ASSESSMENT OF GROUNDWATER RESOURCE IN THE TSINENG AREA, NORTHERN CAPE: A GEOPHYSICAL SURVEY PERSPECTIVE

Tumelo Mokgatle

Submitted in fulfilment of the requirements for the degree

Magister Scientiae in Geohydrology

Faculty of Natural and Agricultural Sciences
(Institute for Groundwater Studies)
at the
University of the Free State

Supervisor: Dr F Fourie

July 2016

DECLARATION

I, Tumelo Mokgatle, hereby declare that the present dissertation, submitted to the Institute for Groundwater Studies, Faculty of Natural and Agricultural Sciences, University of the Free State, Bloemfontein, South Africa, in the fulfilment for the degree of Magister Scientiae, is my own work. It has not previously been submitted by me to any other institution of higher education. In addition, I declare that all sources cited have been acknowledged by means of a list of references.

I furthermore cede copyright of the dissertation in favour of the University of the Free State.

Tumelo Mokgatle

15 July 2016

ACKNOWLEDGEMENTS

I would hereby like to express my sincere gratitude to all who have motivated and helped me in the completion of this dissertation.

- To my supervisor Dr François Fourie, I am sincerely thankful for your guidance and for availing yourself for the contact sessions. Your inputs are appreciated and I am grateful to have you as my supervisor.
- Mr Collen Monokofala, I appreciate your guidance during the field investigations and thanks to Golder Associates for allowing me to use their field equipment.
- Thanks to Mr. Golden Manganyi, for your help during the field work and for your continuous support.
- Thanks to the Department of Water and Sanitation for allowing me to use the data from their funded project.
- The Institute of Groundwater Study staff and Prof Danie Vermeulen thank you for creating a wonderful studying experience at the institute.
- My family and wife, thanks for your support.

TABLE OF CONTENTS

LIST OF FIGURES

LIST OF TABLES

CHAPTER 1:
INTRODUCTION

1.1 BACKGROUND

Groundwater is becoming an important resource to augment the surface water supply in South Africa, and to address the problem of water scarcity faced by the country. The climate is variable and the country has an average rainfall of about 490 mm per year (mm/a), well below the world average of about 860 mm/a (DWA, 2013).

Approximately 25% of the mean annual runoff of 49 000 million m^3/a in South Africa, needs to remain in the rivers and estuaries to support the ecological functioning of the catchments, depending on the specific river systems. Surface water from dams and direct abstraction from rivers accounted for 9 500 million m^3/a, with a significant volume of the surface water yield (3 000 million m^3/a) moved via inter-basin transfers to areas in the country where requirements exceed supply (DWA, 2013).

The replenishment of groundwater is controlled by long-term climatic conditions. Since recharge of the groundwater resource is dependent on rainfall, climate change may have a significant impact on the resources. The sustainability of the groundwater resource therefore has to be of primary concern when managing the resource. Management of the groundwater resource should not only focus on controlling the volumes of water abstracted from the aquifer systems, but should also entail the protection of the quantity of the resource (DWA, 2010).

The most recent estimate of sustainable potential yield of groundwater resources at high assurance is 7 500 million m^3/a, while current groundwater use is estimated at around 2 000 million m^3/a. Allowing for an underestimation on groundwater use for about 3 500 million m^3/a of which could be available for further development (DWA, 2013).

The use of groundwater over surface water is more favourable because the costs of maintaining groundwater schemes are lower as compared to the costs involved in constructing and operating a dam (DWA, 2010). Groundwater is not affected by evaporation/evapotranspiration because, due to its location, it is shielded from these effects (Thomas *et al*, 1998).

Groundwater is also less susceptible to pollution compared to surface water because of the overlying unsaturated zones that protect it from contaminant impacts (Morris *et al*, 2003).

The majority of South Africa's iron ore, manganese, diamonds, lead and copper are mined in the Northern Cape Province of South Africa. The Kalahari Basin hosts one of the world's high grade manganese deposits and mining companies like BHP and Anglo American have been mining there since 1940.

The local municipality where some of these mines are situated in is called Gamagara municipality which originally consisted of two towns namely; Sishen and Kathu. A mining company called Iscor started developing Sishen in 1953 because it started mining there and later it in 1974 it developed Kathu. The towns are commonly known to have camel thorn trees, salt pans and different bird species in the bushes. The municipality currently has three additional towns namely; Shesheng, Dibeng and Olifantshoek. Sishen Mine is situated in Kathu, which is regarded as one of the largest iron open pit mines in the world (www.gamagara.gov.za).

New manganese mines such as United Manganese of Kalahari are now operating within the Kalahari Basin. According to the Khatu Gazette, the mine has 282 million tonnes of manganese in resource and 41 million tonnes in reserve.

In 2012 Tshipié Ntle Mine exported their first manganese production load from their Tshipi Borwa Project (www.tshipi.co.za). Another new mine Kudumane Manganese commenced production in mid-2013.

Production of manganese ore from the project is expected to eventually increase to two million tonnes per annum and later to two and half million tonnes per annum, with the introduction of underground operations in 2019. The expected life of the mine is 10 to 15 years for the open pit or combination mining operations, after which underground mining will continue for an estimated 30 years (http://www.bus-ex.com/article/kudumane-manganese-resources).

Due to the mining activities described above, new property developments, new infrastructure and an influx of people to these areas can be expected, which implies that the social and economic aspects of these areas have changed and will continue to do so in the years to come. Therefore, an increased water demand for agriculture (crop and livestock), steel industries, mining contractors and domestic use is expected.

Geophysical techniques can provide information about the subsurface distribution of geological/geohydrological units and therefore are routinely used in groundwater exploration projects.

The use of the techniques can greatly contribute to the success of an exploration project. Because the technology of geophysical techniques is constantly improving, allowing more reliable data to be recorded and leading to better interpretation techniques, geophysics is expected to play an ever-increasing role in groundwater exploration projects.

Sedibeng Water was founded in 1979 as an organisation that provides water and sanitation services. The organisation currently provides water and sanitation services to two million people in the Free State, North West and Northern Cape (new.sedibengwater.co.za).

Sedibeng Water is also responsible for operating and maintaining the Vaal Gamagara (VGG) water scheme on behalf of the Department of Water and Sanitation (DWS). The scheme is situated approximately 80 km west of Kimberley near Delportshoop. The core function of the scheme is the distribution of purified bulk water for mining, industrial and domestic use (www.ewisa.co.za).

The scheme consist of a raw water pump station, purification works, booster pump stations, several reservoir facilities and a pipeline network of about 1 7000 km. Raw water is abstracted from the Vaal and Hartswater Rivers. The water is purified and then pumped to the various reservoirs. The scheme runs through areas managed by six different water service authorities which involves three local municipalities (Dikgatlong, Kgatelopele and Gamagara) and two district municipalities (Francis Baard and John Taole Gaetsewe) (www.ewisa.co.za).

According to the John Taole Gaetsewe memorandum dated 21 May 2012, the following water services challenges were experienced:

- In the John Taole Gaetsewe area, 5 364 households did not have any formal water systems.
- There were 1 870 households that resided outside the existing water reticulation infrastructure and 200 meter stand tap radius.
- There were 7 041 households that rely on groundwater as a source development. Due to some boreholes drying up and the lack of rainfall these households don't have access to basic water supply.
- During 2012 for a period of 6 months, a total of 147 truckloads [7 500 LT/load] were delivered to various villages experiencing water shortages due to operation and maintenance related failures, breakdowns and other issues.

The DWS and Sedibeng Water appointed KV3 Engineers in association with various consultants to conduct a study named: Development of reconciliation strategies for the area serving with Sedibeng Water Vaal Gamagara scheme as well as a master plan (DWA, 2011). The study inferred that there is a high risk of water shortage to be expected in Kuruman and surrounding areas.

The involved stakeholders decided that an alternative water resource should be sourced to augment the bulk water supply, which lead to the appointment of Worley Parsons Consulting, who in turn appointed Golder Associates to conduct a pre-feasibility study to determine how the current water supply scheme can be augmented by the use of groundwater.

The primary objective of the project was to assess the groundwater resource in those areas that were identified as having potential groundwater resources during the pre-feasibility study. Golder Associates proposed that the study be conducted in two phases:

- **Phase 1** - Exploration and assessment of groundwater resources of the targeted areas and the feasibility of using the existing water facilities to manage the additional water supply.
- **Phase 2** - Development of available groundwater resources.

This project included actions taken to address some of the objectives of Phases 1 and 2. The following actions were taken:

- Geophysical surveys were conducted to delineate geological structures and identify potential areas for groundwater resources.
- Boreholes were drilled at suitable locations, as determined using geophysical surveys.
- Aquifer hydraulic testing was done on boreholes that had a blow-yield in excess of >2 *l*/s.
- Groundwater sampling and hydrochemical analyses were done to determine if the groundwater quality is suitable for drinking purposes.

1.2 AIM AND OBJECTIVES

The main aim of the study was to investigate the possibility of using the groundwater resource to augment the current water supply to the John Taole Gaetsewe. The groundwater resource in the study area was to be assessed in terms of 1) the quantities of groundwater that can be sustainably abstracted, and 2) the quality of the groundwater and its suitability for human consumption. A strong focus was placed on the use of both airborne and ground geophysical methods during the groundwater exploration phase of the study. The current research project aimed to assess the

effectiveness of using these techniques to characterise the geological and geohydrological conditions within the study area and to allow the drilling of successful production boreholes on suitable geological structures. The specific objectives of the research project were as follows:

- To gain information on the distribution of geological units and structures within the study area. This was achieved by conducting both a desktop study of the available information (geological maps, reports) and a geophysical survey. The geophysical survey employed both airborne and ground techniques.
- To assess the effectiveness of using a particular airborne electromagnetic system (the SkyTEM system) during groundwater exploration in the study area.
- To assess the effectiveness of using different ground geophysical techniques to perform detailed investigations across potential targets for production boreholes as identified from the SkyTEM data.
- To drill productions boreholes at suitable locations as determined from the results of the geophysical investigations.
- To investigate the hydraulic properties of the aquifer systems intersected by drilling. This was done by performing pumping tests on selected boreholes.
- To assess the volumes of water that can be sustainably abstracted from the aquifers systems.
- To evaluate the quality of the groundwater from the aquifer system in terms of its suitability for human consumption.
- To make recommendation regarding the possibility of using groundwater to augment the water supply to the John Taole Gaetsewe.

1.3 RESEARCH METHODOLOGY

To achieve the aim and objectives of the investigation, certain methods need to be employed to ensure its successful completion. The project was completed in phases and the methodology was structured according to phases. As part of the investigation, the first five (5) actions were conducted in phase 1 and the other five (5) actions were performed in phase 2. The following actions were taken:

- A literature review was done to understand the hydrogeological setting of the study area, previous work conducted and the principles of the geophysical techniques applied in the investigation.
- A desktop study was conducted which included the collection and collation of available information.
- Hydrocensus was undertaken which included visiting farms and surrounding villages to gather information about the study area.
- Geophysical surveys were performed to detect and delineate geological structures within the study area. Both airborne and ground geophysical investigations were done. The geophysical techniques employed were the magnetic, electromagnetic, gravity and 2D resistivity methods.
- Based on the interpretation of the geophysical data, boreholes were sited at positions of potential high-yielding aquifers
- Production boreholes were drilled at the selected sites. Drilling supervision and geological borehole logging was done during the installation of new production boreholes.
- Aquifer hydraulic tests were performed on existing and newly drilled boreholes to determine the hydraulic properties of the intersected aquifer systems.
- Using the information in the hydraulic properties of the aquifer systems, sustainable yields for the new production boreholes were calculated.
- Groundwater samples were collected and submitted to accredited laboratories for hydrochemical analyses.
- The results of all the components of the investigation were combined to assess to possibility of using groundwater to augment the municipal water supply.

1.4 STRUCTURE OF DISSERTATION

The dissertation is divided into nine chapters, the contents of which are summarised below:

Chapter 1: Provides an introduction to the study which gives background information, describes the aim and objectives of the research and the methodology to be followed.

Chapter 2: Gives a literature review of research pertaining to groundwater exploration using geophysical techniques, as well as previous work done in the study area.

Chapter 3: Gives a description of the site under investigation. This entails the locality of the study area, climate, rainfall, geology, geohydrology, surface drainage, vegetation type, groundwater recharge, groundwater elevations and flow directions.

Chapter 4: The different geophysical techniques employed in the investigation are discussed in terms of the fundamental principles, theory and their application.

Chapter 5: Describes how the geophysical surveys that were conducted as part of the current investigations and the results of these investigations.

Chapter 6: Provides a discussion of the drilling conducted, the borehole construction and the geological borehole logs.

Chapter 7: Describes the results of the aquifer hydraulic tests performed on the new and existing boreholes. Gives a discussion on how the pumping tests were conducted and on the estimated hydraulic parameters of the aquifer systems.

Chapter 8: Discusses the hydrochemistry of the groundwater. Water quality analyses are done and the water type is determined by using the Expanded Durov and Piper Diagrams.

Chapter 9: Conclusions. The entire study is summarized in this chapter. It is discussed how the objectives of the study were achieved. Recommendations are put forward based on the findings of the investigations.

CHAPTER 2:
LITERATURE REVIEW

2.1 INTRODUCTION

The literature review was aimed at ensuring that concepts about groundwater exploration using geophysical techniques are understood. Emphasis was placed on the geophysical techniques employed during groundwater exploration, in particular the Time-Domain Electromagnetic (TDEM) method, and understanding how these techniques can be applied in groundwater exploration programmes.

2.2 CONCEPTS

Some of the concepts encountered in this study are briefly described below:

2.2.1 Groundwater resource management

Kotze *et al.* (2012) defines groundwater resource management as the implementation of programmes for the protection of natural recharge, variation in the volume and abstraction of groundwater over time. The author lists the main groundwater resource management tools by government to protect groundwater resource. Furthermore the author highlights that more guideline frameworks need to be developed to ensure effective groundwater resource management in South Africa.

Hiscock (2005) highlights that groundwater in developing countries is a critical resource and is used extensively for drinking purposes, agriculture and mining. It remains a challenge to continually provide sustainable water for the people because the demand is ever increasing and the management of the resource is often lacking or completely absent. The author also highlights that the lack of protection of water resources could result in the failure of groundwater management schemes.

2.2.2 Groundwater recharge

Groundwater recharge is a hydrologic process where water moves downward from precipitation or surface water to groundwater. This process usually occurs in the vadose zone below plant roots and is often expressed as a flux to the water table surface (https://en.wikipedia.org.wiki/groundwater).

Groundwater recharge is the most important factor in the determination of available and sustainable groundwater resources in the country (DWA, 2010).

Healy (2010) states that understanding groundwater recharge is essential for the successful management of water resources and modelling fluid and contaminant transport within the subsurface. The author furthermore discusses the challenges in estimating recharge because there is an element of uncertainty and there are various methods that can be used in the estimation. It is important that the methods that are relevant to the specific study area are chosen.

According to Kinzelbach (2002), recharge estimates are made particularly difficult in arid and semi-arid areas by the vast variability of hydrological events in time and space. Potential evapotranspiration surpasses average precipitation, which means that only in certain conditions are precipitation events sufficient for recharge to occur.

2.2.3 **Groundwater availability**

Groundwater is the water found in the subsurface in the saturated zone below the water table. The amount of water that an aquifer (a geological formation which has structures or textures that hold water or permit appreciable water movement through them) may yield is dependent upon the porosity and permeability of the material found in the earth layer (DWA, 2013).

The aquifer is replenished naturally by the groundwater recharge process, mainly from precipitation. Groundwater availability depends on the volumes stored underground and other contributing factors are the current abstraction rates, recharge and climatic processes (DWA, 2013).

The utilizable groundwater exploitation potential (Figure 1) in South Africa is estimated at 10 353 Mm^3 per year (DWA-GRA2, 2005). Currently the country uses 2 000 – 4 000 Mm^3 of groundwater per year.

2.2.4 **Groundwater exploration**

Groundwater exploration is the process of locating groundwater resources by studying the hydrogeological settings and the environment of a site.

The exploration of groundwater is often conducted using various geophysical methods. In order for the exploration to commence, a geophysical survey must be designed. Part of the design phase is to clearly set the objectives to be achieved in the investigation and choosing the appropriate method.

Kirsch (2006) provides a guide to various geophysical techniques which are used by hydrogeologists during groundwater explorations. He also describes the application of the different geophysical techniques available for groundwater exploration.

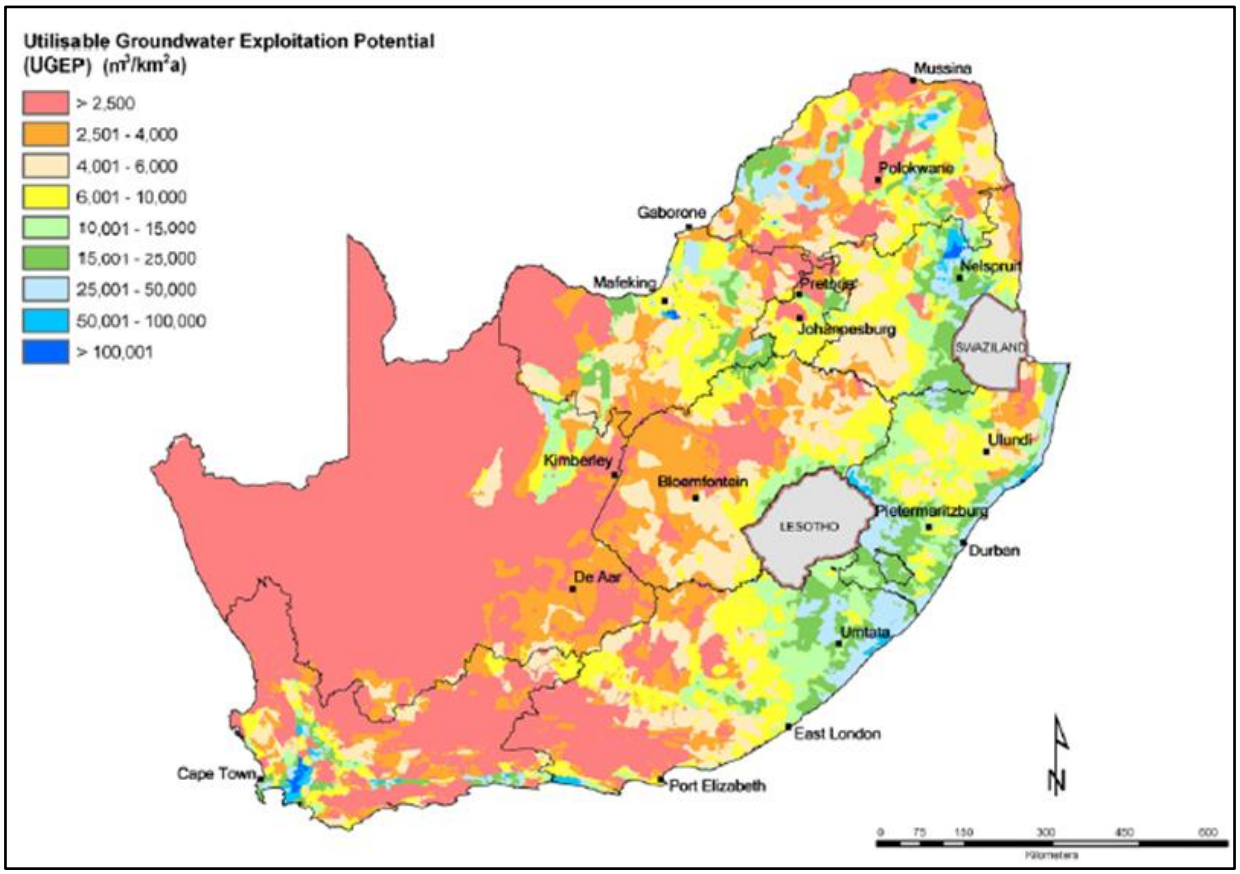

Figure 1: Utilisable groundwater exploitation potential in South Africa (DWA-GRA2, 2005)

2.2.5 Aquifer hydraulic testing

Kruseman and de Ridder (1994) describe the principles of aquifer hydraulic testing as tests that are often conducted by pumping water from a well while measuring the discharge rate as well as the drawdown within the pumped well or within observation wells in its vicinity (refer to Figure 2). The measured discharge rates and draw downs can be used to determine the hydraulic characteristics of the aquifer.

According to Jones (1963) the rate at which water can be withdrawn from a well is dependent on various factors such as: the permeability of the aquifer, the thickness of water bearing zone and the hydrostatic head above the aquifer to which water will rise in the well.

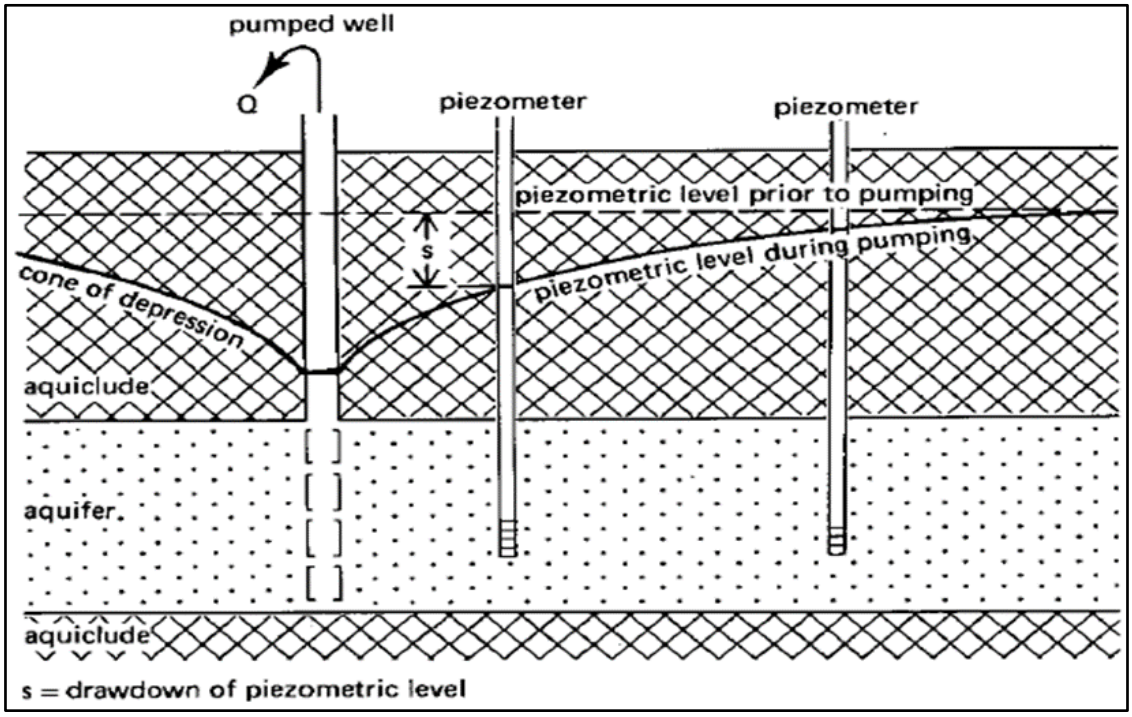

Figure 2: Aquifer testing illustration (Kruseman and de Ridder, 1994)

2.2.6 Hydraulic parameters

The hydraulic parameters of an aquifer determine the volumes of water that can be stored within the aquifer, as well as the rates at which water can be released from the aquifer. The following parameters are critical during the assessment of groundwater resources:

Storage coefficient (S_c): the volume of water released per unit plan area of aquifer for a unit fall in head (DWA, 2011):

$$S_c = \rho g D(\alpha + n\beta) \qquad \text{eq.1}$$

where:

ρg = specific weight of water = 9 804 N/m^3

α = compressibility of the rock (m^2/N)

n = porosity

β = compressibility of the water (4.47×10^{-10} m^2/N for water at 10^{o}C)

D = thickness of the aquifer

Establishing the sustainable exploitable potential requires the determination of the quantity of water held in storage and what percentage can be removed for the resource not to be compromised.

Bredenkamp *et al.* (1995) caution against obtaining an S_c-value from a single observation borehole in secondary (fractured) aquifers, as the value appears to decrease with distance from the pumped borehole. The authors highlight that S-values obtained from pumping tests in a fractured rock system can be unreliable. Furthermore the author suggests that the reason why the S-value changes with distance is because of the pressure relationship between groundwater in the matrix and in the fracture.

Hydraulic conductivity (*K*): A measure of the ease with which water will pass through the earth's material; defined as the rate of flow through a cross-section of one square metre under a unit hydraulic gradient at right angles to the direction of flow (DWA, 2011). The hydraulic conductivity can be determined through the analysis of pumping test data (Murray, 1996).

The hydraulic conductivity of fractured rocks depends on the density of the fractures and the width of the crack. Fractures can increase the hydraulic conductivity of solid rocks (Kruseman and de Ridder, 1994).

Woodford and Chevallier (2002) highlight the importance of establishing the hydraulic properties of an aquifer and understanding the geological environment in which the boreholes are located.

Transmissivity (*T*): The rate at which water is transmitted through a unit width of an aquifer under a unit hydraulic gradient. It is expressed as the product of the average hydraulic conductivity and thickness of the saturated portion of an aquifer (DWA, 2011).

Transmissivity can be expressed as follows:

$$T = KD \qquad \text{eq.2}$$

where:

T = transmissivity in m^2/d

K = hydraulic conductivity in m/d

D = thickness of the confined aquifer in m

2.2.7 Groundwater sustainability

Good management of groundwater resource is the key to reliable, efficient groundwater supply. Monitoring the water level, water quality and abstraction rates are some aspects that need to be taken into consideration (DWA, 2010).

Morris *et al.* (2003) define sustainable groundwater use as the level of development of groundwater that meets the needs of the present generation without compromising the ability of future generation to meet their needs.

Vivier (2013) regards the determination of a sustainable groundwater yield as a complex and challenging task because of the high degree of uncertainty with aquifer parameters. According to the author, the principle of sustainability requires that the environment, social and economic considerations be taken into account. A popular method to determine groundwater sustainability is to compile a groundwater balance taking into account all losses and gains to the groundwater system.

2.2.8 Groundwater use

The volume of groundwater abstracted in South Africa is currently underestimated, since many groundwater users in the country do not register their groundwater use with the Department of Water and Sanitation. This makes quantifying groundwater use in the country difficult (DWA, 2013)

Most rural villages rely solely on groundwater since large volumes of the surface water resource has already been allocated to other uses. Irrigation is the main consumer of groundwater, followed by mining and municipal water supply, as shown in (Figure 3).

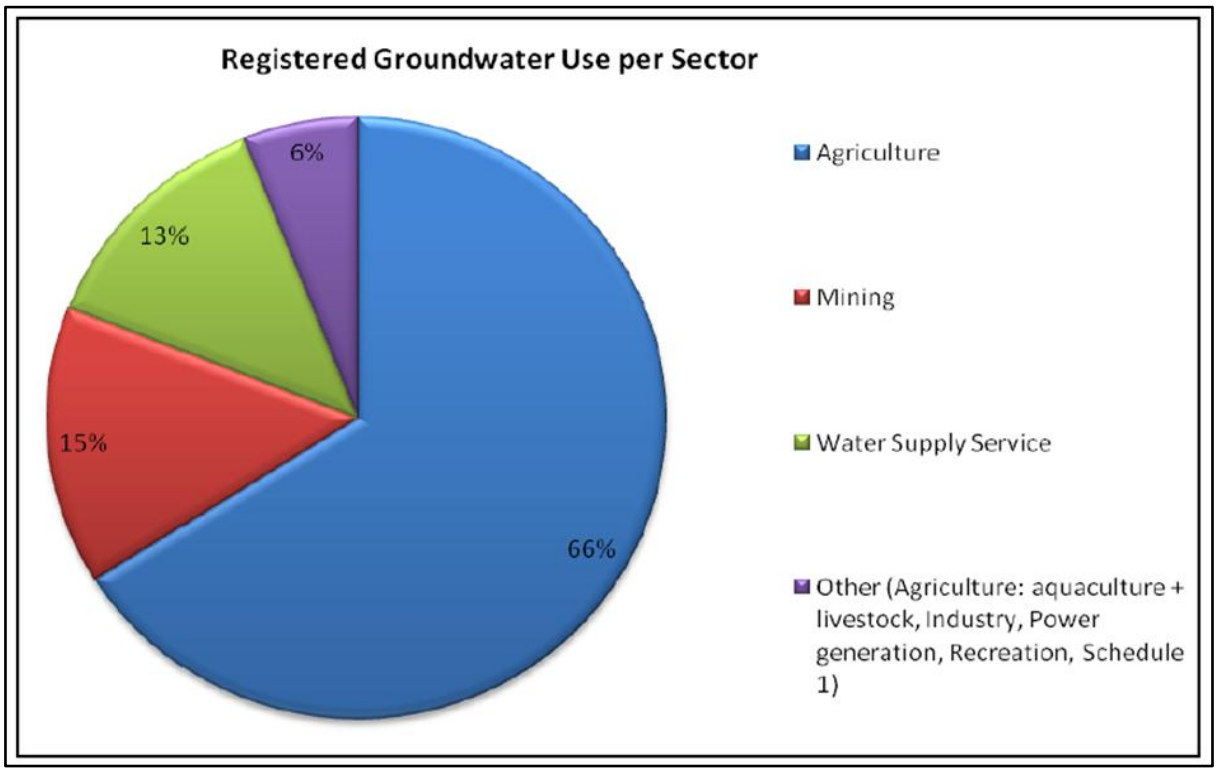

Figure 3: Registered groundwater use per sector in South Africa (DWS-WARMS, 2014)

2.2.9 **Groundwater quality**

The nature and extent of the chemical, physical, and biological processes that control the fate and transport of microorganisms in South African aquifers have not been investigated fully (du Preez *et al.*, 2013). For this reason, the health risk to humans exposed to infectious organisms from groundwater is also not well understood by the general public.

Groundwater can also be contaminated from septic tanks, industries, mining, waste disposal sites and agricultural activity. Generally, the groundwater quality in South Africa is good for potable drinking and requires little or no treatment before consumption (du Preez *et al.*, 2013), as shown in (Figure 4). According to the South African National Standards (241:2011), water that has an electrical conductivity limit below 170 mS/m is suitable for ingestion.

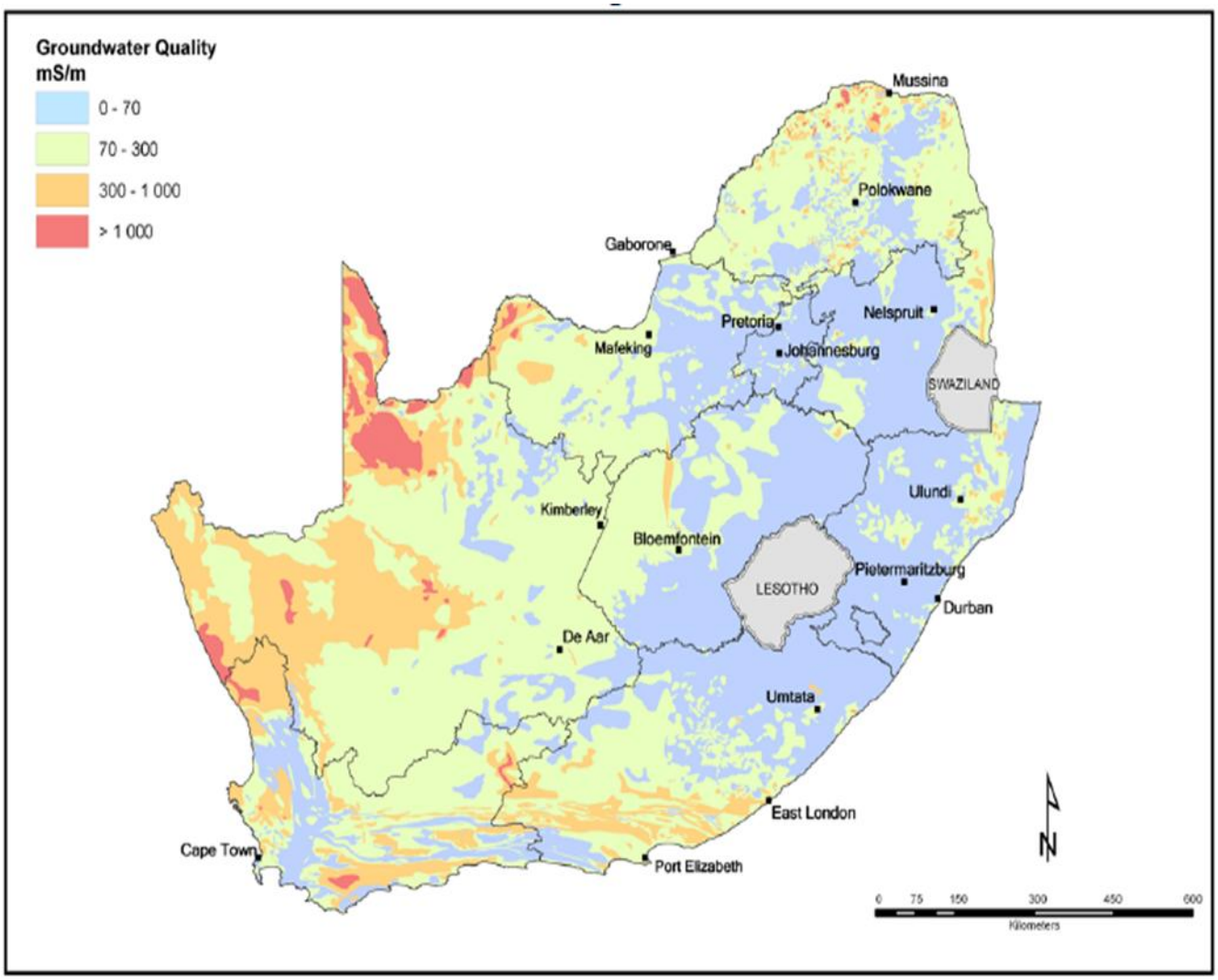

Figure 4: Groundwater quality map in South Africa (DWA-GRA2, 2005)

2.2.10 Airborne and ground geophysical techniques

This study focuses on the application of both ground and airborne geophysical techniques during a groundwater exploration programme in John Taole Gaetsewe. A proper description of the geophysical techniques employed during the investigations is therefore required. A literature review of the geophysical techniques used during the current investigation is provided in Chapter 4 where each of the techniques is discussed in detail.

2.3 PREVIOUS INVESTIGATIONS IN THE STUDY AREA

The previous work in the study area was used to establish the baseline information and conditions about the area. The information was also used to get a better understanding of the water demands and needs of the area and lastly to identify potential areas that can be targeted for the exploitation purposes.

2.3.1 Gravenhage manganese project

Jones and Wagener (2011) conducted a hydrogeological assessment and groundwater modelling for Aquila Steel. The project was within a portion of the study area in the D41M quaternary sub-catchment. Some of the findings of the investigation were:

- The aquifer present could be classified as intergranular and fractured.
- The median borehole yield varied between 0 and 0.10 litres per second.
- The groundwater quality had elevated electrical conductivity levels within the study area.

2.3.2 Kgalagadi District Municipality: groundwater assessment

Wiegmans (2006) conducted various field investigations for the former Kgalagadi District Municipality, now known as the John Taole Gaetsewe. Eighteen maps were produced that provide information on the groundwater situation in the area. Each map encapsulates different aspects about the Kalahari Bain such as: the rainfall, geology, piezometric contours, ecological reserve and groundwater balance

2.3.3 Development of a reconciliation strategy for towns that receive water from Sedibeng water through the Vaal Gamagara Scheme

The detailed study (DWA, 2011) conducted by KV3 Engineers in association with Kayamadi Development Services, WRP Consulting Engineers and Golder Associates covered the social and economic aspects of the towns, with emphasis on the water demand. The consolidated base data

was obtained from reviewing the latest municipal documents, latest housing development plans and personal interviews with the community.

Water benchmarks, i.e. are water use limits that were set for every town by the responsible stakeholders for water supply, were calculated using all the collected data. The overall findings were:

- The water use in 2010 for the towns of Delportshoop, Longlands, Koopmansfontein and Vaal Gamagara was 0.582million m^3/a (1.593 Mℓ/d, 99 ℓ/c/d) and was projected to increase to 0.990 million m^3/a (2.710 Mℓ/d, 124 ℓ/c/d)by the year 2030.
- The water use for the Vaal Gamagara village was 0.150million m^3/a (0.410 Mℓ/d). The village in 2010 had a population of 250 people, which meant that the per capita unit consumption of water was at a high level of 1 643 ℓ/c/d against a benchmark of 137 ℓ/c/d.
- Koopmansfontein was expected to increase its water use in 2010 from 0.004 million m^3/a (0.011 Mℓ/d, 59 ℓ/c/d) to 0.005 million m^3/a (0.014 Mℓ/d, 67 ℓ/c/d) by the year 2030.
- The water use for the Kathu Cluster was estimated at 5.344 million m^3/a (14.631 Mℓ/d). The population of the area was 16 701 which meant that the capita unit consumption of water was at a high level of 876 ℓ/c/d against a benchmark of 303 ℓ/c/d.
- A preliminary analysis of Kathu estimated that the water requirements could potentially be reduced to 8.619 million m^3/a (23.598 Mℓ/d) in 2030 through the implementation of water demand management.
- The water use for Hotazel was estimated at 0.343 million m3/annum (0.939 Mℓ/day). The population in the area was 1 558 which meant that the capita unit consumption of water was at a high level of 602 ℓ/c/d against a benchmark of 272 ℓ/c/d.

Based on the study, the water benchmarks set for the respective towns are lower than the set benchmarks for the towns. This means that additional water needs to be made available and the set benchmarks must be reviewed.

2.4 GEOPHYSICAL METHODS

Previous geophysical investigations conducted for groundwater exploration related to the current investigation are summarised below:

2.4.1 **Application of time domain methods for groundwater exploration**

Danielsen *et al.* (2003) explain how the Transient Domain Electromagnetic (TDEM) method was used during a project in Skjød, Denmark.

The aim of the survey was to identify potential groundwater resources and to estimate the hydraulic properties of the aquifer system. Based on the survey conducted, it was concluded that:

- A buried valley system is present and a basal layer with resistivity below 15 Ωm was detected.
- Valley features which could not be identified on geological or topographic maps were identified using elevations and resistivities adopted from the TDEM data.

Wightman *et al.* (2001) discuss the use of the Transient Domain Electromagnetic (TDEM) method to define shallow stratigraphy and groundwater salinity distribution with the Kurkar aquifer in Gaza, Israel. A Geonics Proton receiver using transmitter loop varying in size between 60 m and 120 m was used. The TDEM sounding results was used to map the distribution of resistivities across Gaza and in addition the method assisted in mapping the boundary between the fresh and saline water. The sounding results were used to map the aerial extent and top elevation of a layer at depth.

Carrasquilla *et al.* (2007) evaluate the performance of different geophysical techniques for groundwater prospecting in Espirito, Brazil. From the use of the TDEM method the following was deduced:

- The results showed that it was possible to detect more resistive areas in the basement complex and separate it from more conductive formations in the fractures/faults.
- The method was able to locate discontinuities within crystalline terrains (fractures/faults), which indicated the best places to drill for new wells.
- The conductive zone in the higher part of the study area was the weathering layer around 25 m wide, which was easily detected by using that method.

Fitterman (1987) explains the use of the Transient Electromagnetic method in groundwater exploration in White Sands, New Mexico. The sounding results were used in an inversion model and the findings were:

- The layer resistivities in the alluvium were interpreted to be 33 Ωm and 7.1 Ωm meanwhile the thickness are 129 m and 101 m respectively.

- The layer resistivities in the confined fresh-water aquifer in bedrock sediments were interpreted to be7 Ωm and 120 Ωm meanwhile the first and second layer thickness were 162 m and 105 m respectively.
- The depth of the salt water layer was estimated to be 110 m and the layer was estimated to have a resistivity of 3.3 Ωm. The thickness of the salt water layer was 33 m.

Atya *et al.* (2012) discuss how they used Transient Domain Electromagnetic method to investigate shallow depths of a particular site in Qarret Abu Rouh, Egypt. The best fitted models were used to construct geoelectric sections. From those sections it was deduced that the layers are sand with gravel, clay beds intercalated with sand lenses and fractured limestone, with marl deposits. The area was delineated based on the different deposits identified.

Porsani *et al.* (2012) conducted a TDEM survey in order to understand the hydrogeological setting of sedimentary and fractured basaltic aquifers in Sao Paulo, Brazil. The findings were:

- The resistive sediments were about 80 to 30 Ωm and were related to the upper layers of the Adamantina formation that consist of clayey sand.
- Below these dry sediments, the geo-electrical models show a conductive layer (about 8 to 12 Ωm) characterised by a saturated clayey sand sediments of the shallow aquifer system in the Adamantina formation.
- The top of the basalt layer (Serra Geral formation) occurs at approximately 70 m depth, and it is characterised as the most resistive layer (about 200 to 600 Ωm).

2.4.2 Application of gravimetric methods for groundwater exploration

Dudash *et al.* (2009) used gravimeter as a practical tool to determine the large density contrast between the igneous and metamorphic bedrock in the Pauma groundwater basin in California, USA. The Scintrex CG5 gravity meter was used in the survey and after the field data was collected, it was processed by using Geosystem'sWinglink software. Based on the investigation the following was deduced:

- The bedrock is shallowest along the western part of the study area and generally slopes to the east-north. Structural features in the northern basin have resulted in deep bedrock and anomalously thick sequence of alluvium is overlying the bedrock.

Bradley *et al.* (2007) discuss the use of microgravity to investigate the geological structures of an area proposed for an aquifer storage and recovery project in north eastern Abu Dhabi Emirate in the

UAE. The CG-5 gravimeter was used in the survey and the data was processed to account for earth tides, gravity drift, elevation and regional variations in gravity. Borehole logs of the study area were compared to the gravity data and findings were:

- Borehole 1, log indicates the bottom of aquifer near the water table elevation and an average density rising to 2.5 g/cm ^{3}at the bottom of the borehole.
- Borehole 2, log is consistent with the gravity profile, the boundaries of the shallow units can be seen on the gravity profile.
- The gravity models clearly show consistent thrust fault in the location and their respective lengths.

Alla *et al.* (2007) conducted an investigation using integrated geophysical techniques to assess the groundwater potential of a site in Sina Penisula, Egypt. The practical tool used was the Scintrex CG3 Autograv with resolution of 0.01 mGal. The conclusion is that:

- The shallow subsurface section of the study area consists of four geoelectric units which are clay, limestone, clayey limestone and sandstone.
- The main aquifer in the study area is the fourth layer and consists of sand of good quality fresh water.
- The area affected by different fault elements of NW-SE, NE-SW and N-S trend.
- The depth of the basement rocks ranges between 120 and 270 metres.

Mochales *et al.* (2007) discuss the use of gravity to detect underground cavities and dolomite structures in Zaragoza, Spain. The Burris gravity meter with a precision of 0.001 mGal was used. The conclusion was that:

- The section of the Bouguer anomaly shows a defined low in the central part of the sinkhole.
- The sinkhole contour shape is well defined by the anomaly gradient and shows a funnel shape.
- Two kinds of filling can be predicted and separated by their densities: a low-density filling, probably resulting from the non-compacted urban debris, and a high-density filling at greater depths, creating the relative gravity highs towards the borders of the negative anomaly.

2.4.3 **Application of magnetic methods for groundwater exploration**

Terblanche and Stroebel (2013) conducted a groundwater exploration programme in basement granites of the Kraaipan Group using geophysical techniques.

A proton magnetometer (Geotron G5) was used to conduct the survey and to identify the drilling targets. In addition to ground geophysics, airborne data from a survey conducted in 2002 was used. The findings of the investigations were:

- The use of airborne geophysical surveys prior to ground geophysical surveys should be considered in large rural groundwater supply projects, especially in traditionally low-yielding aquifers where geological and aerial maps provide little guidance in terms of groundwater bearing structures.
- Vast areas were covered in a short time with the airborne method, while ground geophysical surveys were used to concentrate on actual targets. Not only can there be cost and time savings on ground geophysical surveys when using airborne data, but drilling of unsuccessful boreholes can be limited.
- The project had a success rate 70% with 46 successful boreholes from 66 drilled. The total yield of the successful boreholes amounted to 360 *l/h*. This yield was achieved in low-yielding igneous geology, due to the improved success rate achievable when using geophysical techniques during groundwater exploration.

Al-Garni (2009) conducted a magnetic survey in order to understand and delineate structures that could be targets to evaluate the groundwater potential in Wadi Fatima, Saudi Arabia. Sixteen magnetic profiles were conducted with spacing intervals ranging from 10 m to 20 m. The GEM19 proton precession magnetometer was used for the survey. The magnetic survey showed an intrusive body, which was highly fractured.

The conclusion was that the basement structures control the groundwater flow and that the south western part of the study area was ideal for drilling because there is intensive faulting and fracture at that particular area.

Sultan *et al.* (2009) conducted a magnetic survey in Sinai Peninsula, Egypt. The objective of the magnetic survey was to determine the depth of the anomalous sources. The authors carried out total intensity magnetic field measurements using the Envimag proton magnetometer. The magnetic survey data was combined with the gravity data conducted separately and the following was deduced:

- The north and southwest of the study area is occupied by high magnetic structures while the eastern part is represented by low magnetic structures.
- The thickness of the granite basement is estimated to be within a range of 1 500 m and 3 150 m.
- The top surface of the deep aquifer is probably at depth ranging from 300 to 1 000 m.

Muturi *et al.* (2014) discussed the application of geophysics for groundwater evaluation in hard rock in the eastern part of Kenya. The geophysical techniques were applied to verify the concealed fault zone and provide information about the high yielding aquifers. The Geometrics 858 proton precession magnetometer was used to measure the total magnetic field to a resolution 0.1 nT. The following was deduced:

- The continuous magnetic lows within high magnetic anomaly are a result of the local magnetic anomaly of the disintegrated basement rock.
- The use of the 2D Euler solution to model the magnetic data clearly showed the subsurface faulting/contact patterns within the geological unit.
- A fault structure extending approximately 200 m in depth and a basin structure of 250 m in depth were identified along one of the traverses.

Shendi *et al.* (2004) conducted an investigation using ground geophysics in the development of groundwater in basement terrain south Sinai Egypt. The magnetic survey was conducted on three traverse lines using the Digital Fluxgate magnetometer as the practical tool. After analysing the collected data, the following was concluded:

- The smoothed magnetic profile showed alternative high and low anomalies, reflecting irregularities in the buried basement and lateral lithogical variations in the basement rocks.
- An estimated depth to the fresh basement bedrock ranged between 27 to 104 m.
- Three sites have thick alluvial deposits and weathered basement rock which will be ideal for storing groundwater.

2.4.4 **Application of frequency domain methods for ground water exploration**

Ahmed *et al* (2009) discuss the use of electromagnetic methods for groundwater exploration in the basement complex in south Sudan. The electromagnetic survey was employed along two traverse lines, which were 875 m and 475 m long respectively. The conclusion of the investigation was that:

- The thickness of weathered and fractured basement rocks above the fresh ones is about 77 m and may reach up to 135 m if drilling goes to deeper depths.
- The centre of the structure is trending in a north - south direction and oriented parallel to the western side structures.
- Drilled borehole data and geophysical interpretation results, showed that the valley in the area is an old buried channel.

Ariyo and Adeyimi (2013) conducted an investigation using integrated geophysical methods in assessing the groundwater prospect of a typical basement terrain in some parts of south western Nigeria. The findings in the investigations were:

- The presence of a sandy layer will enhance availability of groundwater.
- The area underlined by granite gneiss will be more prolific in terms of groundwater exploitation than the area underlayed by migmatised gneiss.

Ugwu (2009) explains how he used the electromagnetic method to detect fractures for groundwater development in Oha Ukwa, Nigeria. The length of the traverse is one thousand metres (1 000 m) with inter-coil separation of 20 m, taken normal to the strike. The Geonics 34-3 instrument was used as the practical tool in the investigation and the following was deduced:

- The data showed that conductivity anomalies, was obtained along the fractured zone
- Where the conductivity values did not change much, the rocks were not generally fractured.
- Potential production wells should be drilled at the identified fractured zones.

2.4.5 Application of 2D resistivity methods for groundwater exploration

Nyabeze *et al.* (2013) discuss the use of geophysics to assess the characteristic of the groundwater aquifer associated to the Sagole hot spring in Limpopo. The Iris Syscal Pro channel multi-electrode system was used to estimate the depth of the bedrock structures. The data from survey was modelled to produce depth section images using the Res 2DINV software. The findings were:

- There was a low resistivity vadose zone with a thickness of approximately 30 m. The low resistivity values below 25 Ωm could be attributed to the presence of water or salinity.
- The resistivity increased with depth from surface to about 70 m and had values above 500 Ωm

- The maximum depth of the investigation of the Electrical Resistivity Tomography configuration was about 70 m. The higher bottom layer resistivity values could be associated with the mapped basalt.

Monokofala and Wiegmans (2013) used the 2D resistivity method coupled with other ground geophysics techniques to investigate the Kalahari sediment thickness and the underlying dolomite bedrock in order to establish potential potable groundwater sources for Henningvlei in the Northern Cape. The ABEM SAS4000 Terrameter and ES 464 switching unit with four multi core cables (150 metres long) and 1 metre stainless steel pegs were used. The Wenner-Schlumberger continuous profiling protocol was used. The findings were:

- High yielding boreholes (>2 *l/s*) were found in basal Kalahari gravel deposits below the Budin clay at a depth in excess of 90 mbgl.

Kellet *et al.* (2000) explain the use of combined borehole geophysics to identify structures in deeply weathered crystalline basement terrains in east Mangochi, Malawi. The authors explain that using geophysical techniques to target the thickest zones of weathering resulted in them achieving a high success rate.

The geophysical tool used in the project was an Iris Syscal R2, an electrical resistivity tomography system using 4 x16 node boxes and 5 m minimum electrode spacing. The conclusions were:

- Geological electric structure of the regolith comprised a thin laterite layer (> 200 Ωm) overlying a thick saprolite layer (20 – 100 Ωm).
- A saprolite layer (30 – 150 Ωm) of at least 30 m was considered optimal for good groundwater potential.
- The low lying regions showed lower resistivities near surface, which indicated the presence of clays that might reduce the groundwater potential.

Oladunjoye *et al.* (2013) discuss the use of the electrical resistivity method to evaluate the subsurface geologic and geoelectric properties that might contribute to the availability of groundwater in southern Nigeria. Vertical Electrical Sounding (VES) data was iterated using the software package Winglink. The VES curves obtained were classified into five different curve types and interpreted per category. The findings of the investigation were:

- VES 1 recorded a resistivity of 112 Ωm which indicates there is no available groundwater in that location.

- VES 3 curve morphology indicates an apparent resistivity of 95 Ωm which extends to depth of 6.5 m; this suggests that the borehole will yield groundwater.
- VES 4 and 6 are characterised by apparent resistivity of 77 Ωm and 605 Ωm respectively, which suggest that the borehole will not yield groundwater.
- VES 7 is characterised by apparent resistivity 0 Ωm with total thickness of 19 m, which suggest no groundwater occurrence.

Prabhu and Ravindran (2012) discussed groundwater exploration using the Wenner-Schlumberger electrode array through the W-4 2D resistivity imaging system at Mahapallipuram, Chennai,

Tamilanadu, India. The authors analysed the pseudo sections and deduced the following:

- Three zones were identified; dry zone, fresh water mixed with sandy clay and hard rock enriched soil zone
- The soil, water and bedrock depth was clearly delineated and the hard rock with calcareous sandstone was identified at a depth of approximately 39 m.
- The maximum recorded apparent resistivity in that terrain was 1 275 Ωm and the resistivity range of the conductivity zone was 100 Ωm.

2.4.6 **Discussion**

The different applications of the geophysical methods mentioned above, demonstrated how the objectives of an exploration project can be achieved. The different findings in each of the investigations, gives guidance on how a similar investigations can be approached in order to obtain good results. Thus, it is important that during an investigation, you review the literature of the study area to acquire more knowledge and information that you might not have access to prior to the investigation.

CHAPTER 3:
SITE DESCRIPTION

3.1 LOCATION

The study area is situated in Tsineng which is approximately 20 km from Hotazel and 60 km to Kuruman. The study area is referred to as Source Development 4 (SD4). The study area is situated in the Northern Cape Province (Figure 5) and falls within the John Taole Gaetsewe District Municipality (JTGDM). The village is near mining towns and attracts different cultural groups from different parts of the country and neighbouring countries.

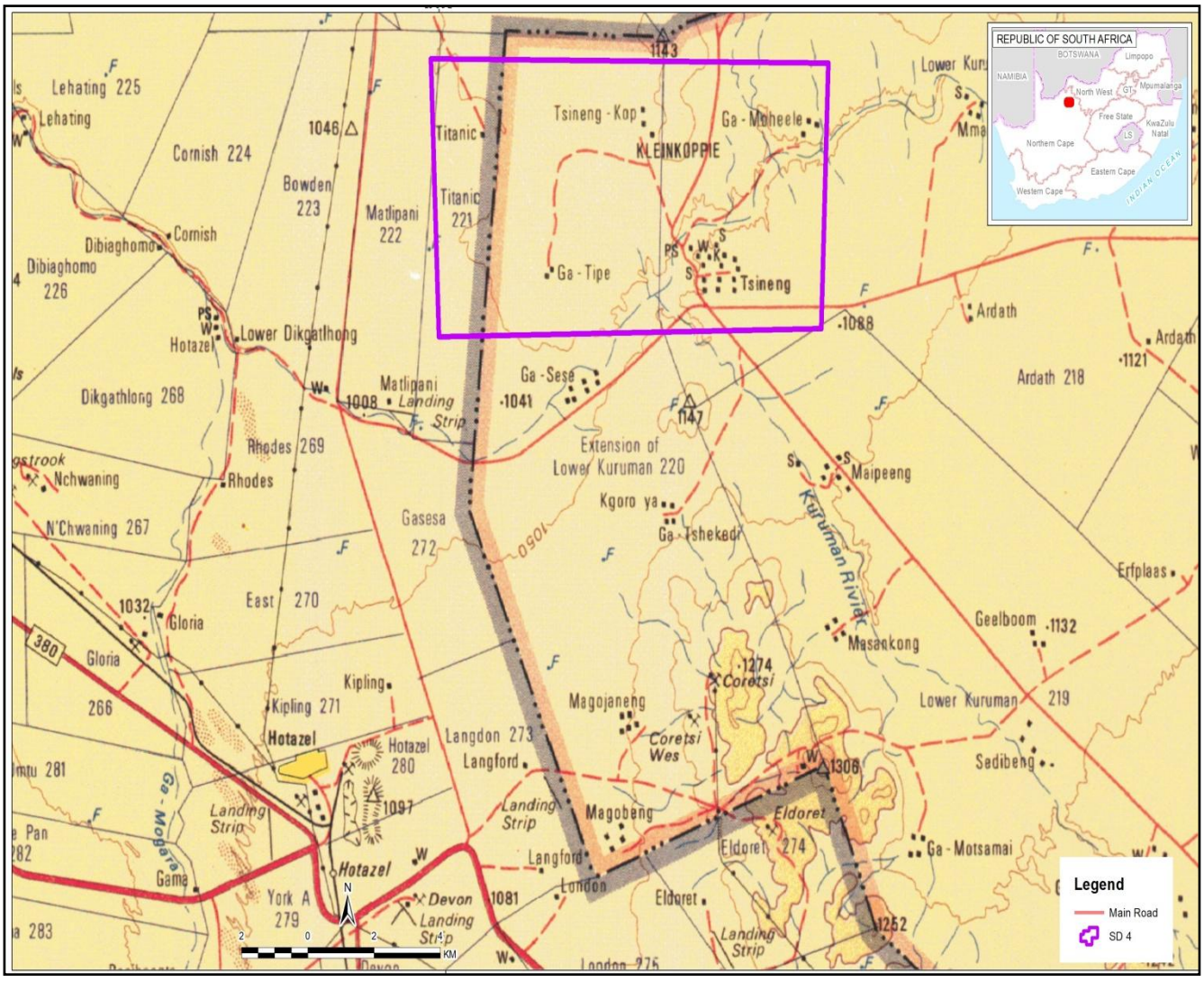

Figure 5: Locality map

3.2 CLIMATE AND RAINFALL

The climate in the study area can be characterised as extremely hot in summer and can be excessively cold in winter. The towns in the study are located in a semi-arid therefore high evaporation rates and dry conditions are expected. Precipitation occurs as a result of thunder showers in the autumn and summer seasons. The village of Tsineng and Titanic receives high rainfall mainly during December to March, while the month of July receives the lowest rainfall (refer to Figure 6 and Figure 7).

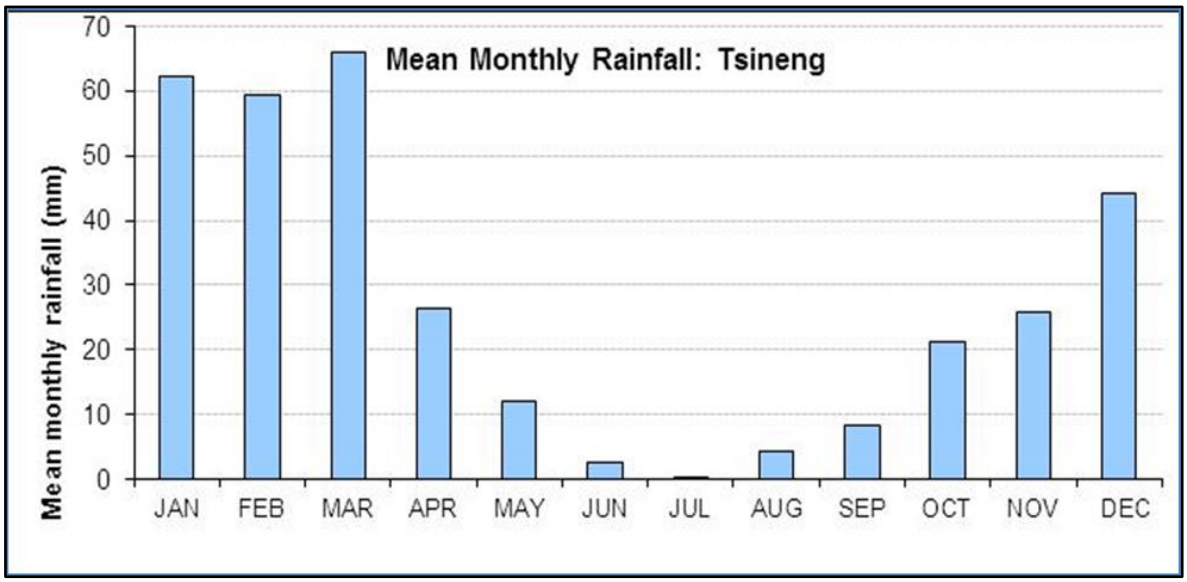

Figure 6: Mean monthly rainfall of Tsineng (Golder, 2014)

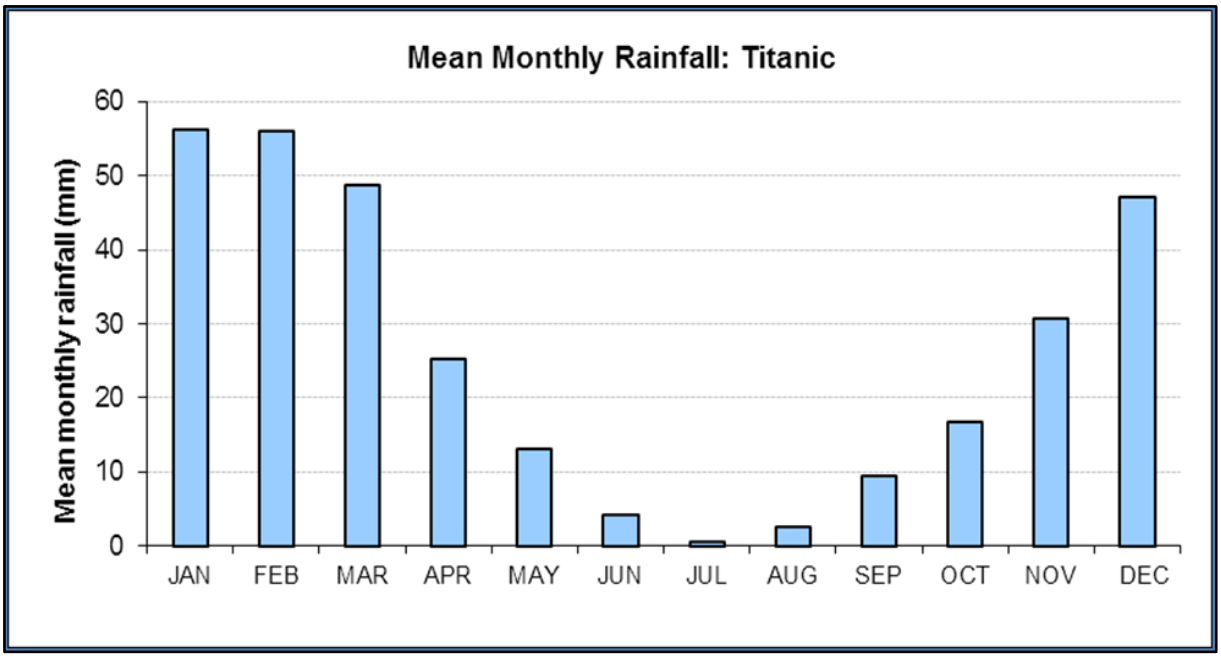

Figure 7: Mean monthly rainfall of Titanic (Golder, 2014)

The annual rainfall recorded for SD4 is shown in (Figure 8). Tsineng's annual precipitation is 339 mm/a while Titanic receives approximately 318 mm/a. According to Vegter (1998), effective rainfall is when the rainfall exceeds 100 mm per month. Effective rainfall is defined as the percentage of rainfall which becomes available to plants and crops. It considers losses due to runoff, evaporation and deep percolation. It is always best to use the actual observation or measurements to estimate the amount of effective rainfall for a particular site (texaset.tamu.edu/effrain.php). The mean annual precipitation of Tsineng and Titanic is approximately 329 mm/a.

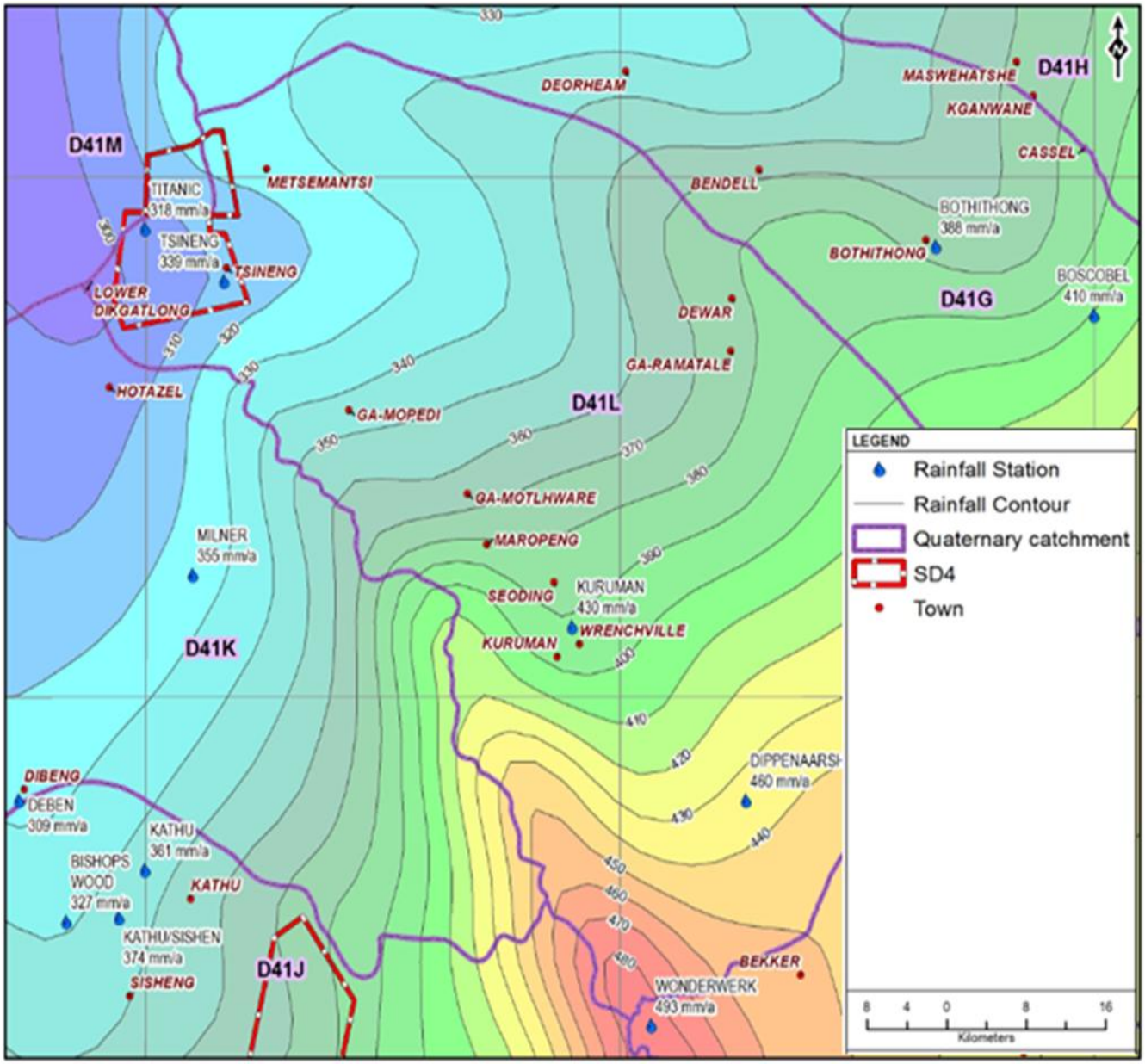

Figure 8: Annual rainfall distribution map (Golder, 2014)

3.3 TOPOGRAPHY AND SURFACE DRAINAGE

The topography is characterized by the flat slope of the Ghaap Plateau. The elevation of Tsineng is approximately 1 067 mamsl (www.floodmap.net). The topographic (See Figure 9) gradient decreases from east to west towards the Kuruman River which is at an elevation of approximately 1 030 mamsl.

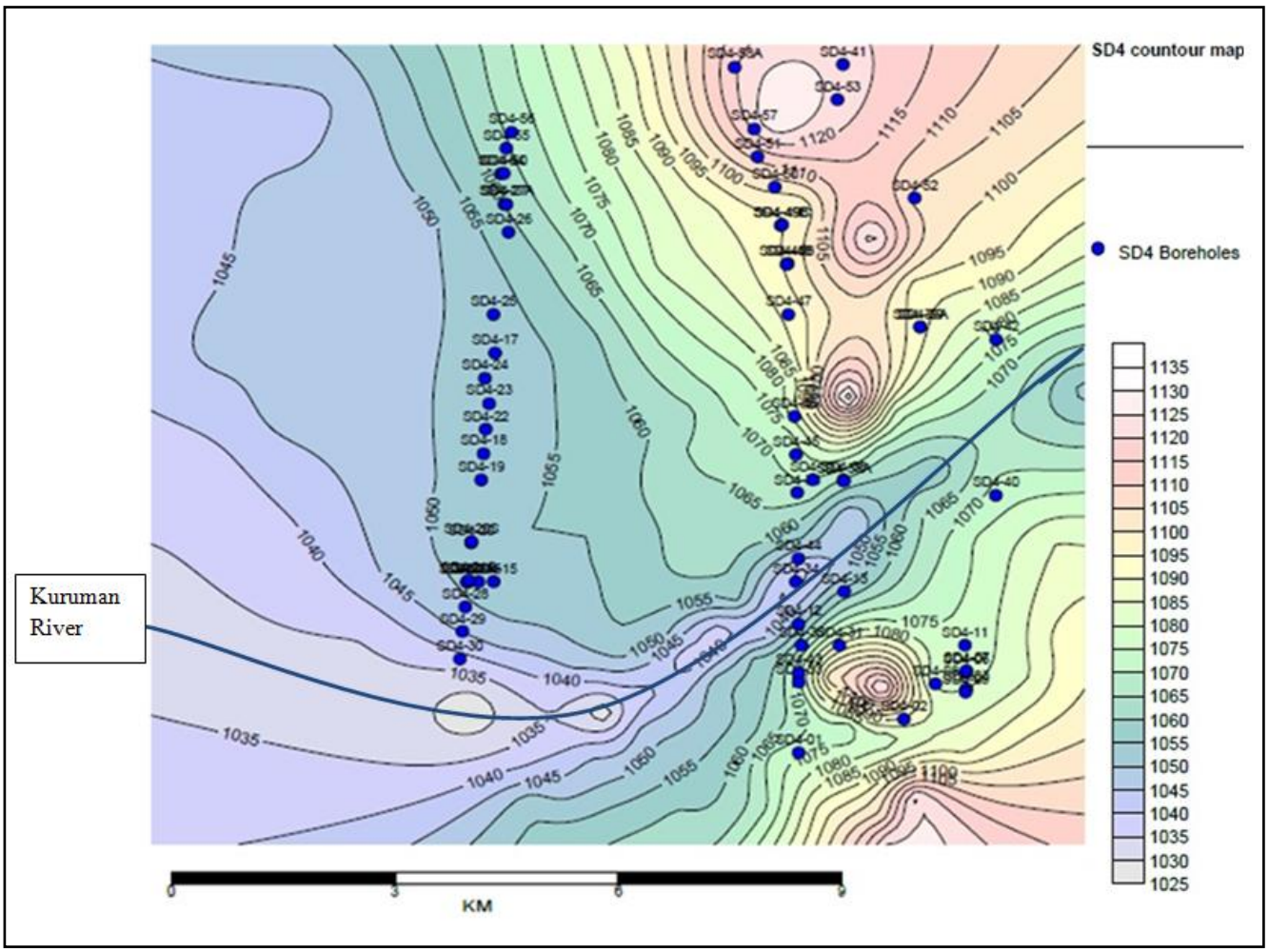

Figure 9: SD4 contour map showing the elevation and distribution of boreholes (Golder, 2014)

The study area is situated in quaternary sub-catchments D41L and D41M (Figure 10). There are three non-perennial rivers present, namely: the Logobate, Matlhwaring and Manyeding Rivers. The Kuruman River is a perennial river which runs through both quaternaries. The rivers flow in a north-easterly direction.

According to data obtained from the SPATSIM database (accessed on 17/04/2013), the ecological water requirement for quaternary sub catchments D41L and D41M is 2.496 Mm^3/a and 0.410 Mm^3/a, respectively.

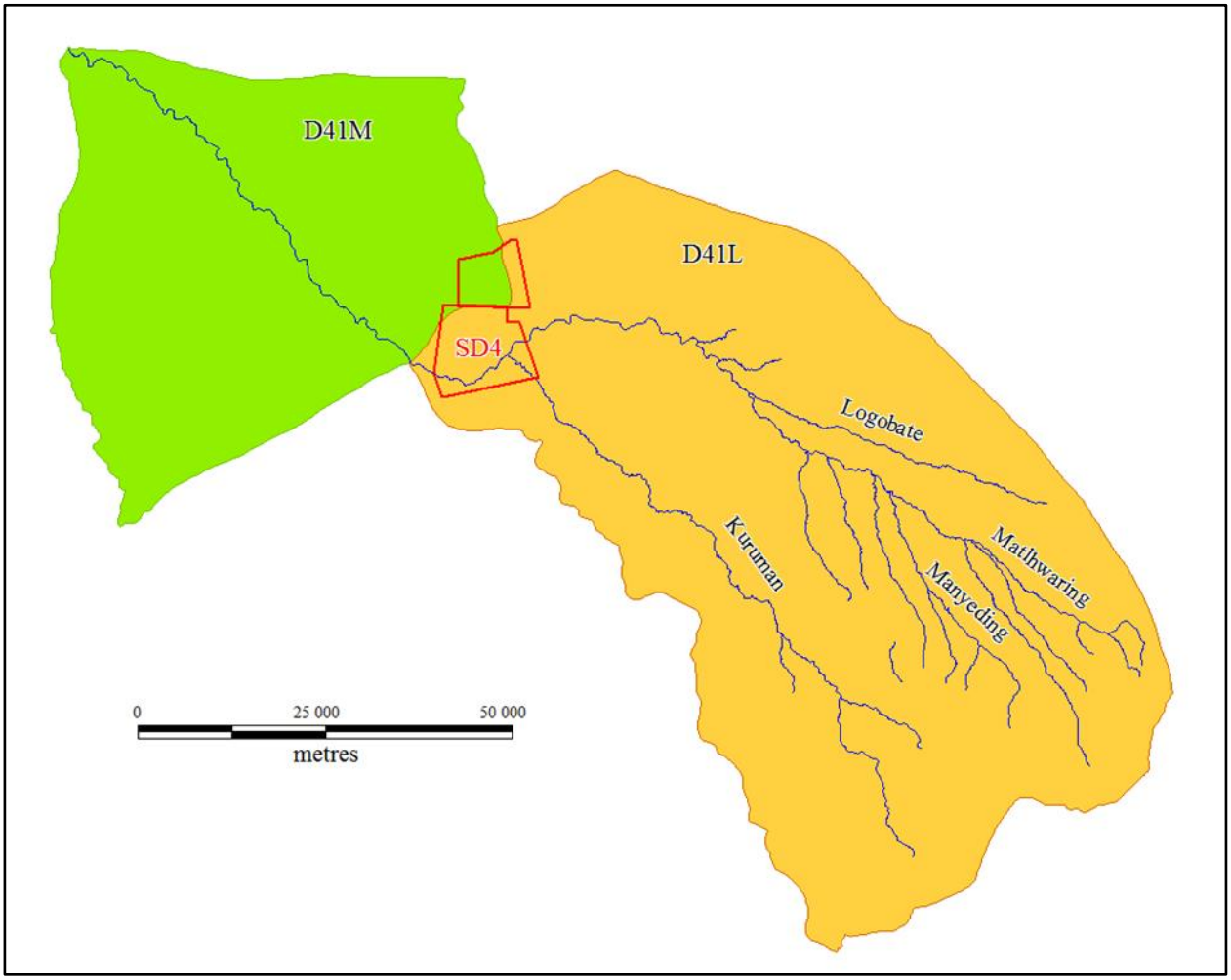

Figure 10: Quaternary sub-catchments and surface drainage in the vicinity of the study area

3.4 VEGETATION

Anderson (2011) conducted a vegetation study for the Gravenhage manganese project north of Hotazel for Aquila Steel. Hotazel is approximately 20 km away from the study area. Similar vegetation can be observed in the study area.

The National Forestry Act 1998 (Act 84 of 1998) protects trees from harm and damage and a permit from the Department of Agriculture, Fisheries and Forestry is required to remove, cut or destroy protected trees. The trees listed in (Table 1), occur within the study area and are classified as protected in the act. During the field investigations, care had to be taken not to cause any damage to these particular trees. Two examples of protected trees occurring in the study area are shown in (Figure 11 and Figure 12).

Table 1: Protected plant species within the study area

Species	Conservation status	Local distribution
Acacia erioloba	Protected	Widespread on sandy areas.
Acacia haematoxylon	Protected	Sandy & limestone areas

Figure 11: Acacia Erioloba (Anderson, 2011)

Figure 12: Acacia Haemotoxylon (Anderson, 2011)

Apart from the protected trees, the study area is covered with natural grass and shrubs. According to Mucina and Rutherford (2006), the Savanna Biome is the largest Biome in Southern Africa, occupying 46% of its area and over one-third the area of South Africa. The Savanna Biome is well developed in the Kalahari Basin as shown in (Figure 13). The red block indicates the study area.

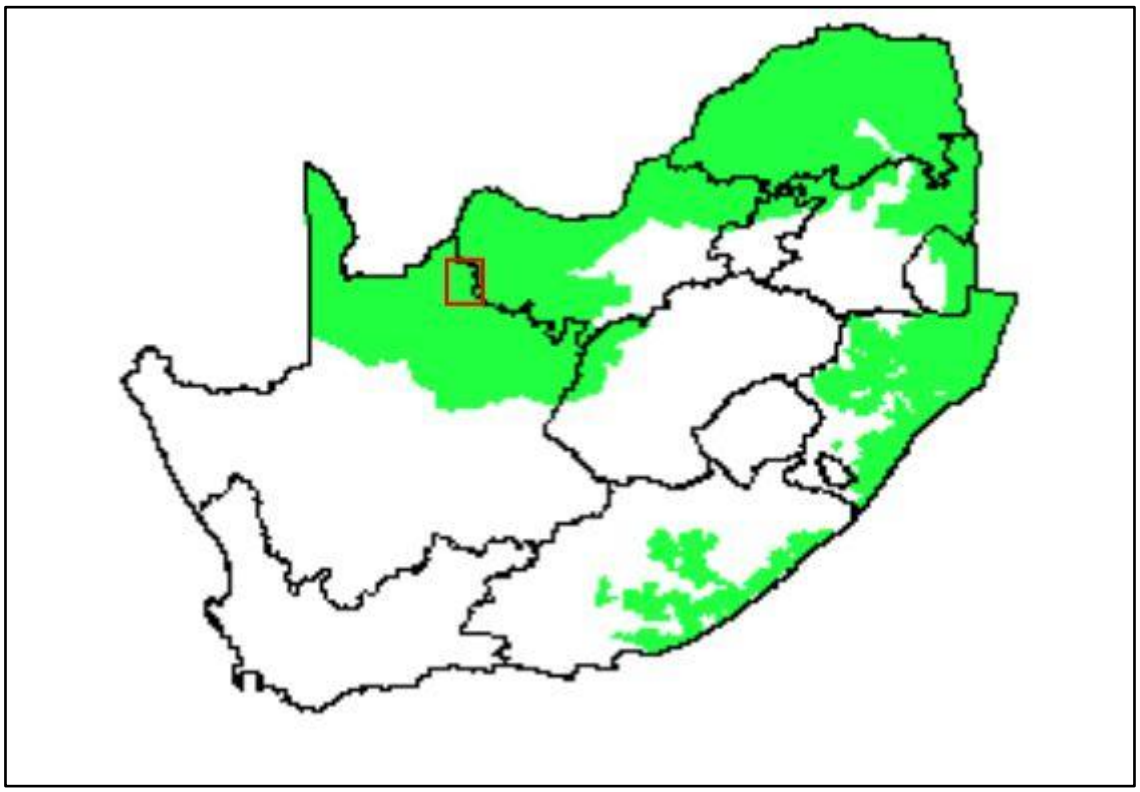

Figure 13: Distribution of Savanna Biome in South Africa (Google images, 2014)

3.5 GEOLOGICAL SETTING

3.5.1 **Regional geology**

The study area is underlain by geological units of the Transvaal Supergroup which is subdivided into two sub basins namely; the Griqualand West Basin and the Transvaal Basin (Figure 14). For this study the focus will be on the Griqualand West Basin. These geological sequences host glacial deposits and are associated with major iron and manganese deposits that are apparently related to the extreme climatic variations that occurred between 2 500 and 2 200 Ma Kirschvink *et al.* (2000).

The Griqualand West Basin consists of two major units, the Ghaap Group and Postmansburg Groups (van Niekerk, 1998).The Ghaap Group comprises of the Schmidtsdrif, Campbellrand, Asbestos Hills and Koegas Subgroups (Figure 14). The stratigraphy of the Griqualand West Basin is shown in (Figure 15).

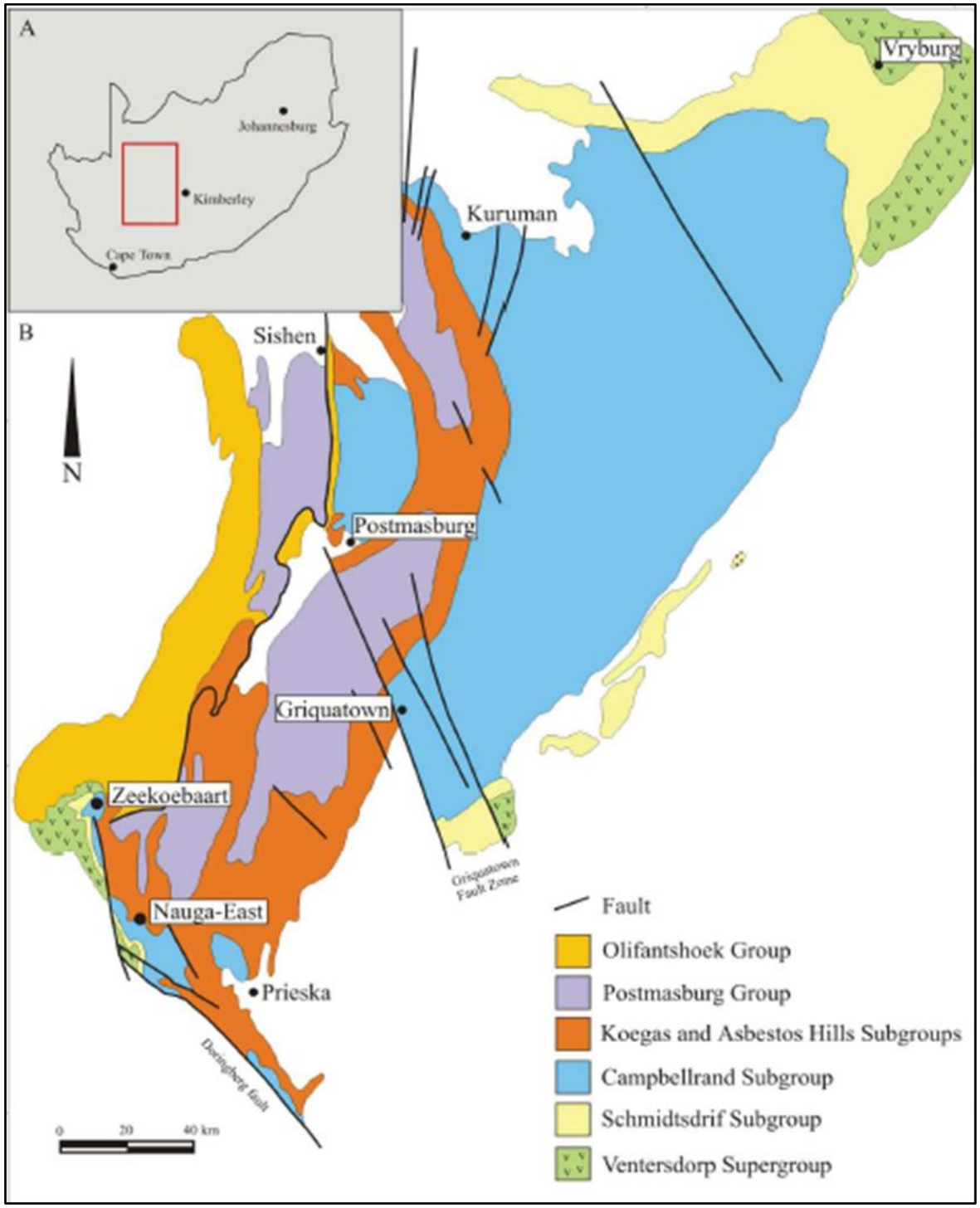

Figure 14: Geological map of the Transvaal Supergroup in the Griqualand West Basin (Harding, 2004)

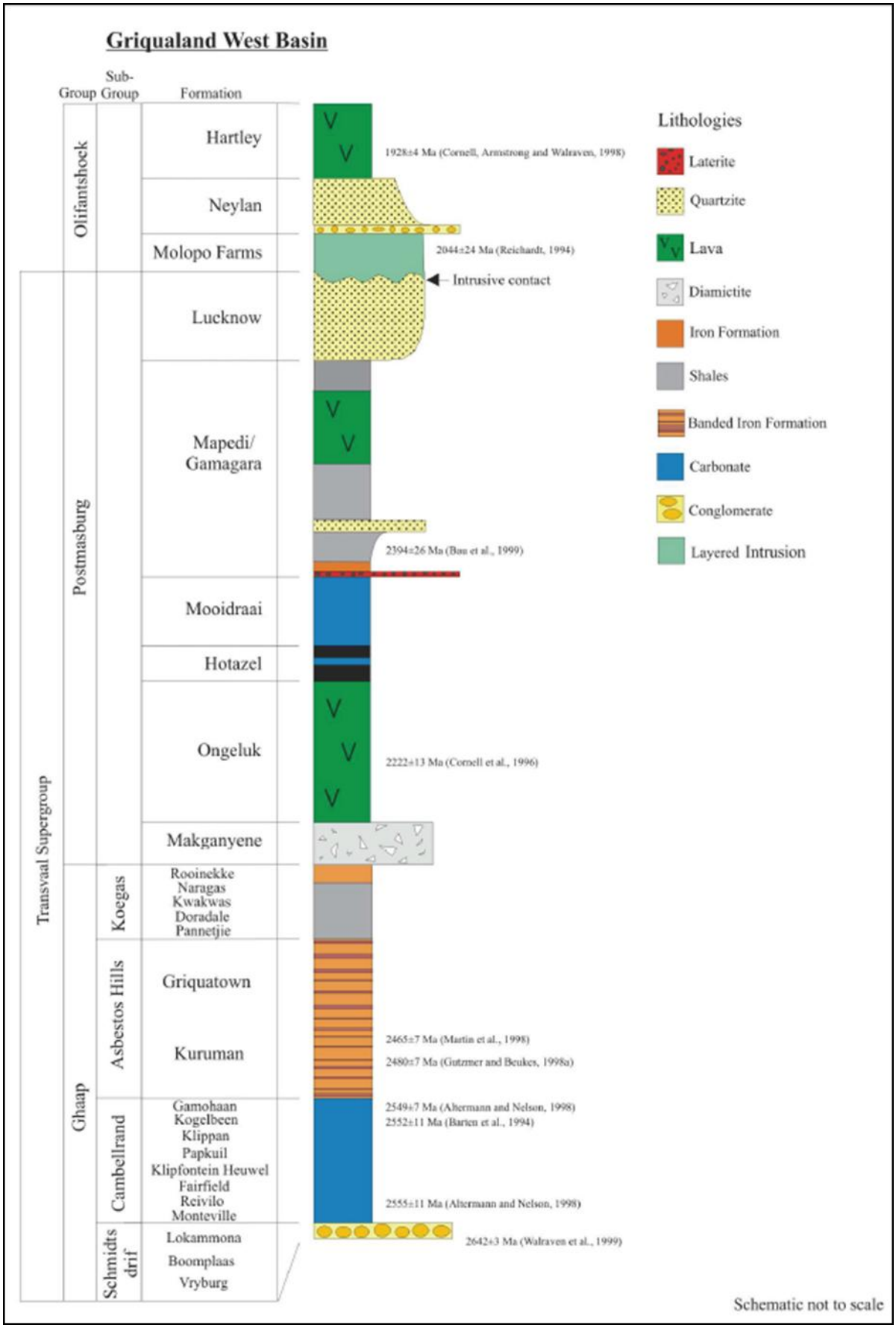

Figure 15: Stratigraphy of the Transvaal Supergroup in Griqualand West Basin (Harding, 2004, adopted from Dorlan, 1999)

3.5.2 **Local geology**

The study area lies within the Ghaap Group and as mentioned in Section 3.5.1, the Ghaap Group comprises three subgroups. The subgroups are described below:

3.5.2.1 The Schmidtsdrif Subgroup

The Schmidtsdrif Subgroup (refer to Figure 15), is divided into three formations namely the Vryburg, Boomplaas, Lokammona Formations. The Vryburg Formation consists of feldspathicarenites, quartz arenites, quartz wackes, argillites, carbonate rocks and lavas while the Boomplaas Formation consists of carbonate rocks and argillites. The Lokammona Formation consists of tuffaceous lagoonal siltstone, shale, oolitic carbonate, stromatolite reef deposits and carbonaceous shale (Beukes, 1983).

3.5.2.2 The Campbellrand Subgroup

The Campbellrand Subgroup (refer to Figure 15), carbonate sequence consists of two major lithofacies of the Ghaap Plateau and Prieska Carbonates. The Ghaap Plateau has a stromalitic carbonate platform while the Prieska Carbonates has clastic algal laminated ferruginous carbonates with carbonaceous shale, banded with ferruginous chert. The platform facies consist of the basal Monteville Formation, followed by the Reivilo, Fairfield, Klipfontein Hills, Papkuil, Klippan, Kogelbeen and Gamahaan Formations. The formations extend laterally into the basinal facies consisting of the Nauga and Naragas Formations (Beukes, 1980, 1983, 1987).

3.5.2.3 Asbestos Hill Subgroup

The Asbestos Hill Subgroup (refer to Figure 15), is a transition from carbonate to BIF-deposition to a major marine transgression and associated to a sea level rise. The clastic-textured basinal facies carbonate rocks of the Campbellrand Subgroup are conformably overlain by carbonaceous Klein-Naute shale (Nauga Formation) and two iron formations of the Asbestos Hills Subgroup namely, the Kuruman and Griquatown Iron Formation (Beukes, 1983).

Kuruman Banded Iron Formation (BIF)

The base of the Kuruman Iron formation hosts the Zeekoebaart and Nauga East high grade iron ore deposits. According to Beukes (1983), the deposition of the Kuruman Iron formation was an open shelf paleoenvironment and the ankerite-banded cherts form the basal unit of the formation. Furthermore the formation consists of chert meso bands alternating with ankeritic or ferruginous dolomitic intramicritemeso bands.

Griquatown BIF

The Griquatown Iron Formation conformably overlies the Kuruman Iron Formation and was deposited in shallow water, storm dominated inland sea. The Griqualand Iron Formation consists of rich banded siderite lutite followed by siderite grainstones and disclutites. The siderite lutites belong to the Danielskuil Member and are considered to be of anabiogenic origin while the chert and magnetite are of diagenetic origin (Beukes, 1984).

3.5.2.4 Koegas Subgroup

The Koegas Subgroup (refer to Figure 14), consists of iron formations similar to the Kuruman and Griquatown Iron Formation but the main difference is that the Koegas Subgroup has a much lower rate of iron formation deposition. The subgroup is underlain by the Pannetjie, Doradale, Kwakwas, Naragas and the Rooinekke Formations (Beukes, 1983).

3.5.2.5 Faults and dykes

The units that were targeted during the investigation were areas that had major faults, dykes as well as the Ghaap Plateau dolomites. The reason for targeting these structures is the fact that they could potentially act as a flow paths or traps for groundwater. The 1:250 000 geological map of the study area (Figure 16) indicates the presence of two major faults within the study area. In the western parts, a fault with an approximate south/north strike extends across almost the entire width of the study area. This fault is known as the Western Fault. Farther to the east, a major fault has been mapped along the contact with the banded iron-formations of the Ghaap Group. This fault, known as the Eastern Fault, also has an approximate south/north strike, although it veers off to the north-west along the northern parts of the study area.

Numerous dykes are known to occur within the study area. These dykes predominantly have south-west/north-east strikes, running parallel to the major linear magnetic anomalies observed in the airborne magnetic map (to be discussed in Section 3.6).

3.6 REGIONAL MAGNETIC SETTING

The total magnetic field intensity recorded across the survey area during an airborne survey conducted by the Council for Geo science shown in (Figure 16). The different magnetic highs and lows are identified by the different colour shades in the survey area. In the eastern part of (Figure 17) are cross cutting yellowish lineaments with an approximate south/west to north/east strike due to the dykes known to occur in that part of the survey area.

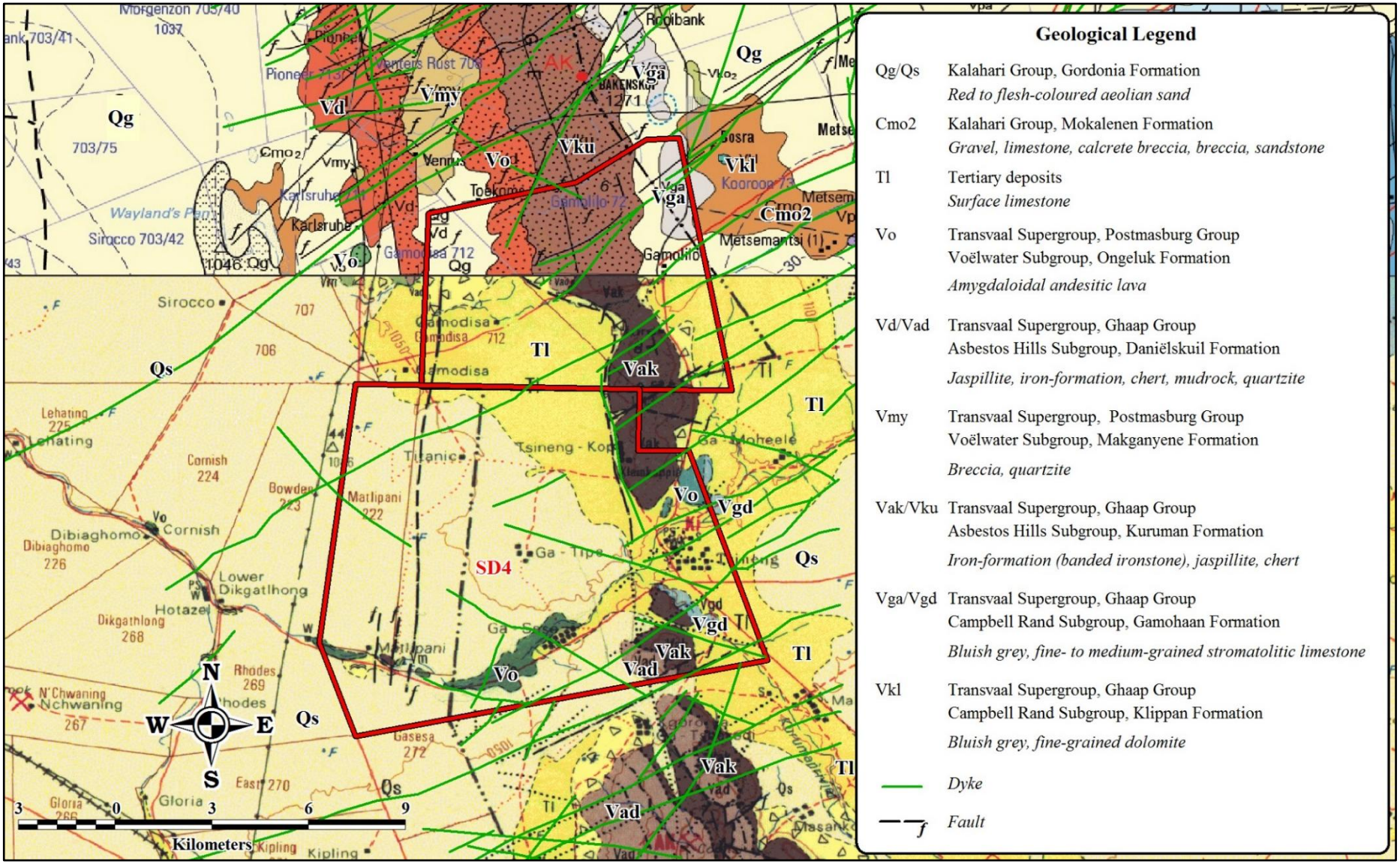

Figure 16: Geological setting of the study area as indicated in the 1:250 000 geology map

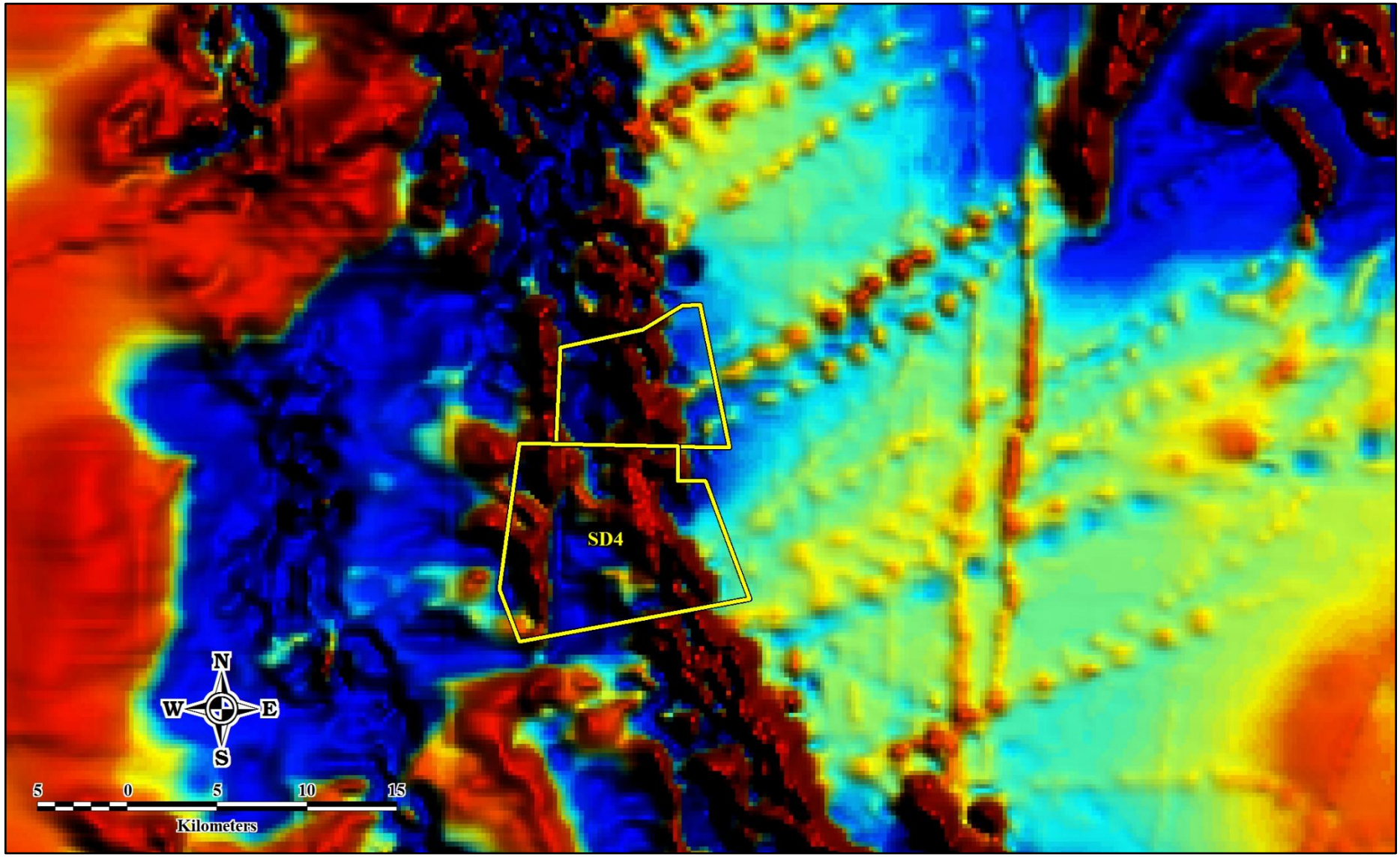

Figure 17: Regional magnetic setting of the study area

3.7 GEOHYDROLOGY

3.7.1 Introduction

The success in evaluating the potential of an aquifer depends on various factors and what is of prime importance is the quantity and quality of the available geohydrological information on the aquifers in the area of interest. It was crucial to ensure that adequate information was obtained for the current investigation.

3.7.2 Groundwater occurrence

The hydrogeological map (Figure 18) shows that the unconsolidated rock hosts intergranular aquifers with limited yields due to the fine and clayey material. However, higher yielding aquifers are no exception in these areas. Fractured aquifers can be present in most rock types with faulting and dolerite intrusions being the major contributors to fracturing (van Dyk *et al*, 2008).

Karst aquifers in calcareous rocks on the Ghaap Plateau can yield large volumes of water and of good quality. Most of the rocks host a combination of intergranular and fractured aquifers. The aquifers are dependent on precipitation for recharge, but other factors such as soil cover and vegetation contribute to the effective recharge of the aquifers (van Dyk *et al*, 2008).

The study area highlighted by the red block (Figure 18) consists of intergranular, karst and fractured aquifers. The map also depicts the groundwater occurrences as well as the median borehole yields, which range between 0.1 *l*/s and 2 *l*/s. However, this does not mean that higher yields do not occur in the study area.

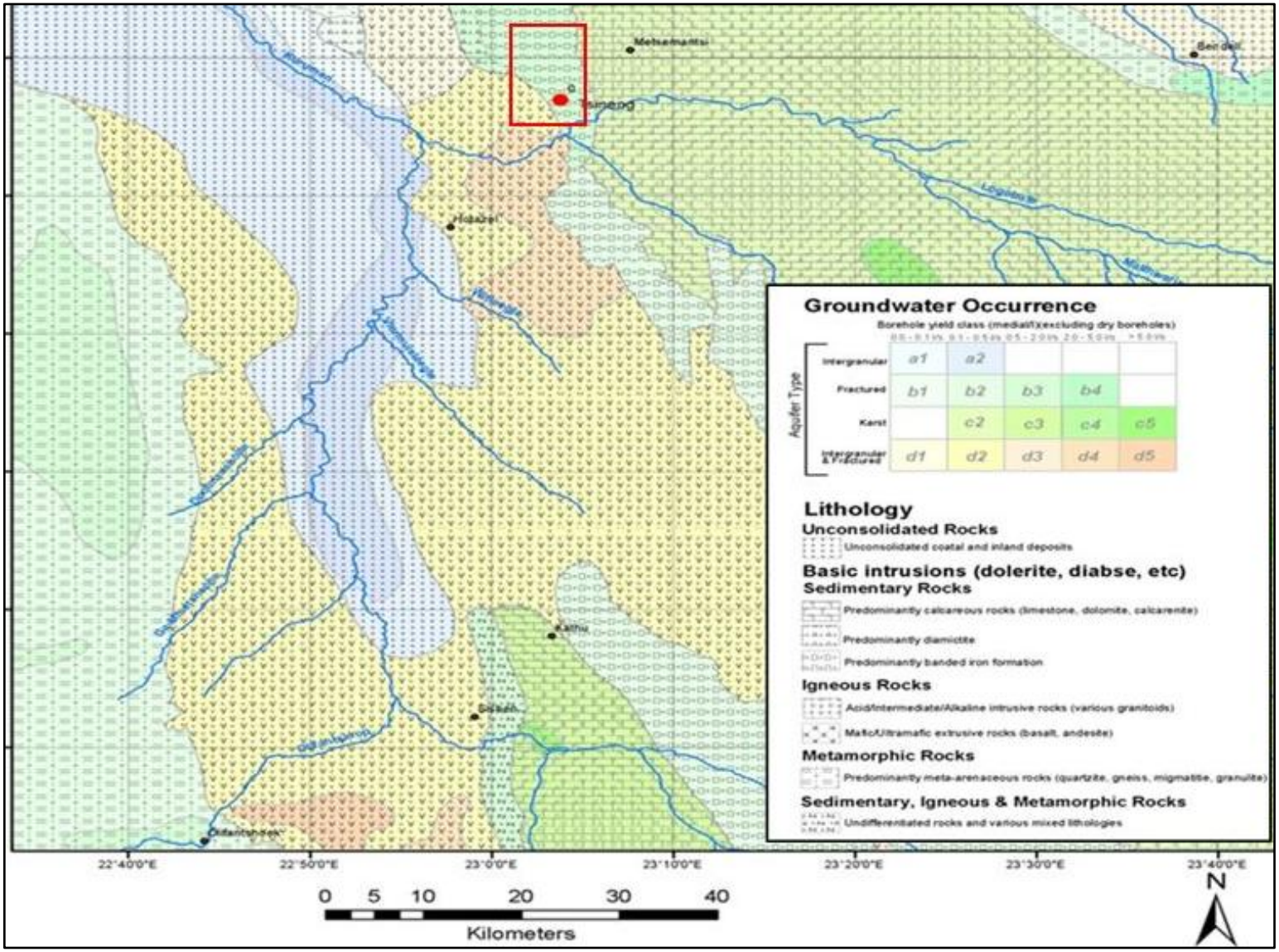

Figure 18: Map showing the distribution of aquifer type and median borehole yield

3.7.3 **Groundwater recharge**

Groundwater recharge represents the portion of rainfall that reaches an aquifer irrespective of whether it follows a preferential flow path through fractures, soil or infiltration from free water in river channels or local surface depression (Lloyd, 1986).

According to Lerner (1990), recharge can occur in a number of ways:

- Direct recharge – water added to the groundwater reservoir in excess of soil moisture deficits and evapotranspiration, by direct vertical percolation through the unsaturated zone.
- Localized recharge – an intermediate form of groundwater recharge resulting from the horizontal (near) surface concentration of water in the absence of well-defined channels.
- Indirect recharge – percolation to the water table through the beds of a surface water course.

Groundwater recharge is dependent on rainfall and a measure of the rainfall that is available for recharge is provided by mean effective rainfall. The effective rainfall is that part of the daily rainfall that seeps into the ground after allowing for losses through interception by vegetation and by storm runoff (Vegter, 1995). Based on the recharge map (Figure 19) compiled by Vegter, the recharge in the study area is estimated at 1-5 mm/a.

Vegter's recharge estimates (Figure 19) are used as a provisional indication of the mean annual groundwater recharge and it might be an overestimate. It must be noted that the lower the rainfall, the more variable and uncertain are the estimates. The estimated recharge values from Vegter's map can be used as a qualified guess and supplemented by other recharge calculation methods (Monokofala, 2013).

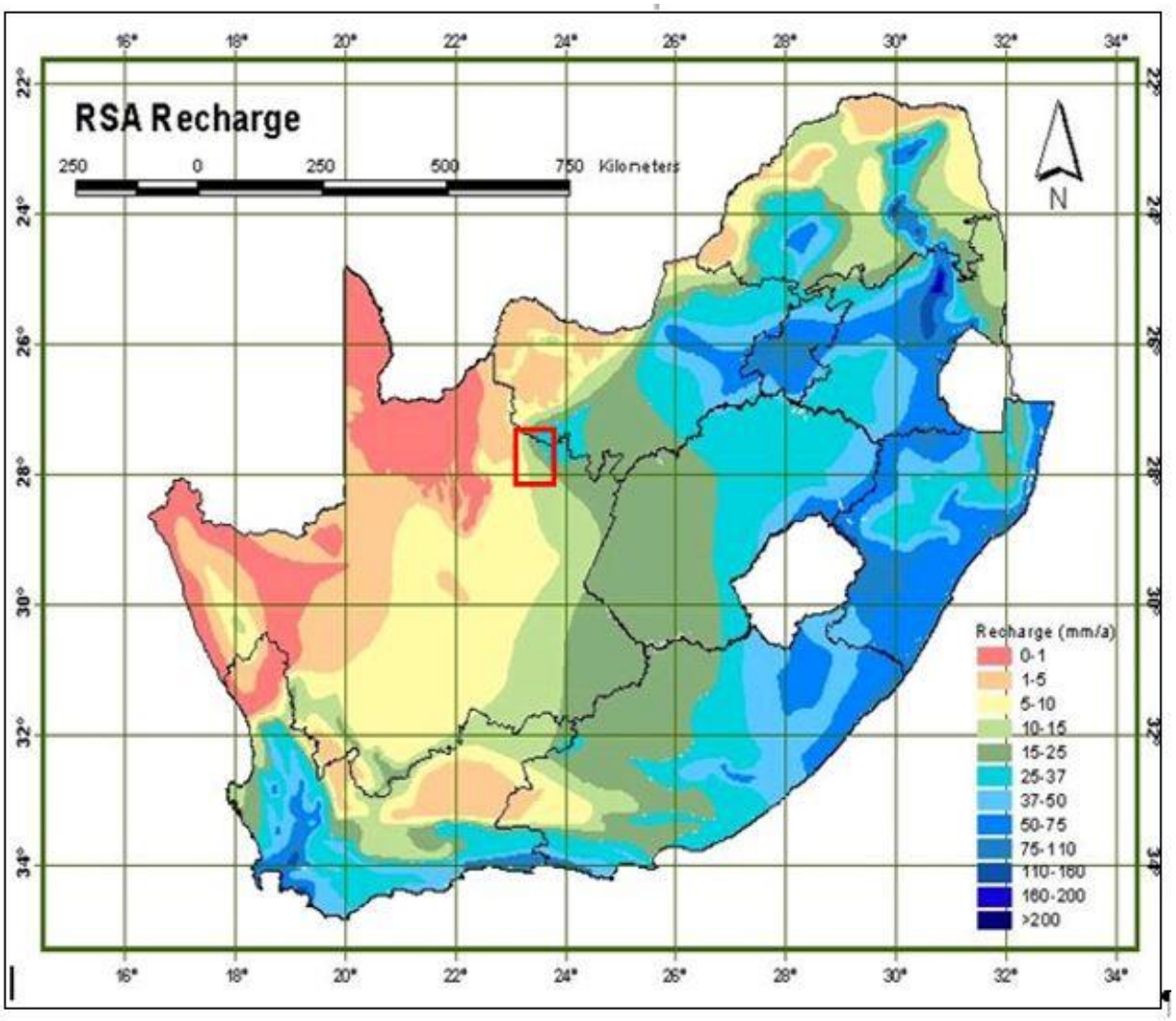

Figure 19: Vegter's recharge map (Vegter, 1995)

The aquifer recharge estimation method used in the study was the Chloride Mass-Balance Method. The average percentage of the rainfall recharged to the groundwater system, can be derived from the ratio of the chloride concentration in the rainfall relative to that of groundwater Bredenkamp *et al.* (1995).

A specific requirement is that no chloride was added by dissolution of aquifer material, from salts contained within the aquifer matrix, or has entered the aquifer via pollution. It is further required that no evaporation of groundwater occurs up-gradient from the groundwater sampling point, and that adsorption of chloride in soils and the vegetation uptake is considered negligible. The chloride concentration should only result from the natural, hydrological, and evaporative processes. The estimated recharge percentage (RE%) can be calculated from:

$$RE\% = \frac{Cl_r}{Cl_{gw}} \times 100 \qquad \text{eq.3}$$

Where Clr is the concentration of chloride in the rainwater (mg/L) and Clgw is the concentration of chloride in the groundwater (mg/L).

The chloride concentration information which was used was adopted from previous investigations in the Kgalagadi area conducted by (Wiegmans, 2006). The recharge estimates using the chloride mass-balance method are summarised in (Table 2). The entire catchment in which the study area occurs was delineated into Groundwater Management Units (GMUs) as shown in (Figure 20). The recharge within the groundwater management units D41L-K10 was used to quantify the available water resources and to calculate the water balance.

Data from four rainfall stations namely: Dippenaarshoop, Wonderwork, Mothibastad and Tsineng in the D41L catchment were combined with six delineated median recharge zones (Table 3) to create a spatial distribution of recharge estimates zones in the study area (Figure 21)

The recharge zones shown in (Table 3) indicate which recharge zones are low to high in recharge value in comparison to some of the surrounding towns/villages near the study area. A relationship between rainfall and recharge can be observed in some of the areas. In the areas where higher rainfall was received, a higher recharge zone was recorded.

The spatial distributed recharge zones that are shown in (Figure 21) were adopted from the Spring program which is a modelling program that uses finite-element approximations to solve groundwater flow equations and other functions. The study area falls within recharge zone 1 and 2. The recharge zone 2 is a high recharge zone which is ideal, because high recharge zones are associated with good water resource potential.

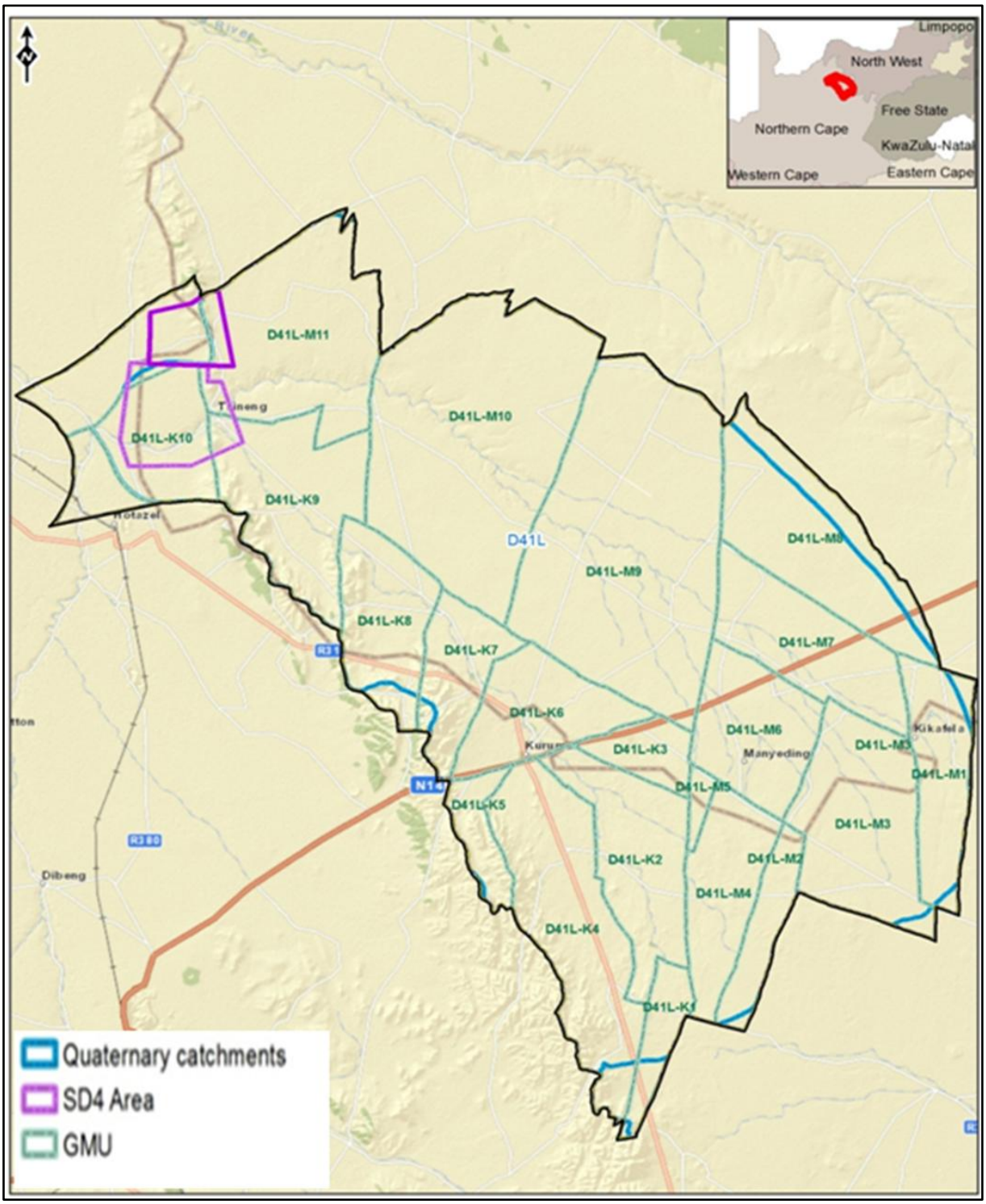

Figure 20: Groundwater Managements Units within quaternary sub catchments D41L (Golder, 2014)

Table 2: GMU recharge estimates (Golder, 2014)

Quaternary catchment area	Groundwater management unit			Effective recharge from rainfall			
	GMU number	Area (km^2)	Name	Mean (Mm^3/a)	Mean (mm/a)	Median (Mm^3/a)	Median (mm/a)
D41L-K: Upper Kuruman River Groundwater Management Area (GMA)							
D41L	D41L-K1	75	Grootkono	1.92	25.7	1.01	13.6
D41L	D41L-K2	238	Kuruman B eye	6.48	27.2	3.47	14.6
D41L	D41L-K3	88	West Derby	2.18	24.8	1.14	12.9
D41L	D41L-K4	368	Kuruman A eye	18.08	49.1	10.84	29.4
D41L	D41L-K5	65	Kuruman Hills	5.15	79	3.25	49.8
D41L	D41L-K6	188	Mothibistad	4.68	24.9	2.45	13
D41L	D41L-K7	141	Batlharos	3.79	23.8	2.02	14.3
D41L	D41L-K8	187	Gamopedi	2.7	14.5	1.13	6.1
D41L	D41L-K9	233	Maipeng	1.85	8	0.47	2
D41L	D41L-K10	174	Gasese	0.82	4.7	0.15	0.9
TOTAL	**10**			**47.65**	-	**25.92**	-
D41L-M: Matlhwaring River Groundwater Management Area (GMA)							
D41L	D41L-M1	96	Kikahela	2.36	24.4	1.22	12.7
D41L	D41L-M2	310	Botheteletsa	7.72	24.9	4.03	13
D41L	D41L-M3	117	Manyeding C	3.07	26.2	1.63	13.9
D41L	D41L-M4	182	Manyeding B	5.11	28.1	2.76	15.2
D41L	D41L-M5	20	Manyending A	0.72	36.3	0.41	20.8
D41L	D41L-M6	209	Manyending L	3.12	15	1.3	6.2
D41L	D41L-M7	297	Metswetsaneng	5.71	19.2	2.72	9.1
D41L	D41L-M8	215	Logobate	2.23	10.4	0.72	3.4
D41L	D41L-M9	268	Gasehunelo	0.79	2.9	0.15	0.6
D41L	D41L-M10	545	Churchill	3.18	5.8	0.71	1.3
D41L	D41L-M11	1216	Tsineng	3.75	3.1	0.75	0.6
Total	**11**			**37.75**		**16.41**	

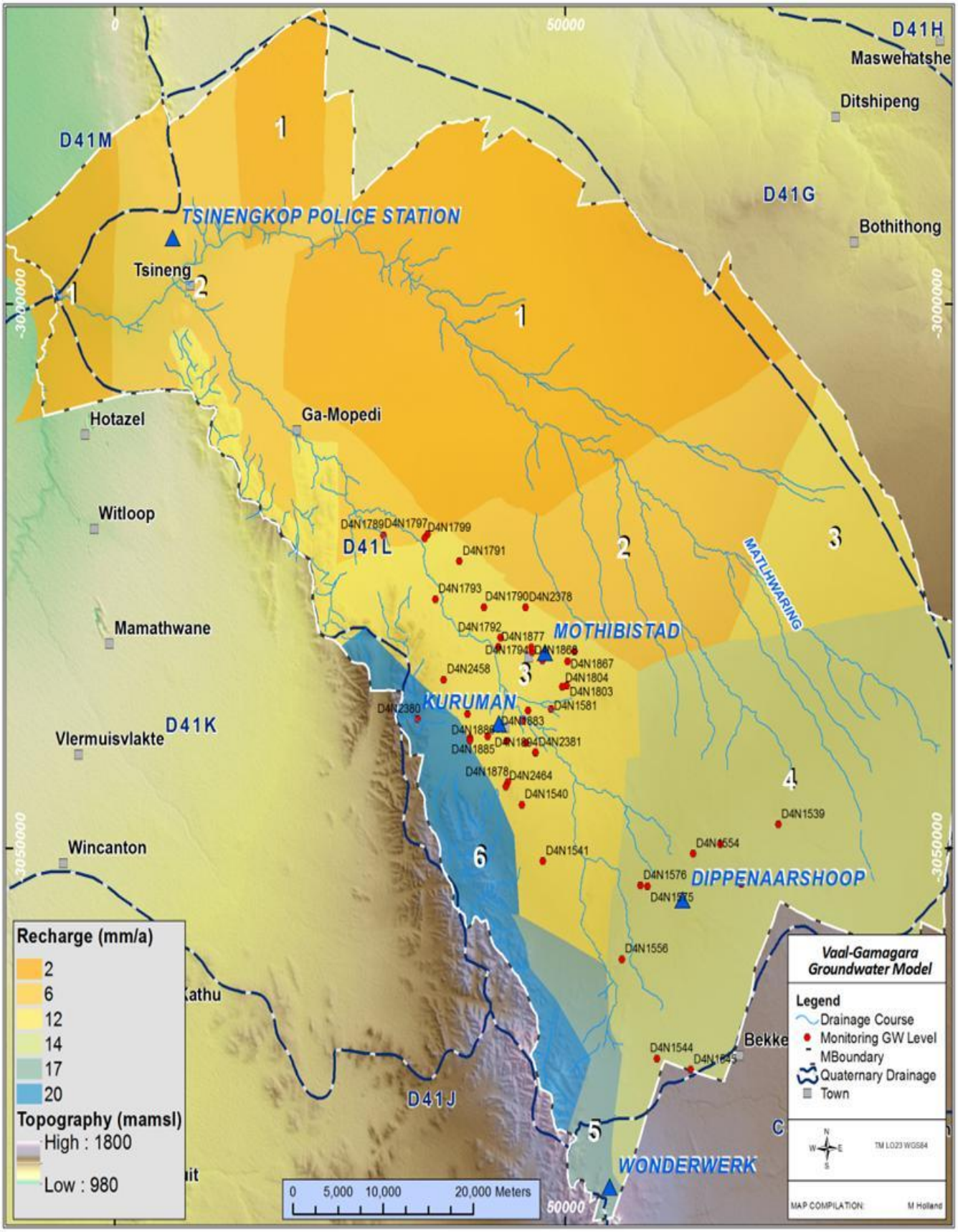

Figure 21: Spatial distribution of recharge zone (Golder, 2014)

Table 3: Median recharge values (Golder, 2014)

Rainfall Station	Recharge Zone	Mean Annual Precipitation(mm)	Groundwater recharge			
			Mean	Median	30 Percentile	70 Percentile
Tsineng kop Low Recharge	1	302	4	2.5	1.9	4.4
Tsineng kop High recharge	2		9	6	4.2	10
Mothibastad	3	300	29	11	6.5	28
Dippenaarshoop	4	460	26	14	10.5	21
Wonderwerk Low recharge	5	490	48	16	11.2	25
Wonderwerk High recharge	6		55	20	15	29

3.7.4 Aquifer classification

The classification of the aquifer systems was done based on a report to the Water Research Commission (WRC) entitled: A South African System Management Classification (Parsons, 1995). The aquifer classification management systems are define as follows:

- Sole source aquifer system: An aquifer that is used to supply 50% or more of domestic water for a given area, and for which there are no reasonable alternative sources should the aquifer become depleted or impacted upon. Aquifer yields and natural water quality are immaterial;
- Major aquifer system: Highly permeable formations, usually with a known or probable presence of significant fracturing. They may be highly productive and able to support large abstractions for public supply and other purposes. Water quality is generally very good;
- Minor aquifer system: These can be fractured or potentially fractured rocks that do not have a high primary permeability, or other formations of variable permeability. Aquifer extent may be limited and water quality variable. Although these aquifer seldom produce large quantities of water, they are both important for local supplies and in supplying base flow for rivers;

- Poor aquifer system: These are formations with negligible permeability that are generally regarded as not containing groundwater in exploitable quantities. Water quality may also be such that it renders the aquifer unusable.

However, groundwater flow through such rocks does occur, although imperceptible, and needs to be considered when assessing risk associated with persistent pollutants;

- Special aquifer system: An aquifer designated as such by the Minister of Water Affairs, after due process.

In (Table 4) the aquifers that occur within the study area are classified according to the above classification system.

Table 4: Aquifer classification of study area

Banded Ironstone and Dolomite (Fractured and weathered)	Major
Dolomite (Karts and fractured)	Major
Lava (Inter granular and fractured)	Minor

3.7.5 Groundwater resource

The groundwater resource can be defined as all the groundwater available for beneficial use, including for human use, aquatic ecosystems and the greater environment. The aquifer should have the potential to supply water at a rate equal to the long-term mean recharge of the aquifer for a sufficient period.

According to Stuickmeier (1989) the groundwater resource potential encompasses the following concepts:

- Accessibility – aquifer depth and drilling risk
- Exploitability – yield and pumping height
- Availability – resource and recharge
- Suitability – chemistry and risk of pollution
- Conservation – size and hydro-dynamic situation

The harvest potential is the maximum volume of groundwater that may be abstracted per square kilometre per annum without depleting the aquifers (Parsons, 1999). The harvest potential is determined from two parameters, namely: groundwater recharge and groundwater storage.

The harvest potential map of the quaternary sub catchments D41L and D41M can be viewed in (Figure 22). From the harvest potential map, the sub catchment D41M has a harvest potential ranging between 2 500 and 4 000 m^3/km^2/annum. The sub catchment D41L has a harvest potential ranging between 15 000 and 25 000 m^3/km^2/annum.

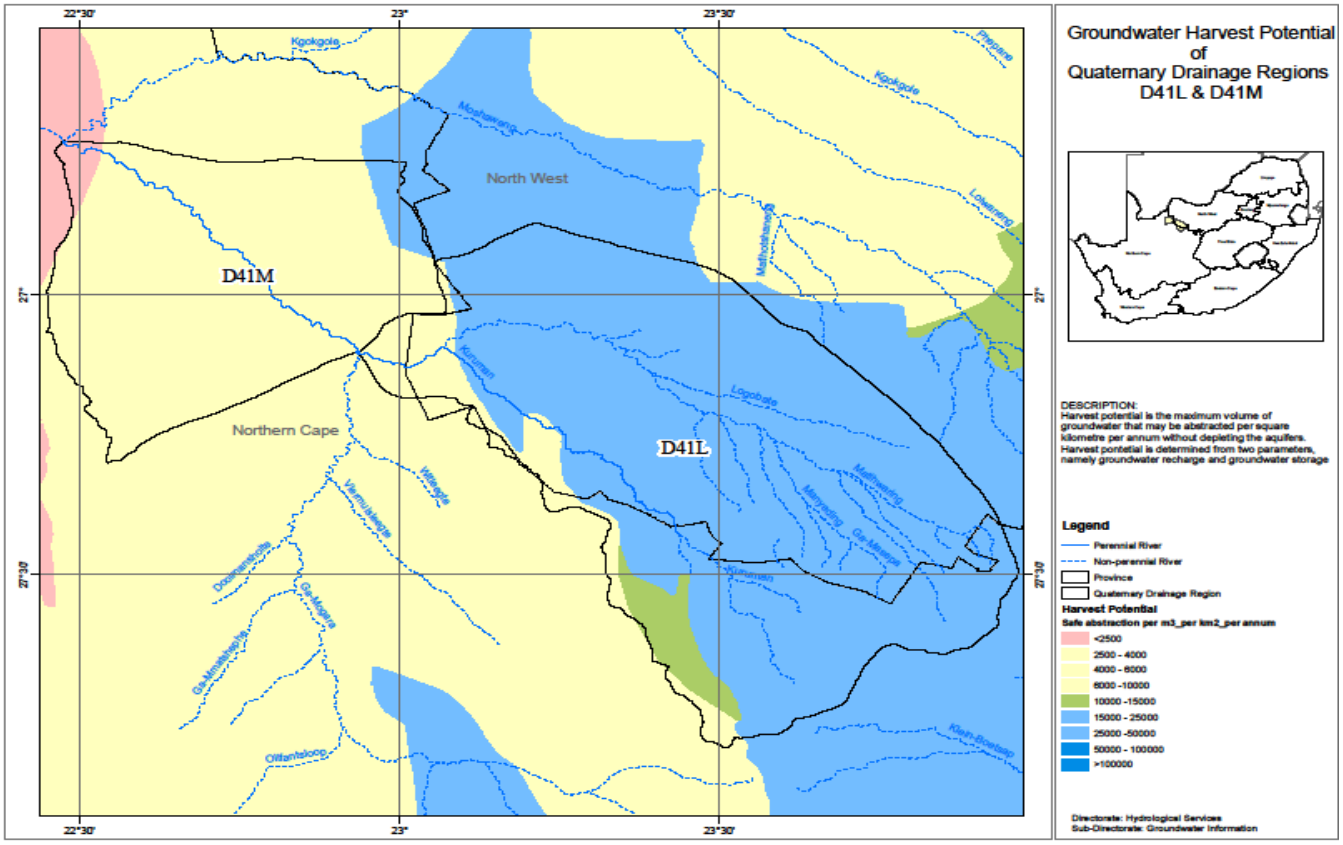

Figure 22: Harvest potential map (DWA-Geo info, 2013)

3.7.6 **Hydrocensus**

During the hydrocensus the static water levels in the boreholes within and around SD4 were measured. In the year 2011 and 2012 Golder Associates conducted a hydrocensus focusing on three farms, namely: Tsineng, Titanic, Gamodisa and Gamolelo. The hydrocensus was also extended to the surrounding communities of Gasese and Gatshekedi. Verification of government, private and trustee owned boreholes was done as part of the process. Existing borehole information from the NGA and the Golder database in the study area is summarised in (Table 5), while the positions of the identified boreholes are shown in (Figure 23).

Recorded borehole data shows that the borehole depth varies between 19 and 151 metres below ground level (mbgl) depending on where the borehole was sited.

It is observed that shallow boreholes are mostly found on the eastern part of the study area which is underlain by dolomites and banded iron formations. Deeper boreholes are found towards the western part which is covered by thick Kalahari sediments and unlined by lava.

The static water levels in the Tsineng locality are highly variable ranging from 8 mbgl and 30 mbgl. The village of Gatshekedi have deep water levels varying from 15 mbgl to 52 mbgl, while the village of Gamolele have shallow water levels that are less than 10 mbgl.

The electrical conductivity (EC) values are ranging between 57 mS/m to 150 mS/m, which suggests that the water is of an ideal quality for drinking water purposes and is unlikely to require extensive treatment before drinking it. According to the South African National Standard SANS (241-2011) water that contains < 170 mS/m is acceptable for human consumption.

Table 5: Summarized information on existing boreholes

Locality	Borehole number	Latitude	Longitude	Borehole depth (m)	Static water level (mbgl)	Reported yield (L/s)	Electrical conductivity (mS/m)
Gasese	13-86228	-27.11677	23.05714	74	11.5	0.3	108
Gatshekedi	13-86646	-27.13494	23.1100	63	52	2.8	61
Tsineng K	13-86744	-27.06962	23.06202	120	30.16	1	105
Gatshekedi	13-86781	-27.14523	23.07515	57	40.64	3.5	64
Tsineng K	13-8672	-27.13131	23.09088	75	12.03	0.5	105
Tsineng	13-87012	-27.07810	23.07861	-	-	-	93
Tsineng	13-87084A	-27.09764	23.07720	41	24.01	6	89
Gasese	13-87101	-27.12647	23.05245	134	15.21	-	120
Gasese	13-87102	-27.13101	23.03967	120	19.25	-	100
Gamolelo	13-87105	-27.07494	23.11104	121	0.5	-	64
Gasese	13-87113	-27.09532	23.06689	50	3.04	-	95
Gasese	13-87114	-27.09701	23.06995	39	-	-	150
Gatshekedi	13-87118	-27.13239	23.07314	73	15.65	8	57
Gamolelo	13-87253	-27.07361	23.10789	78	0.76	2	69
Tsineng	13-87484	-27.08755	23.07718	33	8.63	-	82
Tsineng K	13-87529	-27.05000	23.06063	54	32.5	3	99
Tsineng K	13-87529A	-27.04989	23.06028	64	-	-	107
Gamodisa	GA4	-27.00853	22.99171	60	15.1	0.3	73
Gamodisa	GA9	-26.99623	23.00041	63	24.28	2	75
Gamodisa	SD4GAA014	-27.01655	23.02795	-	7.6	-	79
Gamolelo	SD4GAA026	-26.99694	23.07617	19	3.8	1	58
Gamolelo	SD4GAA027	-26.99659	23.07591	28	5.06	3	65
Gamodisa	SD4GAA030	-27.01669	23.02480	151	9.02	0.4	80
Tsineng	13-87085	-27.09494	23.08988	94	11.78	0.8	100
Titanic	SD4GAA015	-27.06043	23.00162	77	34.01	0.3	84
Titanic	SD4GAA017	-27.08271	22.99831	101	37.74	1.5	88
Titanic	SD4-GAA18	-27.05771	23.05142	99	8.5	-	79
Titanic	SD4-GAA10	-27.05800	23.01522	43	9.9	-	82

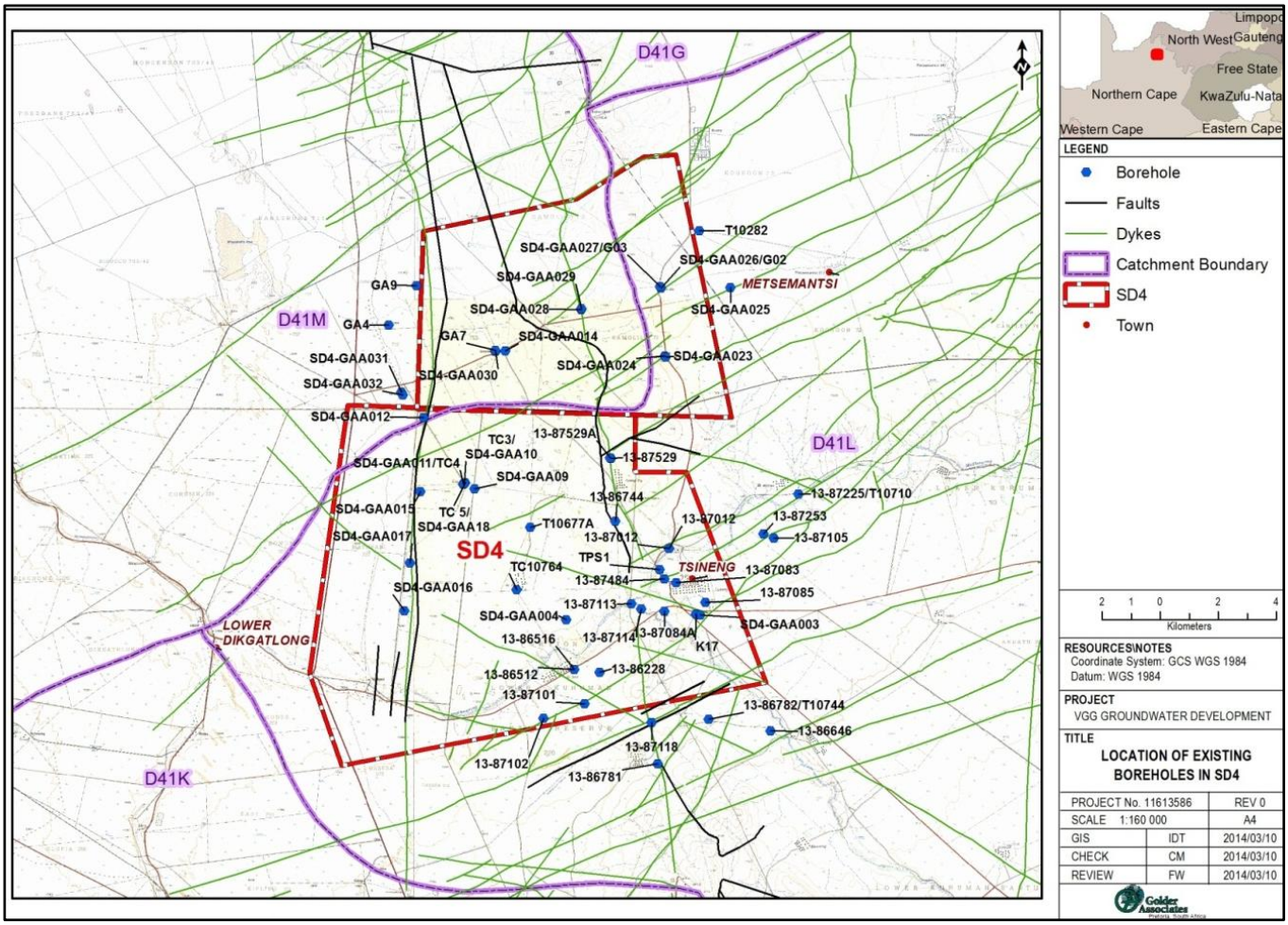

Figure 23: Location of existing boreholes within and near SD4 (Golder, 2014)

3.7.7 Groundwater elevations and flow direction

Knowing the groundwater flow direction is important in groundwater exploration and understanding the flow regime allows you to identify potential groundwater sites to be exploited. Such information can also be used to locate recharge zone. Groundwater piezometric contours shown in (Figure 24) were mapped at 10 m intervals using water level elevation information sourced from previous investigations conducted by (Wiegmans, 2006). Groundwater piezometric levels emulates the surface topography and ranges from 950 to 1 050 mamsl in the study area. The piezometric contour map indicates that the groundwater flow is towards the Kuruman River in the north-west direction.

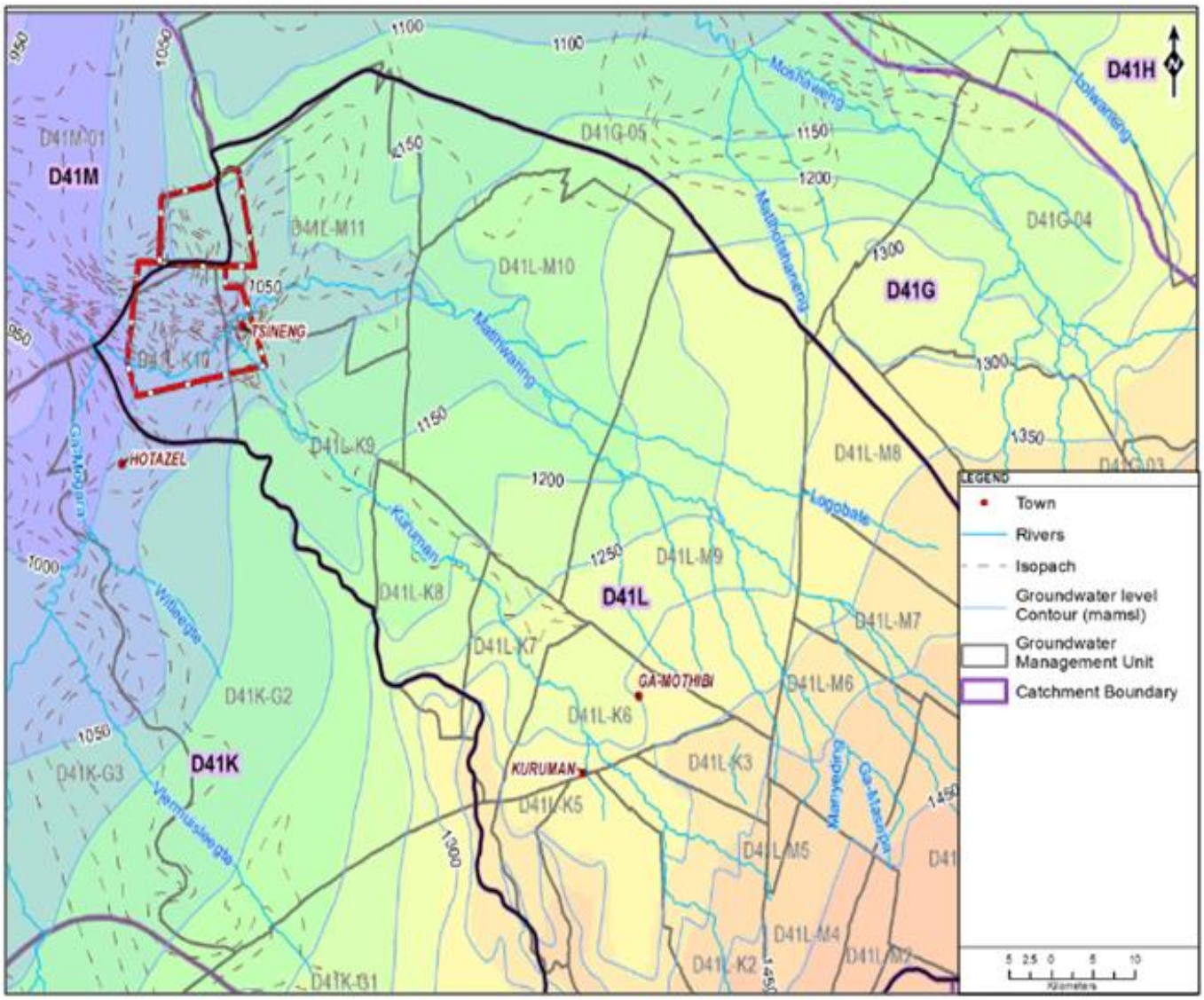

Figure 24: Groundwater piezometric contours of study area (Golder, 2014)

CHAPTER 4:
GEOPHYSICAL TECHNIQUES EMPLOYED DURING THE INVESTIGATIONS

4.1 INTRODUCTION

The application of geophysical techniques in groundwater exploration programmes is common and the choice of the applied method is important to ensure that the aims of the exploration project are achieved. Modern geophysical techniques are now designed to make exploration less complicated and can provide results in a short period of time. However, understanding the fundamental principles of the geophysical techniques is essential; having the background and knowledge on how the technique functions can certainly facilitate and become vital during the geophysical results interpretation.

Geophysical techniques respond to a physical contrast in earth properties such as density, magnetic susceptibility, electrical resistivity, seismic velocity and heat flow/absorption (Stettler, 1979).

Since the study area is covered by Aeolian sand, electromagnetic techniques were appropriate for the groundwater exploration programme. The techniques are not detrimentally affected by the presence of near-surface materials of high resistivity, such as the dry sands that occur in the study area. The area is underlain by iron-rich rocks that are expected to be magnetic. The magnetic method was therefore included in the exploration programme to detect and delineate magnetic structures in the subsurface. Intrusive dykes are also often strongly magnetic so conducting magnetic surveys would be essential to delineate such features.

Faults are generally electrically conductive structures and electromagnetic (EM) techniques were again deemed appropriate for the investigations to detect these structures. Intrusive dykes often consist of minerals with different electrical properties than the surrounding host rock. EM techniques may therefore be successful in detecting and delineating such intrusive structures. Furthermore, dykes are often associated with fractured and weathered zones in the host rock which are also likely to be more conductive than the host rock.

Parts of the study area are underlain by dolomite formations. Thus dissolution cavities in dolomites are often targeted during groundwater exploration programmes due to the fact that these features are associated with very high transmissivities and have generally high borehole yields. Since water is much less dense that dolomite, dissolution cavities are associated with mass deficits in the subsurface. The gravity method is used to measure the gravitational acceleration of the Earth.

A local mass deficit will cause a slight decrease in the gravitational acceleration, which may be detected with the gravity method.

This method was therefore used to investigate the presence of such zones of dissolution in the dolomites that occur within the study area.

The time-domain electromagnetic (TDEM) method is an effective method for determining electrical conductivity of soils at great depths. TDEM is a powerful tool for mapping soils and changes in soil types at different depth ranges. TDEM is useful in mapping sand and gravel aquifers, as well as clayey layers. Considering the fact the study is underlain by Aeolian sand of the Kalahari Basin the technique was invaluable to the investigation.

A two-dimensional (2D) resistivity survey was conducted on profiles located at positions where the results of the other geophysical surveys had indicated possible changes in the subsurface geology. The 2D resistivity method was used to obtain a model of the subsurface resistivity distribution, which was then interpreted in terms of the local geological condition. The resistivity survey also served to verify the findings of the other geophysical techniques.

4.2 GRAVITY METHOD

4.2.1 **Introduction**

The gravity method involves measuring the gravitational attraction exerted by the Earth at a measurement station on the surface. The strength of the gravitational field is directly proportional to the mass and therefore the density of subsurface materials. Gravity anomalies will occur where there is density contrast in the Earth (see Figure 25).

During a gravity survey, the gravitational acceleration is measured at a specific position. The gravitational acceleration is the time rate of change of the speed at which a body falls under the influence of the gravitational force.

Figure 25 shows constant gravity acceleration and when it comes into contact with a geological structure the gravitational acceleration changes.

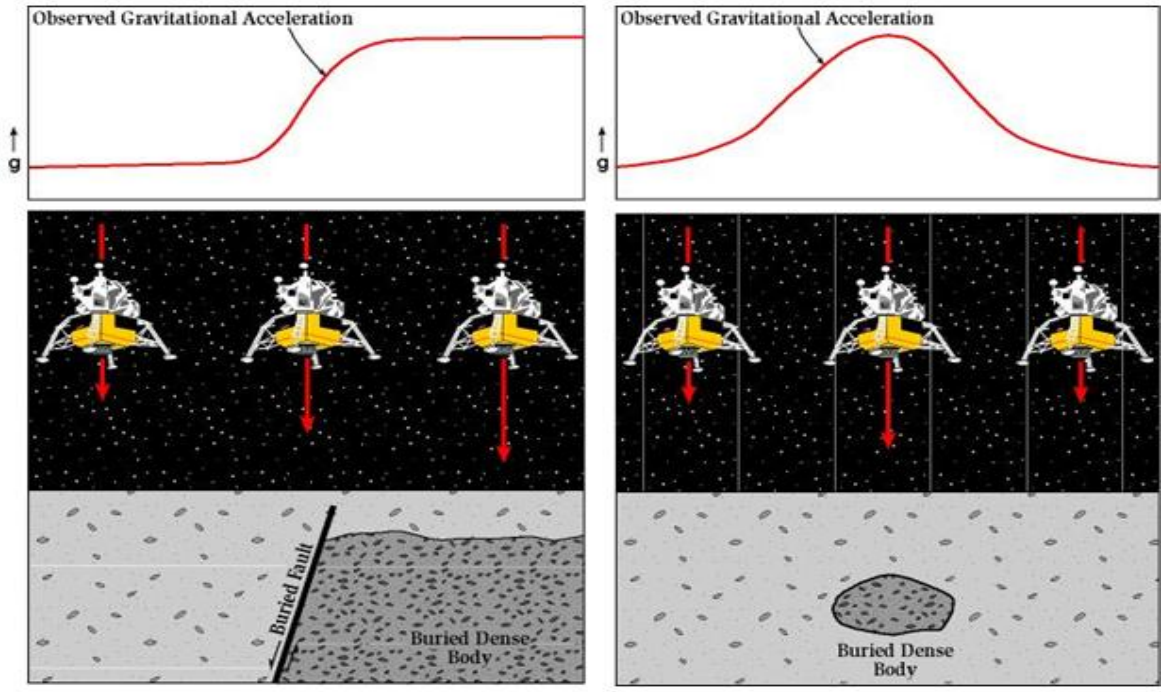

Figure 25: Illustrations showing the relative surface variation of Earth's gravitational acceleration over geologic structures (geoinfo.nmt.edu/geoscience/projects/astronauts/gravitymethod.html)

The gravity method is used as a reconnaissance tool in groundwater, oil and gas exploration. It is used to associate variations in the gravitational acceleration with the differences in the distribution of mass densities.

4.2.2 Basic principle

The basis of the gravity method depends on two laws by Sir Isaac Newton, namely: the Universal Law of Gravitation and the Law of Motion. The first law states:

- The force of attraction between two bodies of known masses is directly proportional to the masses of the objects and inversely proportional to the square of the distance between their centres of mass.

The above law may be expressed mathematically as:

$$F = \frac{Gm_1m_2}{r^2} \qquad \text{eq 4}$$

Where:

F = the attractive force between the bodies (N)

G= gravitational constant (6.67×10^{-11} N m^2 kg^{-2})

m_1= mass of body 1 (earth)

m_2= mass of body 2 (falling body)

r= distance between centres of mass of the two bodies

The second law states:

The force acting on an object is equal to the mass of the object (m) multiplied by the acceleration it experiences. If the Earth exerts and attractive force on an object, the acceleration that the object experiences is known as the gravitational acceleration (g):

$$F = m\ x\ g \qquad \text{eq 5}$$

4.2.3 Gravity reduction

The gravitational acceleration at a particular position on the Earth's surface is affected by a number of factors, namely: 1) Earth tides, 2) instrument drift, 3) the latitude of the measurement position, 4) the elevation of the measurement position, 5) topographic variations (hills, valleys) in the vicinity of the measurement position, and 6) local variations in the mass densities of the subsurface earth materials. The purpose of gravity reduction is to remove the influences of the first five of these factors, so that only the effects due to local density variations remain (Reynolds, 1997). After removal of these influences, the remaining data is referred to as the Bouguer anomaly data.

The factors influencing gravity measurements, and the procedures to remove these influences, are briefly described below:

4.2.3.1 Earth tides and instrument drift

The Earth's rotation and the gravitational pull of the sun and moon create tides. Because the moon is much closer to Earth than the sun, the moon exerts a much stronger gravitational pull (http://education.nationalgeographic.org/media/earths-tides/).

Instrument drift refers to changes in the gravity measurements taken at a specific position at different times and occurs due to changes in the elastic properties of the components of the gravimeter giving rise to an apparent change in the gravity at the specific position (Reynold, 1997).

To compensate for the earth tides and instrumental drifting during a survey, repeated measurements at a selected base station should be taken at different times (usually one hour apart). The observed temporal drift in the measurements is then used to calculate the variation in the gravitational acceleration at those stations where gravity data was recorded in the time spanned by the two base station measurements.

4.2.3.2 Latitude correction

Variation of gravity on earth with latitude is attributed to two factors namely: shape and rotation of the earth.

1) Shape: the radius difference of the Earth measured at the equator differs from the radius measured at the poles. The polar radius is 6 357 km while the equatorial radius is 6 378 km, which means the value of gravity at the poles is greater than that at the equator.
2) Rotation: the Earth's rotation reduces the observed gravitational field because part of the Earth's gravitational acceleration goes into supplying the centrifugal acceleration. The centrifugal acceleration is responsible for keeping the measuring system in a constant orbit around the earth (Pinsker, 1972).

Latitude corrections are made by subtracting the normal gravity (g_n), calculated from the International Gravity Formula (IGF), from the observed or absolute gravity value. The IGF is given by:

$$g_n = 978031.85 * (1.0 + 0.005278895 \sin^2(lat) + 0.000023462 \sin^4(lat) \text{ (mGal)}$$

where

1at is the latitude of the measurement station expressed in radians.

Changes in the elevation of the measurement station cause changes in the measured gravitational acceleration. The gravitational acceleration varies as the square of the inverse distance between the gravimeter and centre of earth. To compensate for the effects of elevation changes on the measured gravity data, an elevation correction has to be done. The free-air correction accounts for gravity variations caused by elevation differences in the observation locations.

The Bouguer correction is a first-order correction to account for the excess mass underlying observation points located at elevations higher than the elevation datum (sea level). Conversely, it accounts for a mass deficit at observation points located below the elevation datum (geoinfo.nmt.edu/geoscience/projects/astronauts/gravity_method.html).

The combined free-air and Bouguer corrections are calculated from:

$g_{fa} = 0.3086h$ (mGal)

where

h is the elevation (in m) at which the gravity station is above the datum (typically sea level).

4.2.3.3 Free-air and Bouguer corrections

The terrain correction accounts for variations in the observed gravitational acceleration caused by variations in topography near each observation point. Because of the assumptions made during the Bouguer correction, the terrain correction is positive regardless of whether the local topography consists of a mountain or a valley (geoinfo.nmt.edu/geosciences/projects/astronauts/gravitymethod).

4.2.3.4 Terrain correction

The main objective of gravity data reduction is to get the Bouguer anomaly, which should correlate only with the lateral variation in density of the upper crust (Reynolds, 1997).

Regional gravitational effects may be removed from the Bouguer values by removing a smoothly varying regional field, either manually or through digital filtering. The gravity values that remain after removal of the regional field are called *residual gravity values* (Fourie, 2012). These residual gravity values reflect only the influences of the near surface density variations.

4.2.4 Instrument

In recent years, the Scintrex CG5 Autograv has become the most commonly used gravimeter for local investigations of density contrasts in the subsurface (see Figure 26). The instrument has a standard resolution of 1 micro Gal with a standard deviation that is <5 micro Gals. The sensing element of the instrument is based on a fused quartz spring system (www.scintrexltd.com).

The gravitational force on the proof–mass is balanced by a spring and an electrostatic restoring force. The inherent strength and elastic properties of the fused quartz, together with limit stops around the proof mass allows the instrument to be operated without clamping (www.scintrexltd.com).

The CG5-Autograv is equipped with a radio frequency remote start transmitter to allow measurements to be taken without disturbing the meter by touch. By using an electronic tilt sensor, the instrument is constantly updating information from the internal tilt sensor. The instrument can automatically compensate measurements for errors in instrument tilt. By selecting a feature, the instrument ensures that when measurements are taken on an unstable ground and an error occurs due to the instrument movement, the errors are automatically removed (www.scintrexltd.com).

Figure 26: Scintrex CG5 Autograv gravimeter (Google image, 2015)

4.3 MAGNETIC METHOD

4.3.1 Introduction

The magnetic method is used to measure the Earth's magnetic field and detect changes (anomalies) in the magnetic field caused by magnetic bodies in the subsurface. Anomalies in the Earth's magnetic field provide information of the location, orientation, depth and degree of magnetisation of the anomaly causing bodies (Fourie, 2012). Figure 27 shows a typical example of magnetic survey conducted with the magnetic strength being measured. The figure depicts that Earth's magnetic field changes over different magnetic geological features.

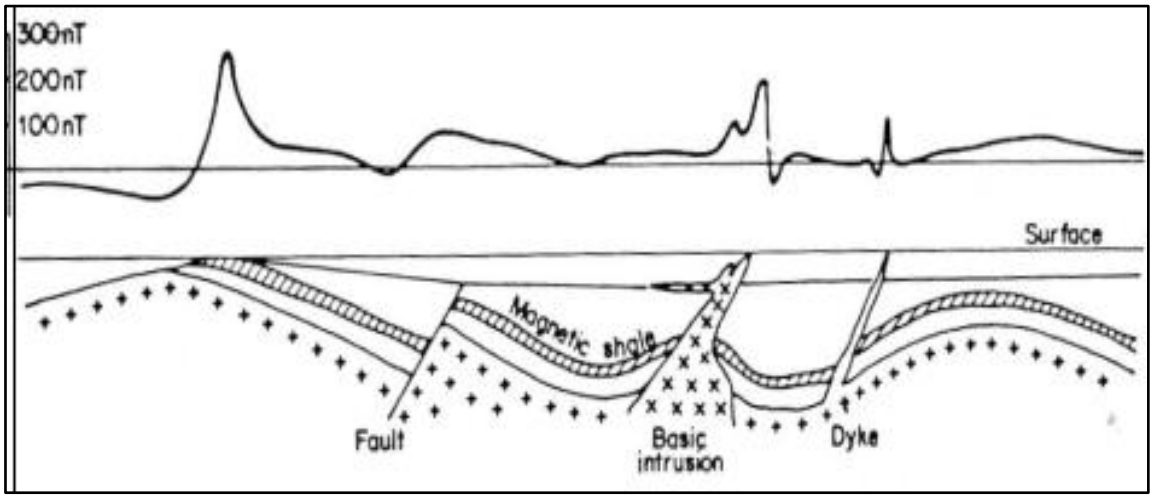

Figure 27: Illustration showing typical changes in the Earth's magnetic field over magnetic geological features (IGS lecture notes, 2012)

4.3.2 Earth's magnetic field

The Earth's magnetic field is generated by the convection currents in the liquid outer core of the Earth. Magnetic minerals may act as magnets or electro magnets and become aligned with the earth's magnetic field (Roux, 1980). The magnetic minerals tend to be magnetised and have their magnetic field (Roux, 1980). This magnetic field is local but at its location will be superimposed on the earth's magnetic field. Anomalies are created from the earth's normal magnetic field and they can be either positive or negative depending on the depth of burial, degree and direction of magnetisation (Roux, 1980).

4.3.3 Induced magnetism and remanent magnetism

Induced magnetism is the process by which iron or steel becomes magnetised by magnetic field (http://www.thefreedictionary.com/). The induced magnetism is produced by the force of the field radiating from the poles of a magnet and works in a similar manner as an electro-magnet (http://www.thefreedictionary.com/). When a piece of soft iron is placed in a magnetic field it will draw lines of the magnetic force towards it and will take properties of a magnet with a north and a south pole (Roux, 1980).

Remanent magnetism is the magnetisation left behind in a ferromagnetic material such iron after an external magnetic field is removed (https://en.wikipedia.org/wiki/). Remanent magnetism may result from the following causes: (1) Molten rock cooling down in a magnetic field; (2) the chemical formation and crystallisation in a magnetic field; (3) magnetic grains tend to be orientated in the direction of the earth's magnetic field during sedimentation; (4) the reorientation of magnetic grains as a result of great pressure (Roux, 1980).

4.3.4 Magnetic properties of rocks and minerals

The susceptibity of a rock depends on the magnetite content, so most rocks that have a significant concentration of ferro and or ferri-magnetic minerals will have the highest susceptibilities. Basic and ultrabasic rocks have the highest susceptibility, while igneous and metamorphic rocks have intermediate to low. Sedimentary rocks have a very small susceptibility (Milsom, 2003). The magnetic susceptibility of common rock and ore is shown in (Table 6).

Table 6: Magnetic susceptibility of common rocks (Modified after Milsom, 2003)

Common rocks	
Slate	0 - 0.002
Dolerite	0.01 - 0.15
Greenstone	0.0005 -0.001
Basalt	0.001 - 0.1
Granulite	0.0001 - 0.05
Rhyolite	0.00025 - 0.01
Gabbro	0.001 - 0.0001
Ores	
Hematite	0.001 - 0.0001
Magnetite	0.1 - 20.0
Chromite	0.0075 - 1.5
Pyrrhotite	0.001 - 1.0
Pyrite	0.0001 - 0.005

4.3.5 **Instrument**

Various magnetometers are available for magnetic surveys and the commonly used magnetometers are: proton precession magnetometers, fluxgate magnetometers and overhauser magnetometers. In this study the proton precession magnetometer manufactured by Geotron was used (see Figure 28).

The proton magnetometer consists of an electronic console battery, processor and a sensor. The sensor consists of a container filled with proton- rich fluid called kerosene (Paraffin) and coil of wire is wrapped around it (Roux, 1980).

The protons in the kerosene act like small spinning magnets and the spin axes wobble about the direction of the earth's magnetic field. When the current is applied to the coil a strong magnetic field is created and the axes of the protons align with the magnetic field (Roux, 1980).

When the current is switched off, the axes of the protons will wobble around the earth's magnetic field and together will produce an oscillating voltage in the coil. The frequency of the oscillating voltage will be equal to the precession rate of the proton spin axes, which is directly proportional to the earth's magnetic field (Roux, 1980).

Figure 28: The Geotron G5 proton precession magnetometer

4.4 RESISTIVITY METHOD

4.4.1 Introduction

The resistivity method is based on the phenomena of electrical current flowing in the subsurface and the fact that the subsurface material exhibits resistance to electrical current flow due the finite resistivity of the earth materials. The resistivity method is practically applied by injecting a direct current (DC) or slow varying alternating current (AC) into the earth by means of grounded current electrodes (Fourie, 2012).

During a resistivity survey, four electrodes are inserted into the earth. The four-electrode array typically consists of two current electrodes (A and B) used to send electrical current into the earth, and two potential electrodes (M and N) used to measure the resulting electrical potential difference, as shown in (Figure 29) for the Schlumberger array. By comparing the measured potential difference together with current and the distances between the electrodes, an apparent resistivity for the earth can be calculated. This is applicable when assuming that the earth is homogenous and isotropic

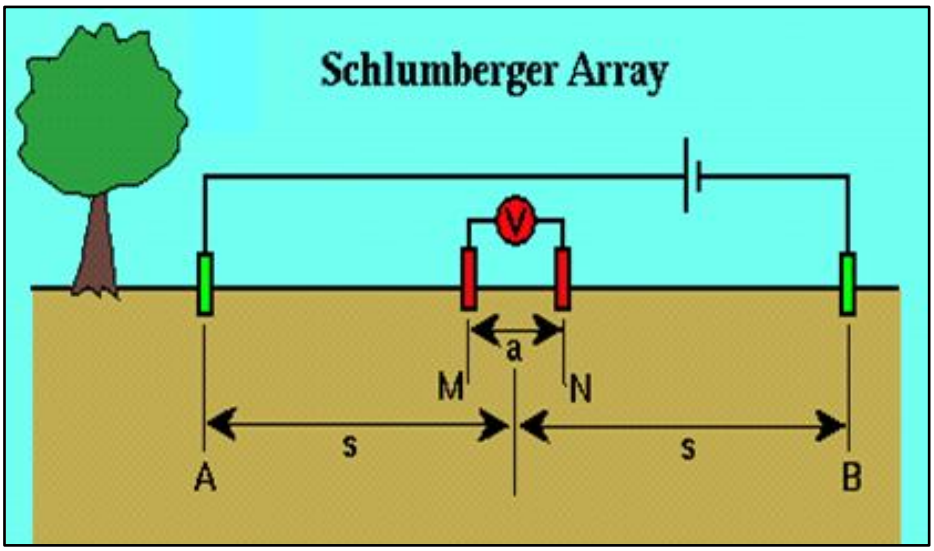

Figure 29: Electrode geometry for the Schlumberger array (IGS lecture notes, 2012)

During a typical resistivity survey energy is lost in the form of heat. The energy losses are caused by the changes in the electrical potential (the potential energy per unit charge). Therefore measuring the electrical potential difference (*V*) between the two grounded potential electrodes can provide information on the subsurface resistivities.

Electrical current flow in the subsurface goes through a 3D volume and not through a single path. The different earth materials that occur within this volume all contribute to the energy losses experienced and therefore affect the measured potential difference. The measured electrical potential difference represents the influence of all the subsurface materials through which the electrical current flows. Various parameters such as the mineral and fluid content, the porosity and degree of water saturation of the subsurface material also influence the resistivity of the subsurface materials (Loke, 2000).

4.4.2 Depth of investigation

The depth of investigation can be determined once information about the subsurface resistivity is known. The separation distance between the current electrodes determines the depth of investigation. The depth of investigation will always be less than the current electrode spacing. The greater the distance between the current electrodes the greater the depth of investigation becomes.

4.4.3 Sounding vs. profiling

The resistivity sounding method is used to investigate the changes in the subsurface resistivities with depth. This method is referred to as vertical electrode sounding (VES). During the sounding measurements, the distance between the current electrodes is gradually increased while the centre of the layout remains at a fixed point.

Apparent resistivities calculated from the current strength and the potential difference readings are used to estimate the resistivities and thicknesses of individual layers in the subsurface (http://www.solution4africa.com/).

Electrical profiling investigations are conducted in order to trace lateral boundaries of lithological units having different electrical properties. The electrode spacing is kept fixed, while the electrode array is moved along a traverse in order to measure lateral changes in the Earth's resistivities. The resistivity profiling method can differentiate less permeable areas from more permeable areas on the basis of apparent resistivity measured in the field (http://www.solution4africa.com/).

4.4.4 Electrical properties of rocks

Earth materials, including soil and rock, have an intrinsic property, called resistivity, which governs the relation between the current density and the gradient of the electrical potential. Variations in the resistivity of earth materials, either vertically or laterally, produce variations in the relations between the applied current and the potential distribution as measured on the surface. Properties that affect the resistivity of a soil or rock include porosity, water content, composition (clay mineral and metal content), salinity of the pore water, and grain size distribution. Table 7 shows the typical electrical resistivities of earth materials.

Table 7: Typical electrical resistivities of earth materials (Telford *et al.*, 1990)

Material	Resistivity (Ωm)
Clay	1 – 20
Sand	20-200
Shale	1 – 500
Porous limestone	100 – 1000
Dense limestone	100 – 1000 000
Metamorphic rock	50 – 1000 000
Igneous rock	100 – 1000 000

4.4.5 Electrode arrays

The electrode configuration (electrode array) is a geometrical pattern of electrodes used in electrical sounding and profiling (www.encyclopedia.com). The value of the apparent resistivity depends of the electrode array used (Reynold, 1997). There are various arrays used in the application of the resistivity method and the commonly used arrays are the Schlumberger, Wenner and Dipole-Dipole arrays (see Figure 30).

The Schlumberger array consists of four collinear electrodes. The outer two electrodes are current (source) electrodes and the inner two electrodes are the potential (receiver) electrodes.

In the Schlumberger array, the current and potential pair of electrodes has a common mid-point but the distance between the adjacent electrodes differ.

In the Wenner array, the current and potential electrodes have a common mid-point and the distance between the adjacent electrodes are equal. The Wenner array consists of four collinear, equally spaced electrodes. The outer two electrodes are typically the current (source) electrodes and the inner two electrodes are the potential (receiver) electrodes.

In the Dipole-Dipole array, the electrode array consists of two sets of electrodes, the current (source) and potential (receiver) electrodes. A dipole is a paired electrode set with the electrodes located relatively close to one another; if the electrode pair is widely spaced it is referred to as a dipole. The convention for a Dipole-Dipole electrode array is to maintain an equal distance for both the current and the potential electrodes (en.openei.org/wiki/DC/Resistivity/Survey).

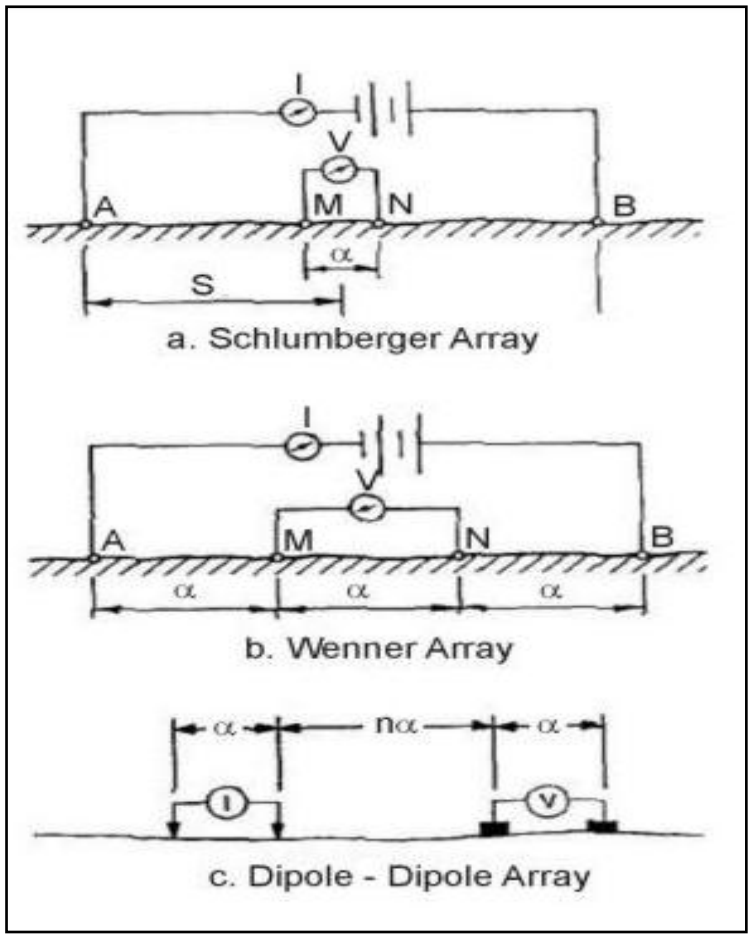

Figure 30: Commonly used electrode arrays (Milsom, 2003)

4.4.6 **Inversion**

During a field survey the resistance measurements are reduced to apparent resistivity values. The multi-electrode meter used in the survey come with computer software that is used in the inversion process.

A good inversion method must simultaneously minimize the effects of data error and model parameter errors. This means that it is necessary for inversion of any geophysical data to utilise a fast forward algorithm for calculating the theoretical data for initial model parameter (Narayan, *et al*, 1994).

4.4.7 **Instrument**

Electrical Resistivity Tomography (ERT) is an advanced geophysics method used to determine the subsurface's resistivity distribution. ERT data is rapidly collected with a multi-electrode resistivity meter. ERT profiles consist of a modelled cross-sectional (2-D) plot of resistivity (Ωm) versus depth.

ERT interpretations, supported by borehole data or alternate geophysical data, accurately represent the geometry, lithology and subsurface geologic formations. This method is ideal for depth investigations and can serve as an excellent basis for planning detail investigations for groundwater resources.

The ABEM Lund Imaging System (see Figure 31) comprises a Terrameter (SAS1000), an Electrode Selector ES464, electrodes, jumpers and four electrode cables. The Lund Imaging System uses a configuration shown in (Figure 32) and during the survey the four multi-core cables are laid out on a straight line (profile) across the area of interest.

Cables 1 to 4 are connected by means of cable connectors. The Terrameter and Electrode Selector are positioned at the midpoint of the four-cable setup. Cable 2 and 3 are connected to the Electrode Selector, which in turn is connected to the Terrameter through a communication cable. During the current investigations, four cables with 21 take-outs each and a standard electrode spacing of 5 m were used to reach a maximum depth of investigation of approximately 60 - 70 m.

Figure 31: The ABEM Lund Imaging System (www.abemlund.com)

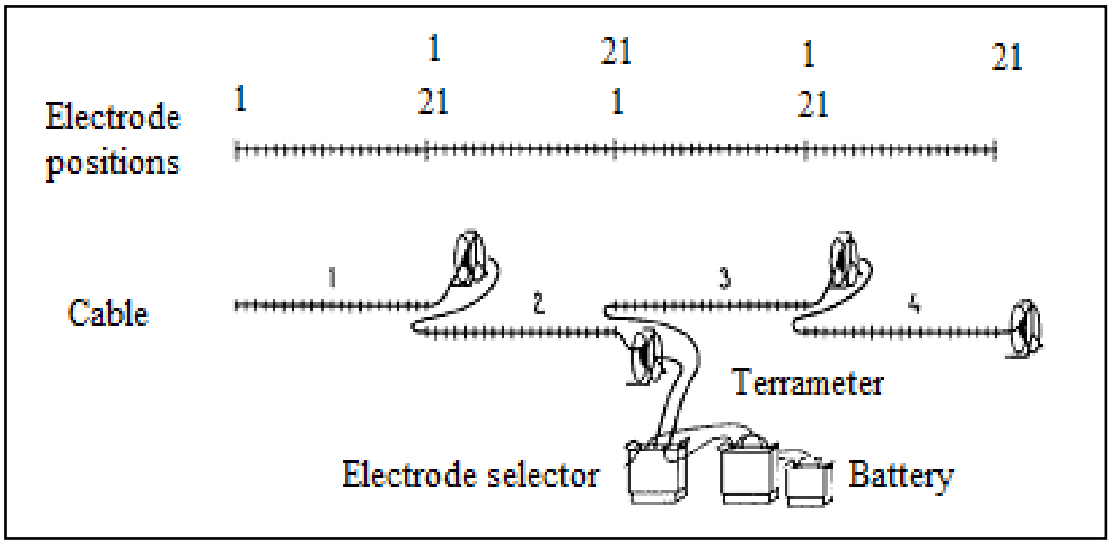

Figure 32: 2-D resistivity survey setup with the Lund Imaging System using the 4-cable approach (Loke, 2000)

4.5 ELECTROMAGNETIC METHOD

4.5.1 Introduction

Electromagnetic (EM) methods are applied in various exploration investigations because of the ability of these techniques to map changes in the subsurface conductivity distribution. Such changes may be due to changes in the lithology, state of weathering and moisture content of the geological units in the study area.

A time-varying primary current flowing through a primary circuit will cause a primary time-varying magnetic field in the vicinity of the circuit. The primary time-varying magnetic field will create a primary time-varying magnetic flux through the subsurface. This magnetic flux will give rise to an electromotive force (*emf*) in conductive bodies intersected by the magnetic field lines. The emf causes electrical currents (eddy current) to flow through the subsurface materials. These induced currents set up their own secondary, magnetic fields, which may be measured at surface at a receiver loop (coil).

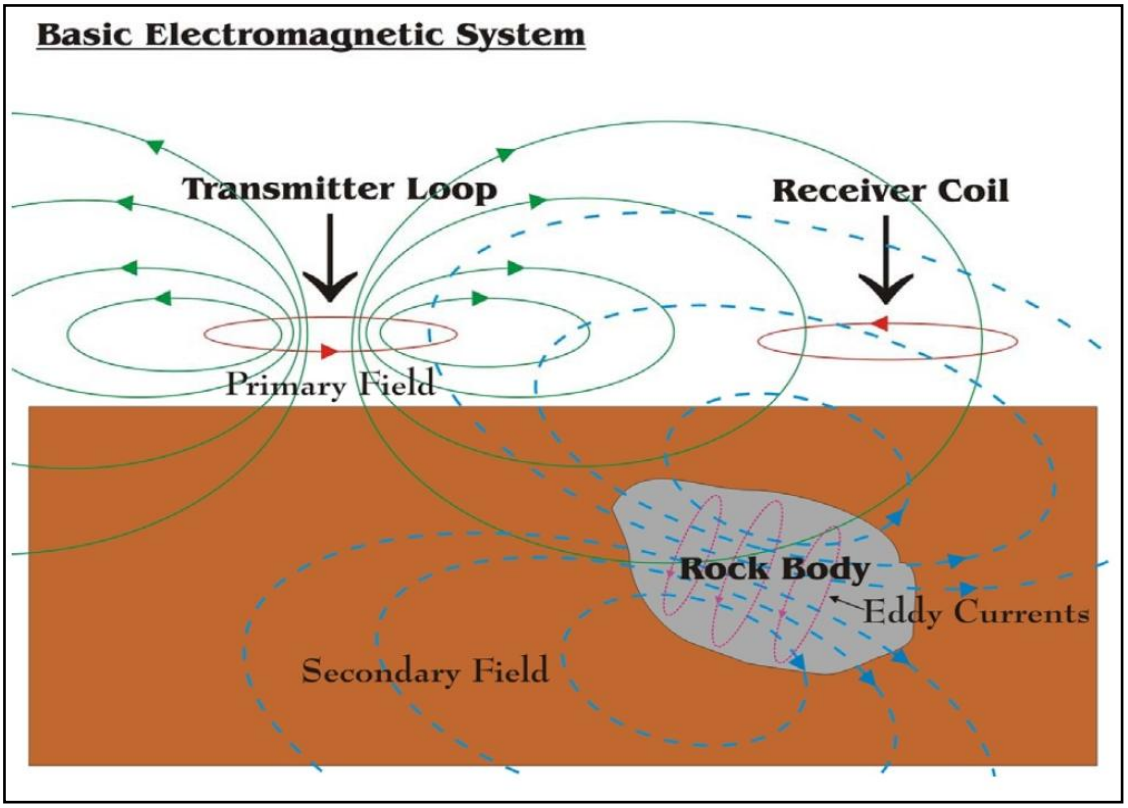

Figure 33: Using electromagnetic induction to obtain information on the subsurface conductivity distribution (Grant &West, 1965)

EM methods may be subdivided into two broad categories, based on their mode of operation, namely: frequency-domain electromagnetic (FDEM) and time-domain electromagnetic (TDEM). The difference between two methods is that the frequency-domain methods make use of sinusoidal (AC) excitation of the subsurface and measures a phase shift between the primary and secondary magnetic fields to calculate an apparent conductivity for the subsurface, while time-domain methods work excite the subsurface through a series of electromagnetic pulses.

The secondary magnetic field is measured over a number of time intervals between the pulses to investigate the rate of decay of this induced field (IGS, 2008). From the decay rate, information on the subsurface conductivity distribution may be derived.

During time-domain surveys, an electrical current flowing in a transmitter loop is switched off abruptly (see Figure 34). The collapsing electromagnetic field induces eddy currents in the conductive underground according to Maxwell's equations. This system of eddy currents produces a secondary magnetic field, whose propagation depends on the conductivity distribution in the subsurface (Nabighian and Macnae, 1991). Measured responses from later times therefore correspond to greater depths of investigation.

Time-domain electromagnetic methods are relatively young compared to the frequency-domain methods, magnetotelluric and geoelectric methods. The first time-domain method was developed in the mid-1980s and the technique has since been refined and has become a popular geophysical tool. Initially the method was used for mineral exploration but because of the introduction of advanced technology, the method was refined and the method can now be used for hydrogeological purposes as well for general geological mapping (Christiansen *et al.*, 2006)

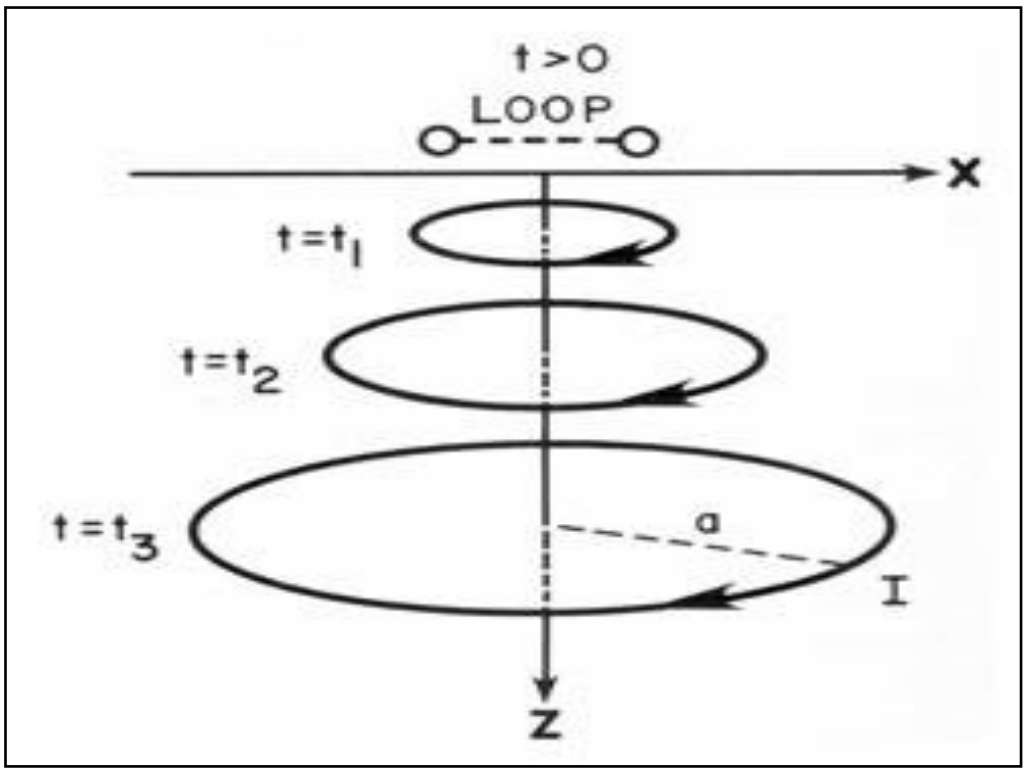

Figure 34: Propagation of current underground (Nabighian and Macnae, 1991)

4.5.2 Electromagnetic systems used during the current investigations

Both frequency- and time-domain systems were used during the current investigations. These are described below:

4.5.2.1 Frequency domain EM system: Geonics EM34-3

During the current study, the Geonics EM34-3 instrument was used for the FDEM surveys. The instrument operates at low induction numbers, which allows an apparent conductivity to be calculated from the ratio of the quadrature component of the secondary magnetic field to the free space primary magnetic field (McNeill, 1980).

During surveying, the transmitter and receiver coils are aligned in a plane, either parallel or perpendicular to the Earth's surface. The parallel alignment is referred to as the horizontal loop (vertical dipole) orientation, while the perpendicular alignment is called the vertical loop (horizontal dipole) orientation (refer to Figure 35 and Figure 36).

The manufacturers of the system, Geonics Ltd, indicate depths of investigation depending on the inter-coil spacing and coil orientation as listed (Table 8). Vertical dipole orientations allow greater depths of investigation than horizontal dipole orientations.

Table 8: Depths of investigation for the Geonics EM34-3 system (McNeill, 1980)

	Exploration depths (m)	
Intercoil spacing (m)	**Horizontal dipole**	**Vertical dipole**
10	7.5	15
20	15	30
40	30	60

During the current survey, measurements of the terrain conductivity were taken with both a vertical dipole and horizontal dipole orientations. The distance between the two coils was kept at a constant coil separation of 20 m and 40 m. The data was recorded at 10 m apart during the survey.

Figure 35: Terrain conductivity survey using the EM34-3 system in horizontal dipole (vertical coil) mode (www.geonics.com)

Figure 36: Terrain conductivity survey using the EM34-3 system in vertical dipole (horizontal coil) mode (www.geonics.com)

4.5.2.2 Time domain EM system: SkyTEM

The SkyTEM system was used in the current investigation because it uses advanced technology and has the capability to measure to large depths (approximately 500 m). The SkyTem system was developed for groundwater investigation by the Hydro Geophysics Group (HGG) at the University of Aarhus, Denmark. Various TDEM system were available but the need for a system that could increase the production time over single-site conventional TEM (Transient Electromagnetic) led to the development of the Pulled Array Transient Electromagnetic (PATEM) system (Sørensen *et*

al.,2000). Furthermore, the necessity for a system that could penetrate to greater depths and required a higher transmitting moment led to the development of an improved TEM system. Based on those systems developments, a platform for the development of SkyTEM became possible.

The SkyTEM system was designed for two reasons: 1) to record data of a quality similar to conventional ground-based systems, and 2) to resolve both shallow and deep earth structures comparably to or better than conventional ground-based systems (Sørensen *et al.*, 2004).

4.5.2.2.1 System design

The system does not require many personnel except for the pilot who flies the helicopter. The transmitter, receiver coil, laser altimeters, global positioning system (GPS) and data logger are mounted to a framework. The framework is hooked onto the helicopter (Figure 37).

During a survey, the array is located using the three global positioning devices and the altitude is measured using the two laser altimeters mounted to the framework. The data is averaged, reduced to data subsets (soundings) and stored together with the global positioning system coordinates, altitude, and inclination of the transmitter and receiver coils.

The data from two of the GPS receivers are recorded by the EM data acquisition system while a third GPS records the magnetic data system. The GPS system is used for time stamping, positioning, correlation of the EM and magnetic datasets (SkyTEM report, 2012).

A base station in the survey area is established, were data is captured every 1.5 hour. The system is monitored whenever the helicopter is refuelled to ensure that the system is stable (Sørensen *et al.*, 2004).

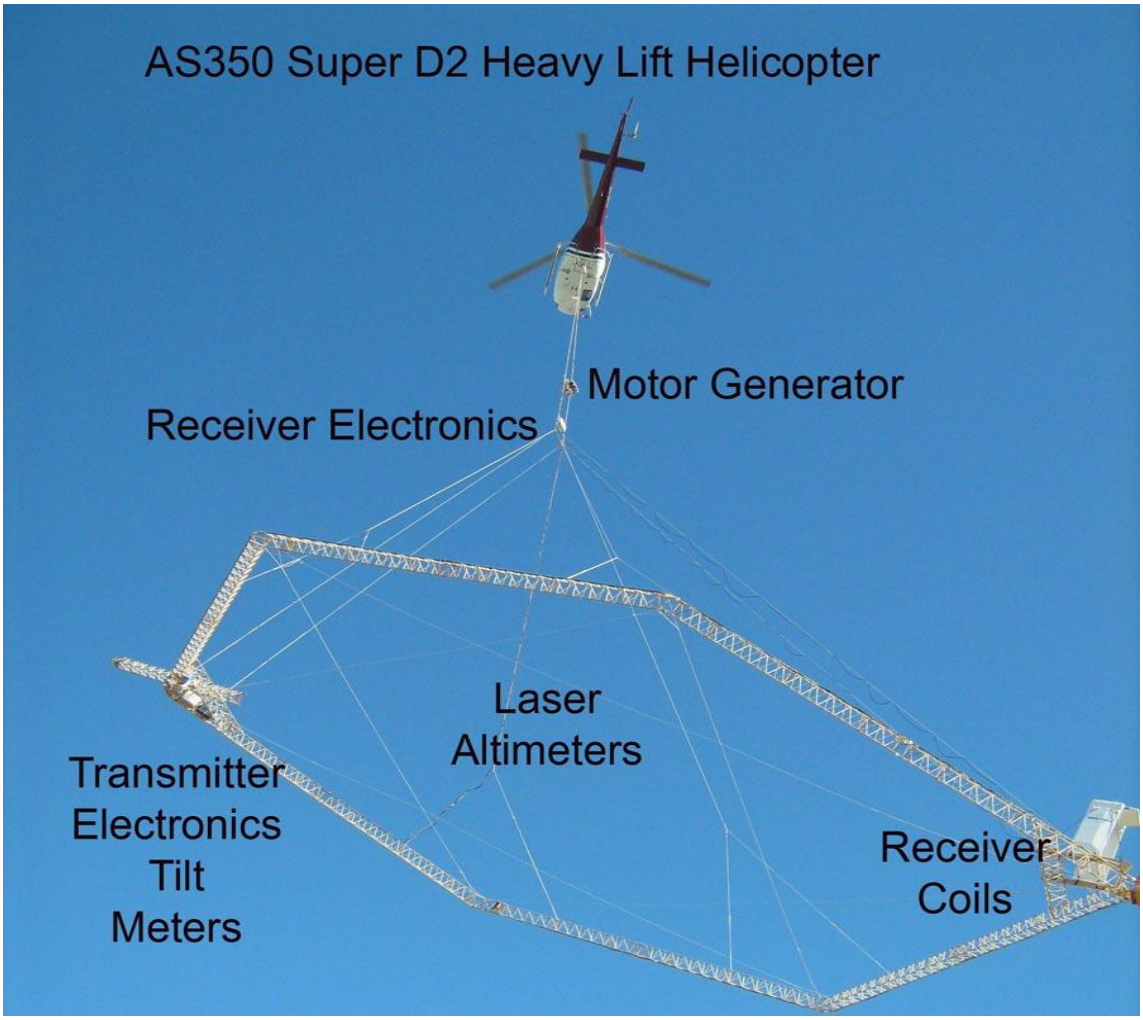

Figure 37: SkyTem system setup (Google images, 2013)

4.5.2.2.2 Transmitter

The transmitter loop is roughly hexagonal with a nominal diameter which can be configured to vary from about 15-30 m. The four turn transmitter loop is mounted on a wooden lattice frame and powered by a generator, which is suspended on the tow cable between the helicopter and the loop. The system is capable of operating in a dual transmitter mode (Reid *et a*l, 2007):

- **Low Moment (LM):** The mode in this instance has the system at a low current and high base frequency which can provide early time data and high spatial sampling for shallow imaging.
- **High Moment (HM):** The mode is at a higher current and lower base frequency which can provide a high quality late time data for deep imaging.

The transmitter waveform can be described as a modified square where the current builds quickly and is turned off within a few microseconds. The very fast turn-off time of the low moment transmitter results in higher vertical resolution of the upper layer (Reid *et al*, 2007).

4.5.2.2.3 Receiver

The receiver coil consists of a multiple-turn loop with a first-order cut-off frequency of 450 Hz. The receiver samples the transient decay at 20 delay time in the LM mode and 24 times in the HM mode. The receiver channel delay times are measured from the top of the current turn-off ramp (Sørensen *et al.,* 2004).

The receiver system uses two computers that are electrically separated; one computer stores the measurements from the receiver coil while the other controls the transmitter, transmitted waveform, GPS coordinates, laser altitude and angle data. The computers communicate and synchronise using the standard Transmission/Internet protocol (TCP/IP) (Sørensen *et al.*, 2004).

The receiver system uses synchronous detection with online data stacking, the stacking size is usually chosen so that the quantity is reduced by a factor of 25 to 50 resulting in a manageable size data set. The receiver integrates the incoming voltage by applying a digital control integrator (Sørensen *et al.*, 2004).

4.5.2.2.4 Flight speed and altitude

The flight speed and altitude operation are crucial parameters for the resolution of the subsurface resistivity distribution. The flight speed determines the lateral average of data and is related to the transmitter magnetic moment (Sørensen *et al.,* 2004).

4.5.2.2.5 Processing of SkyTem data

Navigation and status data for the SkyTem system make up a substantial amount of data. According to Christiansen *et al* (2006) the basis for the processing is the following:

- GPS data is measured every second with three independent devices.
- The inclination of the frame is measured every second by two independent devices.
- The altitude of the frame is measured 20 times per second with two laser devices.
- The transmitter current is stored for every 50– 100 transients.
- The transmitter also monitors parameters such as battery voltage and temperature.
- Every transient is stored and saved for further processing.

Processing of GPS and inclination data is done by adaptive filtering of the datasets. The inclination data is used to calculate normal reflection altimeter data and for calculation of exact transmitter and receiver altitudes and a field correction factor. The field correction factor accounts for the reduction in the *z*-directed magnetic moment caused by the movements of the transmitter/receiver-plane when flown in the wind (Christiansen *et al.*, 2006).

The processing of the transient datasets is done in two steps. The first step uses adaptive filters to eliminate noise. The stack size after the first step is approximately 100 – 200 transients. At this stage all datasets that are coupled due to man-made installations are removed. This process is quite time-consuming and requires a close integration of gate profile plots, individual dataset plots and a GIS-map. In the second step, the datasets from the first step are averaged into dataset sequences. The dataset sequences are the final soundings used in the inversion (Christiansen *et al.*, 2006).

4.5.2.2.6 Modelling and inversion of data SkyTEM

The model used for inversion of SkyTem data is a multi-layer model (MLM) with typically 30 layers. The layer thicknesses increase downwards as a hyperbolic sine function of the layer number. This means that the depth of the layer boundaries increases linearly for small depths, so that the top layers are all of approximately the same thickness (SkyTEM report, 2012).

For large depths, the depth to the layer boundaries increases exponentially with depth, so that the thickness of a layer is a factor times the previous layer (SkyTEM report, 2012)

The initial model for deep inversion is a 30 layer MLM with a homogenous resistivity layer, i.e. the initial model is essentially a homogenous half space. Model optimisation can be carried out in both a L1 and L2 norm formulation where the former produces more blocky models than the latter (SkyTEM report, 2012).

4.5.2.2.7 Noise model

The inaccuracy of TDEM data is caused by ambient noise. This noise is reduced by selective stacking of delay time series, and by applying appropriate filters in the receiver system. For the SkyTEM data, the noise voltage is most often described by a simple model: log (noise) which is a linear function of log (time) (SkyTEM report, 2012).

When the width of the time gates increases proportional to delay time, the slope of the linear function is close to -0.5 (SkyTEM report, 2012).

CHAPTER 5: GEOPHYSICAL INVESTIGATION

5.1 INTRODUCTION

Geophysical investigations often play an important role in groundwater exploration projects. Investing time and money in this phase of the exploration programme can only contribute to the success of the project. In this study, the company SkyTEM was contracted to conduct a time-domain electromagnetic survey across the study area. The results of the SkyTEM survey were then used to identify geological features of interest to the groundwater exploration programme, as well as to plan the subsequent ground geophysical investigations targeting the identified geological features.

Although the SkyTEM technique is technologically advanced and has yielded great results in many investigations (Christiansen *et al.*, 2006), the geological and hydrogeological setting of the study area of the current investigations is different from conditions at study areas where investigations were previously conducted. One of the main objectives of this study is to evaluate the effectiveness of the technique for groundwater exploration programmes in this particular environment.

5.2 SKYTEM SURVEY

The SkyTEM survey was conducted across the study area to map the conductivity/resistivity distribution of the subsurface and to relate this distribution to the presence of different geological structures that could have an influence on the occurrence and distribution of groundwater. The SkyTEM survey preceded the ground geophysical investigations; targets for the ground geophysical surveys were identified from the results of the SkyTEM survey

5.2.1 **Survey geometry**

The time-domain electromagnetic survey, was flown with a helicopter and covered area SD4, but also extended across its eastern boundary. The grid on which the SkyTEM data were recorded is shown in (Figure 38)

.The flight survey lines were separated by a distance of approximately 30 m. The source and receiver loop system was maintained at a constant altitude of 30 metres above ground level. Resistivity depth soundings were obtained every 2 m and a base station was established for data capturing and storage.

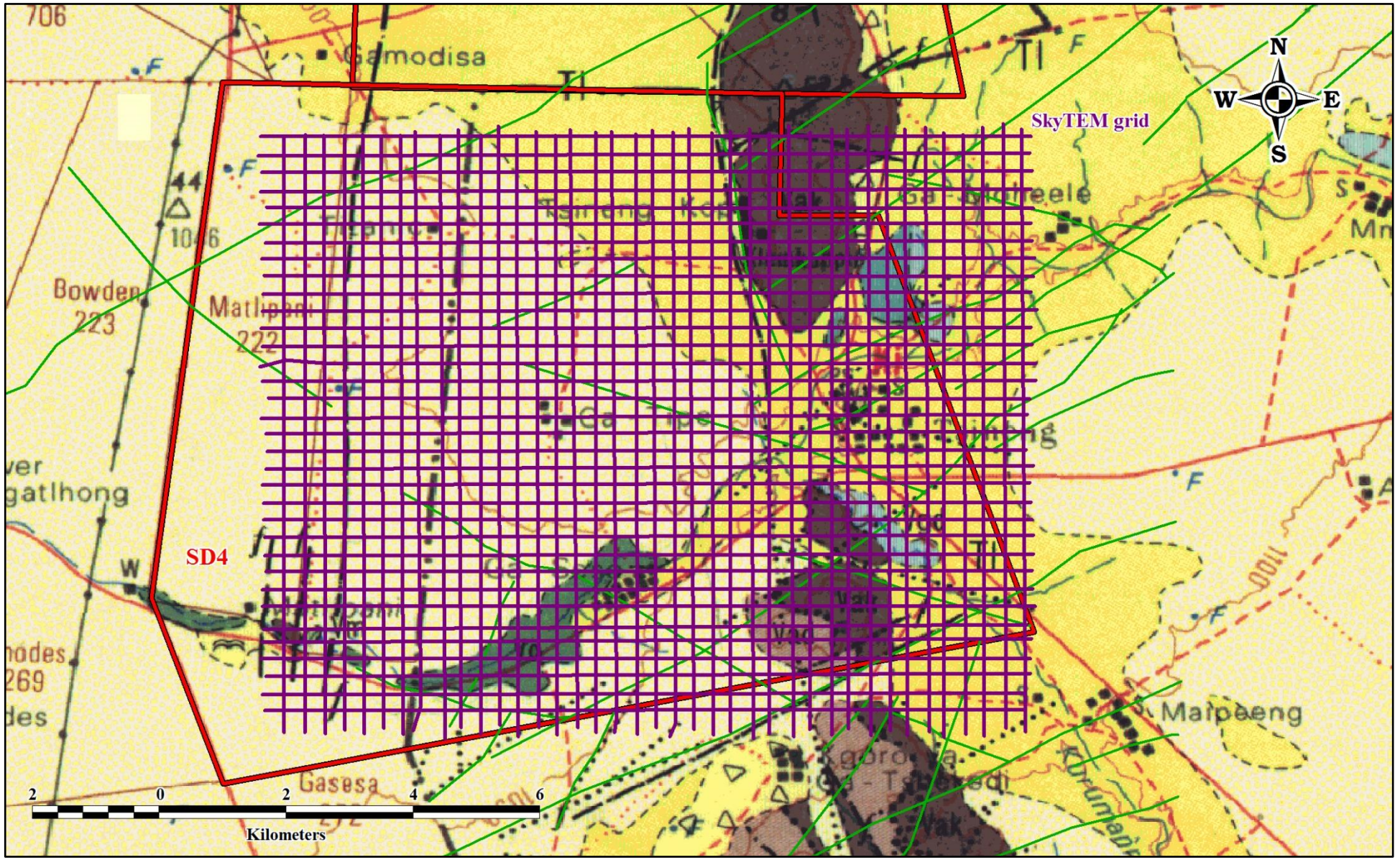

Figure 38: Grid on which the SkyTEM data was recorded within and across area SD4

5.2.2 **Results of the SkyTEM survey**

The data recorded during the SkyTEM survey were processed to yield contour maps of the resistivity distribution across the survey area at various depths of investigation. These depths of investigation ranged from surface (0 m) to depths in excess of 500 m. A total number of 30 depth sections were compiled in this way.

The results of the SkyTEM survey are presented as contour maps of the apparent resistivities recorded at different depths. From these contour maps, inferences regarding the subsurface distribution of the different lithologies underlying the study area can be made. The resistivity sections corresponding to 10 selected depths of investigation are presented in (Figure 39 to Figure 48). These depth sections (layers) were selected to highlight certain features of the subsurface resistivity distribution.

Layer 1 (0.0-5.0 m)

The distribution of resistivities from surface (depth of 0 m) to 5.0 m is shown in (Figure 39). Also indicated in this figure are the positions and orientations of the two major faults (Eastern Fault and Western Fault, refer to Section 3.5.2.5), as well as the numerous dykes that have been mapped. A zone of higher resistivities (in excess of 700 Ωm; blue colours) is seen in the north-western parts of the survey area. A similar but smaller zone of high resistivities is also seen in the southern parts of the survey area. The reason for these localised high resistivities is unknown, since most of the western parts of the survey area are covered by Kalahari sands. More conductive near-surface materials are present in the eastern and south-eastern parts of the survey area. These materials may be due the weathering of the tertiary deposits (limestones) that are known to occur in the area.

No prominent resistivity anomalies are associated with the Western Fault at these shallow depths of investigation. However; there is some indication that lower resistivities are associated with the Eastern Fault, even at these shallow depths.

None of the mapped dykes appear to be associated with prominent resistivity anomalies at shallow depths.

Layer 3 (10.1-15.2 m)

The distribution of resistivities at depth 10.1 m to 15.2 m is shown in (Figure 40). Similar to (Figure 39), zones of higher resistivities (in excess of 700 Ωm; blue colours) are seen in the north-western and southern parts of the survey area .These zones have very similar spatial extents than in Layer 1.

More conductive materials are present in the eastern and south-eastern parts of the survey area. These materials may be due to the tertiary deposits (limestones) that are known to occur in the area.

No prominent low resistivities are associated with the northern parts of the Western Fault; however, low resistivities (approximately 7 – 21 Ωm) are observed in the southern-most part of this fault. A low resistivity zone is observed along the Eastern Fault. Due to the small lateral extent of this zone of low resistivity, it appears to be related to the fault and not the banded iron formations occurring in this part of the survey area.

The mapped dykes show no association to the resistivity anomalies that were observed in the survey area.

Layer 6 (26.1-32 m)

The distribution of resistivities at depth 26.1 m to 32.0 m is shown in (Figure 41). At this depth, more prominent zones of low resistivities (red colours) coincide with the position of the Western Fault. These zones also extend farther to the north along the fault than in Layer 3. The low resistivities associated with the fault could be due to a higher degree of fracturing and weathering, as well as a higher water content in the more permeable zones created through fracturing.

The high resistivities zone values (blue colour) in the western parts of the survey area decrease in size and also become more scattered as compared to Layer 3. However, the zone of high resistivities in the south is more prominent with a larger lateral extent than in Layer 3. This zone could be due to the lavas of the Ongeluk Formation known to underlie the survey area in these parts.

A low resistivity zone along the Eastern Fault is clearly visible at this depth of investigation. This zone follows the strike of the fault and is clearly associated with the fault.

Towards the south of the Eastern Fault, prominent zones of low resistivities are observed. These zones generally occur in a broad band that coincides with the outcrops of the banded iron formations occurring in the area. A localised anomaly with a resistivity value that is approximately less than 2 Ωm is observed towards the eastern boundary of the study area. This reason for this localised zone of low resistivities at this depth is uncertain.

Another prominent linear low resistivity feature is observed in the south-eastern corner of the survey area. This zone coincides well with a fault (and possibly a parallel dyke) that has been mapped in this part. Again, the low resistivities may be due to increased fracturing and higher water content along the fault.

Layer 9 (44.8-51.9 m)

The distribution of resistivities at depth 44.8 m to 51.9 m is shown in (Figure 42). The north-western parts of the survey area display a very drastic change in resistivities as compared to Layer 6. Whereas in Layer 6, resistivities in the order of several hundreds of ohmmeters were observed, in Layer 9, these resistivities are below 5 Ωm. This indicates a prominent vertical change in the subsurface lithologies. However, the zone of high resistivities in the south extends from Layer 6 to Layer 9 and even becomes more prominent in Layer 9. This observation clearly shows that different lithologies underlie the northern-western and south-western parts of the survey area. The high resistivities in the south are thought to be due to the lavas of the Ongeluk Formation (confirmed during drilling, refer to Chapter 6). The origin of the low resistivities in the north were unknown at the time of the survey, but was later confirmed to be thick clay layers (refer to Chapter 6).

There is still some indication that the Western Fault is associated with low resistivities at the depths of investigation, although the presence of the zone of low resistivities in the north partially masks it presence.

Linear zones of low resistivities are also noted along many of the dykes running through the survey area, particularly in the north-western and south-eastern parts. Since the dykes themselves are expected to have resistivities (dolerite and diabase are generally associated with high resistivities), these linear zones of low resistivities along the dykes suggest that the dykes are associated with fracturing of the host rock and could potentially be water-bearing features.

The eastern parts of the survey area also exhibit low resistivities, again within a broad band roughly corresponding to the mapped outcrops of banded iron formations. However, the localised zone of low resistivities observed in Layer 6, is even more prominent in Layer 9. This anomaly is likely to be due the banded ironstones of the Kuruman Formations.

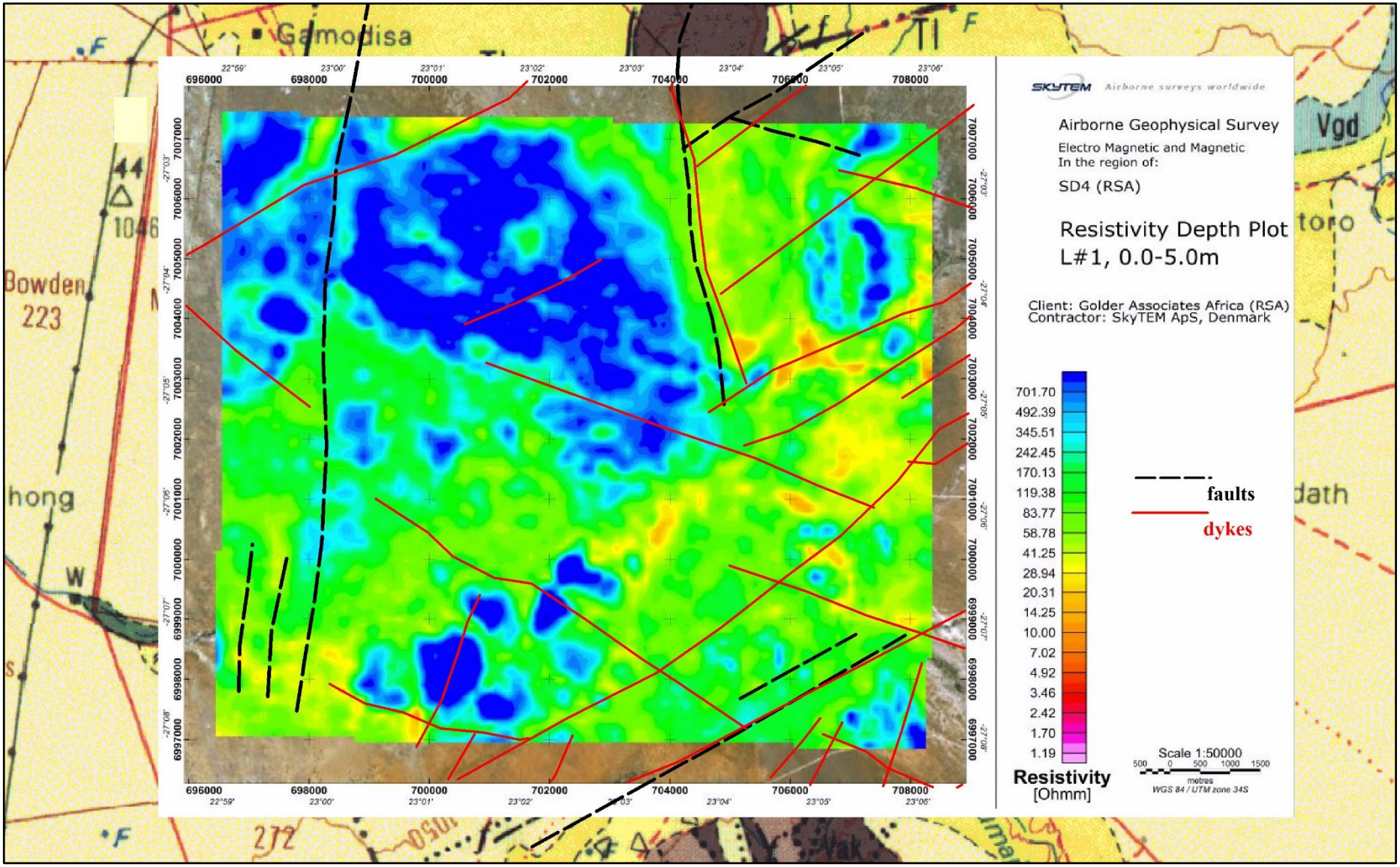

Figure 39: Resistivity distribution at depths ranging from 0.0 to 5.0 m

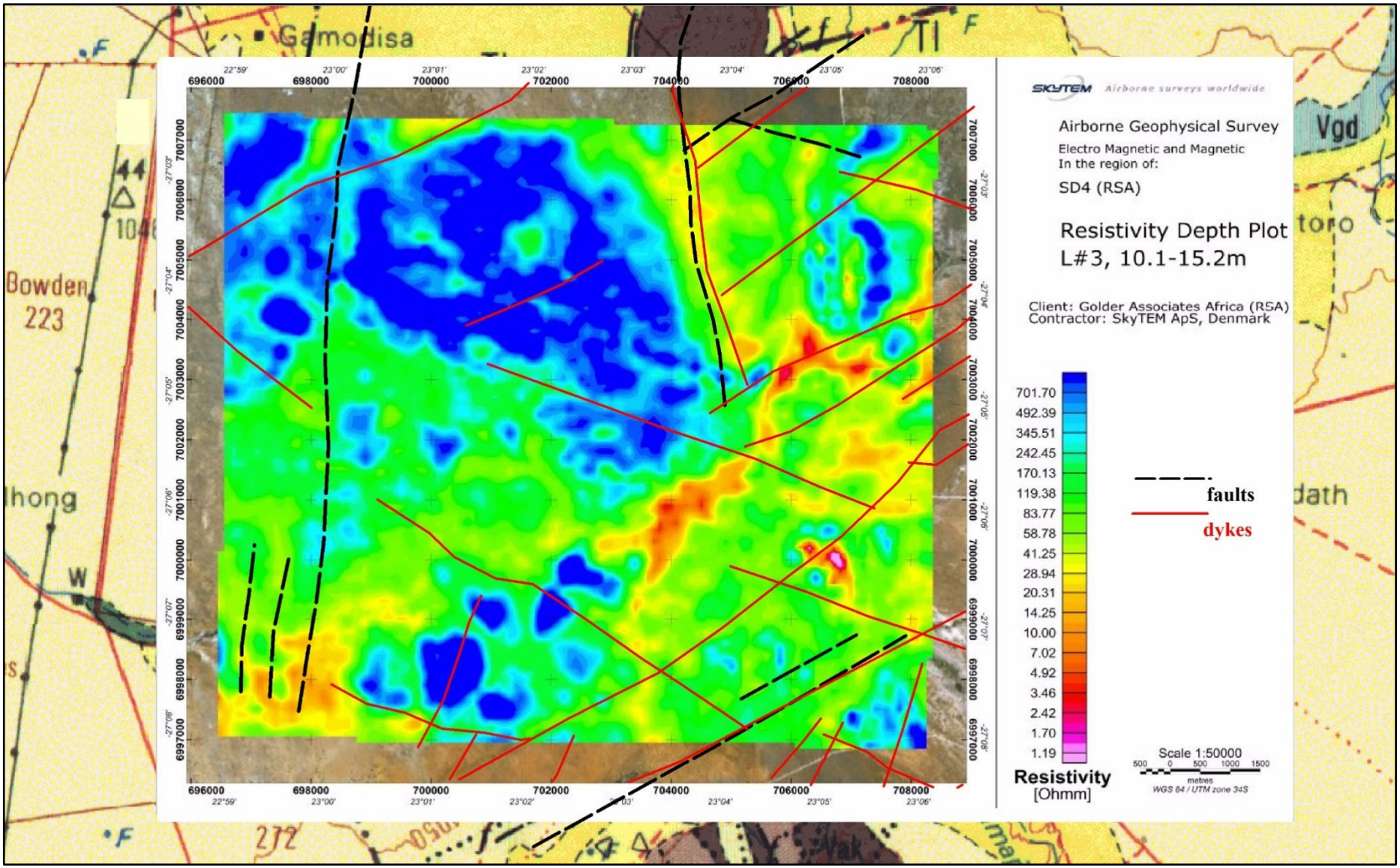

Figure 40: Resistivity distribution at depths ranging from 10.1 to 15.2 m

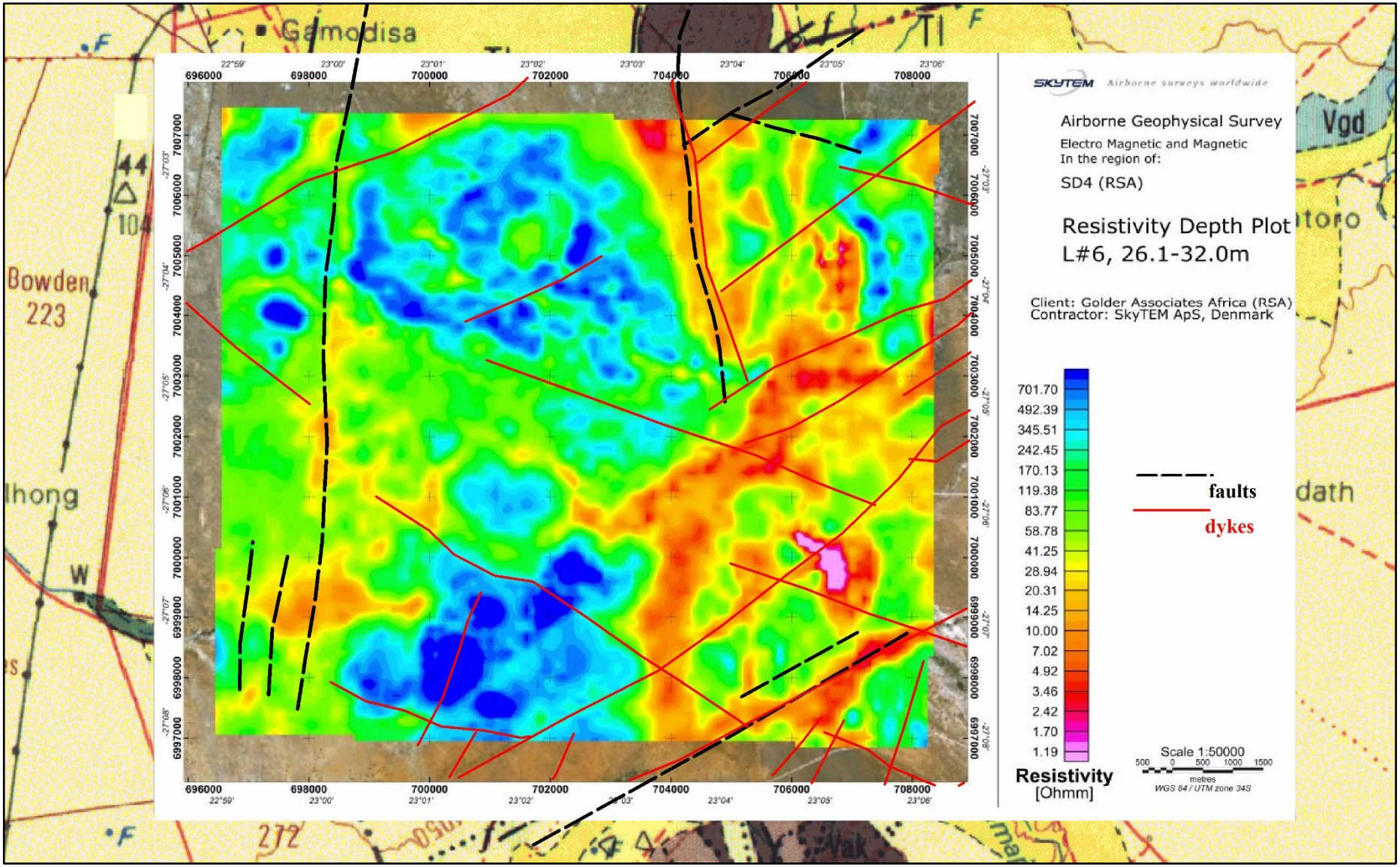

Figure 41: Resistivity distribution at depths ranging from 26.1 to 32.0 m

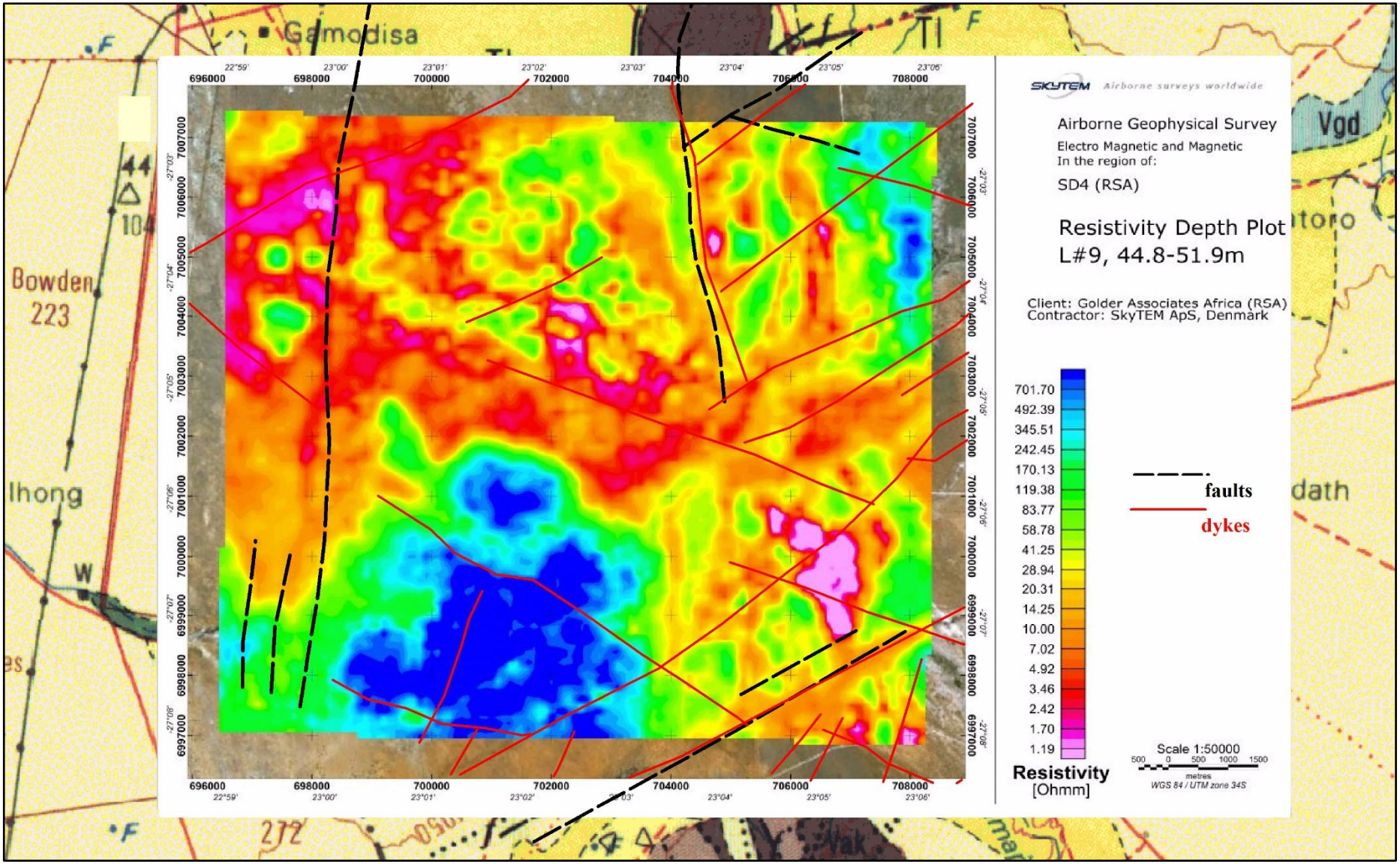

Figure 42: Resistivity distribution at depths ranging from 44.8 to 51.9 m

Layer 12 (68.0-77.1 m)

The distribution of resistivities at depth 68.0 m to 77.1 m is shown in (Figure 43). Again a drastic change in the resistivities is observed in the north-western parts of the survey area. The resistivities increase significantly from Layer 9 to Layer 12. This shows that the horizon of low resistivities observed in Layer 9 does not extend to the depths of investigation of Layer 12.

Zones of low resistivities still appear to be associated with the Western Fault, but now occur on the western side of the fault. A prominent lateral change in resistivities is seen between the western and eastern sides of the fault. The fault therefore appears to be associated with lateral changes in lithology. This observation suggests that the fault is a thrust or normal fault (not a strike-slip fault). The absence of low resistivity zones coinciding with the position of the fault suggests that the fault may not associated with groundwater at these depths.

The Eastern Fault also appears to be associated with lateral changes in resistivities at the current depth of investigation. Much lower resistivities are observed on the eastern side of the fault than on the western side. This change in resistivities is clearly due to changes in the subsurface lithology, since the low resistivities coincide with the areas in which banded iron formations are known to occur. The Eastern Fault appears to form the boundary between the banded iron formations and the host rock to the east.

Towards the south of the Eastern Fault, the zones of low resistivity seen in Layers 6 and 9 are still visible. These anomalies can be attributed to the banded iron formations that are known to occur in this area.

The high resistivity zone in the south-western parts of the survey area is more prominent in Layer 12 than it was in Layer 6 and 9. The lavas of the Ongeluk Formation therefore seem to extend to the depths of investigation of Layer 12.

A weaker correlation between the mapped dykes and linear low resistivity zones is observed at this depth of investigation. This could mean that the zones of fracturing and higher water content associated with the dykes do not extend to the current depths of investigation.

Layer 15 (98.0-110.0 m) and Layer 21 (191.6-213.4 m)

Very similar resistivity distributions are observed in Layers 15 and 21 in (Figure 44 and Figure 45), despite the large difference in depths of investigation. This observation shows that the subsurface geology remains relatively uniform over a large range of depths (98 to 213.4 m).

Apart from a localised anomaly along the northern parts of the fault, the Western Fault does not appear to be associated with prominent resistivity anomalies at the current depth of investigation. This could indicate that the fault does not extend to these depths. However, the loss of resolution with depth of the SkyTEM data could also be the reason for the lack of prominent anomalies.

The Eastern Fault neatly maps the western boundary of the zones of low resistivity associated with the banded iron formations. Comparing the resistivity distributions of Layers 15 and 21 indicates that the banded iron formation occur farther to the west at increasing depths. These formations therefore appear to be dipping to the west.

No prominent resistivity anomalies are observed along the mapped dykes. This observation suggests that the fractured zones associated with the dykes do not extend to the current depths of investigation. However, the loss of resolution of the SkyTEM data with depth could also be responsible for the absence of resistivity anomalies associated with the dykes.

The high resistivity zone in the south-western parts of the survey continues to be prominent at this depth of investigation. The Ongeluk lavas therefore appear to extend to these large depths.

Layer 26 (327.3-364.0 m), Layer 28 (404.7-449.8 m) and Layer 30 (>500 m)

The distribution of resistivities within Layers 26, 28 and 30 are shown in (Figure 46, Figure 47 and Figure 48), respectively. These distributions are all very similar in character.

The localised zone of low resistivities observed along the northern parts of the Western Fault in Layer 15 can still be seen in Layers 26, 28 and 30. The origin of this anomaly extending to these large depths is at present unknown.

At all three depths of investigation, the Eastern Fault seem to form part of the western boundary of the banded iron formations occurring in the area.

The lateral extent of the low resistivity zone due to the Ongeluk lavas seems to decrease with increasing depth of investigation. Localised anomalies seen surrounding this zone are thought to be noise effects contaminating to the data at such large depths of investigations.

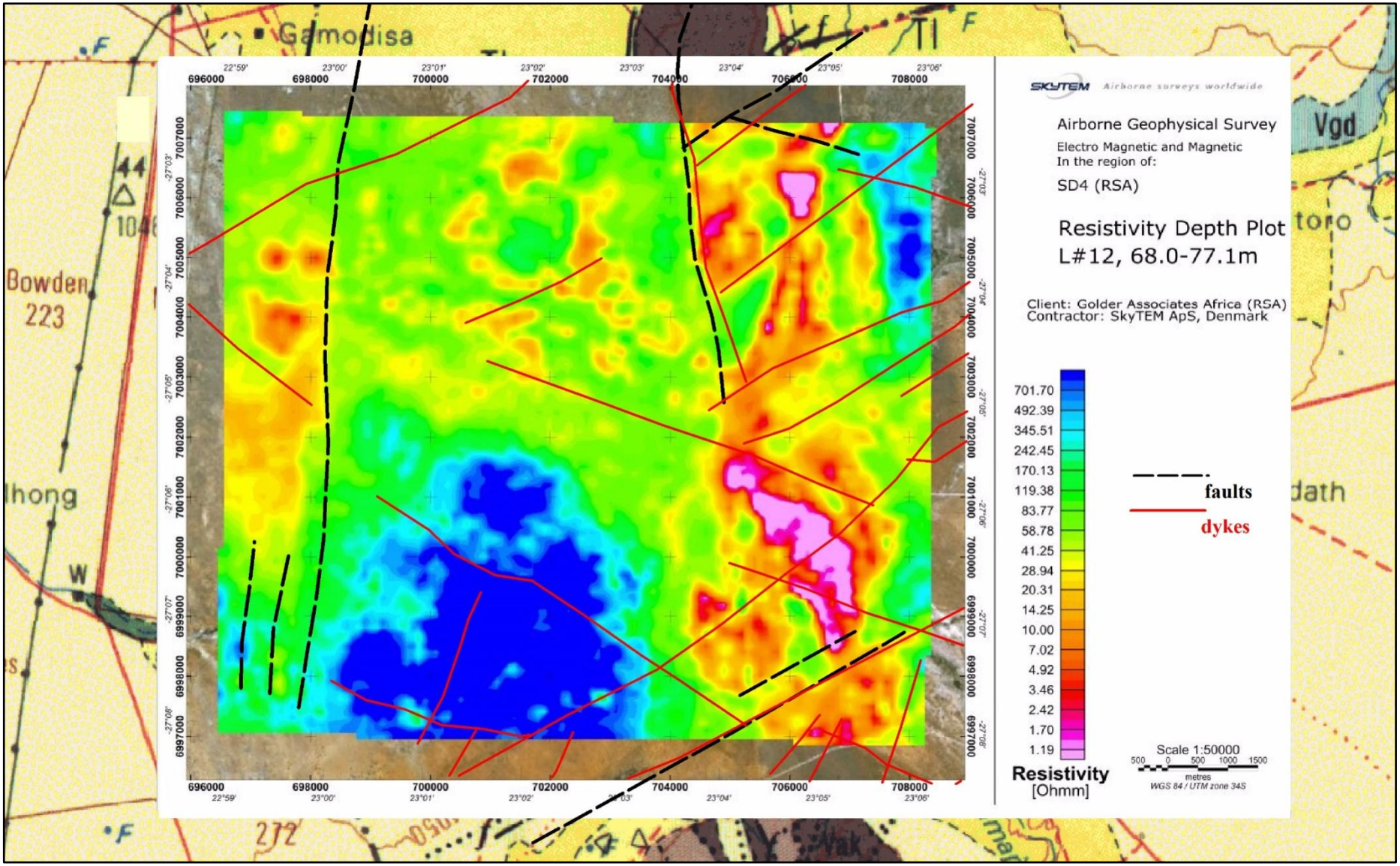

Figure 43: Resistivity distribution at depths ranging from 68.0 to 77.1 m

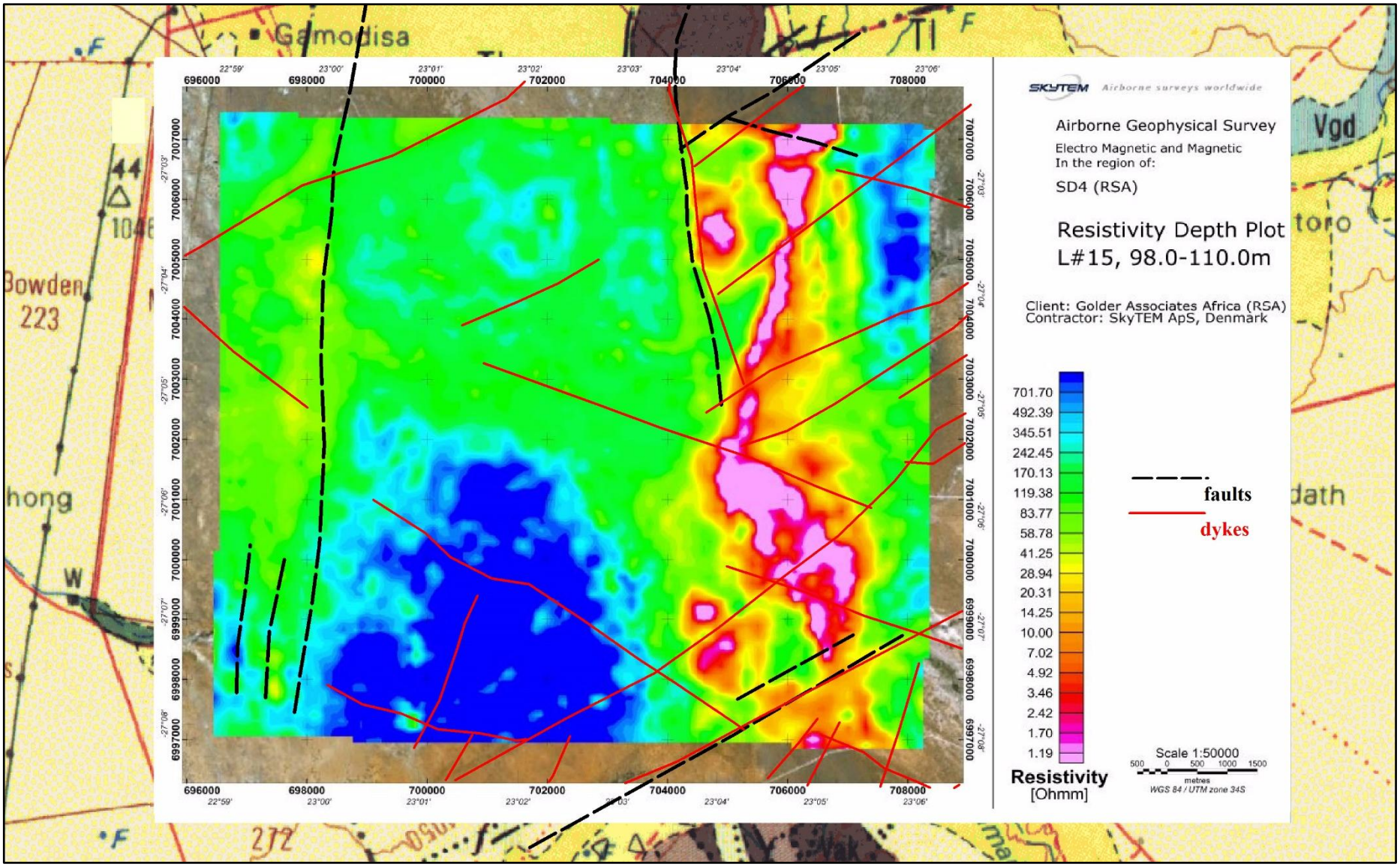

Figure 44: Resistivity distribution at depths ranging from 98.0 to 110.0 m

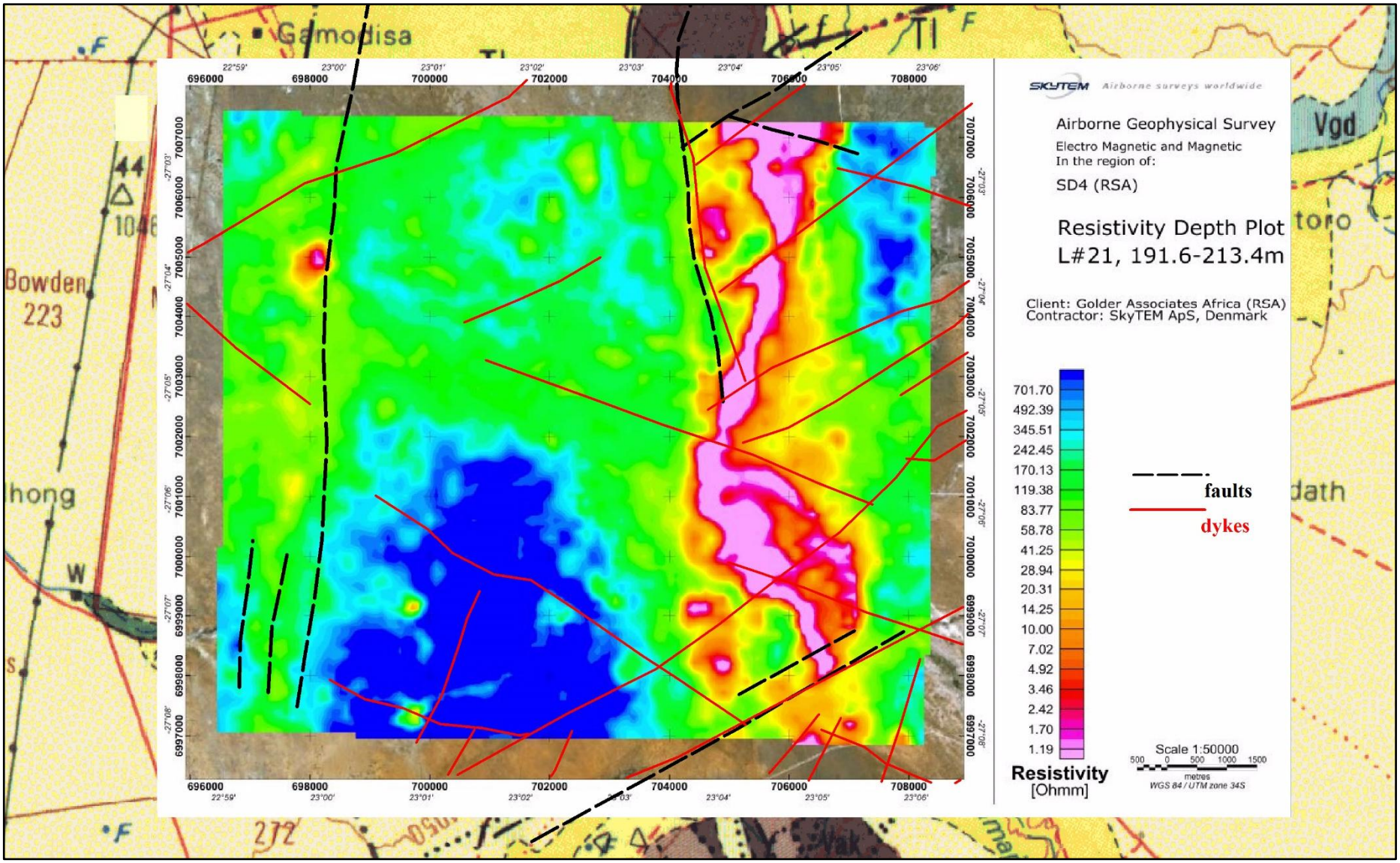

Figure 45: Resistivity distribution at depths ranging from 191.0 to 213.4 m

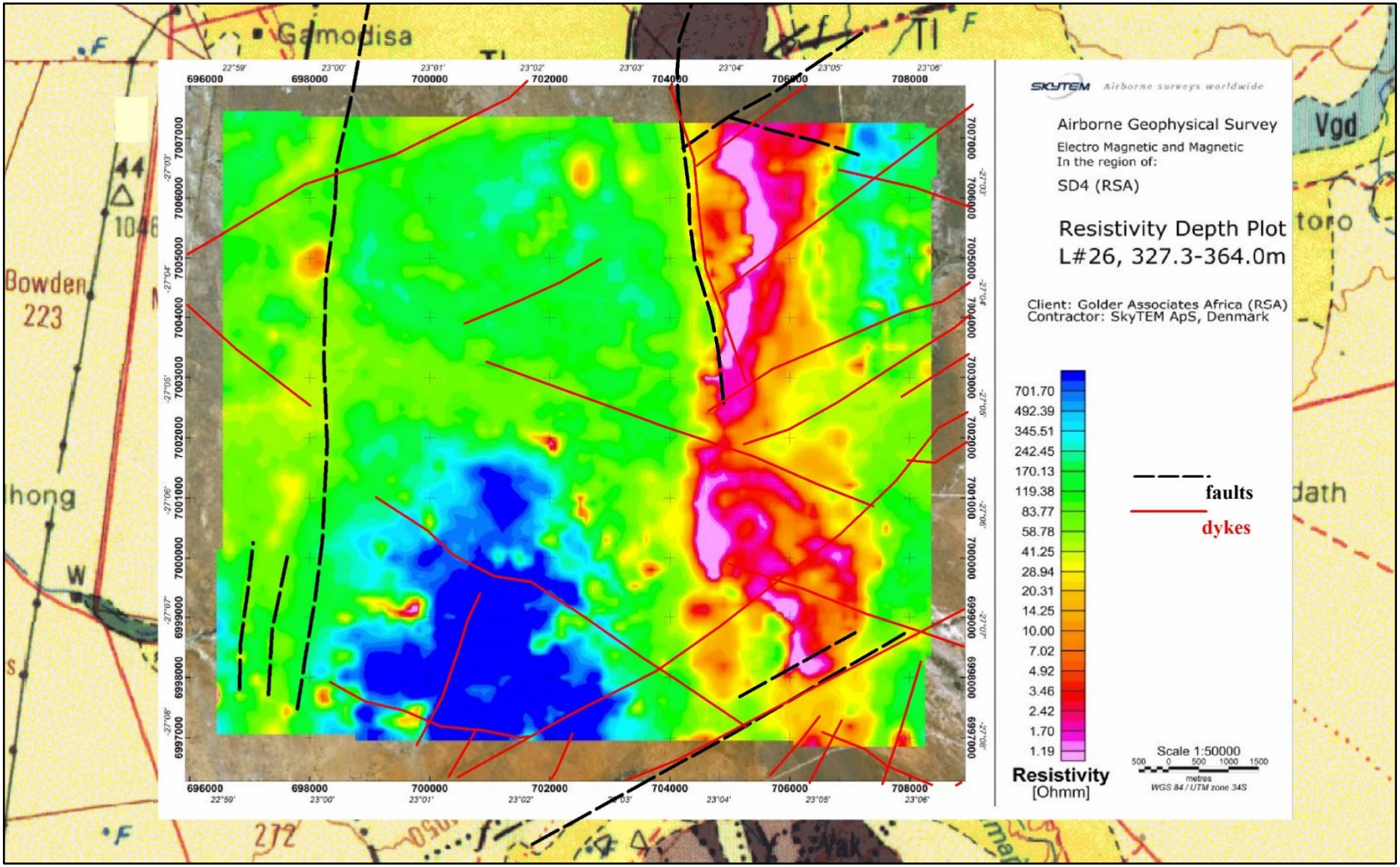

Figure 46: Resistivity distribution at depths ranging from 327.3 to 364.0 m

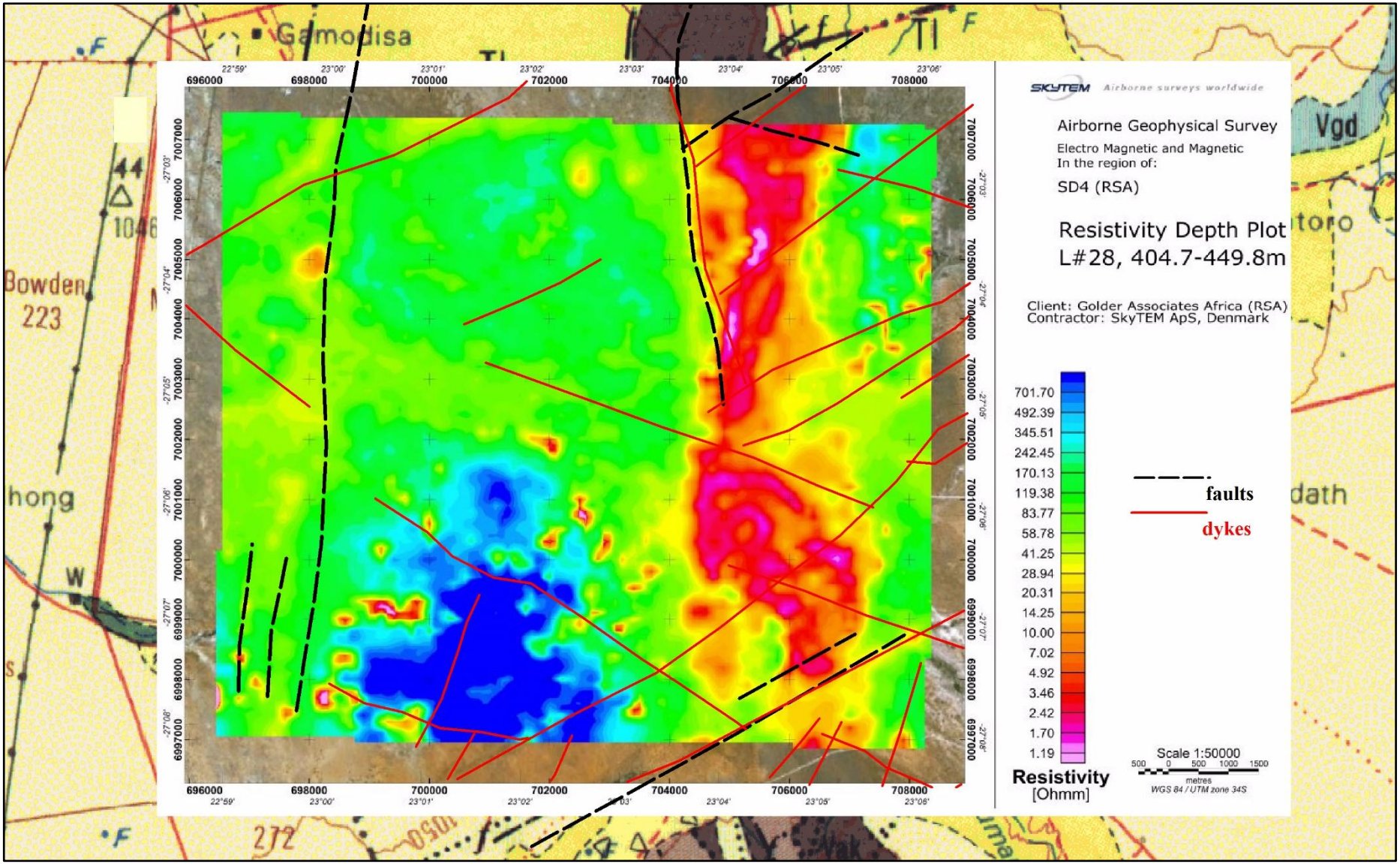

Figure 47: Resistivity distribution at depths ranging from 404.7 to 449.8 m

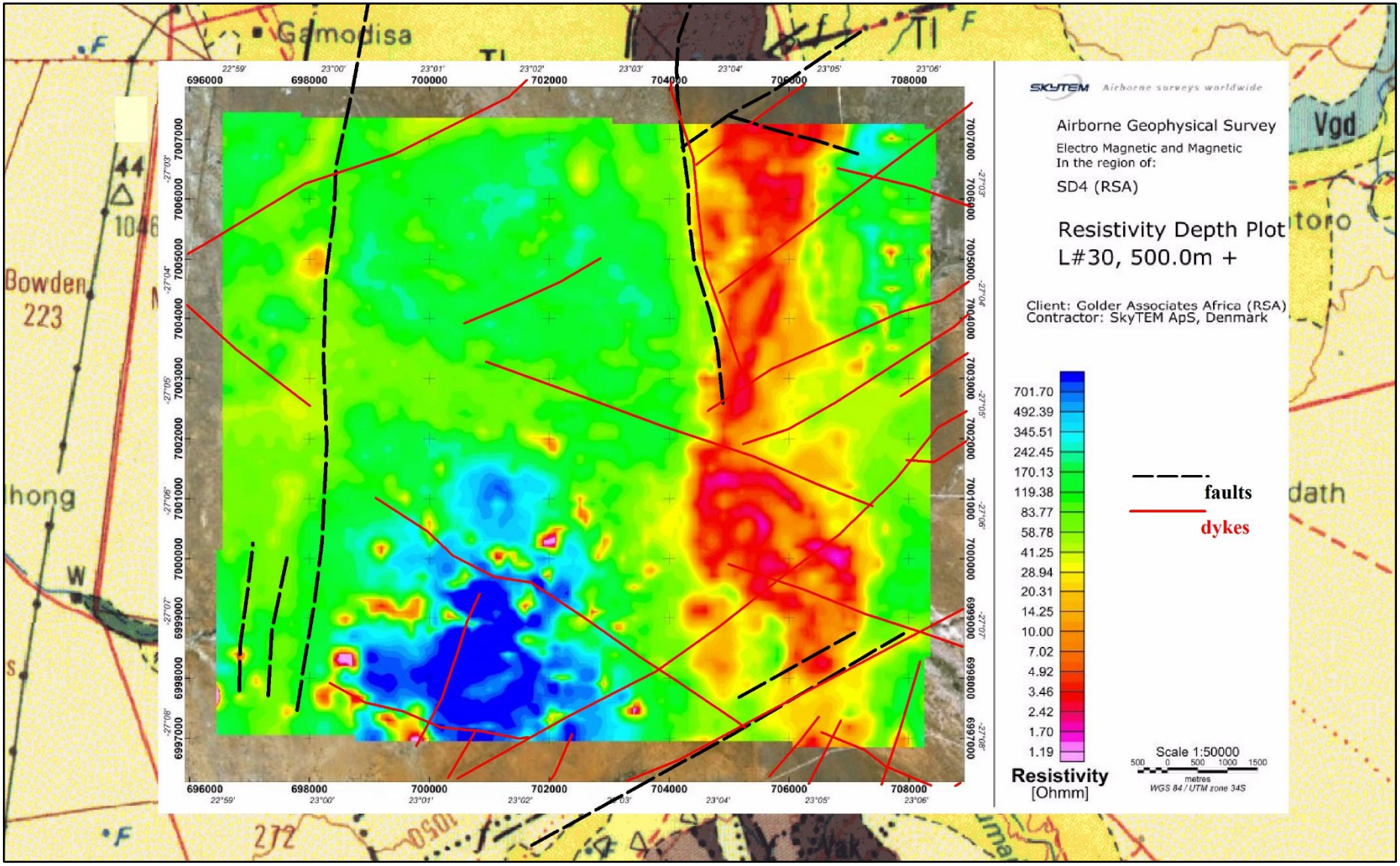

Figure 48: Resistivity distribution at depths in excess of 500 m

5.2.3 **Discussion**

The results of the SkyTEM survey show that this technique can be used to not only map regional changes in the subsurface geology, but also reveal the presence of secondary features of interest during groundwater exploration programmes, such as faults and dykes. The SkyTEM data was also valuable in obtaining first estimates of the depth extents of the various subsurface geological units and secondary geological features.

The geological features identified during the SkyTEM survey can be used to identify preliminary targets for ground geophysical surveys focussing on obtaining more detailed data at a greater resolution in order to site production borehole with greater confidence. In the current investigations, the major geological features that were targeted during the ground geophysical surveys were the Western Fault, the Eastern Fault, the prominent fault in the south-eastern parts of the survey area, as well as localised occurrences of dolomites in the eastern parts of the survey area. The ground geophysical investigations are discussed in Sections 5.3.1 to 5.3.4.

5.3 GROUND GEOPHYSICAL SURVEYS

Ground geophysical work, which consisted of magnetic, electromagnetic, resistivity and gravity surveys, was conducted within area SD4 boundary, as well as across its eastern boundary. The SD4 area was later extended towards the north to include more traverse lines; however, the extended part does not form part of this study. The SD4 traverse lines within and across area SD4 are shown in (Figure 49). The positions and orientations of these traverses were selected so as to run across geological features of interest to the groundwater exploration project, such as dykes, faults, geological contacts and dolomitic areas. These features were identified from the geological map as well as from the results of the SkyTEM survey.

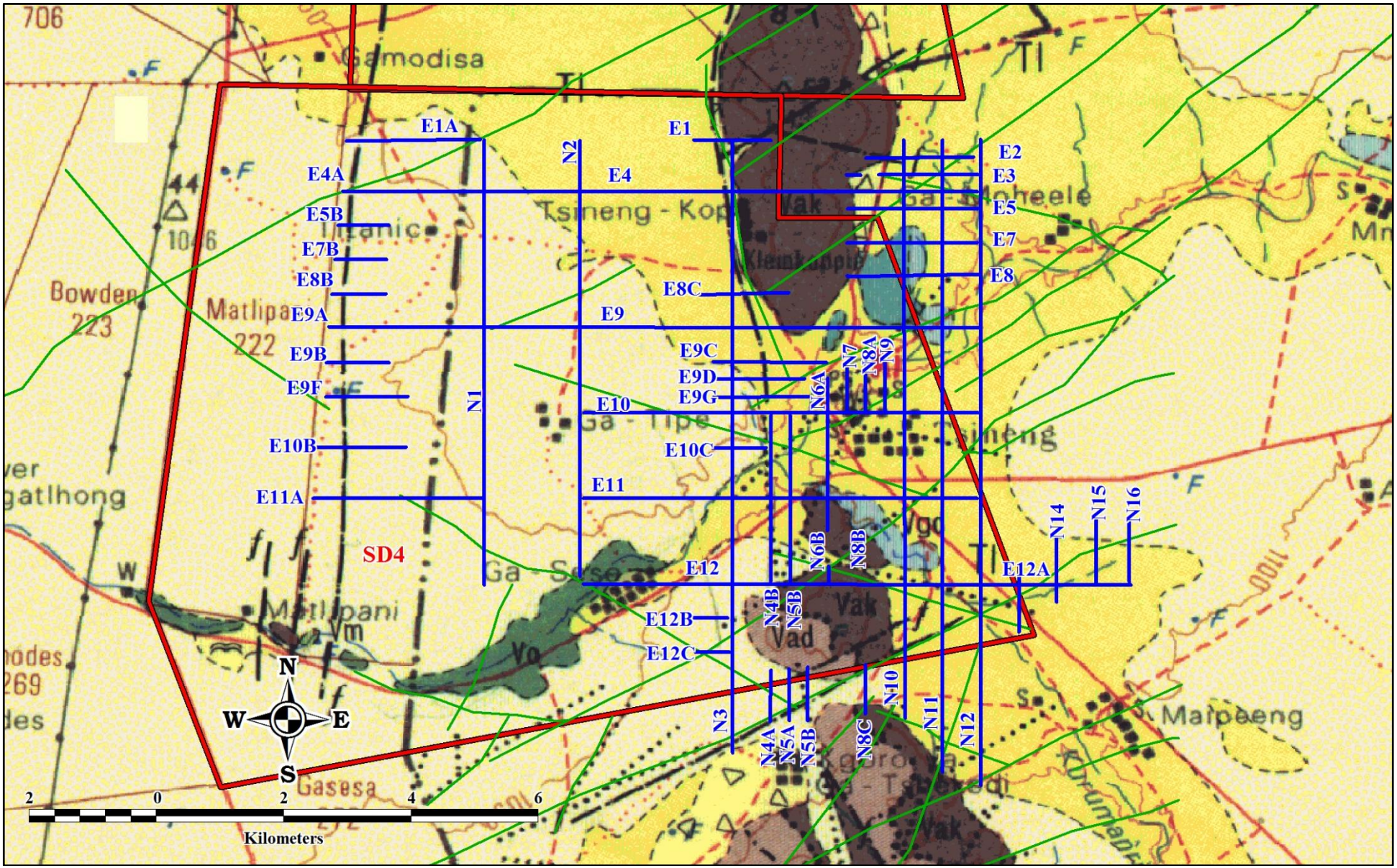

Figure 49: Positions and orientations of the traverses along which ground geophysical data were recorded

5.3.1 **Gravity survey**

The purpose of the gravimetric survey was to provide information on the distribution of subsurface units of differing mass densities. Variations in the mass densities can then be interpreted in terms of the geological units underlying the study area.

The interpretation of gravity data must always be related to the rock densities in the area that is being surveyed. The variations in the rock densities produce the potential field differences that can be observed after data reduction. It is ideal that the rock densities of the area to be surveyed are known prior to the survey being conducted.

The gravity survey of the current investigations was conducted along traverse lines using a Scintrex CG-5 Autograv instrument. The traverse lines were chosen to intersect geological structures such as dykes, faults and contact zones since such structures are often associated with groundwater resources. In addition, the gravity survey targeted those areas within SD4 where dolomitic rocks are known to occur. Dissolution cavities in these rocks are often considered targets during groundwater exploration.

Gravity data was recorded on a station spacing of 50 m. Data was recorded on all the traverses shown in (Figure 49). The lengths of the north-south traverses varied between 270 m and 11.4 km, while the lengths of the east-west traverses varied between 660 m and 10.3 km.

5.3.2 **Magnetic survey**

The purpose of magnetic survey was to detect and map changes in the magnetic properties of the subsurface materials within the study area. From such changes, inferences regarding the subsurface lithology and the presence of geological structures can be made. Magnetic structures, such as dykes, may influence the groundwater regime and may be associated with preferential flow paths.

During the magnetic survey, measurements of the Earth's magnetic field were taken along some of the traverse lines that were also used during the gravity survey (refer to Figure 50). For the magnetic survey, traverses were selected that cross geological features of interest to the groundwater exploration programme. Such features include prominent faults, dykes, and contacts between different geological units. Measurements were taken using a proton precession magnetometer on a station spacing of 10 m.

5.3.3 **Frequency-Domain EM survey**

The purpose of the frequency-domain survey was to measure the variation in ground conductivity. Conductivity data was recorded using the Geonics EM34-3 system along the same traverse lines as

the magnetic survey (Figure 50). This allowed comparison of the results of the EM survey with those of the magnetic survey. Measurements were recorded on a station spacing of 10 m. Both vertical dipole (VD) and horizontal dipole (HD) measurements were taken at each station. Data was recorded using inter-coil spacing of 20 and 40 m, except for traverse E9A on which data was recorded using only a 40 m inter-coil spacing.

5.3.4 **ERT survey**

The purpose of the electrical resistivity tomography (ERT) survey was to detect changes in the subsurface resistivity distribution that could reveal the presence of geological structures along which groundwater may be found.

The ERT survey targeted the major faults known to occur within area SD4, but also incorporated the results of the other geophysical methods to select possible targets. The survey was conducted on selected extents of the 11 traverse lines listed in (Table 9) to investigate the responses of the faults and the origin of some of the anomalies detected with the other geophysical surveys. The positions and orientations of these traverses are shown in (Figure 51).

Table 9: Information on the ERT profiles

Traverse no.	Traverse Length	Technique used	Target Structures	Lithology
N3	1 000 m	Lund	Dyke/Fault	BIF
N4A	900 m	Lund	Dyke/Fault	BIF/Dolomite/Shale
N5A	900 m	Lund	Dyke/Fault	BIF/Dolomite/Shale
N5B	900 m	Lund	Dyke/Fault	BIF/Dolomite/Shale
N8C	850 m	Lund	Dyke/Fault	BIF/Dolomite/Shale
N10	1 200 m	Lund	Dyke	Dolomite/Mudstone
N11	900 m	Lund	Dyke	Dolomite
E4	1 100 m	Lund	Dyke/Fault	BIF/Dolomite
E4A	2 200 m	Lund	Dyke/Fault	BIF/Lava
E9A	900 m	Lund	Dyke/Fault	BIF/Lava
E10B	1 200 m	Lund	Dyke/Fault	BIF/Lava

The Wenner-Schlumberger arrays were selected for the survey, because this array is moderately sensitive to both horizontal and vertical structures. The Wenner-Schlumberger array also has a slightly better horizontal coverage as compared with other common arrays (Loke, 2000).

The field data sets were inverted using the RES2DNV software to obtain models of the subsurface resistivity distribution along the selected profiles.

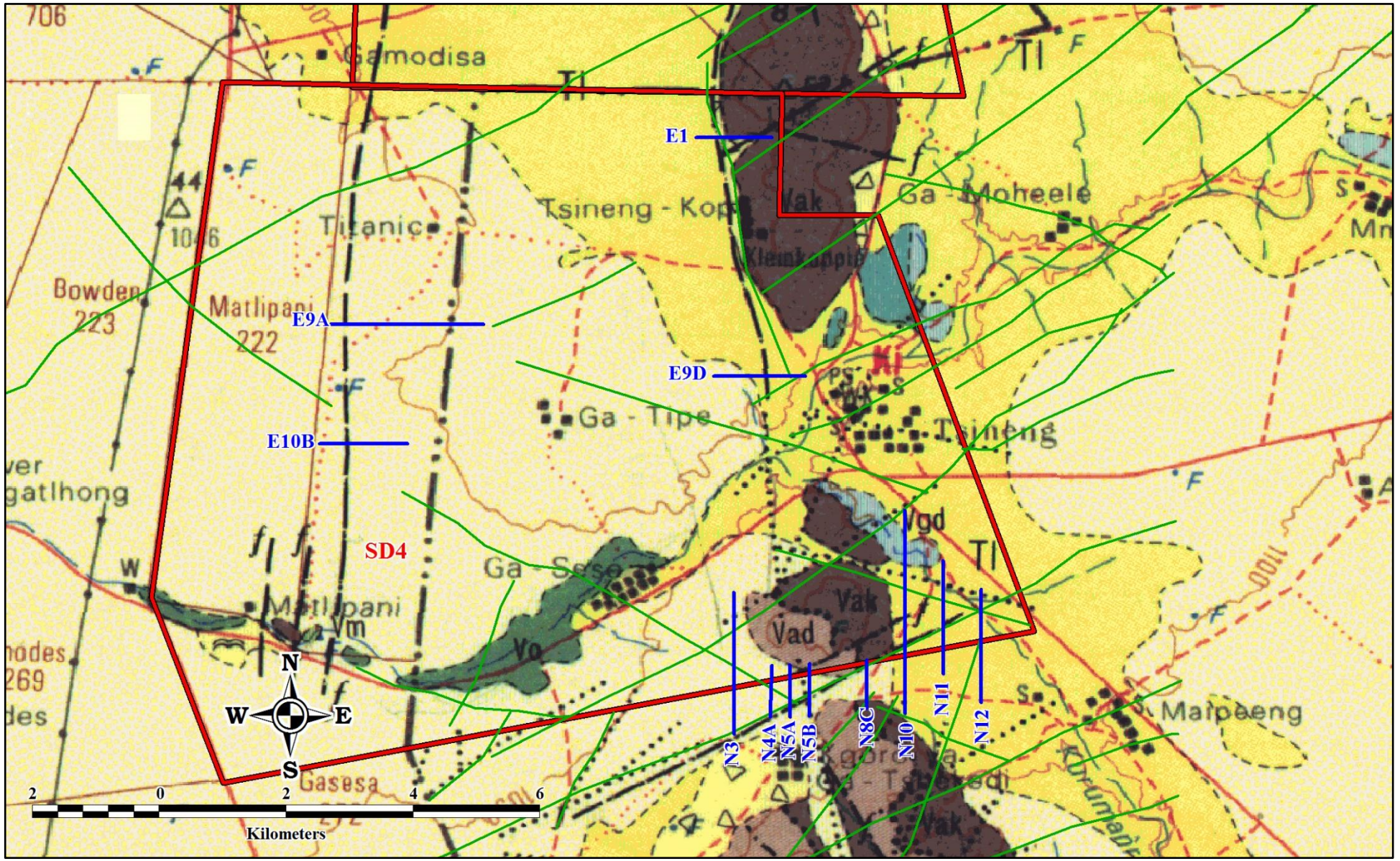

Figure 50: Positions and orientations of the traverses along which ground magnetic and EM data were recorded

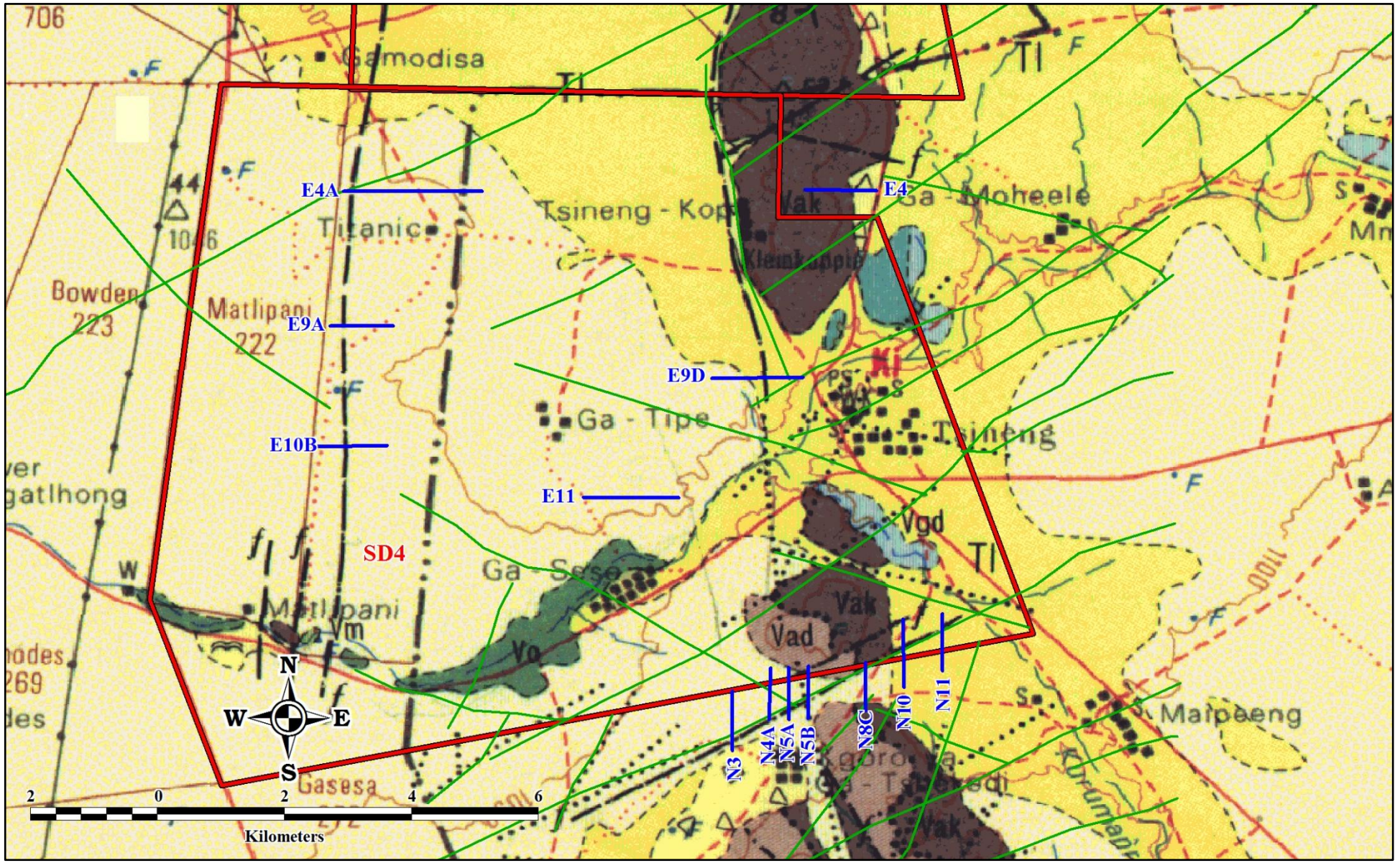

Figure 51: Positions and orientations of the profiles along which ERT data were recorded

5.3.5 Ground geophysical survey results

5.3.5.1 Results of gravity survey

A contour map of the residual gravity values is present in (Figure 52). Areas of mass surplus (red colours) and mass deficit (blue colours) can clearly be discerned in the contour map.

The manifestation of the prominent Western Fault is seen in the contour map as the transition from an area with a mass surplus to a near-linear zone of mass-deficit running approximately parallel to the mapped position of the fault (refer to the geology map in Figure 16). The Eastern Fault also manifests itself in the gravity contour map as a linear zone of local mass deficit (refer to Figure 52).

A broad near-linear zone of mass deficit with an approximate south/north strike corresponds well with the outcrops of banded iron formation within the study area. This mass deficit is surprising because banded iron formation typically have large specific mass densities (5.0-5.3 g/cm^3). It is possible that the observed mass deficit relates to the presence of dolomitic rocks known to occur in the area.

5.3.5.2 Results of geophysical surveys on selected traverses

Since many of the geophysical traverses investigate the same geological features, the results of the surveys on only a selected number of traverses are discussed here:

- Gravity, magnetic, EM and ERT data were recorded across the Western Fault on traverses E9A and E10B.
- Gravity, magnetic, and EM data were recorded across the Eastern Fault on traverse E1, while gravity and magnetic data were recorded across this fault on traverse E9D.
- Gravity data and ERT data were recorded on traverse E11 at a position near the centre of area SD4.
- Gravity, magnetic, EM and ERT data were recorded on traverses N3, N8C, N10 and N11 across a fault, and possibly a parallel dyke, near the southern border of SD4.

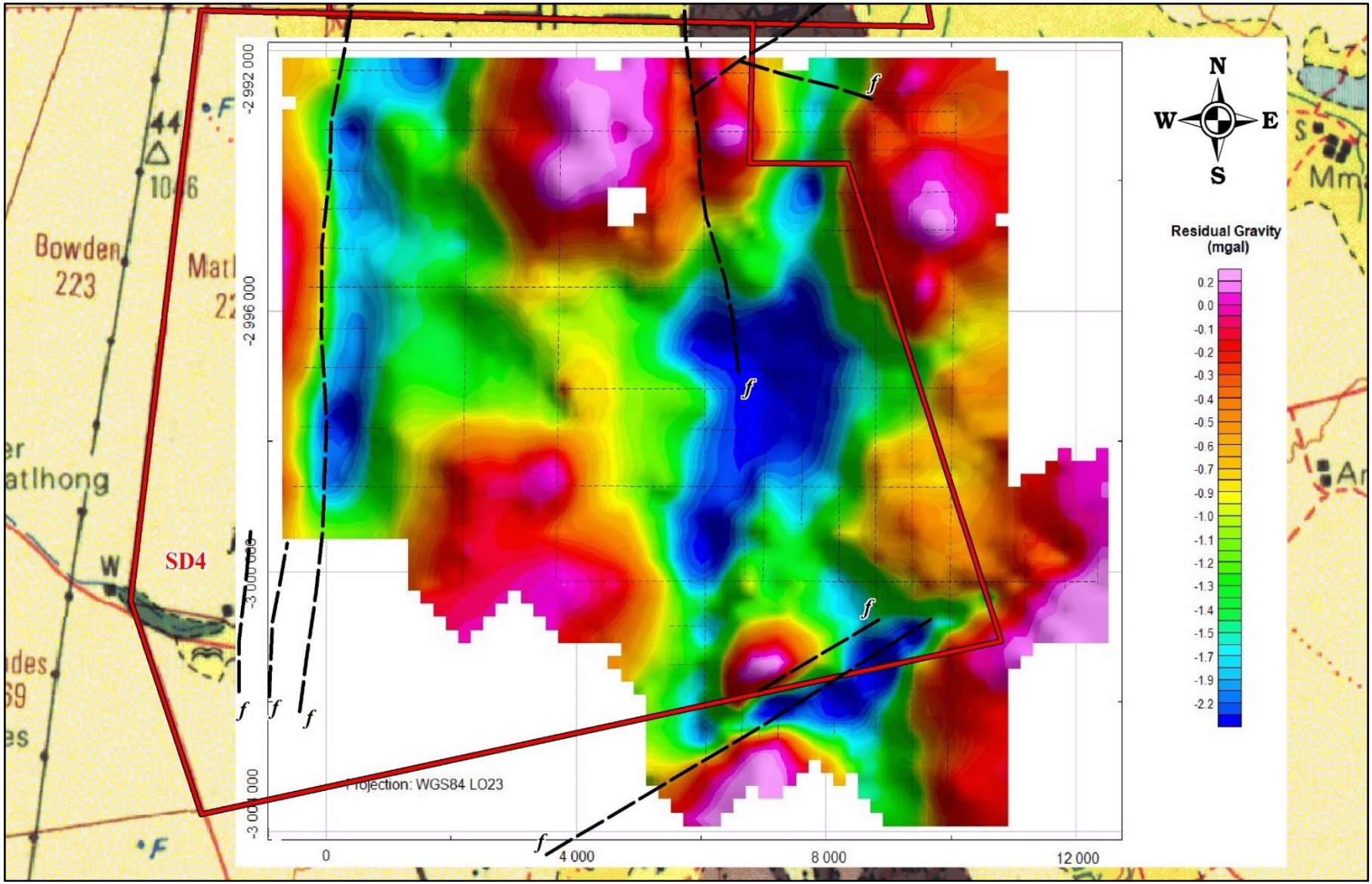

Figure 52: Contour map of residual gravity value

5.3.5.2.1 Results of geophysical surveys across Western Fault

Traverse E9A

Traverse E9A had a total length of 2 400 m. Gravity data was recorded along the entire length of the traverse, while magnetic and EM data were recorded along the western 1 500 m and ERT data along the western 900 m of the traverse. The results of the gravity, magnetic and EM surveys are presented as profile plots in (Figure 53, Figure 54 and Figure 55), respectively. The inverse resistivity model created from the ERT data recorded along this traverse is shown in (Figure 56).

In the profile plot of the residual gravity values, a prominent change in the average mass densities of the earth materials can be seen in the western parts of the profile where the residual gravity values decrease from approximately -0.4 mgal to approximately -1.85 mgal over a distance of 400 m (refer to Figure 53). This change in the mass densities is probably related to the presence of the Western Fault and suggests that rocks of different densities occur on either side of the fault.

The profile plot of the total magnetic field displays a very similar response to the behaviour of the residual gravity values. A prominent decrease in the magnetic field strength from approximately 28 250 nT to 27 000 nT is observed across the first 400 m of the traverse (refer to Figure 54). This observation also suggests that there is material of different magnetic properties that are in contact with one another in the western part of the traverse. This is again likely to be due to the presence of the Western Fault.

The apparent conductivity values recorded with in the VD mode show a very prominent increase in conductivities in the vicinity of station 400 m (refer to Figure 54). This anomaly coincides with the positions of the gravity and magnetic lows as observed in (Figure 53 and Figure 54), respectively. A less prominent anomaly is also observed in the profile of the data recorded using the HD mode. Since the VD mode has a greater depth of exploration, it appears that the changes in conductivity associated with the Western Fault are more pronounced at greater depths.

The inverse resistivity model for the ERT data recorded along the first 900 m of the traverse reveals a zone of high resistivity at shallow depths, underlain by more conductive material. The resistive material at the surface is in all likelihood representatives of the Kalahari sands known to occur in the area. The more conductive material at depth is likely to be Ongeluk lavas. A prominent zone of very low resistivities occurs near the centre of the ERT profile. This zone starts near station 400 m and seems to extend farther to the east. This zone is in all likelihood associated with the Western Fault known to occur in this area.

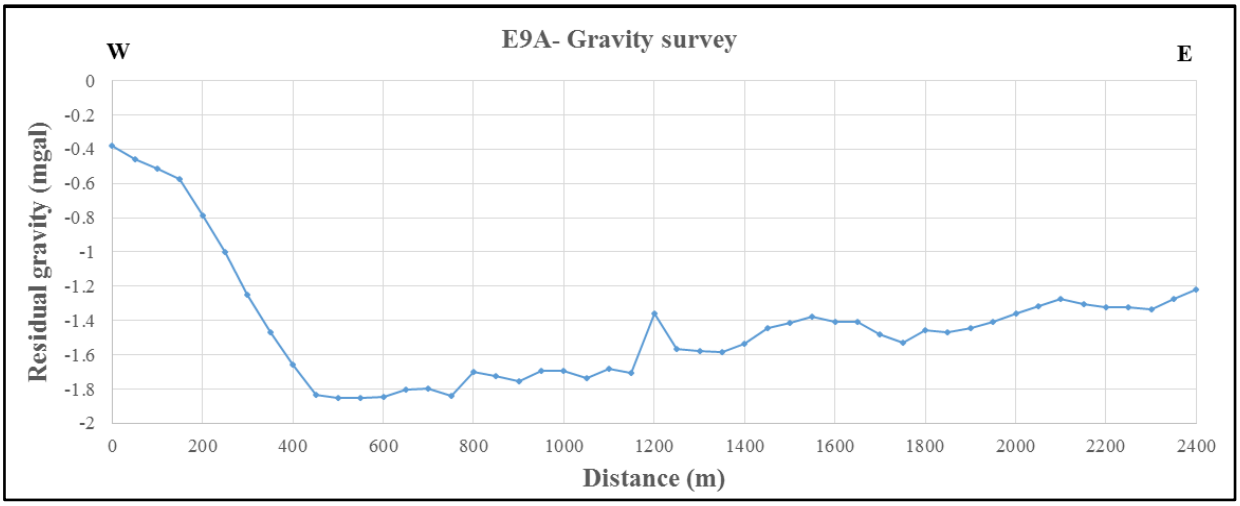

Figure 53: Residual gravity values along traverse E9A

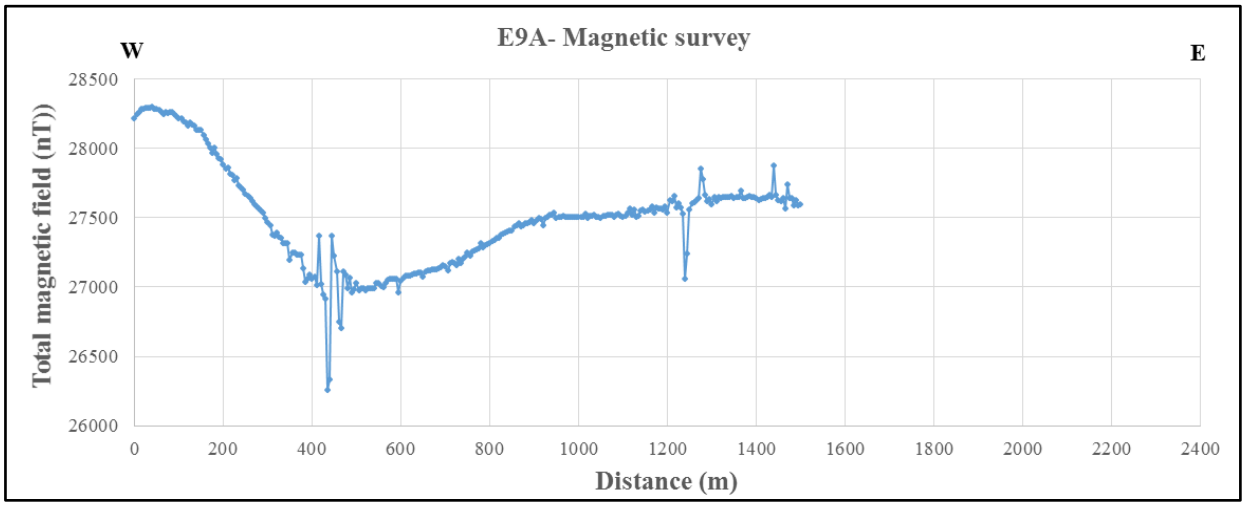

Figure 54: Total magnetic field recorded along traverse E9A

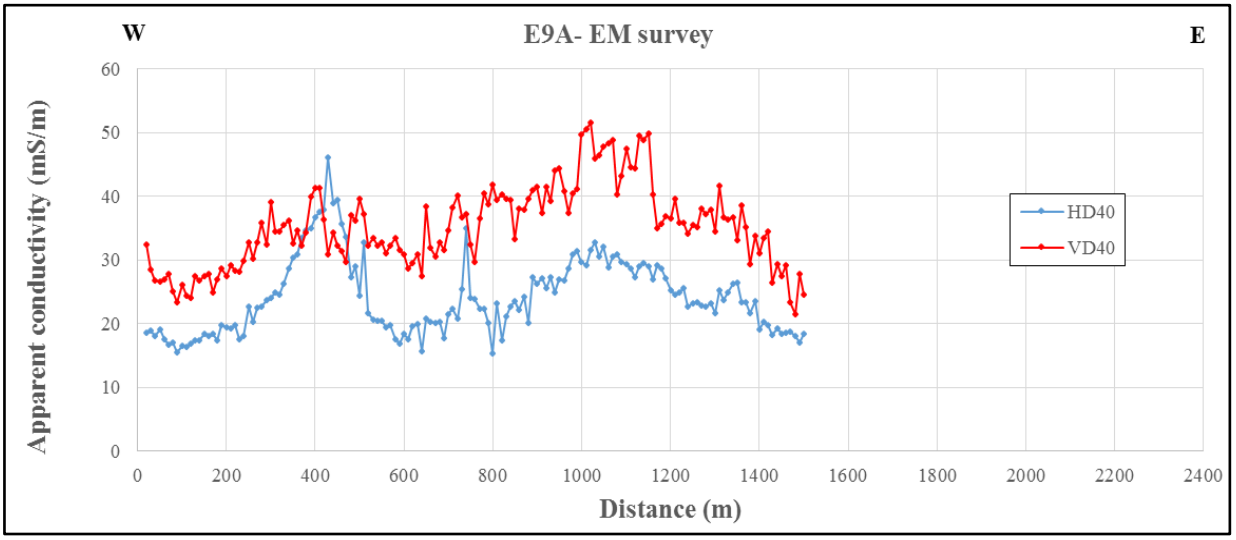

Figure 55: Apparent conductivity values along traverse E9A

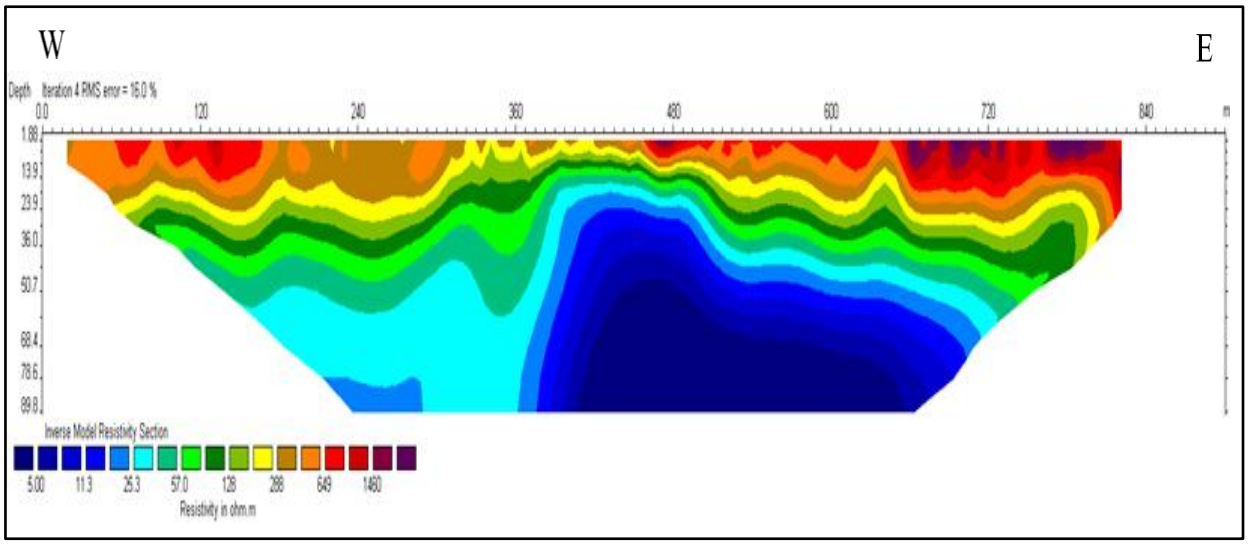

Figure 56: Inverse resistivity model along traverse E9A

Traverse E10B

Traverse E10B had a total length of 1 400 m. Gravity, magnetic and EM data were recorded over the entire the length, while the ERT data was recorded along the western 1 200 m traverse. The results of the gravity, magnetic and EM survey are presented as profile plots in (Figure 57, Figure 58 and Figure 59), respectively. The inverse resistivity model created from the ERT data recorded along this traverse is shown in (Figure 60).

In the profile plot of the residual gravity values, a prominent change in the average mass densities of the earth materials can be seen in the western parts of the profile where the residual gravity values decrease from approximately -0.9 mgal to approximately -2.5 mgal over a distance of 550 m (refer to Figure 57). This change in the mass densities is probably related to the presence of the Western Fault and suggests that rocks of different densities occur on either side of the fault.Farther east, along the traverse; a gradual increase in the average mass densities of the subsurface materials is observed. The geological reason for this gradual increase is at present unknown.

The profile plot of the total magnetic field displays a very similar response to the behaviour along Traverse E9A (refer to Figure 54). A prominent decrease in the magnetic field strength from approximately 28 800 nT to 26 600 nT is observed between station 200 m and 400 m (refer to Figure 58). This observation also suggests that there is material of different magnetic properties that are in contact with one another in the western part of the traverse. This is again likely to be due to the presence of the Western Fault.

The apparent conductivity profiles recorded along Traverse E10B are shown in (Figure 59). Since the HD mode has a shallower depth of investigation than the VD mode, and since larger coil separations lead to greater depths of investigation, it can be concluded that the conductivity of the

subsurface materials increases with depth. The four profiles exhibit the same general behaviour and suggest near-horizontal layering (a layered earth model).

For the 40 m coil separations, the maximum conductivities are seen to occur near station 500 m. The HD mode in particular displays a prominent increase in the conductivities near this position. This zone of increased conductivities corresponds well with the position of the local magnetic minimum recorded across the Western Fault (refer to Figure 58). The increased conductivities may indicate a higher degree of weathering and/or a larger moisture content in the subsurface associated with the Western Fault.

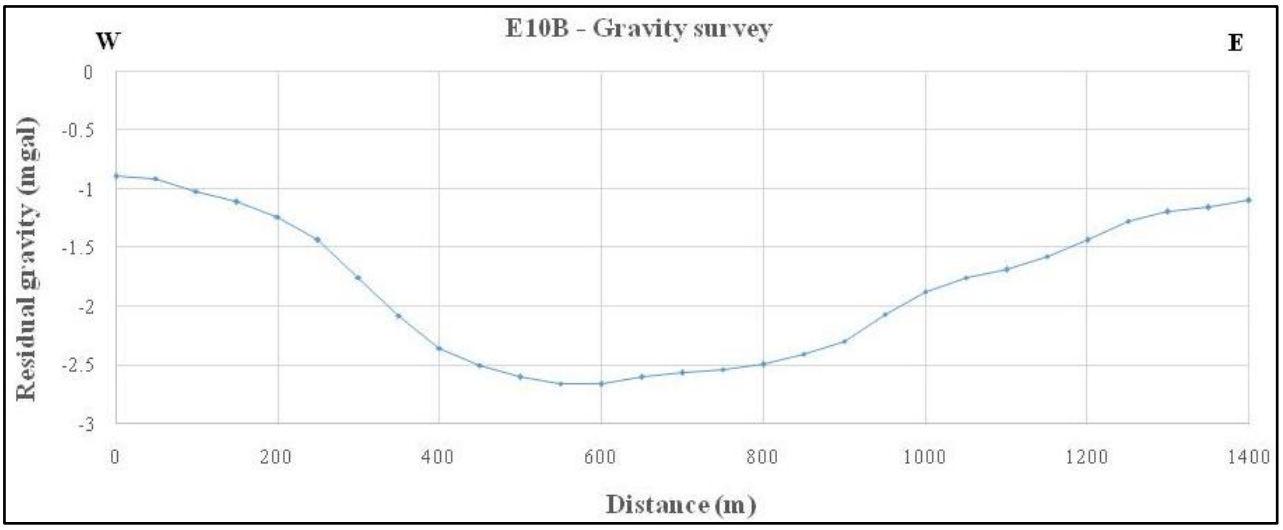

Figure 57: Residual gravity values along traverse E10B

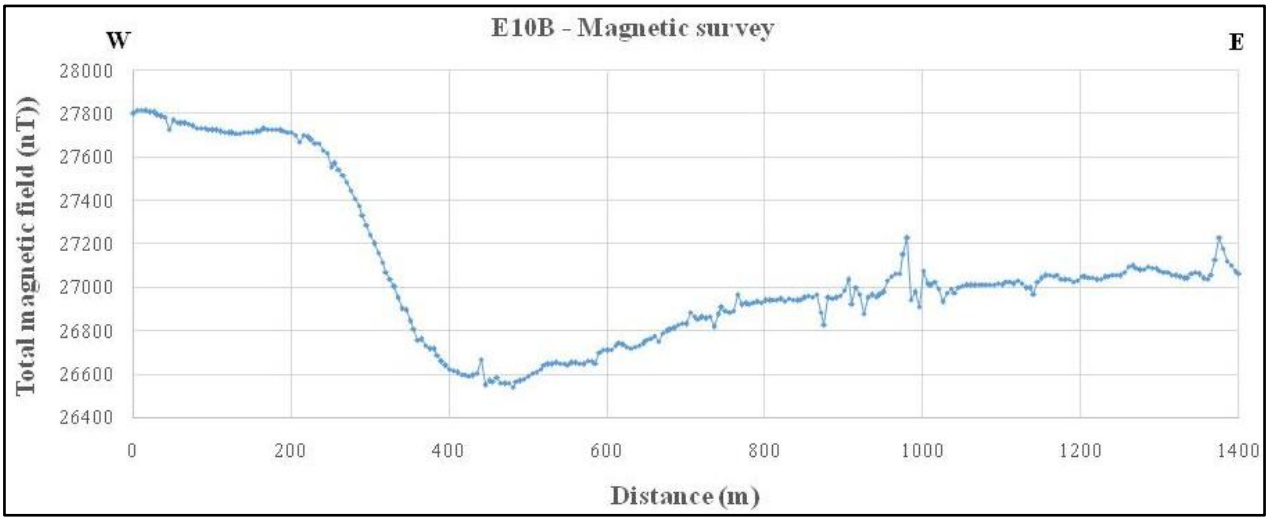

Figure 58: Total magnetic field recorded along traverse E10B

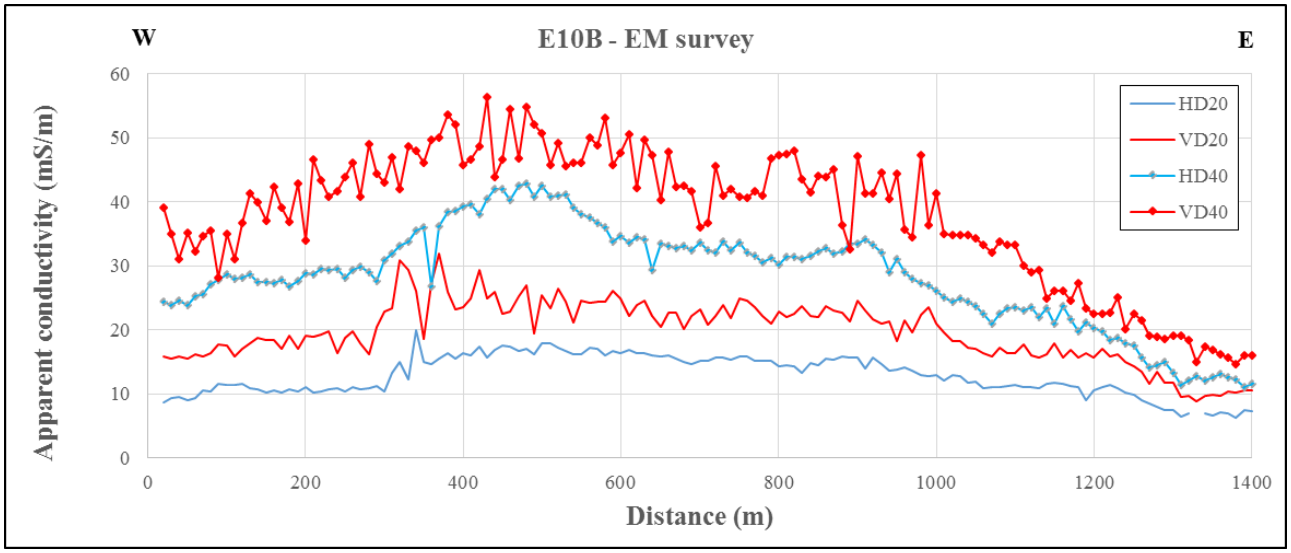

Figure 59: Apparent conductivity values along traverse E10B

The inverse resistivity model for the ERT data recorded along the 1 200 m of the traverse reveals a zone of high resistivity at shallow depths, underlain by more conductive material. The resistive material at surface is in all likelihood a representative of the Kalahari sands known to occur in the area. This layer is underlain by a less resistive layer of varying thickness. A localised zone of very low resistivities occurs between stations 300 m and 500 m. This zone corresponds well with the zone of local increased conductivities observed in the EM profiles (see Figure 59), and may be due to the fracturing associated with the Western Fault. The resistive material that underlies the less resistive layer is likely to be Ongeluk lavas.

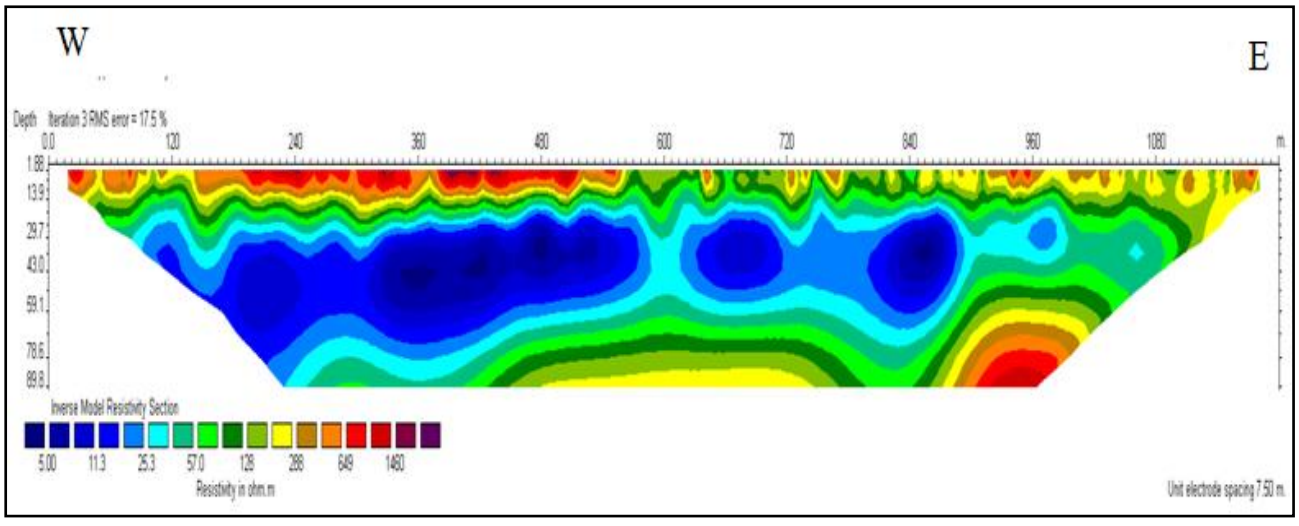

Figure 60: Inverse resistivity model along traverse E10B

5.3.5.2.2 Results of geophysical surveys across Eastern Fault

Traverse E1

Traverse E1 had a total length of 1 200 m. The gravity, magnetic and EM were recorded over the entire the length of the traverse. No ERT was done along this traverse. The results of the gravity, magnetic and EM survey are presented as profile plots in (Figure 62, Figure 63 and Figure 64), respectively.

Although some variations in the values of the residual gravity data are observed, no prominent anomalies can be identified (Figure 61). It does; however appear that local mass deficits are present along the first 400 m of the traverse. These mass deficits may be related to the presence of the Easter Fault, which occurs near these positions (see Figure 49). Farther to the east along the traverse, positive residual gravity values occur, indicating that more dense material underlies these parts of the traverse. These denser materials appear to be the banded iron formations known to underlie the area.

The total magnetic field profile shows a stable magnetic field from station 0 m to 380 m, with a decreasing regional trend (refer to Figure 62). This stable behaviour is in sharp contrast to the erratic magnetic field observed at positions to the east of station 380 m. The variable magnetic field intensity to the east of station 380 m is in all likelihood due to the banded iron formations that occur in the study area.

The profile plots of the apparent conductivity show prominent conductivity increases near station 380 m. This is true for both the VD and HD modes, and both the 20 m and 40 m coil separations. The positions of these increases in conductivity coincide with the position where the magnetic field changes from stable to erratic (see Figure 62). The increased conductivities are most probably due to the presence of the Eastern Fault, which occurs to the west of the outcrops of banded iron formations (refer to Figure 49). The fact that conductivity anomalies are seen on all the profiles, corresponding to different depths of investigation, suggests that the zone of higher conductivity extends from surface to depths in excess of 40 m.

Near station 900 m, another local increase in the apparent conductivity is observed. This anomaly occurs in the both the profiles recorded with the HD mode, but is prominent in only the 20 m-profile recorded with the VD mode. The increases in the apparent conductivities are most likely associated with another fault cross cutting the traverse (refer to Figure 49). The fact that this zone of high conductivity is not observed in the VD mode with a 40 m separation, suggests that the conductive zone associated with the fault has a limited depth extent.

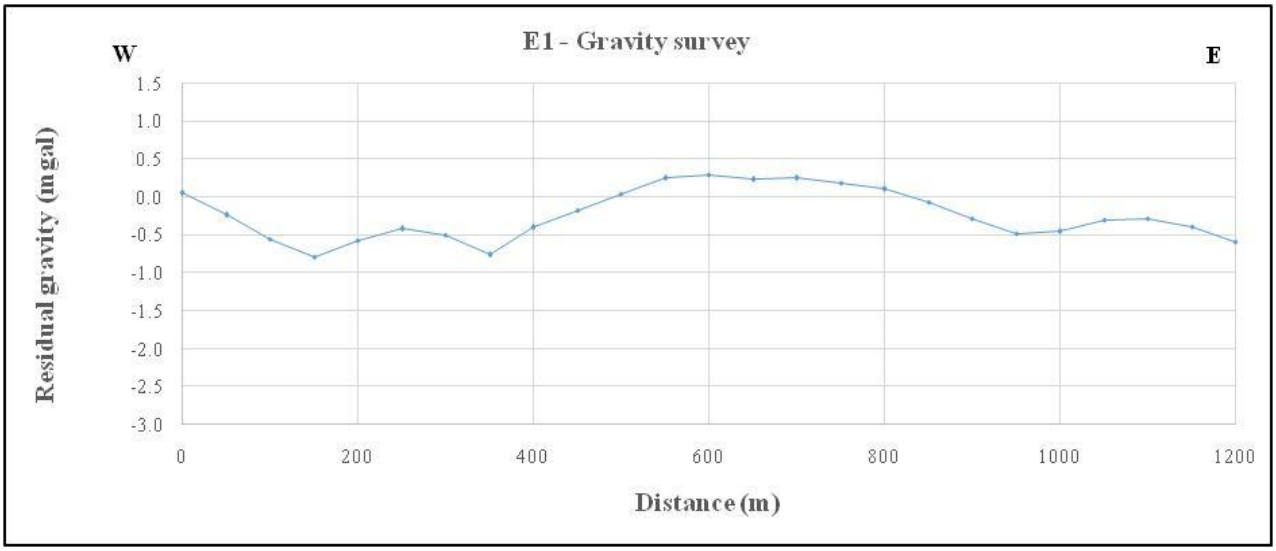

Figure 61: Residual gravity values along traverse E1

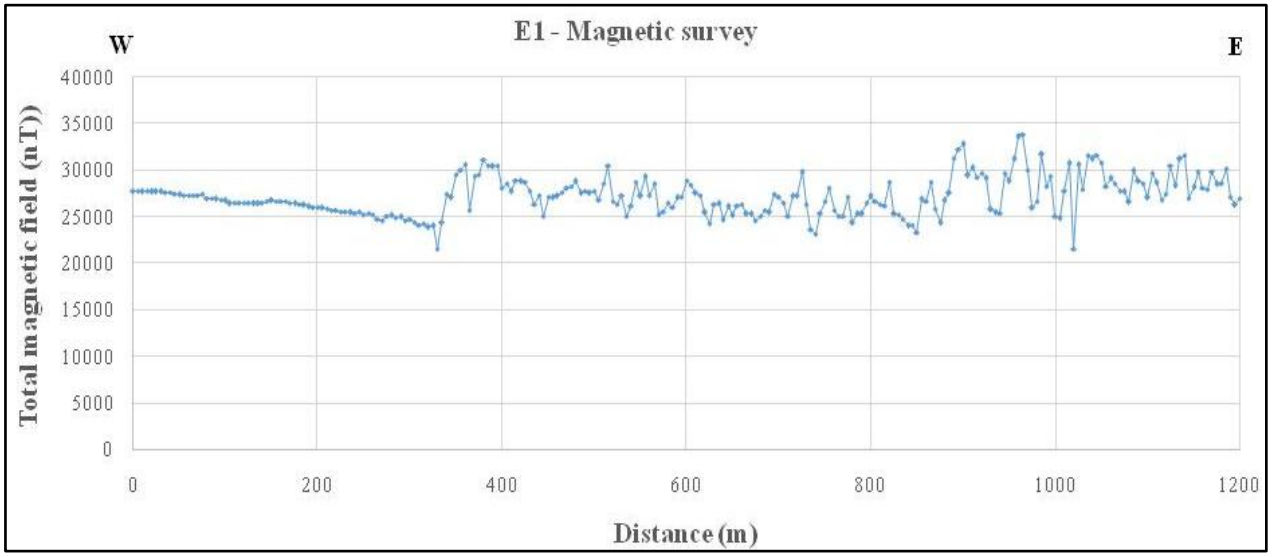

Figure 62: Total magnetic field recorded along traverse E1

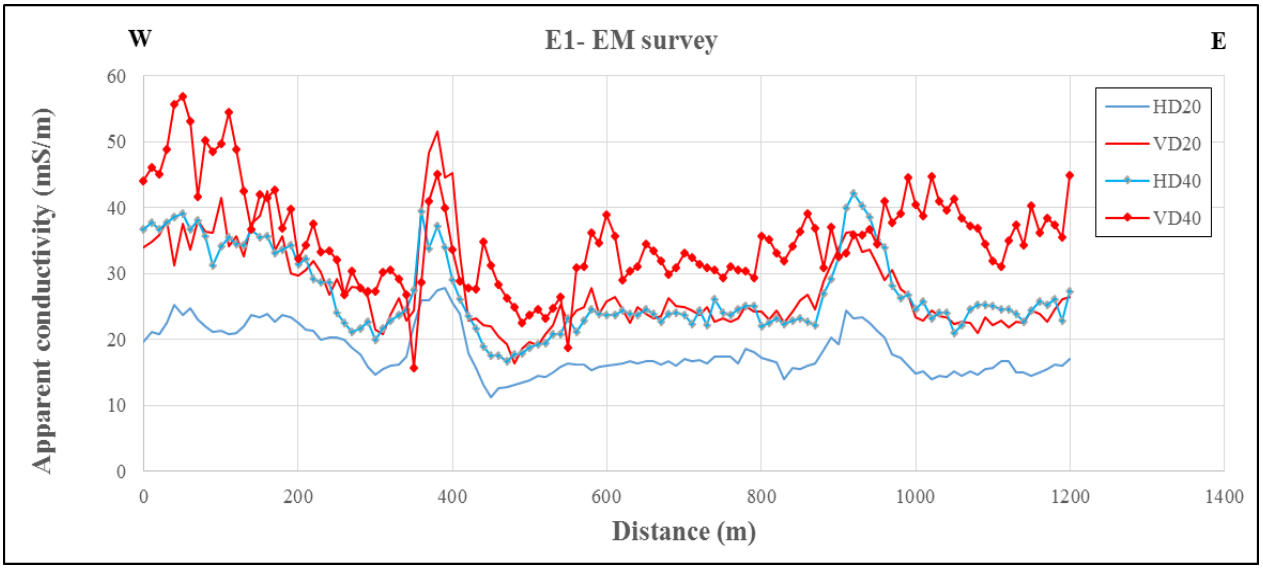

Figure 63: Apparent conductivity values along traverse E1

Traverse E9D

Traverse E9D had a total length of 1 450 m. Gravity data was recorded for the entire length while magnetic was recorded for the first 1 400 m of the traverse. The results of the gravity and magnetic are presented as profile plots in (Figure 64 and Figure 65). ERT data was also recorded on this traverse but unfortunately the data was lost prior to processing.

In the plot the residual gravity decreases from approximately -2.25 mgal to approximately -3.1 mgal over a distance of 200 m. The change in residual gravity is in all likely due to the different earth materials traversed. The western part of the traverse occurs in an area underlain by Kalahari sands overlying Ongeluk lavas, while Tertiary deposits occur in the eastern part. Different mass densities can be expected for the lavas and limestones. The Eastern Fault has been mapped near the centre of the traverse; however, no prominent gravity anomaly is observed in the vicinity of the mapped fault.

The profile of the total magnetic displays a gradual decrease in magnetic field strength between stations 0 m and 500 m. To the east of station 500 m, a gradual increase in the magnetic strength in observed. These regional changes in the magnetic field reflect regional changes in the magnetic properties of the subsurface materials. An erratic magnetic field is observed between stations 1 000 m and 1 300 m. The variable magnetic field indicates the presence of highly magnetic materials, and could be attributed to the banded iron formations outcropping in the area. As on Traverse E1, the position where the magnetic field changes from stable to variable is likely to indicate the position of the Eastern Fault which occurs immediately west of the banded iron formations.

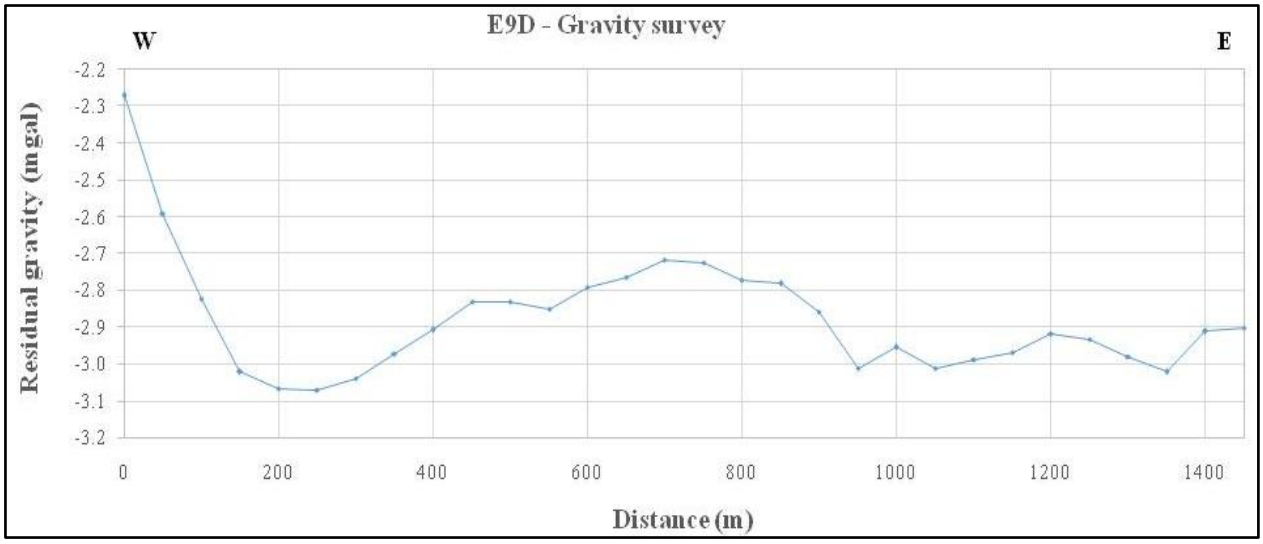

Figure 64: Residual gravity values along traverse E9D

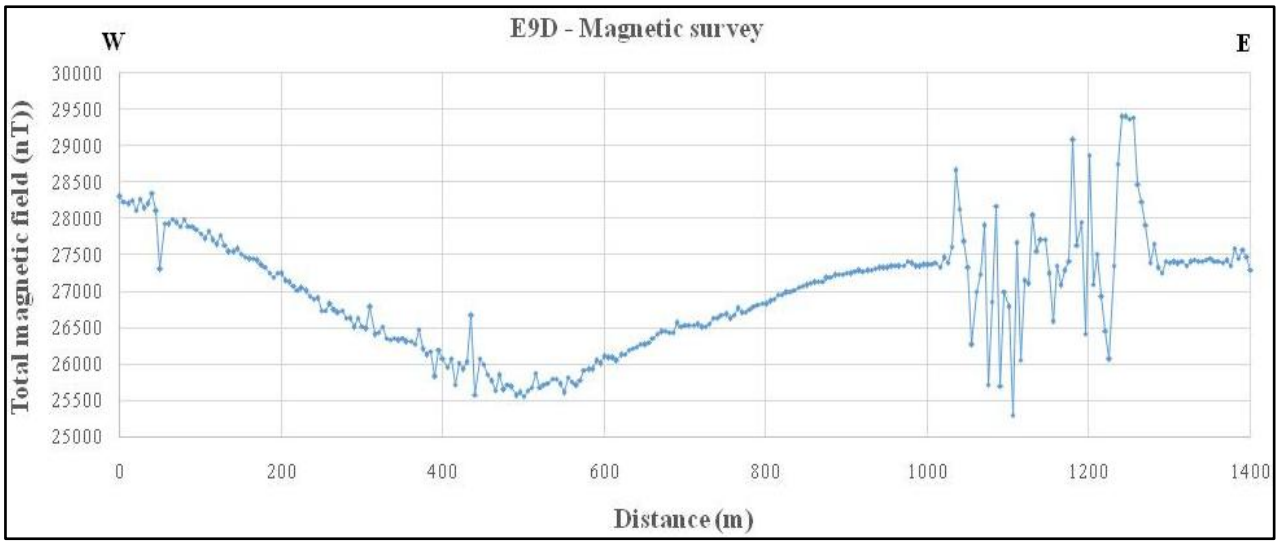

Figure 65: Total magnetic field recorded along traverse E9D

5.3.5.2.3 Results of geophysical surveys across fault and dyke near southern border of SD4

Traverse N3

The traverse N3 had a total length of 2 550 m and a south/north strike. Gravity, magnetic and EM data were recorded along the entire length of the traverse, while ERT data was recorded on 1 000 m stretch of the traverse. The results of the gravity, magnetic and EM are presented in (Figure 66, Figure 68 and Figure 68), respectively. The inverse resistivity model created from the ERT data recorded along this traverse is shown in (Figure 69).

The gravity profile shows a fluctuating residual gravity value along most of the traverse. The negative gravity anomalies in the northern parts of the traverse may be related to the presence of the Eastern Fault. Along the remainder of the traverse, the changing gravity values may reflect the different lithologies with different mass densities crossed by the traverse. These lithologies include: surficial Kalahari sand deposits, Tertiary limestone deposits, Ongeluk lavas, and banded iron formations (refer to Figure 49).

The total magnetic field strength in (Figure 67) displays large variability along the northern and southern parts of the profile. These variable fields again point towards the presence of banded iron formations at surface and in the subsurface. Between stations 700 m and 1 700 m, the magnetic field displays more gradual changes (the spikes in the data near the centre of the profile are due to bad data). Along this stretch of the traverse, Ongeluk lavas are thought to underlie the Kalahari sand and Tertiary deposits.

The apparent conductivity values recorded with the 20 m coil separations were generally significantly lower than with the 40 m coil separations (see Figure 68). This shows that the deeper earth materials along the traverse are generally more conductive than the shallower materials.

A number of prominent localised conductivity anomalies are observed along the traverse. The anomaly near station 450 m could be due to intensive fracturing associated with the Eastern Fault. The geological reason for a large anomaly near station 1 600 m is at present unknown. A prominent anomaly near the southern end of the profile may be related to the fault that has been mapped in this area.

The apparent anomaly near station 1 040 m is in all likelihood due to overhead power lines that occur at this position.

The inverse resistivity model for the ERT data recorded along the first 1 000 m of the traverse is shown in (Figure 69). The ERT profile shows a high resistivity layer near surface which overlies a thick zone of low resistivity. The shallow high resistivity layer is most probably due to the Kalahari sands present in the study area. A localized zone of low resistivities is observed near station 450 m. This zone corresponds to the position of the conductivity anomalies (refer to Figure 68) and may again be related to the Eastern Fault.

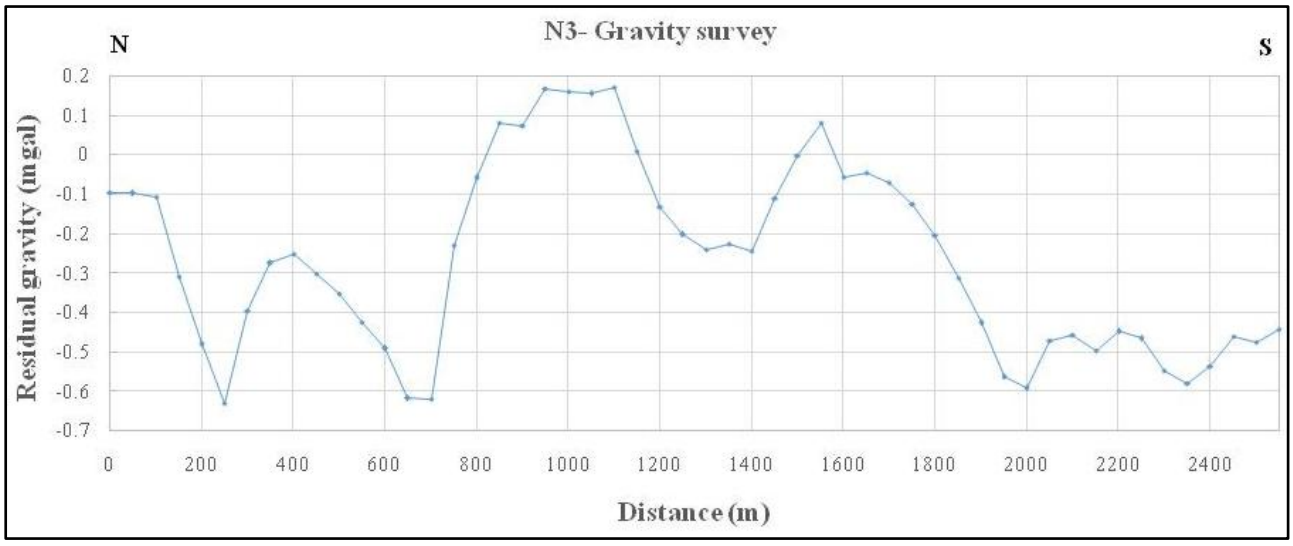

Figure 66: Residual gravity values along traverse N3

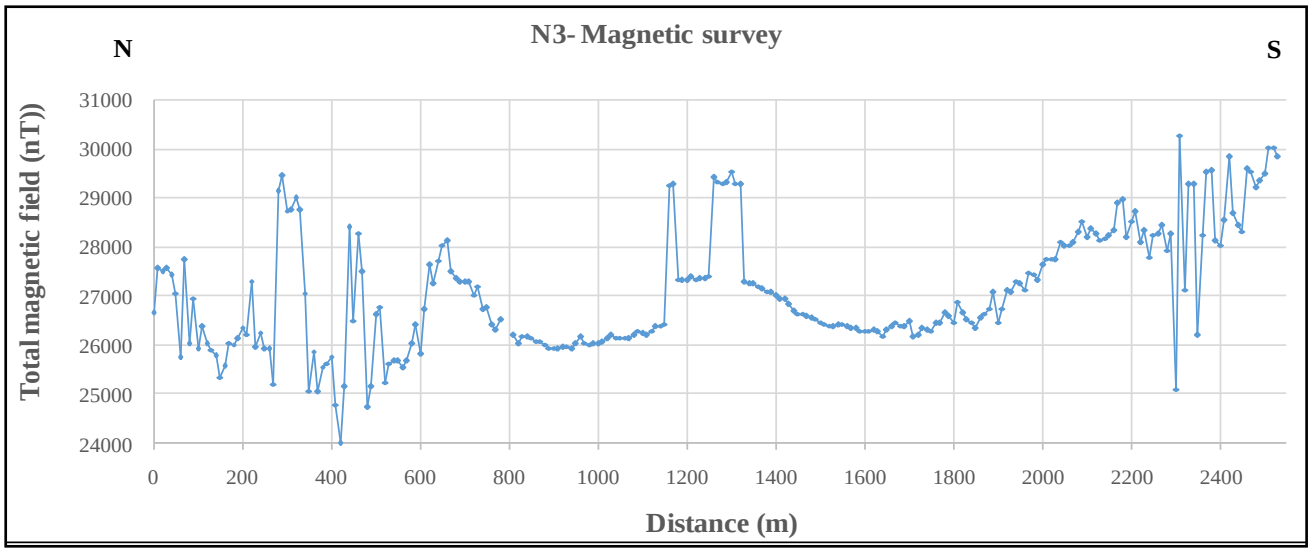

Figure 67: Total magnetic field recorded along traverse N3

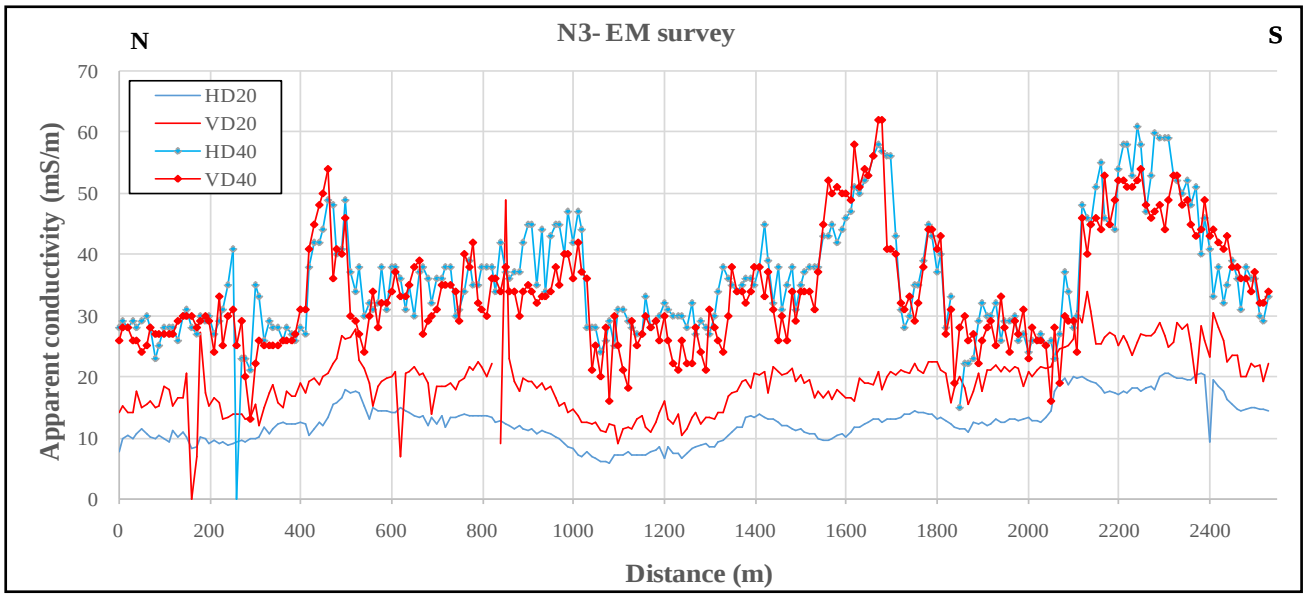

Figure 68: Apparent conductivity values along traverse N3

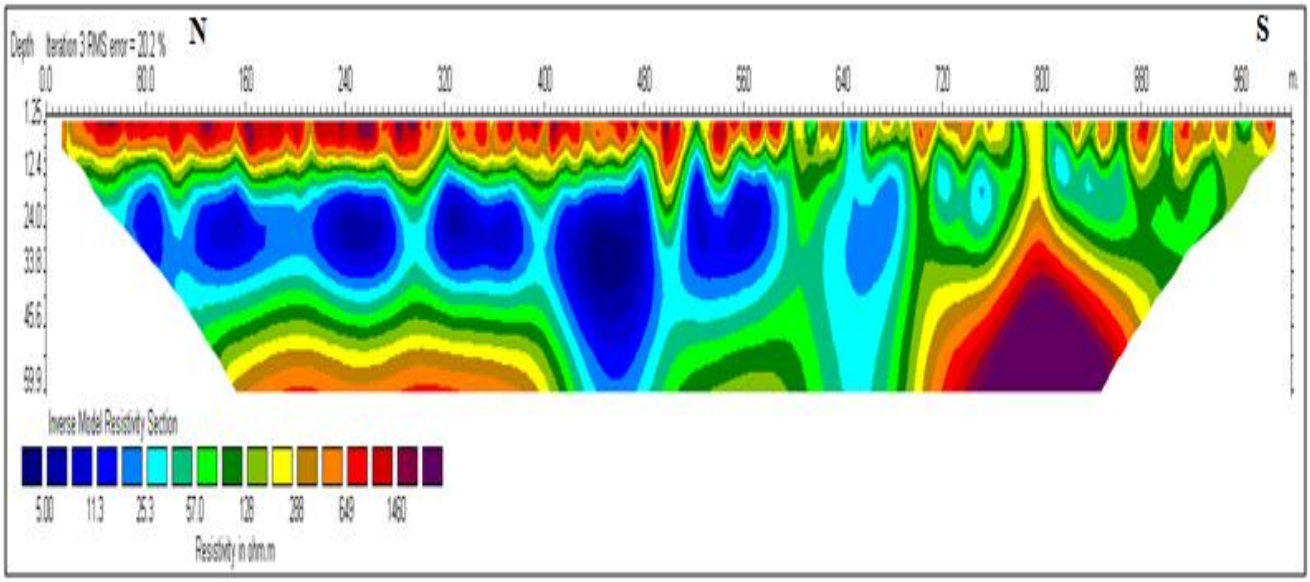

Figure 69: Inverse resistivity model along traverse N3

Traverse N8C

Traverse N8C had a total length of 900 m. Gravity data was recorded for the first 850 m of the traverse. The results of the gravity, magnetic and EM data are presented as profile plots in (Figure 70, Figure 71 and Figure 72), respectively. The inverse resistivity model created from the ERT data recorded along this traverse is shown in (Figure 73).

The residual gravity values show that the central part of the traverse is underlain by material of lower mass density than the near the start and end of the traverse (see Figure 70). The higher densities at the respective ends of the traverse appear to be due to the banded iron formations outcropping in these areas (refer to Figure 49). Although a prominent fault appears to be associated with the northern outcrop, no clear evidence for the presence of this fault is seen in the gravity data.

The magnetic profile in (Figure 71) shows a variable data in the northern and southern parts of the traverse. These variable magnetic field strengths may again be attributed to the presence of the banded iron formations at these positions. The profile shows stable readings between stations 50 m and 800 m, suggesting that this stretch of the traverse is not underlain by rocks with high magnetic susceptibilities.

The plots of the apparent conductivity data (Figure 72) show lower conductivities in the northernmost and southernmost parts of the traverse. These lower conductivities are likely to be due to the outcrops of banded iron formations in these areas. Higher apparent conductivities in the central parts of the traverse most probably reflect the conductivities of the Tertiary limestones that occur at these positions. The apparent conductivity data show that the deeper earth materials are generally more conductive than the shallower materials.

A positive conductivity anomaly occurs in the vicinity of station 250 m. This anomaly is seen on all the profiles, although its presence is less clear on the VD profile with a 40 m coil separation. This anomaly may be associated with the fault that occurs in the northern parts of the traverse.

The inverse resistivity model (Figure 73) confirms the presence of this zone of low resistivity (high conductivity) observed in the EM data near station 250 m.

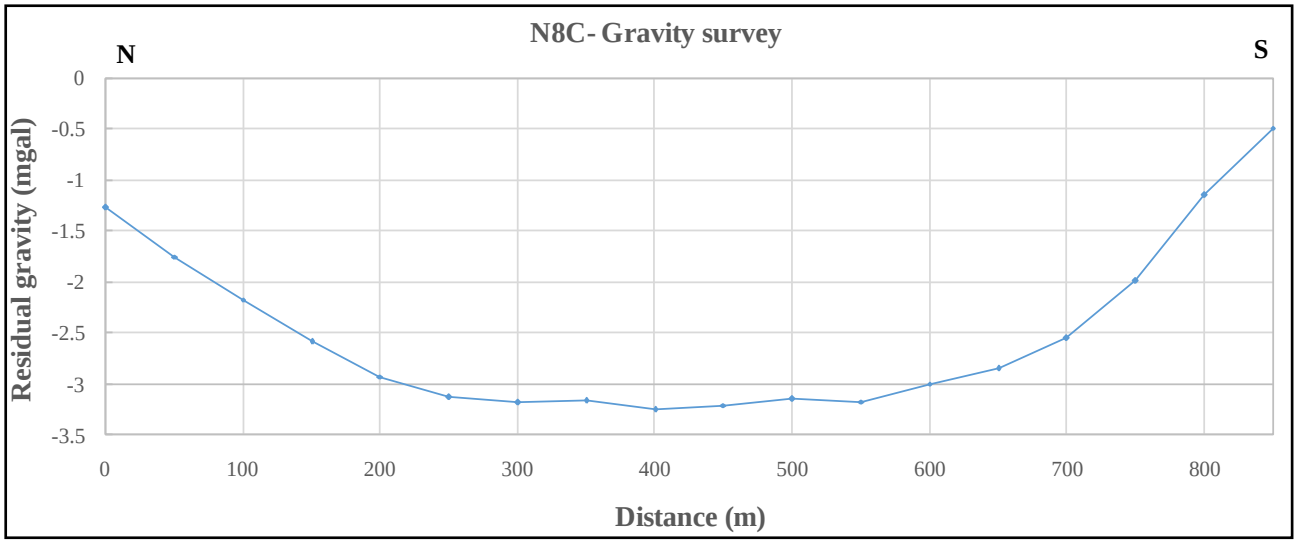

Figure 70: Residual gravity values along traverse N8C

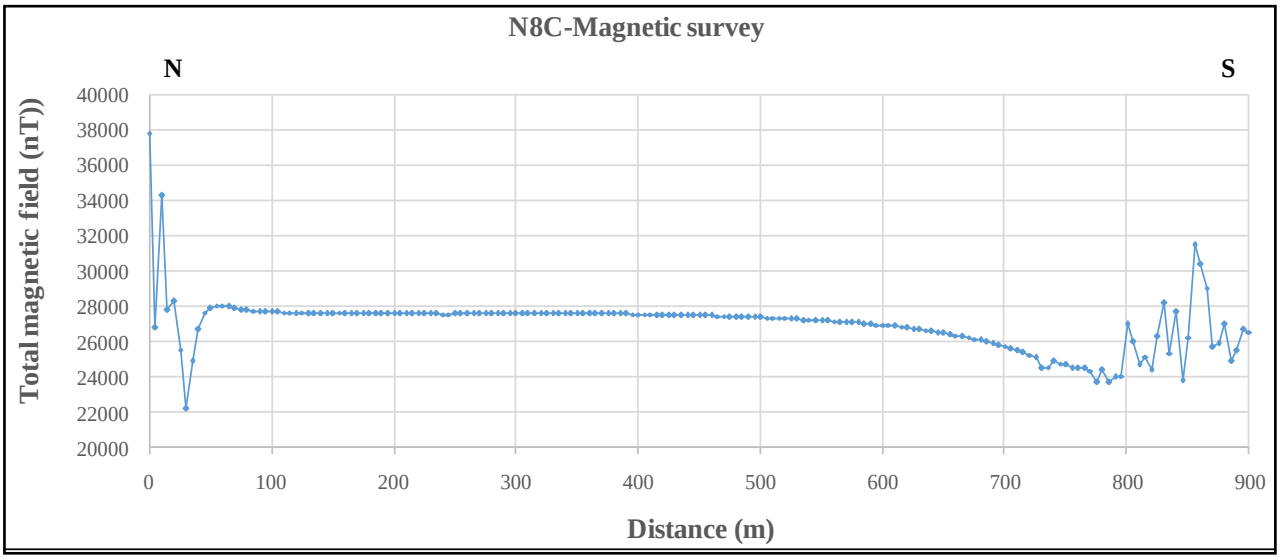

Figure 71: Total magnetic field recorded along traverse N8C

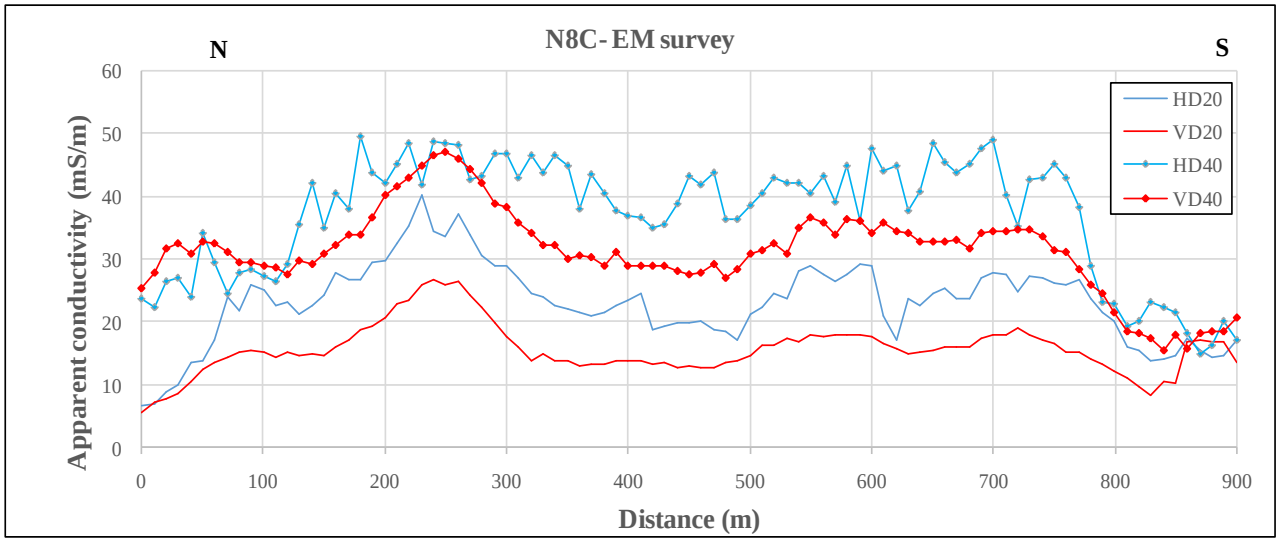

Figure 72: Apparent conductivity values along traverse N8C

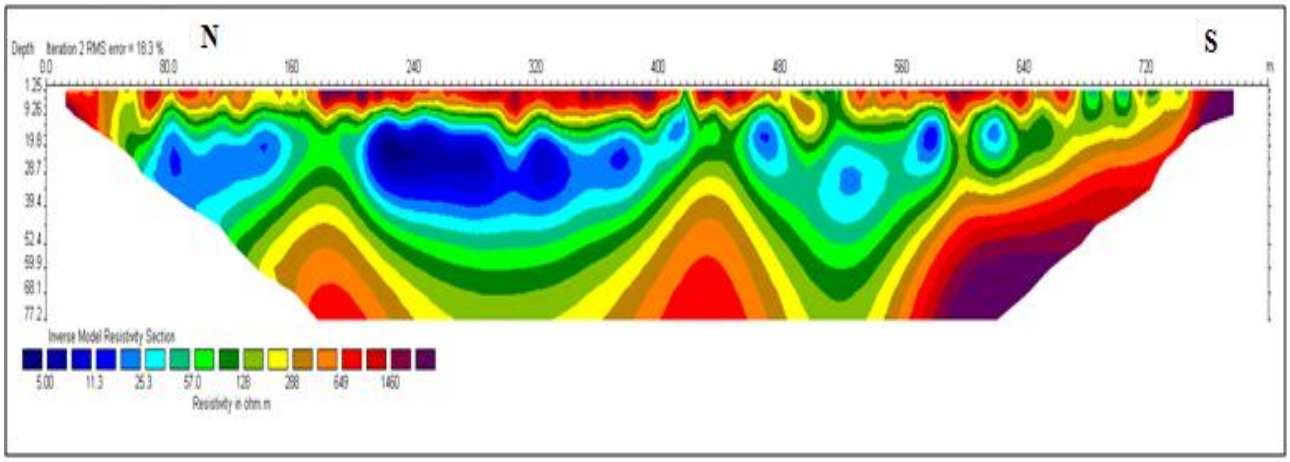

Figure 73: Inverse resistivity model along traverse N8C

Traverse N10

Gravity, magnetic and EM data was recorded over a distance of 2 400 m along Traverse N10, in north-south direction. The gravity, magnetic and EM data are presented as profile plots in (Figure 74, Figure 75 and Figure 76). The inverse resistivity model created from the ERT data recorded along a 1 200 m stretch of this traverse is shown in (Figure 77).

The gravity profile (Figure 74) displays one prominent negative anomaly in the northernmost part of the traverse. The reason for this anomaly is at present unclear, but it could be related to the presence of dolomites in the subsurface. However, other parts of the traverse which cross dolomite outcrops do not display similar negative anomalies.

The total magnetic field plot (Figure 75) shows a stable magnetic field for the northern most 700 m of the traverse. Between stations 700 m and 1 100 m, more variable magnetic data was recorded. The variable nature of the magnetic field at these positions points towards the presence of banded iron formations. The magnetic field displays a regional decrease between stations 1 100 m and 1 400 m, after which a gradually increasing trend is observed. These regional changes in the magnetic field are due to regional changes in the magnetic properties of the subsurface materials. South of station 2 200 m, variable magnetic field strengths are again observed, indicating the presence of banded iron formations. No anomaly that could clearly be attributed to the fault in the southern parts of the traverse can be identified in the magnetic profile.

The apparent conductivity profiles (Figure 76) show that the shallower earth materials are generally less conductive than the deeper materials. These shallow, low conductivity materials are most likely surficial Kalahari sands and Tertiary limestones. Prominent conductivity anomalies are observed in both profiles using the 40 m coil separation, showing the presence of conductive earth materials at depth. The anomalies observed between stations 400 m and 1 000 m are most likely due to the presence of the dolomites outcropping in these parts of the traverse (see Figure 49).

The high conductivities suggest that the dolomites contain dissolution cavities in which groundwater are likely to occur.

Resistivity data was recorded along the traverse over a distance of 1 200 m. The resistivity model shows distinct horizons of differing electrical resistivity properties (see Figure 77). The near-surface material, up to a depth of approximately 20 m, displays high resistivities, generally greater than 100 Ωm. This layer is in all probability due to the presence of surficial Kalahari sands and Tertiary deposits. The high resistivity layer overlies a thick layer of low resistivities, generally below 20 Ωm. Localised zones of very low resistivities are observed within this layer. These zones correspond with the zones of high conductivity seen in (Figure 76), and are again probably related to the presence of dolomitic rock underlying the survey area at these positions.

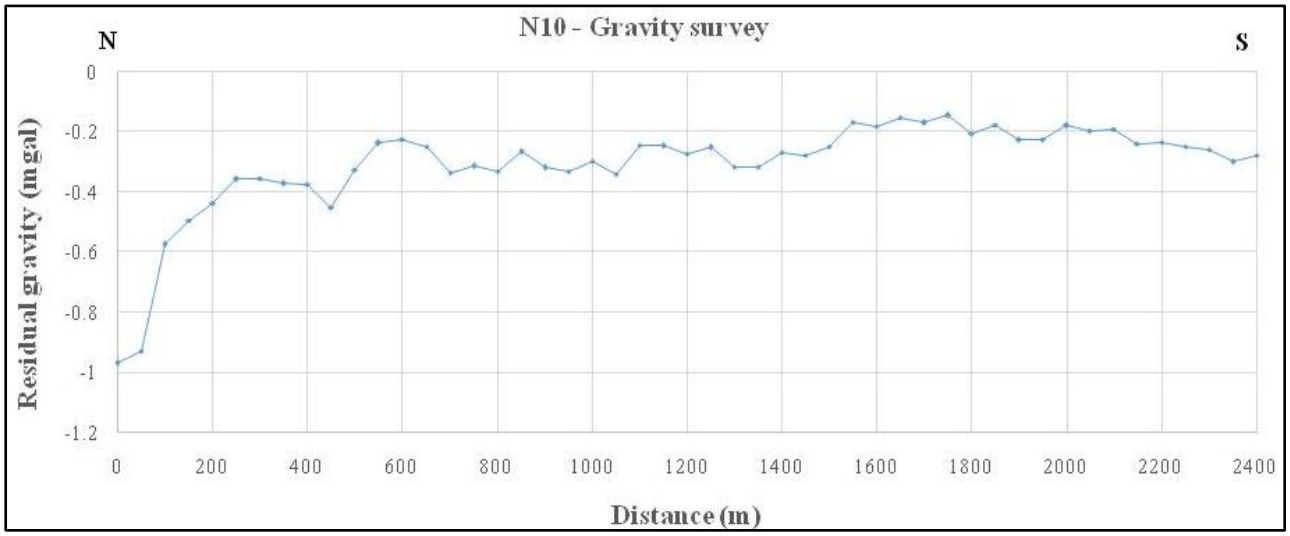

Figure 74: Residual gravity values along traverse N10

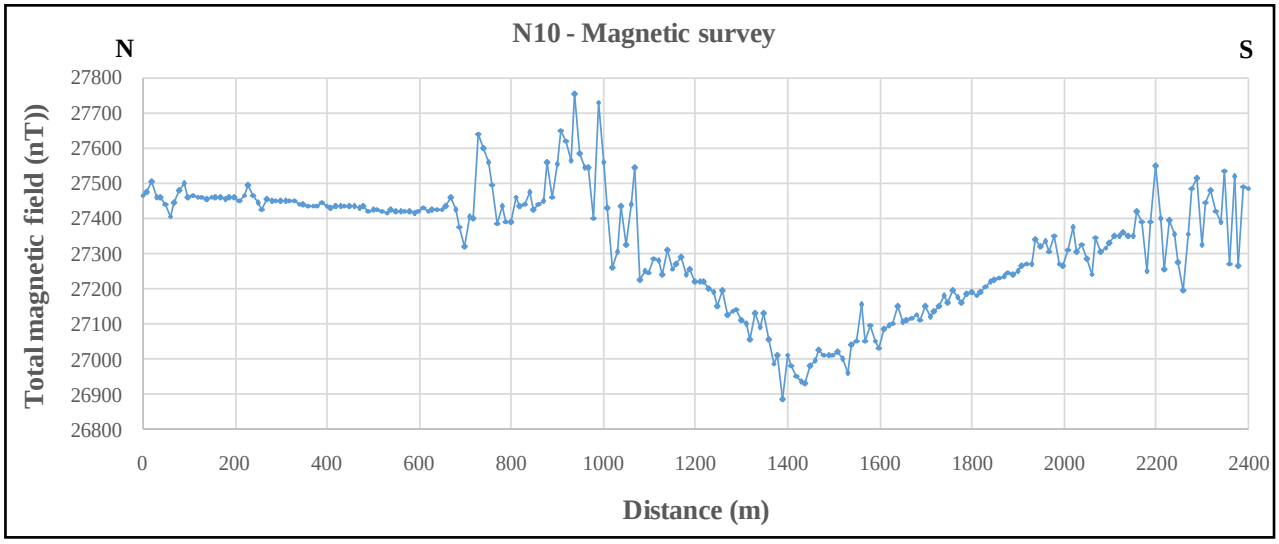

Figure 75: Total magnetic field recorded along traverse N10

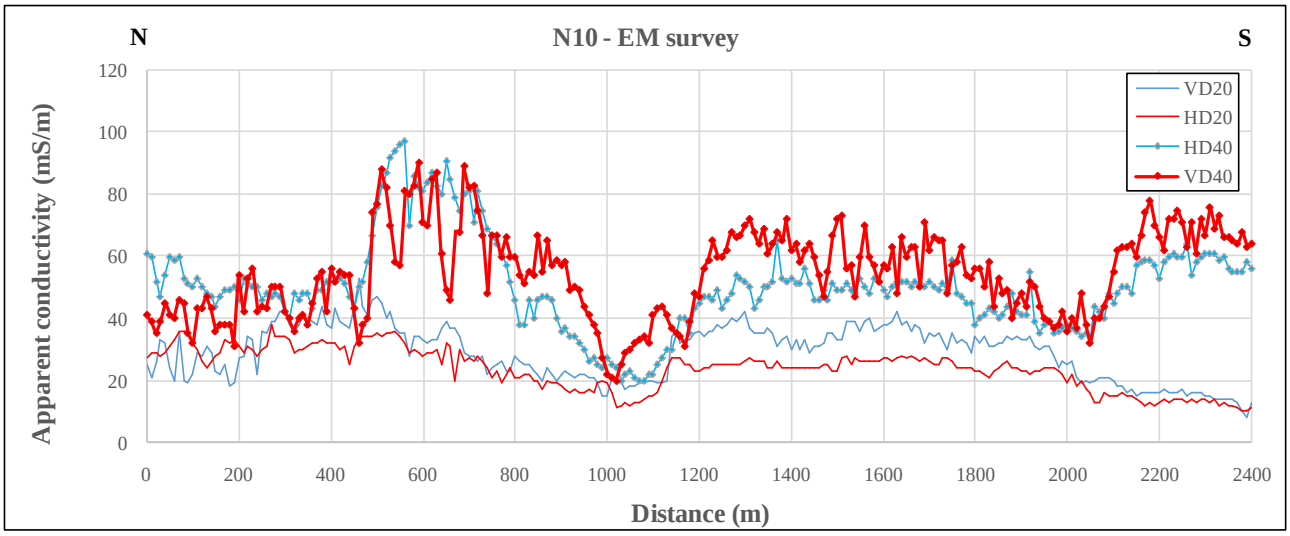

Figure 76: Apparent conductivity values along traverse N10

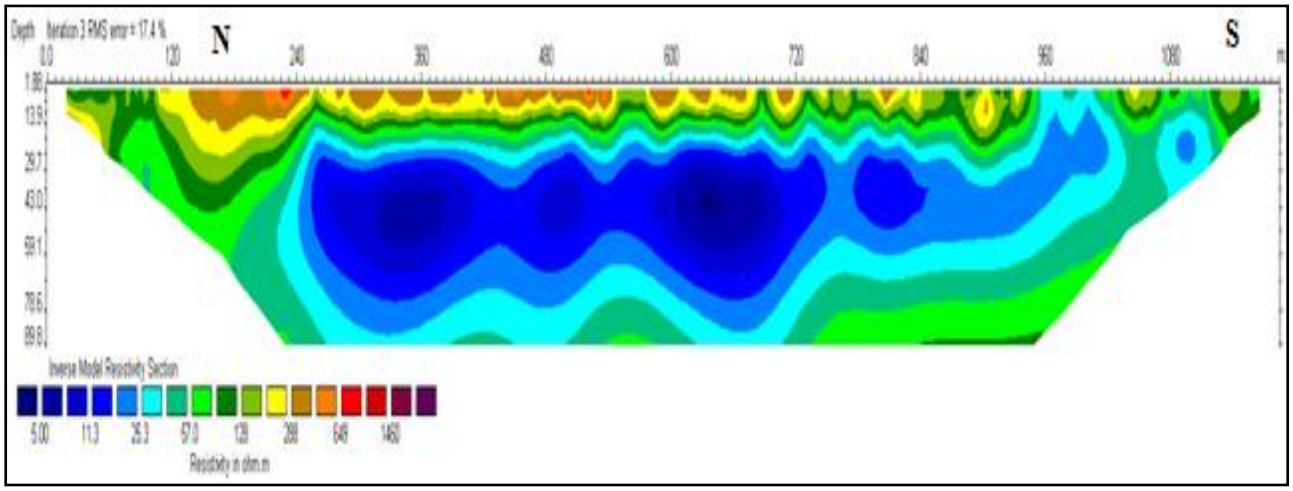

Figure 77: Inverse resistivity model along traverse N10

Traverse N11

Traverse N11 had a north/south strike and extended over a distance of 2 400 m. Gravity was recorded along the first 2 250 m of the traverse, while magnetic and EM data were recorded along the entire length of the traverse. ERT data was recorded on a 1 000 m stretch of the traverse across a prominent conductivity observed in the EM data. The gravity, magnetic and EM data are presented as profile plots in (Figure 78, Figure 79 and Figure 81), respectively. The inverse resistivity model created from the ERT data was recorded along the apparent conductivity profiles is shown in (Figure 82).

The gravity data shows the presence of a broad zone with generally lower mass densities between stations 200 m and 1 450 m (refer to Figure 78). This zone may be related to the presence of dolomitic rock with dissolution cavities in the subsurface at these positions.

The total magnetic field along the traverse is stable for the first 2 000 m of the traverse, after which highly variable data was recorded (see Figure 79). The variable magnetic field is most likely due to the banded iron formation that occurs in the southern parts of the traverse.

Figure 80 shows the total magnetic field recorded along the first 2 000 m of the traverse. A magnetic anomaly is observed between stations 200 m and 400 m. This anomaly may be due to a dyke crosscutting the traverse (see Figure 49). Near station 1 400 m, a change in the regional magnetic field strength is observed. This change may indicate that transition between different lithologies with different magnetic properties.

Two major conductivity anomalies are observed in the apparent conductivity data (Figure 79). The first occurs between stations 800 m and 1 400 m. The conductivities within this zone are seen to increase with depth of investigation. The origin of this zone of high conductivities is at present unknown, but it may be associated with the dolomites known to occur in the area (see Figure 49). The second conductivity anomaly occurs at the southern extreme of the traverse. This anomaly is thought to be associated with the dykes that are known to crosscut the traverse at these positions.

The 2D resistivity model along the traverse (Figure 82) shows a very prominent zone of low resistivities in the central parts which corresponds to the zone of high conductivities observed in the EM data. Again, this zone is thought to be associated with the dolomitic rocks that occur in this part of the survey area.

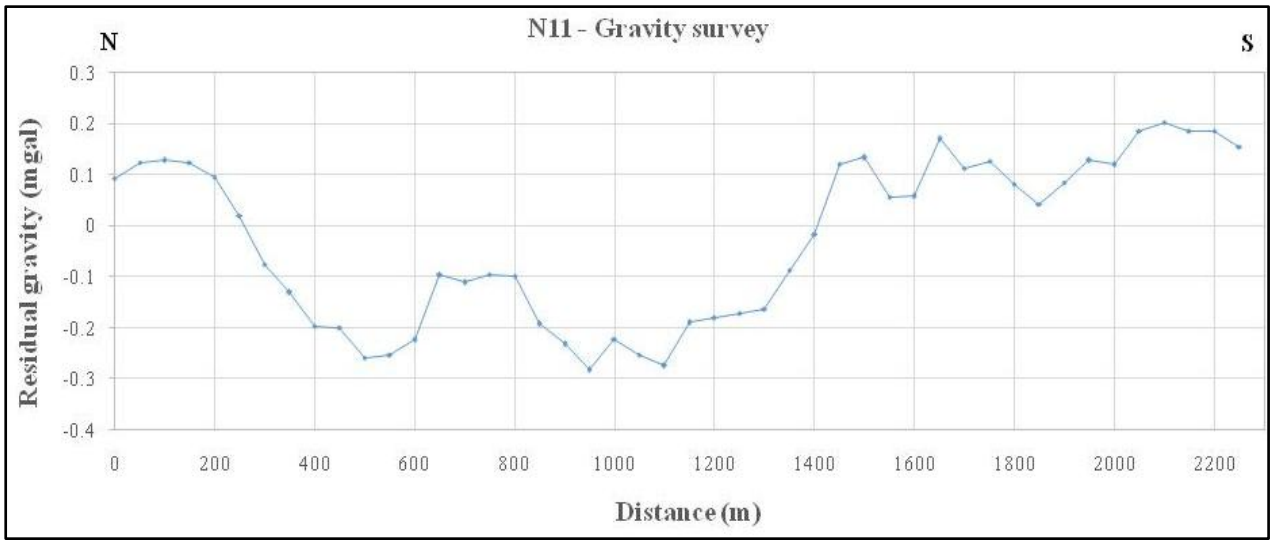

Figure 78: Residual gravity values along traverse N11

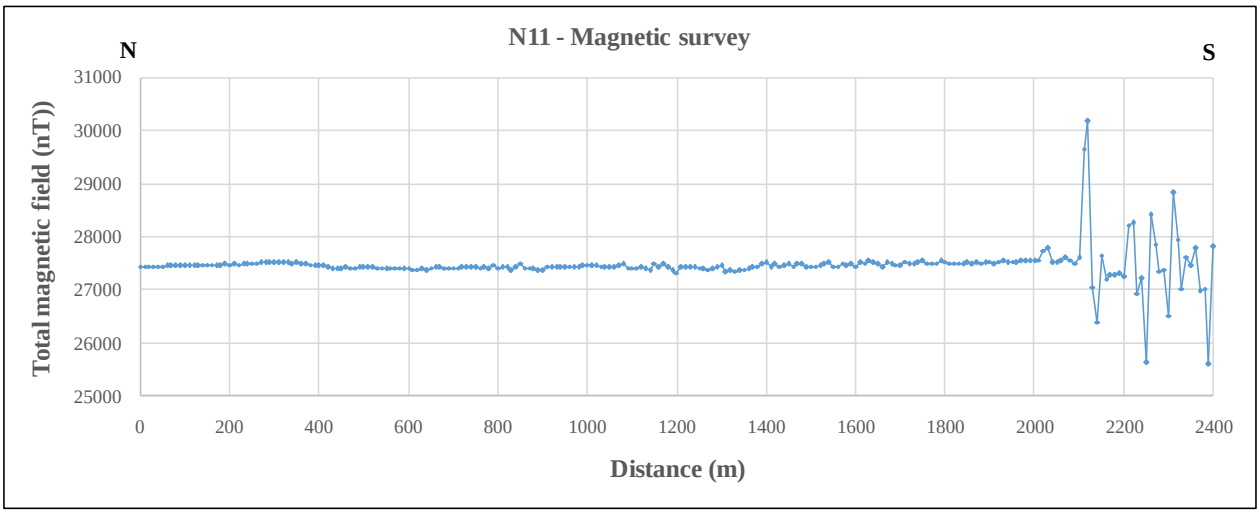

Figure 79: Total magnetic field recorded along traverse N11

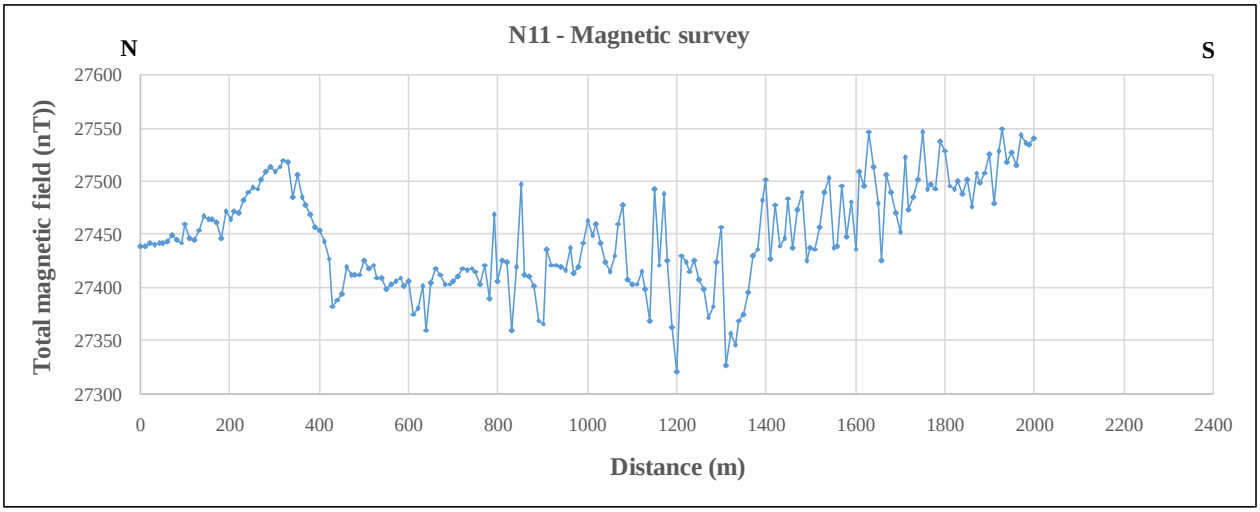

Figure 80: Total magnetic field recorded along the first 2000 m of traverse N11

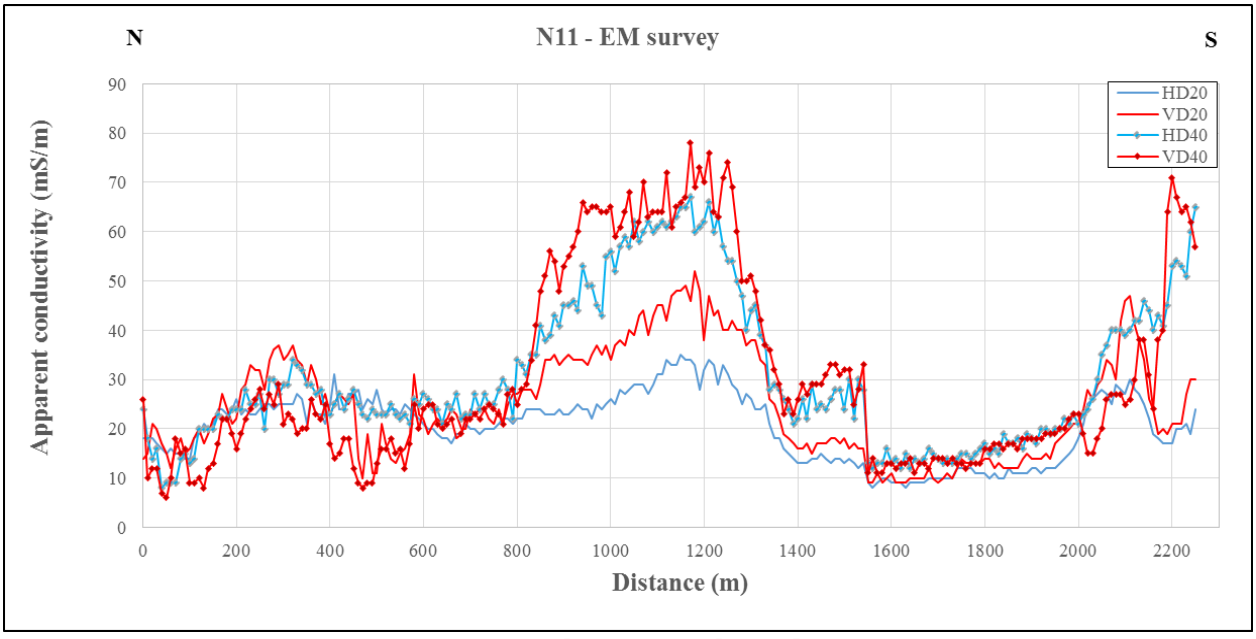

Figure 81: Apparent conductivity values along traverse N11

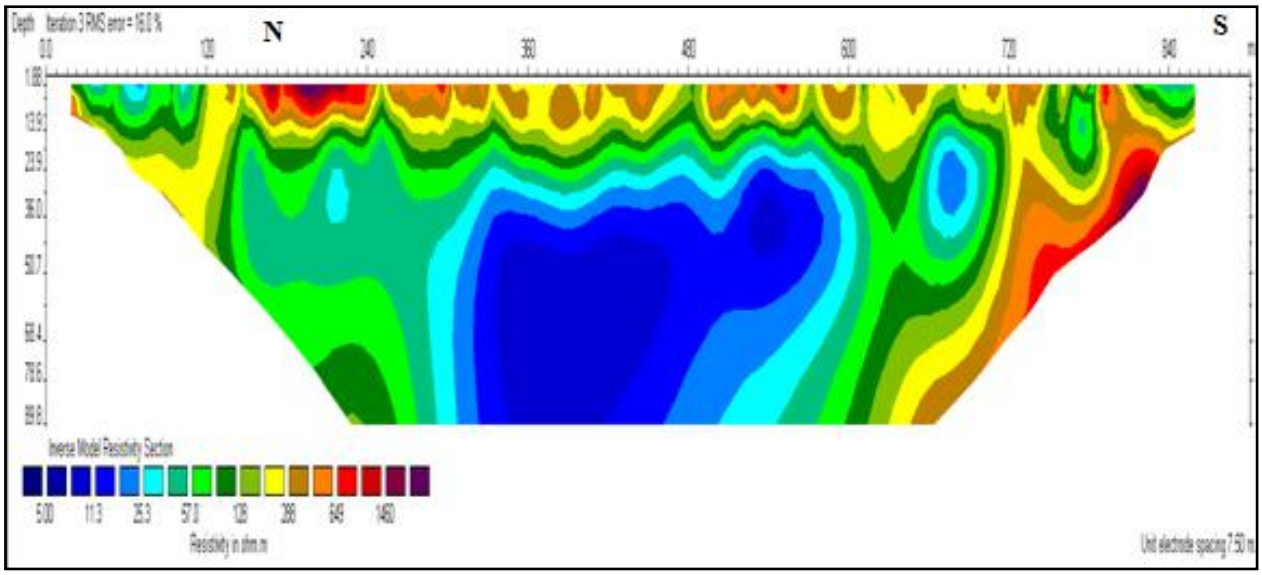

Figure 82: Inverse resistivity model along traverse N11

5.3.6 **Discussion**

The results of the ground geophysics investigations demonstrated in detail the changes near surface and subsurface geology. The use of different geophysical techniques increased the level of confidence of the SkyTEM data discussed in Section 5.2. Based on the ground geophysical investigations conducted, the geological features were clearly identified. The ground geophysics investigation confirmed the two major faults and other geological features known to occur in the western and eastern part of the study area.

The gravity method allowed the delineation of distinct areas of mass differences, and successfully detected the changes in mass on either side of the prominent faults in the study area. Mass deficits in the subsurface could also possibly be attributed to dissolution cavities in areas underlain by dolomites.

On most traverses the results of the different geophysical surveys correlated well. Magnetic anomalies were often associated with changes in the subsurface resistivity/conductivity distribution as measured by the EM and ERT methods. The combined use of these methods allowed a more reliable interpretation of the subsurface conditions responsible for the observed anomalies, and also contributed to the sitting of successful boreholes on the identified geological structure. The results of the drilling programme are discussed in Chapter 6.

CHAPTER 6: EXPLORATION DRILLING

6.1 INTRODUCTION

The purpose of the drilling programme was to drill production boreholes at positions as determined from the results of the geophysical investigations. These boreholes were drilled at positions deemed most favourable for the intersection of high-yielding aquifer systems. Unfortunately information on the specific choices for the drilling positions on the observed anomalies was unavailable during the current project. This should be seen as a limitation of the current study.

Drilling was conducted according to the minimum standards prescribed by the Borehole Water Association (BWA, undated) to secure the long-term viability and serviceability of the installation (DWA guideline, 1996).

6.2 DRILLING AND BOREHOLE CONSTRUCTION

Drilling was conducted by JM Drilling under supervision of qualified geohydrologists. The boreholes were drilled to various depths, depending on the depths at which major fractures were intersected. Drilling was done by means of the percussion drilling technique. Percussion drilling was done using hammers with a minimum diameter of 165 mm and a maximum diameter of 381 mm.

Drill cuttings were collected every metre to allow geological logging of the boreholes. Information on water strikes (depths, blow yields) was recorded for all the installed boreholes.

In Chapter 5 it was established that the study area has two distinctive major fault structures. These fault zones and other geological structures identified by the geophysical investigations were targeted during the drilling programme.

The actual drilling diameters depended on the lithologies encountered in the targeted areas. Boreholes with a blow yield >2 l/s were reamed at a diameter of 216 mm and equipped with steel casing, which was either plain or slotted. Gravel packs were used and a sanitary seal of 5 m thickness was installed.

A total of 78 boreholes were drilled as part of the drilling programme. Sixty of these boreholes were considered successful in terms of serving as production boreholes. The locations and distribution of the boreholes drilled by 29 January 2013 are shown in (Figure 83). A few more boreholes were drilled after this date.

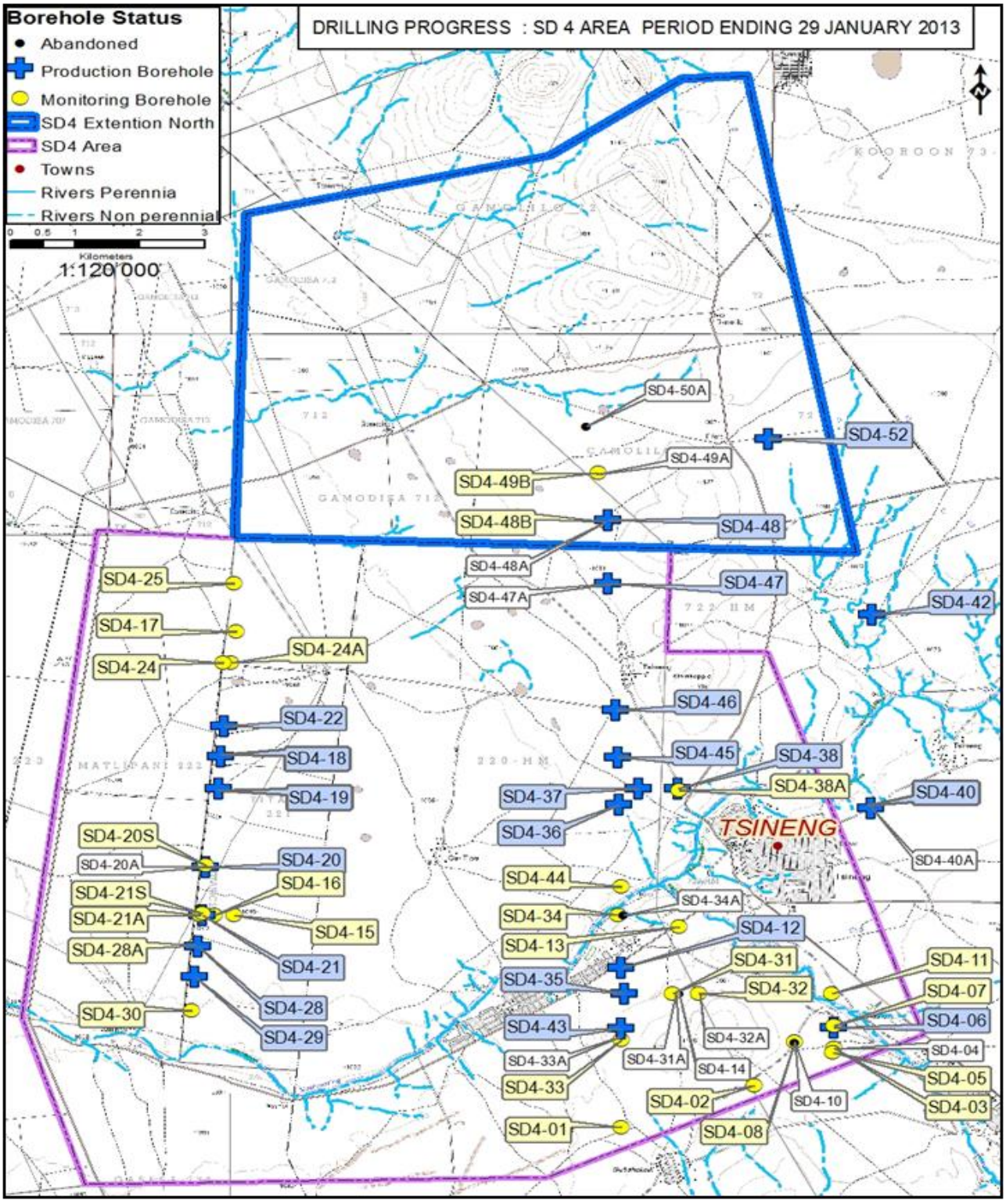

Figure 83: Location and distribution of the drilled boreholes in SD4

6.2.1 Boreholes and geological logs along the Western Fault

Boreholes were drilled along the western fault because the results of the geophysical investigations suggested that this fault has the potential to be associated with highly fractured rock materials likely to produce high-yielding boreholes.

Twenty-one boreholes were drilled along the fault zone with depths ranging between 40 mbgl and 161 mbgl (refer to Appendix A1). Most of the successful boreholes were cased, and equipped with gravel packs and sanitary seals. The geological borehole logs of three of the boreholes targeting the Western Fault are discussed below:

Geological log of borehole SD4-16

The geological log of borehole SD4-16, as well as the water strike encountered during drilling, is shown in (Figure 84). At shallow depths, layers of calcrete and clay are observed followed by prominent layers of lava. Water was struck in the fractured lava at a depth of approximately 92 mbgl. The measured blow-yield was 21 l/s.

Geological log of borehole SD4-18

The geological log of borehole SD4-18 (Figure 85) shows calcrete followed by clay material from surface up to a depth of approximately 85 mbgl. A weathered and fractured banded iron formation layer with cobbles and pebbles is observed just below the calcrete. Two water strikes occurred in the banded iron formation, at depths of 86 mbgl and 90 mbgl and with blow-yields of 2 and 4 l/s, respectively.

Geological log of borehole SD4-28

The geological log of borehole SD4-28, as well as the water strikes encountered in this borehole, is shown in (Figure 86). Alternating layers of calcrete are seen for the first 47 mbgl followed by a layer of fine weathered red clay. A water strike occurred at a depth of approximately 66 mbgl in the brownish red shale formation. This water strike had a blow-yield of 0.5 l/s. Another water strike occurred at approximately 82 mbgl in the yellowish brown shale formation. This water strike had a blow-yield of 3.5 l/s. A black shale formation was intersected from 90 to 110.65 mbgl

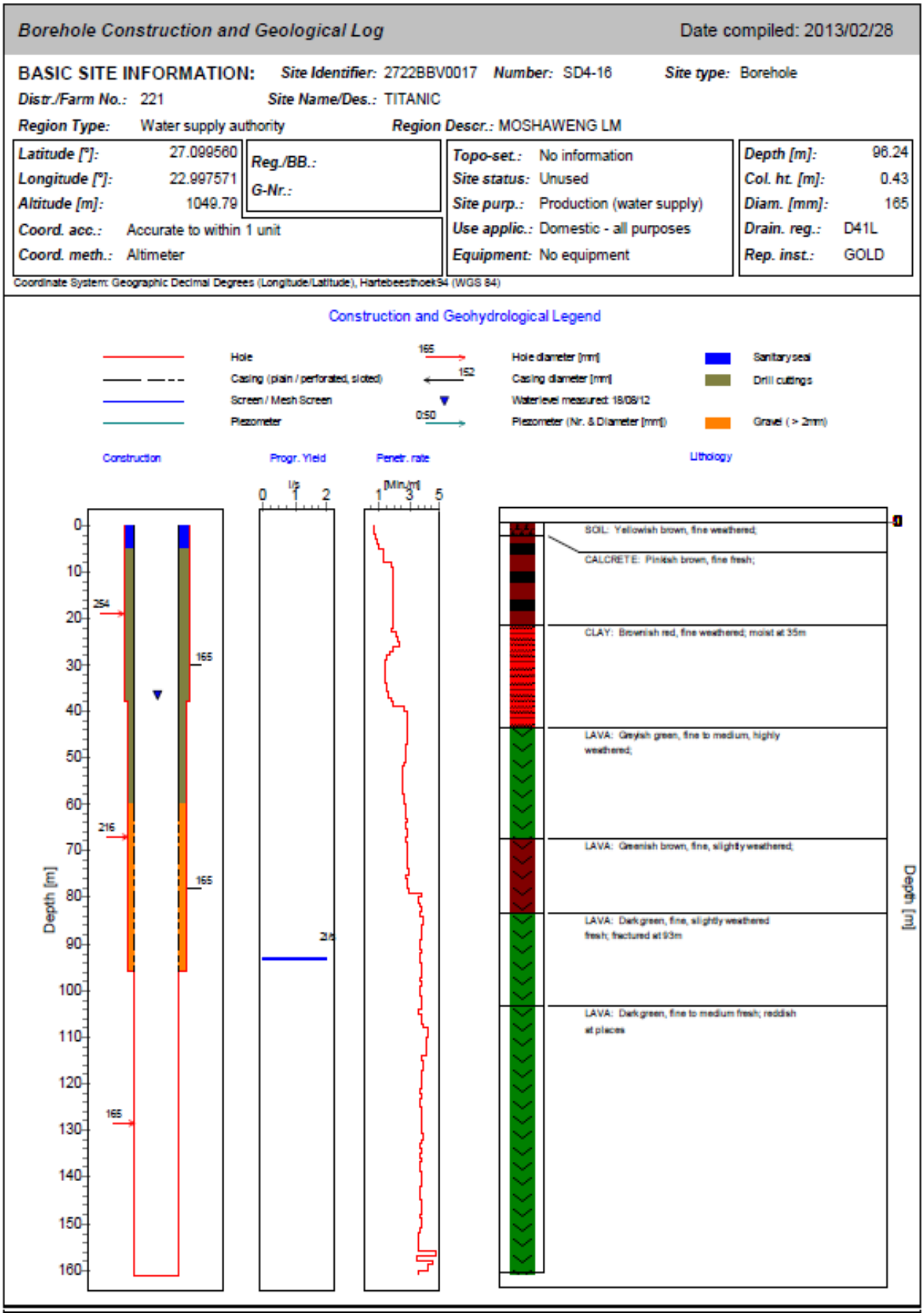

Figure 84: Geological log of SD4-16, showing the lithology and water strikes

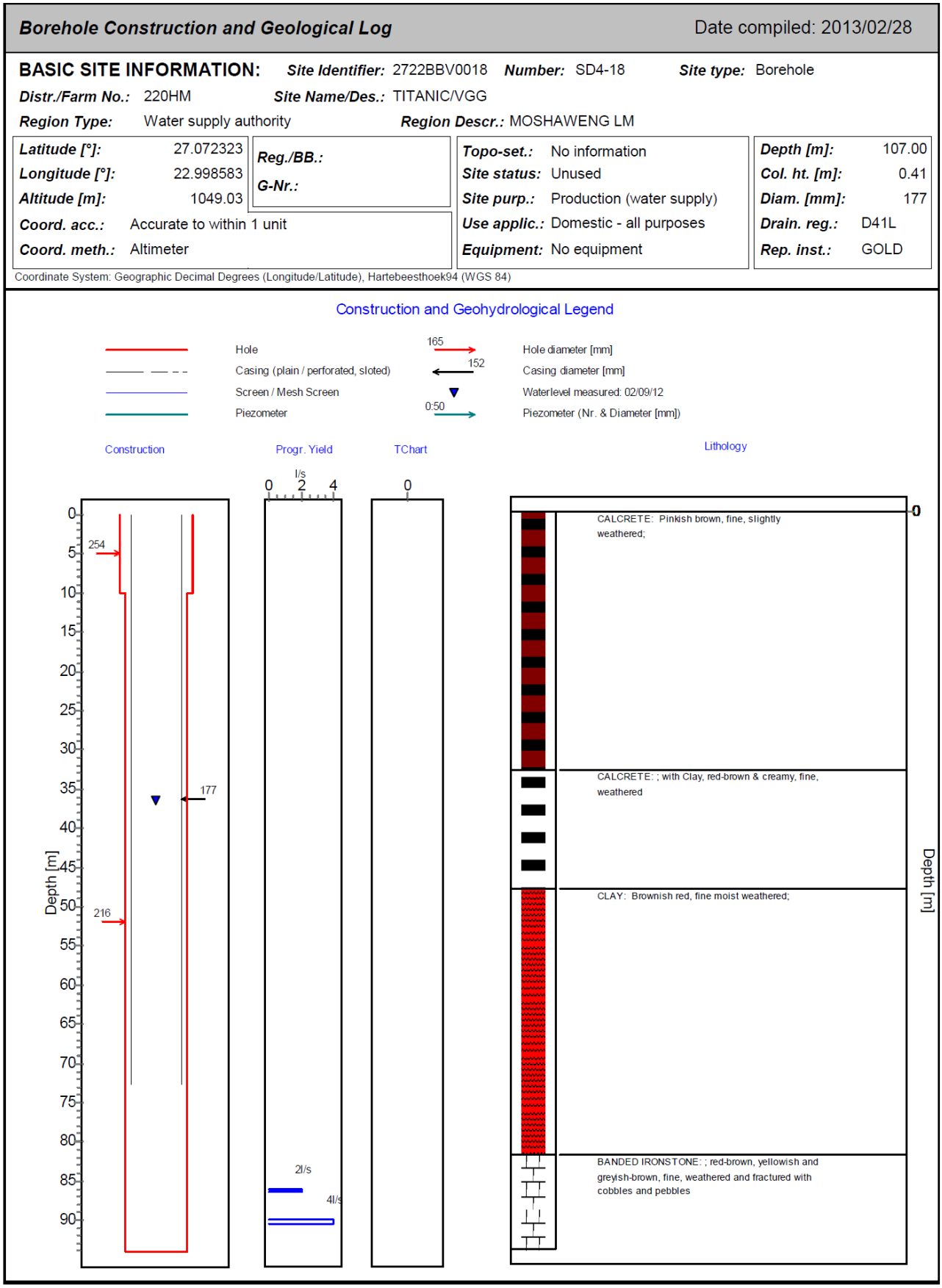

Figure 85: Geological log of SD4-18, showing the lithology and water strikes

Borehole Construction and Geological Log Date compiled: 2013/02/28

BASIC SITE INFORMATION: ***Site Identifier:*** 2722BBV0026 ***Number:*** SD4-28 ***Site type:*** Borehole

Distr./Farm No.: 221 ***Site Name/Des.:*** TITANIC

Region Type: Water supply authority ***Region Descr.:*** MOSHAWENG LM

Latitude [°]:	27.104885	***Reg./BB.:***	***Topo-set.:***	No information	***Depth [m]:*** 110.65
Longitude [°]:	22.994961	***G-Nr.:***	***Site status:***	Unused	***Col. ht. [m]:*** 0.51
Altitude [m]:	1048.02		***Site purp.:***	Production (water supply)	***Diam. [mm]:*** 216
Coord. acc.:	Accurate to within 1 unit		***Use applic.:***	Domestic - all purposes	***Drain. reg.:*** D41L
Coord. meth.:	Altimeter		***Equipment:***	No equipment	***Rep. inst.:*** GOLD

Coordinate System: Geographic Decimal Degrees (Longitude/Latitude), Hartebeesthoek94 (WGS 84)

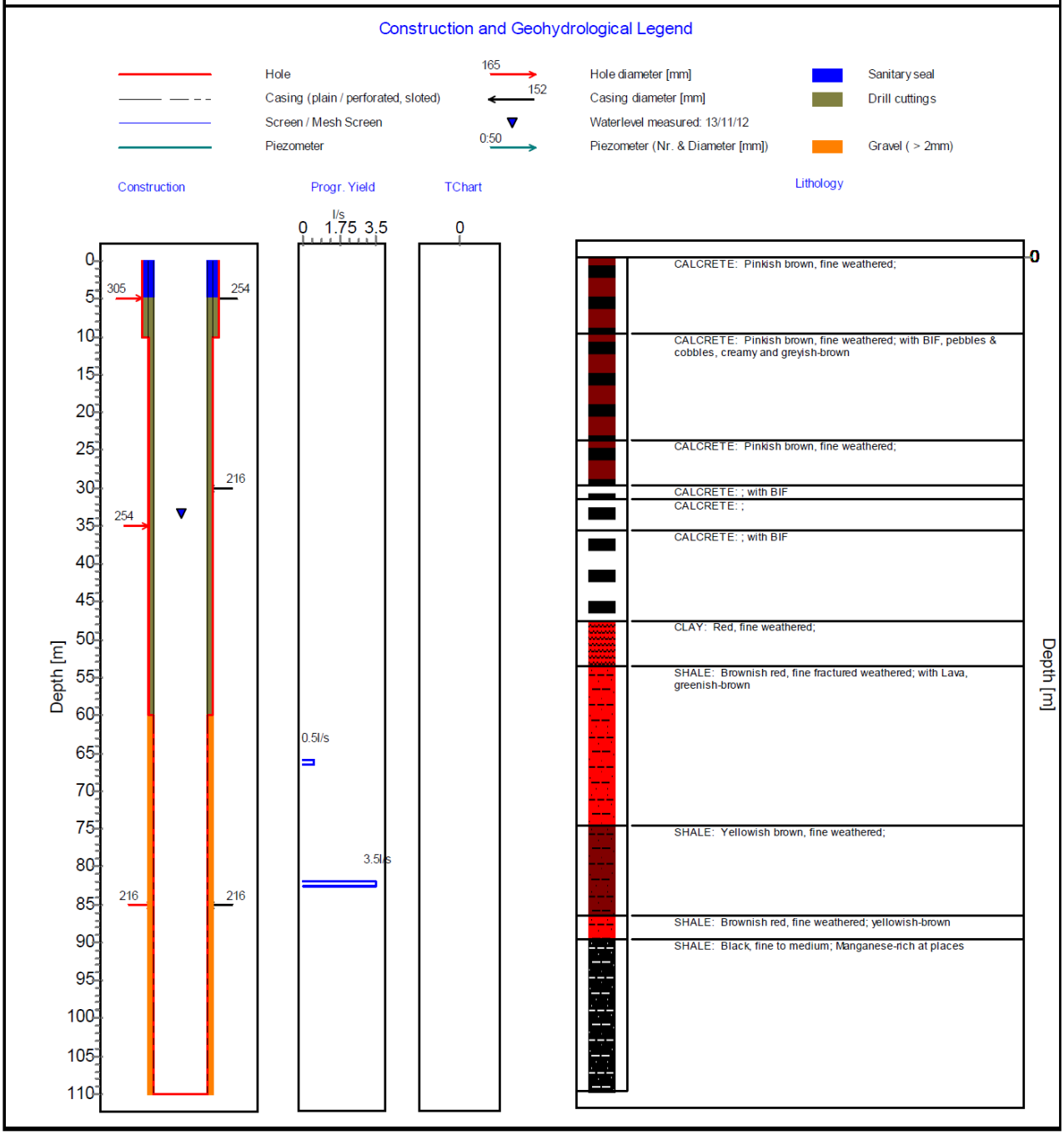

Figure 86: Geological log of SD4-28, showing the lithology and water strikes

6.2.2 Borehole and geological logs along the eastern fault

Very similar to the western fault, the boreholes were drilled along the eastern fault targeting the major fault zone which was also expected to be associated with higher water content because of the fracturing and weathering caused by the fault. Twenty-three boreholes were drilled along the fault zone with depths ranging between 37 mbgl and 120 mbgl (refer to Appendix A2). Again, the majority of the successful boreholes were cased, and equipped with gravel packs and sanitary seals. The geological borehole logs of three of the boreholes targeting the Eastern Fault are discussed below:

Geological log of borehole SD4-36

The geological log and water strikes of borehole SD4-36 are shown in (Figure 87). Alternating clay layers were observed from ground level up to a depth of 62 mbgl. A layer of limestone was intersected between depths of 63 mbgl and 65 mbgl. Two major water strikes were encountered in the banded iron formation at depths of approximately 76 mbgl and 80 mbgl. These water strikes had blow yields of 10 l/s and 20 l/s, respectively.

Geological log of borehole SD4-43

The geological log of borehole SD-43 (Figure 88) shows multiple fractures in the banded iron formation with blow yields ranging from 0.5 to 9.3 l/s. The observed water strikes occurred between approximately 49 mbgl and 60 mbgl.

Geological log of borehole SD4-45

Alternating layers of calcrete are observed for the first 12 m of borehole SD4-45 (see Figure 89). From a depth of 12 to 50 mbgl clay was intersected. Two major water strikes with blow yields of 2.2 l/s and 13.6 l/s were encountered in the banded iron formation at depths of approximately 58 mbgl and 67 mbgl.

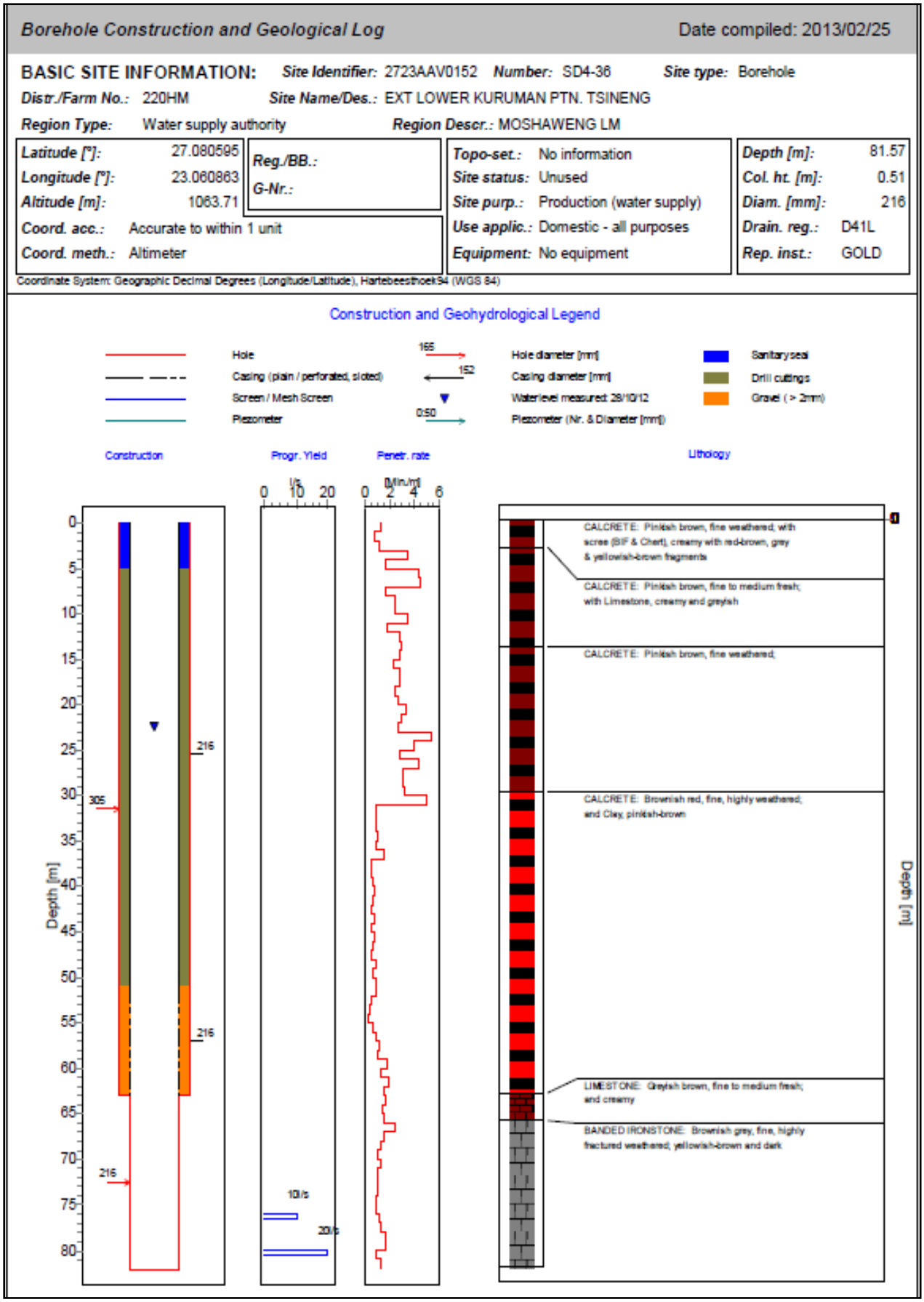

Figure 87: Geological log of SD4-36, showing the lithology and water strikes

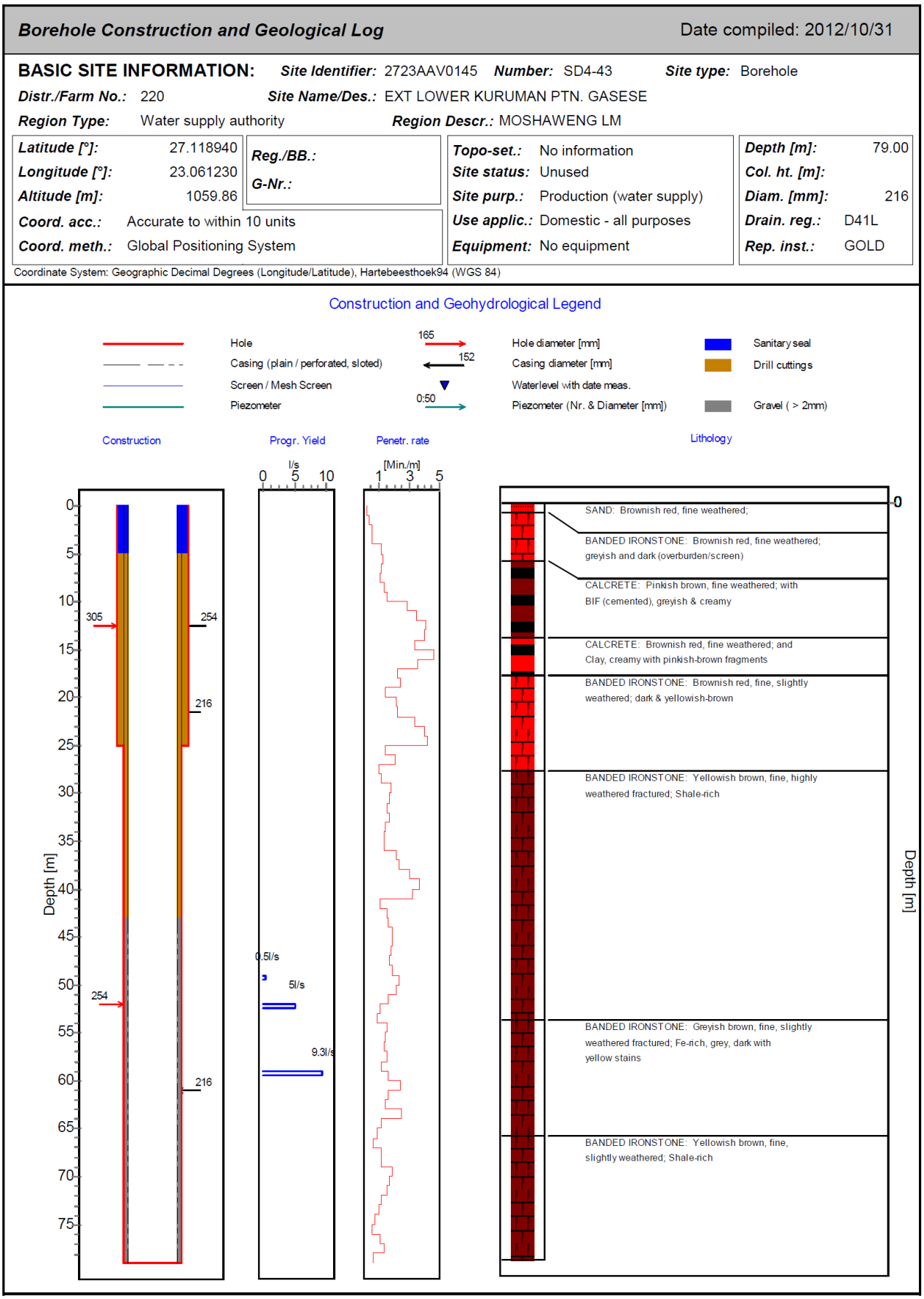

Figure 88: Geological log of SD4-43, showing the lithology and water strikes

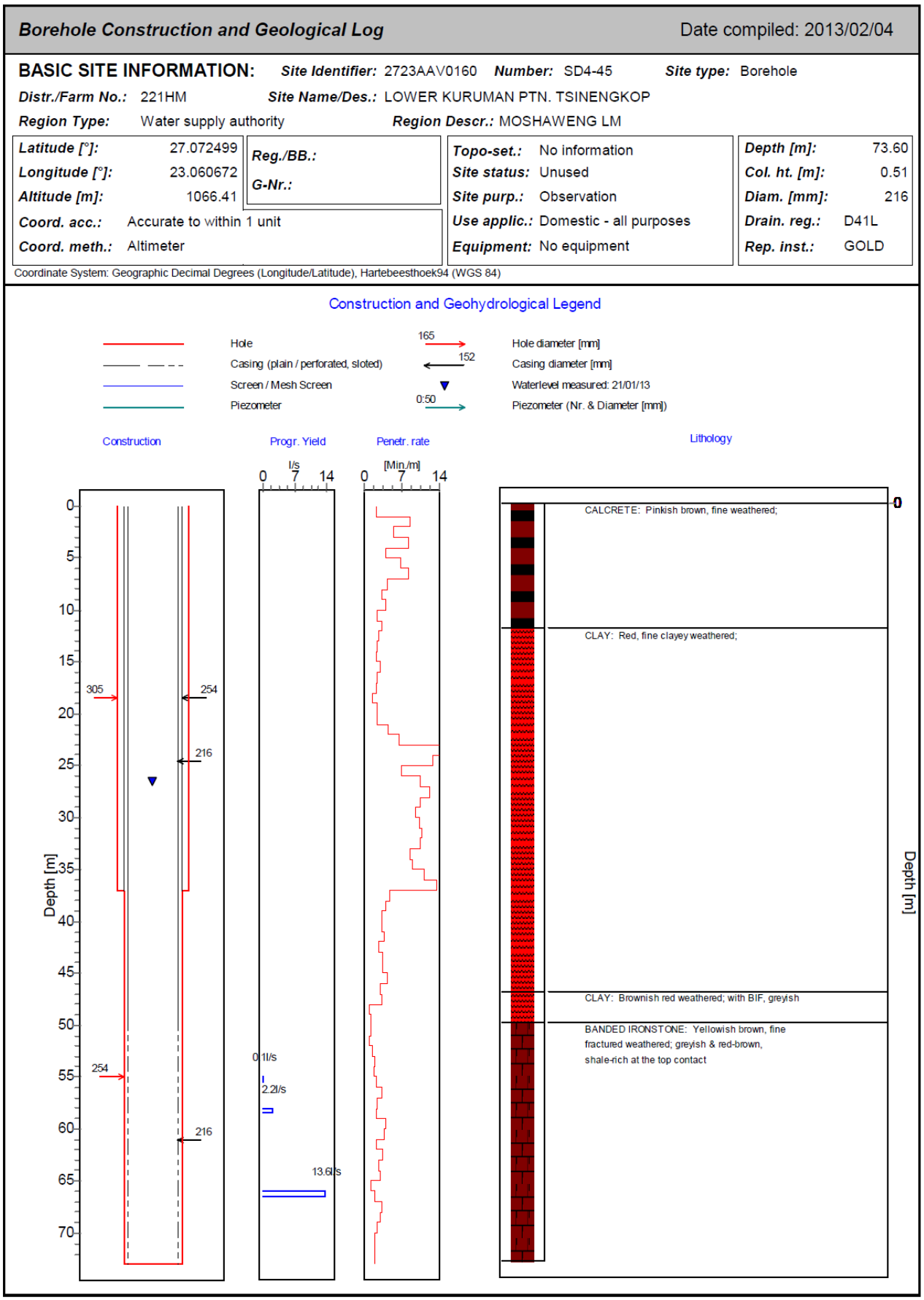

Figure 89: Geological log of SD4-45, showing the lithology and water strikes

6.2.3 Borehole and geological logs along the south boundary

Boreholes were drilled near the southern boundary of the SD4 study area, targeting geological structures such as faults and dykes. Sixteen boreholes were drilled with depths ranging between 26 to 179 mbgl (refer to Appendix A3). The geological borehole logs of two of the boreholes drilled along the southern boundary of the study area are discussed below:

Geological log of borehole SD4-02

The geological log of borehole SD4-02 (refer to Figure 90) shows calcrete and banded iron formation at shallow depths. A minor water strike with a low blow yield of 0.01 l/s occurred at the contact between the banded iron formation and limestone/dolomite layer. From 52 to 179 mbgl, black shale was intersected.

Geological log of borehole SD4-06

Figure 91 shows the geological log of borehole SD4-06. Alternating layers of calcrete are observed for the first 19 metres below ground level. A major water strike with a blow yield of 8.5 l/s was intersected in the banded iron formation at a depth of approximately 20 mbgl.

6.2.4 Discussion

During the current study, boreholes were sited on geophysical anomalies as observed in the airborne and ground geophysical data. These anomalies often corresponded to the positions of known geological structures, such as prominent faults and dykes. Of the 78 drilled boreholes, 60 were considered successful in terms of serving as production boreholes. This high success rate (77%) suggests that the use of geophysical surveys was highly successful in the sitting of high-yielding production boreholes. Unfortunately no information is available on the expected success rate of drilling production boreholes in the absence of geophysical data, so that the improvement in the success rate using geophysical techniques cannot be directly evaluated.

The drilling results show that the Western Fault is associated with high-yielding aquifers in the fractured lavas, shales and banded iron formations along the fault. The major water strikes occurred between depths of 66 mbgl and 92 mbgl. The strongest borehole (SD4-16, blow-yield of 21 l/s) was installed in the fractured lavas.

The high-yielding aquifers associated with the Eastern Fault all occur in the fractured banded iron formations occurring in this part of the study area. Water strikes were encountered at depths ranging from 49 to 80 mbgl. Blow-yields of up to 20 l/s were recorded.

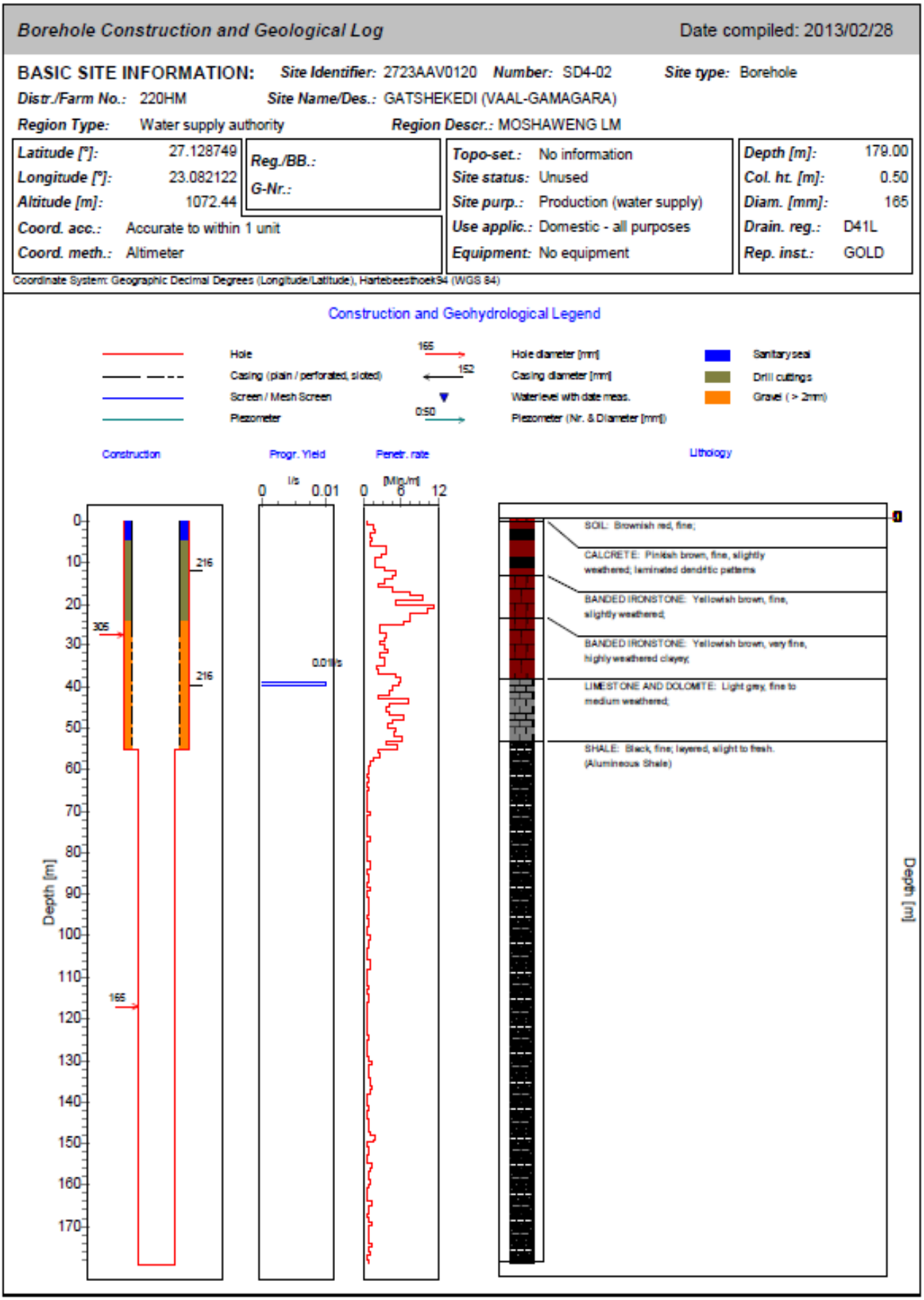

Figure 90: Geological log of SD4-02, showing the lithology and water strikes

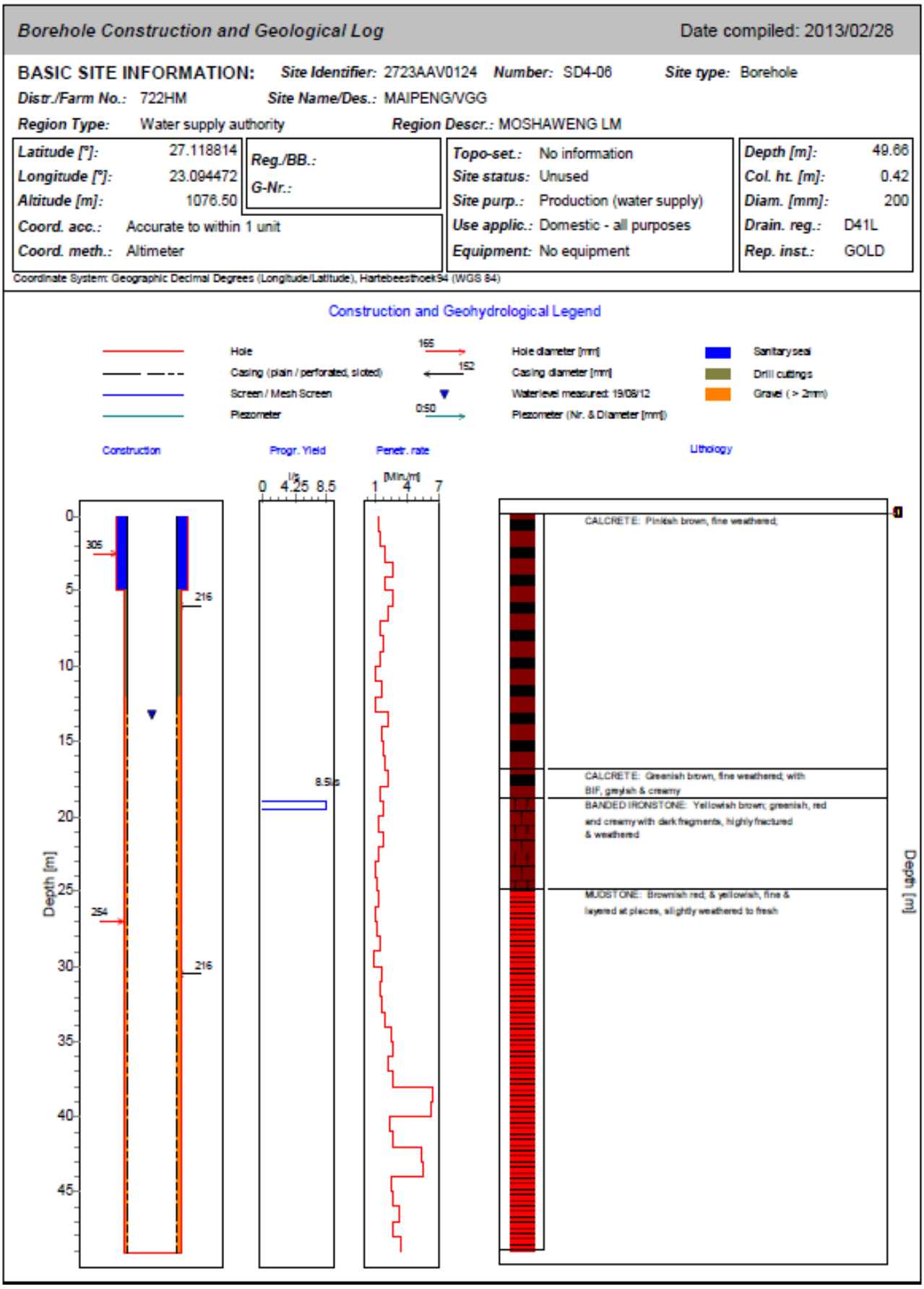

Figure 91: Geological log of SD4-06, showing the lithology and water strikes

The high-yielding borehole installed on the southern boundary (SD4-06, blow-yield of 8.5 l/s) also encountered a major water strike in fractured banded iron formations, but at a much shallower depth (20 mbgl) than the boreholes on the Western and Eastern Faults.

The drilling results confirm that the Western and Eastern Fault are associated with major aquifer systems. Boreholes drilled on these faults could potentially be used as abstraction boreholes for groundwater supply.

CHAPTER 7: HYDRAULIC TESTS ON AQUIFERS

7.1 INTRODUCTION

In the current study, boreholes that were installed as part of the drilling programme (refer to Chapter 6), and had blow-yields larger than 2 l/s were earmarked as potential production boreholes. These boreholes were considered potential production boreholes able of yielding suitable quantities of groundwater. Hydraulic tests (pumping tests) were performed on the selected boreholes to determine the hydraulic properties of the intersected aquifers. These properties are of significant importance when estimating the sustainable yield of a borehole.

The pumping test data were analysed using the Flow Characteristic (FC) software package developed by the Institute for Groundwater Studies (van Tonder, 2001). The FC software is used as a tool to estimate sustainable yields of boreholes by considering the behaviour of the drawdown in the water levels during pumping. The Cooper Jacob method was used to analyse the results of the pumping tests to determine the aquifer hydraulic parameters (transmissitivity and storativity). Diagnostic plots were used to characterise the flow regimes and to determine the behaviour of the aquifer system under stress. *The manual on pump test analysis in fractured-rock aquifers* (van Tonder, 2001) and *The analysis and evaluation of pumping test data* (Kruseman and de Ridder, 1994) were used for interpretation purposes

7.2 AQUIFER TESTING

Prior to testing the aquifers by means of a constant discharge tests, step drawdown tests were performed on all the boreholes. Step drawdown tests involve pumping of a borehole at three or more sequentially higher pumping rates. The rates are maintained for an equal length of time. The purpose of the test is to assess the productivity of a borehole. Based on the measured water level drawdown and the pumping rate recorded during the step test, a constant discharge rate is selected.

A total of 40 boreholes were subjected to the pumping test. The test involved monitoring the drawdown in the boreholes while the discharge rate was kept at constant rate for the duration of 12 to 72 hours. The available drawdown during the assessments was selected based on the behaviour of the borehole observed on the derivative plots.

In the FC method, information of the available drawdown and main water strikes is critical, because such information is used to estimate the sustainable yield of the boreholes.

The flow regimes were identified using derivative and diagnostic plots. These plots are used to assess the behaviour of the aquifer under stress and to understand drawdown time trends which assist in the determination of transmissivity and storativity values.

7.3 AQUIFER TEST RESULTS AND ANALYSIS

Four boreholes (SD4-18, SD4-28, SD4-43 and SD4-47) were selected for the discussion of the results of the aquifer tests. Two of these boreholes (SD4-18 and SD4-28) are located on the Western Fault, while the other two boreholes (SD4-43 and SD4-47) are located on the Eastern Fault. Diagnostic plots were used to determine the typical flow regimes and behaviour of the aquifers in the study area. The log-log derivative of drawdown versus time and semi-log plot of drawdown versus time were used to identify the position of the fractures as well as the inner and outer boundary conditions, thus determining the aquifer characteristics.

The geological logs of the selected boreholes were discussed in Chapter 6. The results of the hydraulic tests performed on the four boreholes will be interpreted with reference to the geological conditions observed in these boreholes.

7.3.1 **Borehole SD4-18**

From the step drawdown test performed on borehole SD4-18, the suitable constant discharge rate was determined to be 5 l/s. Borehole SD4-18 was pumped at this constant rate for a period of approximately 48 hours. The available drawdown for this borehole was 19.38 m, based on the derivative plots showing the position of the main water strike. The available drawdown was chosen so as not to dewater the main fractures.

In the semi-log plot in (Figure 92), the first 10 minutes indicate a linear flow, which means flow was from the fracture to the borehole. From 10 minutes until the end of the test, a secondary matrix flow was observed, thus making the flow bilinear. According to Kruseman and de Ridder (1994) the curve indicates a confined aquifer.

The depths of the fracture positions showed in the derivative plot (Figure 93) are calculated from the FC software by taking the drawdown of the different fractures and adding the static water level of the borehole. In this instance for the first fracture the drawdown was 17.1 m and the static water level is 36.42 mbgl (see Table 11). By combining the two values one can determine the depth of the fracture. However, when referring to the geological log of SD-18 (refer Figure 85) the fractures observed in the derivative plot in (Figure 94) are not present at same depth in the geological log. A possible explanation for the discrepancy it that not all the fractures were logged during the logging of borehole SD4-18.

The derivative plot in (Figure 93) shows that the aquifer system is multi-fractured. Two major fractures are positioned at depths of approximately (53.5 mbgl and 54.23 mbgl). There is a possibility of another fracture at approximately 55.5 mbgl judging by the behaviour observed on the derivative plot; however, the duration of the pumping test was insufficient to conclude this with certainty.

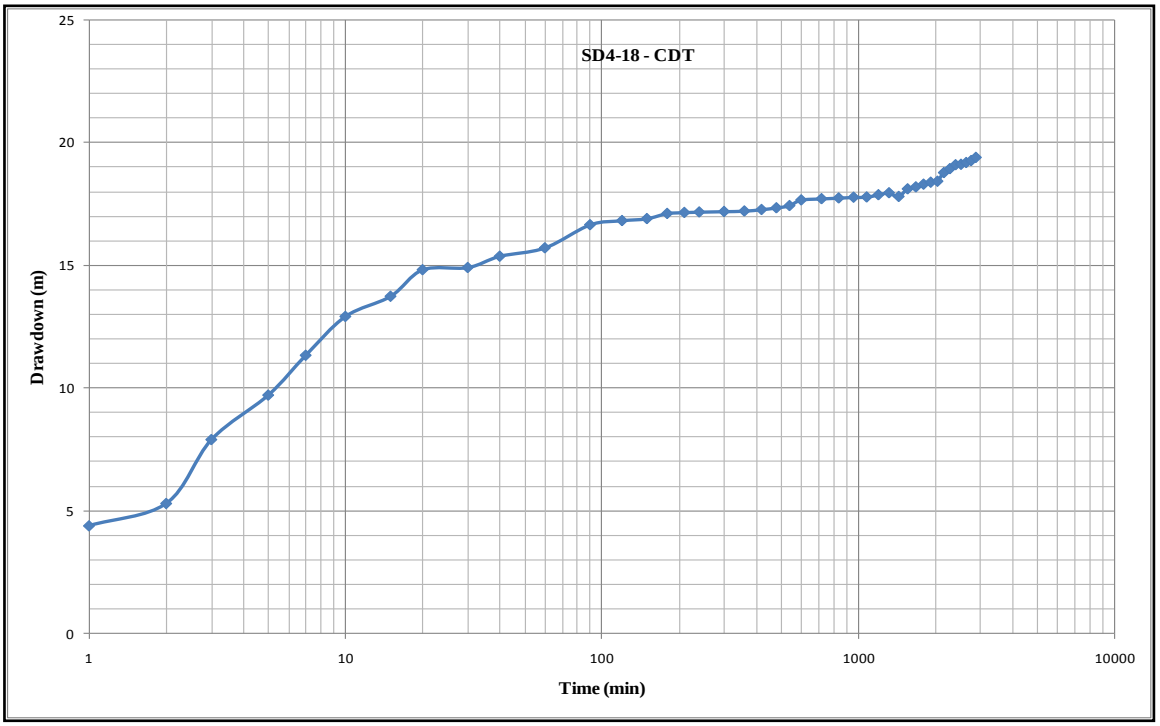

Figure 92: SD4-18 Semi log drawdown plot

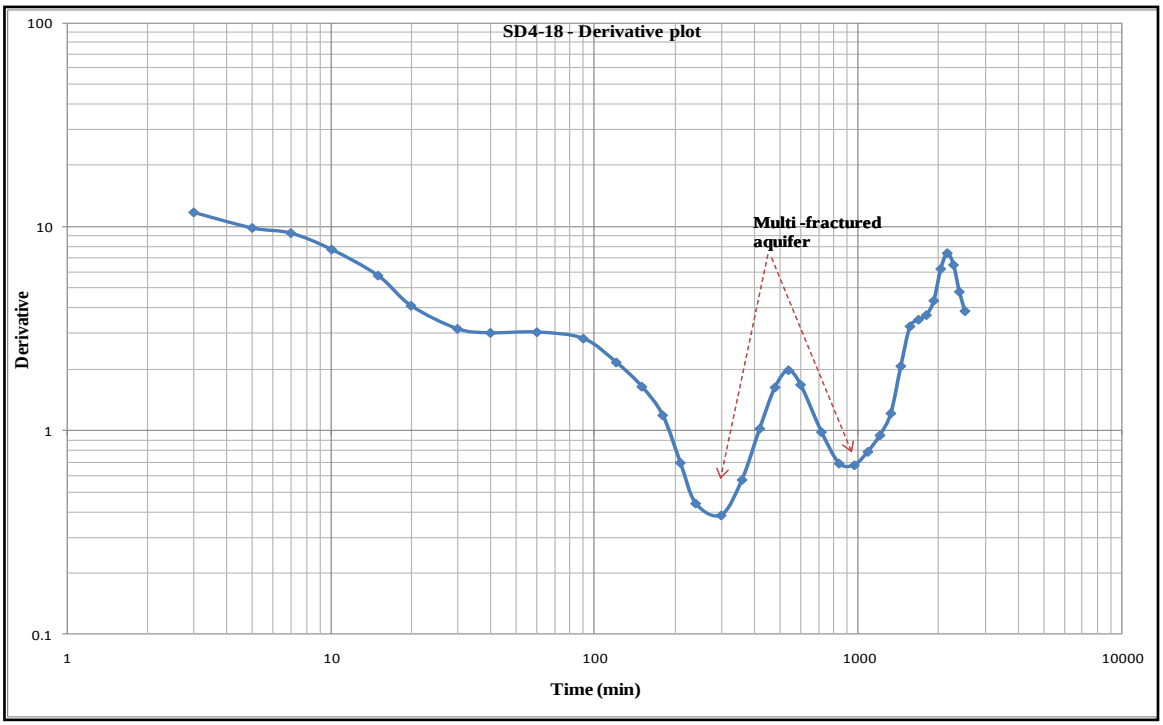

Figure 93: SD4-18 Derivative plot

7.3.2 **Borehole SD4-28**

The step down test performed on borehole SD4-28 determined that the suitable constant discharge rate was 5 *l*/s. Borehole SD4-28 was pumped at this constant rate for a period of 48 hours. The selected available drawdown was 26.01 m based on the derivative plots showing the position of the main water strike.

In the semi-log plot in (Figure 94), the first 10 minutes indicates that the borehole was pumping from the wellbore storage. At medium pumping time (10-1 000 minutes), a flattening segment is observed, which indicates recharging from the overlying, less permeable formation. From the late time (1 000-10 000 minutes), a bilinear flow is observed. According to Kruseman and de Ridder (1994) the curve indicates a confined aquifer.

The same principle as in Borehole SD4-18 was applied in determining the depth of the fractures of this borehole. The geological log of this borehole shows that the fractures are at different depths compared to the derivative plots; again this has to do with the geological logging of the borehole. Ideally the fractures on the derivative plots should correspond to the fractures on the geological logs (refer to Figure 86).

The derivative plot in Figure 95 shows that a multi-fractured aquifer is observed. The major fracture is at approximately (53.67 mbgl), followed by two minor fractures positioned at approximately (55.26 and 56.32 mbgl), respectively.

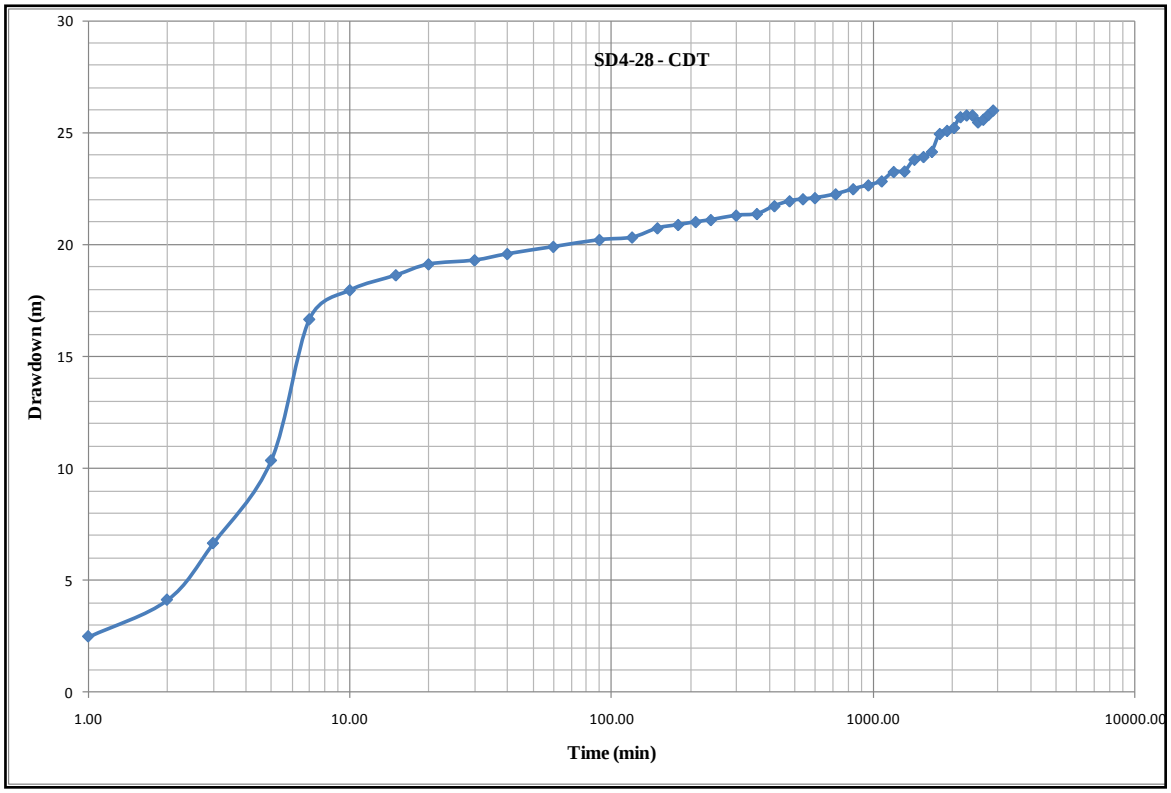

Figure 94: SD4-28 Semi log drawdown plot

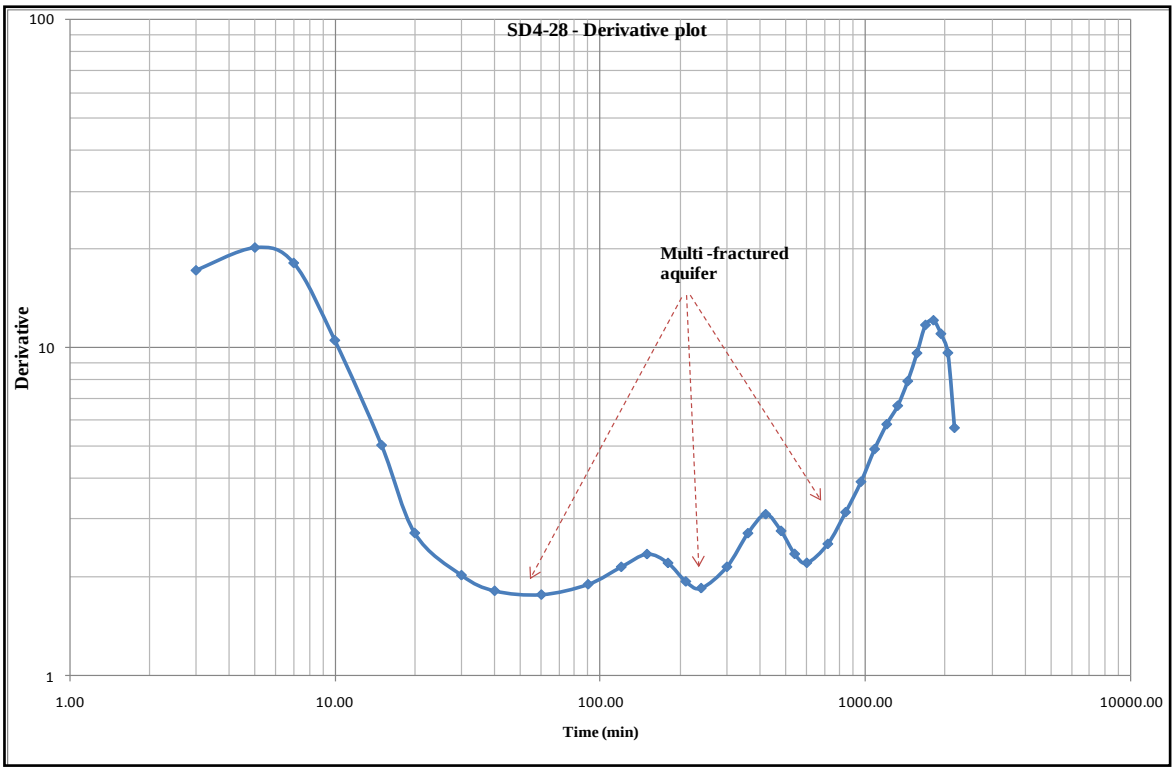

Figure 95: SD4-28 Derivative plot

7.3.3 Borehole SD4-43

From the step drawdown test performed on borehole SD4-43, the suitable constant discharge rate was determined to be 10 *l*/s. Borehole SD4-43 was pumped at this constant rate for a period of approximately 48 hours. The selected available drawdown was 13.51 m based on the derivative plots showing the position of the main water strike.

Based on the semi-log plot in (Figure 96), a linear flow is observed at the early time (0-8 minutes) followed by a bilinear flow from 8-11 minutes. The flow regime stabilised from 11 minutes until the end of the test. Matrix flow is observed at the late times, which means flow is from the overlying, less permeable formation. According to Kruseman and de Ridder (1994) the curve indicates a confined aquifer.

The fracture positions were determined by adding the static water level to the selected drawdown of the fractures. The geological log (refer to Figure 87) and the derivative plot fractures do not correlate well, possibly due to inaccurate geological logging.

The derivative plot in (Figure 97) shows that the aquifer is multi-fractured with fractures positioned at approximately (35.85 mbgl, 39.54 mbgl and 40.26 mbgl). It is possible that additional minor fractures could have been intersected if the duration of the test had been longer.

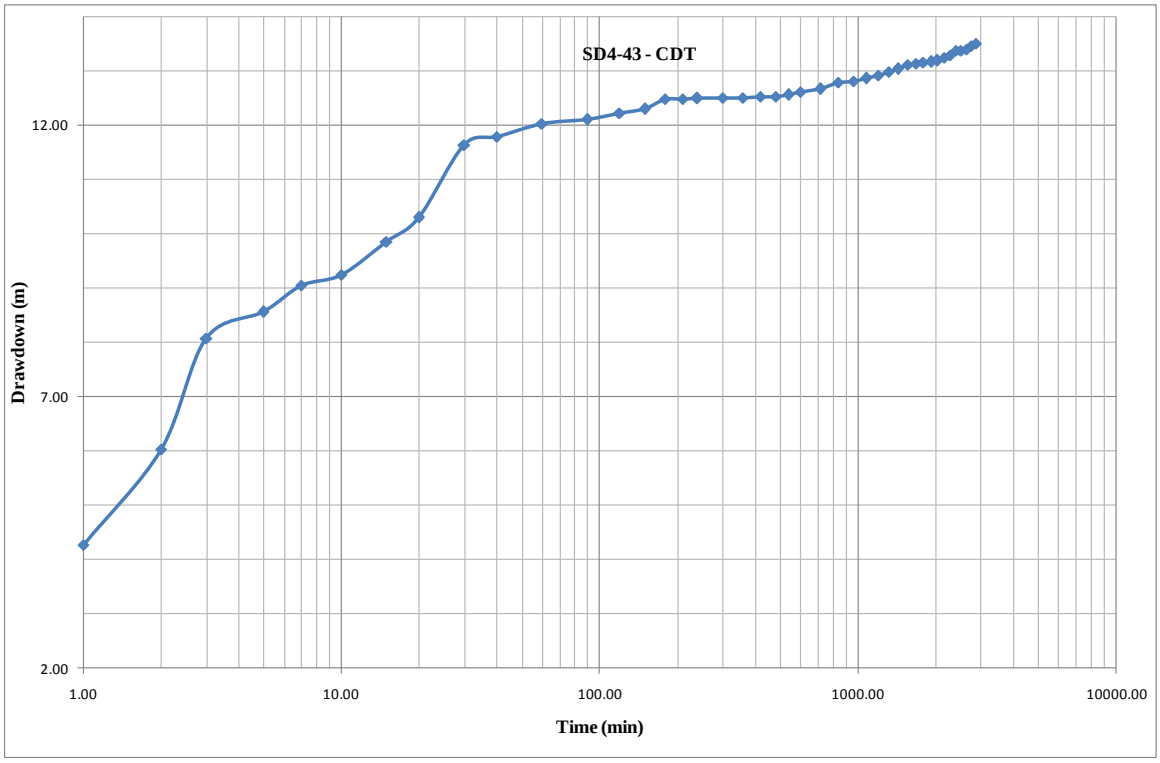

Figure 96: SD4-43 Semi log drawdown plot

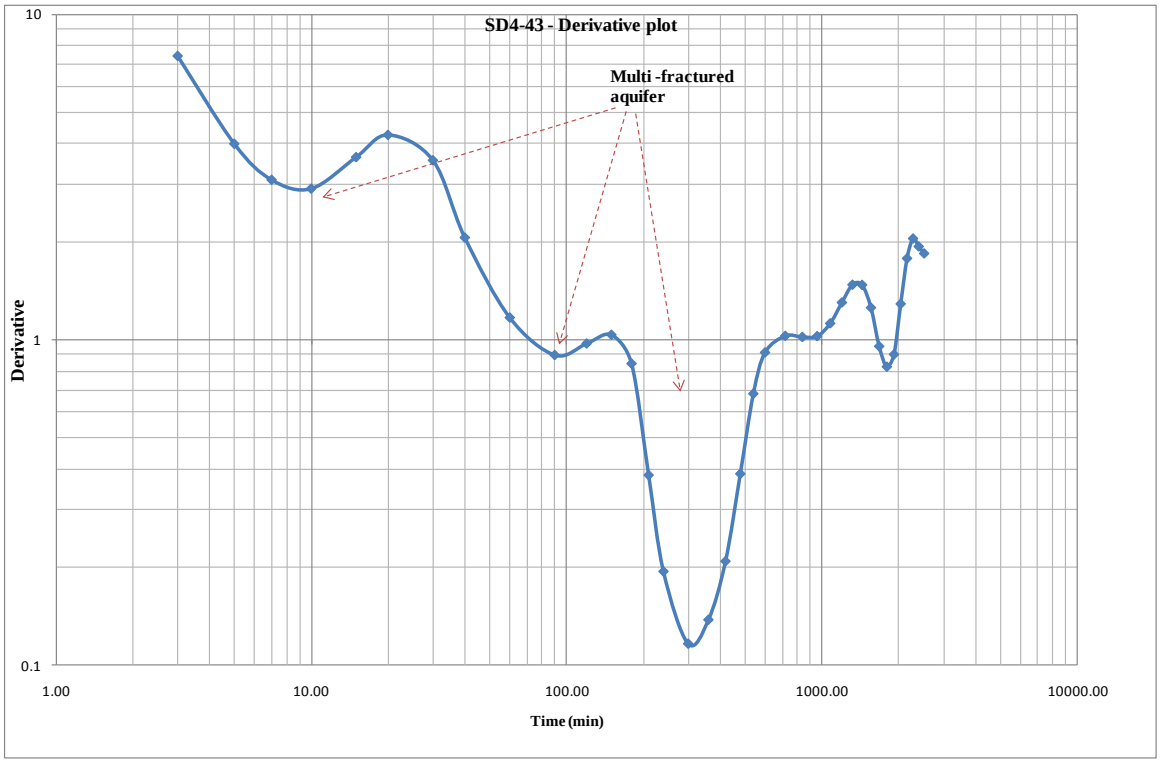

Figure 97: SD4-43 Derivative plot

7.3.4 Borehole SD4-45

The step down test performed on SD4-45 determined that the suitable constant discharge rate was 10.32 l/s. Borehole SD4-28 was pumped at this constant rate for a period of 72 hours.

The selected available drawdown was 12.39 m based on the derivative plots showing the position of the main water strike.

The semi log plot in (Figure 98) shows well bore storage at the early time (0-2 minutes). From 2-11 minutes a linear flow is observed. A bilinear flow is observed from 100 minutes, although the borehole was strong enough and signs of dewatering are evident. According to Kruseman and de Ridder (1994) the curve indicates a confined aquifer.

The fracture positions were determined by adding the static water level to the selected drawdown of the fractures. The geological log (refer to Figure 88) and the derivative plot fractures do not correlate, possibly due to inaccurate geological logging.

The derivate plot in (Figure 99) shows a multi-fractured aquifer system. The fractures are positioned at approximately (36.46 mbgl, 37.58 mbgl and 38.08 mbgl).

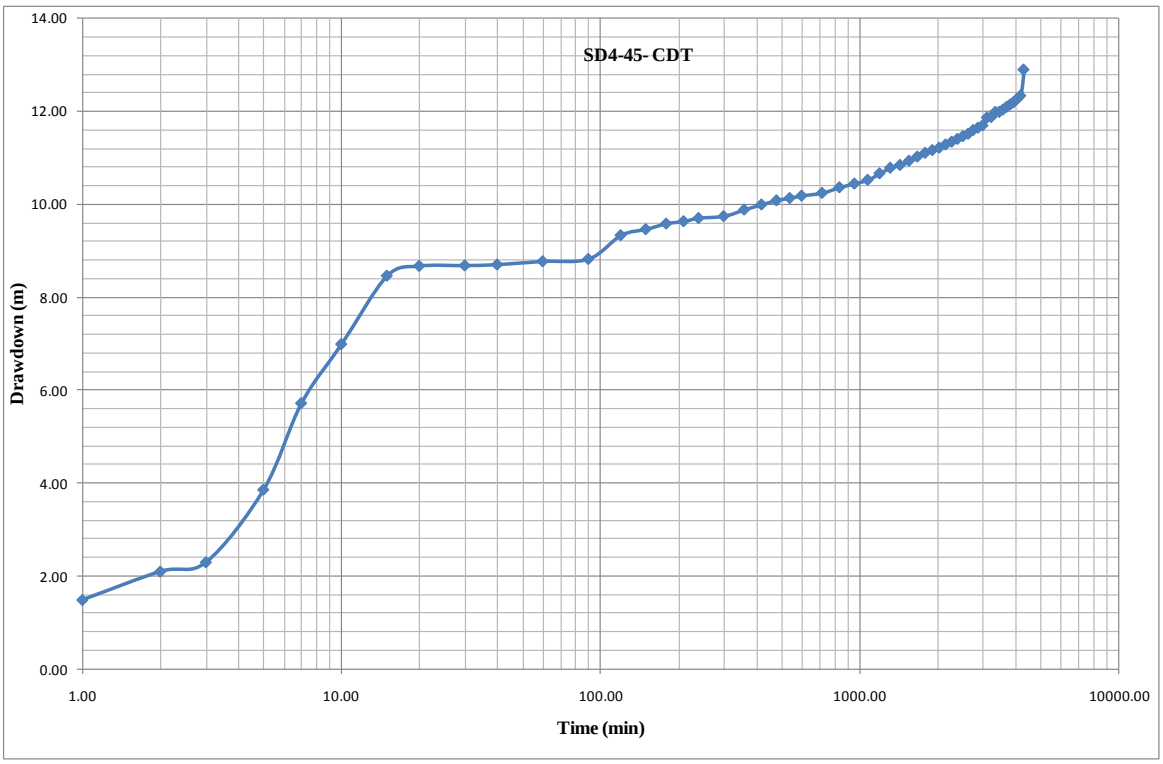

Figure 98: SD4-45 Semi log plot

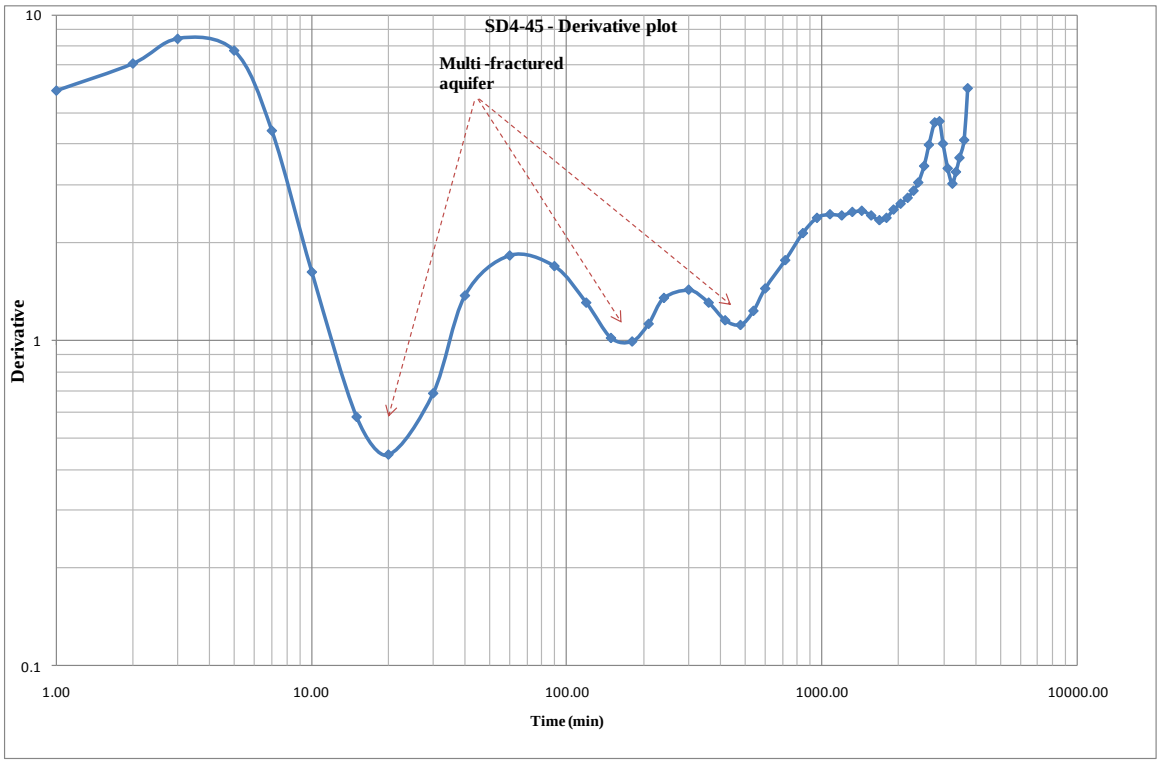

Figure 99: SD4-45 Derivative plot

7.3.5 Aquifer parameters

The transmissivity of the study was analysed using the Cooper-Jacob method which is included in the FC spreadsheet. The storativity and hydraulic parameters were obtained from the Spring model which uses finite-element approximations to solve groundwater flow equations. Hydraulic properties are assigned to nodes and elements that run a series of iterations to solve matrix problems (Golder, 2014).

7.3.5.1 Cooper Jacob method

The Cooper Jacob solution (or Jacob's modified non-equilibrium method) is useful for determining the hydraulic properties (transmissivity and storativity) of non-leaky confined aquifers. Analysis involves matching a straight line given by the solution to drawdown data plotted as a function of the logarithm time since the start of pumping (Cooper Jacob, 1946).

The Cooper Jacob method was used because it can provide realistic aquifer characteristic estimates with ease. The combination of derivative analysis and Cooper Jacob method improves the reliability of the estimates.

7.3.5.2 Validity assumption of Cooper Jacob method

During the application of the Cooper Jacob the following assumptions are made:

- The aquifer is confined,

- The aquifer has infinite areal extent,
- The aquifer is homogeneous, isotropic and of uniform thickness over the area influenced by the test,
- Prior to pumping, the piezometric surface is horizontal over the area that will be influenced by the test,
- The aquifer is pumped at a constant discharge rate and,
- The well penetrates the entire aquifer thickness.

These assumptions however are not always valid and realistic for all aquifers due to the complex mechanisms of fluid flow in the aquifer systems. For instance, one assumption is that the aquifer is homogenous, isotropic and of uniform thickness but if an aquifer is made up of alluvial sand and gravel, this assumption is incorrect (Kruseman and de Ridder, 1994). According to van Tonder (2001) all analytical methods have problems and limitations, therefore choosing the best method must be done with utmost cation.

7.3.5.3 Storativity

The groundwater system in the study area is diverse and changes in storativity are expected to occur in the different parts of the study area. The storativity values were calculated by the spring model using data of 21 observation boreholes in the study. The storativity of a confined aquifer, which varies with specific storage and aquifer thickness, typically ranges from 5×10^{-5} to 5×10^{-3} (Todd, 1980), while in an unconfined aquifer the storativity ranges from 0.1 to 0.3 (Lohman, 1972). Table l0 lists the summary of the storativity values in the study area.

Table 10: Storativity values determined for SD4 (Golder, 2014)

Parameters	Storativity (S)	
	Western Fault (9 boreholes)	Eastern Fault (12 boreholes)
Minimum	0.0001	0.00013
Maximum	0.0191	0.0382
Mean	0.00758	0.01929

7.3.5.4 Hydraulic conductivity

Western Fault aquifer

The aquifer is found at depths from 60 m to 110 m below surface. This aquifer is present below the gravel beds of the Eden Formation and above the andesitic lava of the Ventersdorp Supergroup.

Dolerite dykes intrudes the lava and the BIF bedrock, which is covered with thick Kalahari sediments with a thickness of up to 85 m (see Figure 100). The hydraulic conductivity ranges between 3×10^{-3} m/day to 2.1 m/day (Golder, 2014).

Eastern Fault aquifer

This aquifer is found at depths between 30 m and 70 m below surface. The aquifer is present below the Eden Formation and above the shale and quartzite of the Schmidtsdrif Subgroup. Dolerite dykes intrude the shale, quartzite and BIF bedrock which is covered with clay and calcrete (see Figure 101). The hydraulic conductivity ranges between 3×10^{-3} m/day to 1.1×10^{-1} m/day (Golder, 2014).

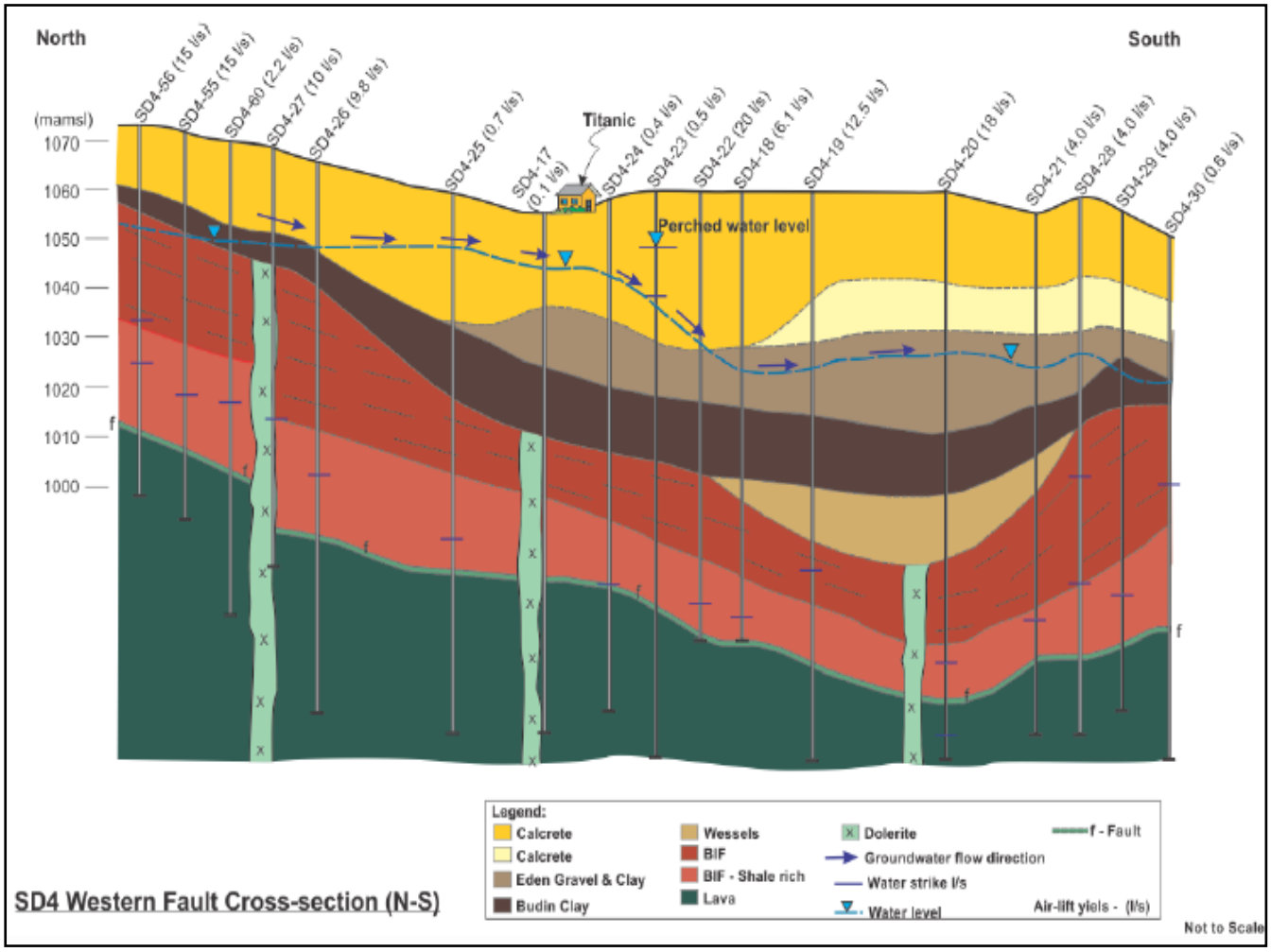

Figure 100: Cross-section of the Western Fault in SD4 from north to south (Golder, 2014)

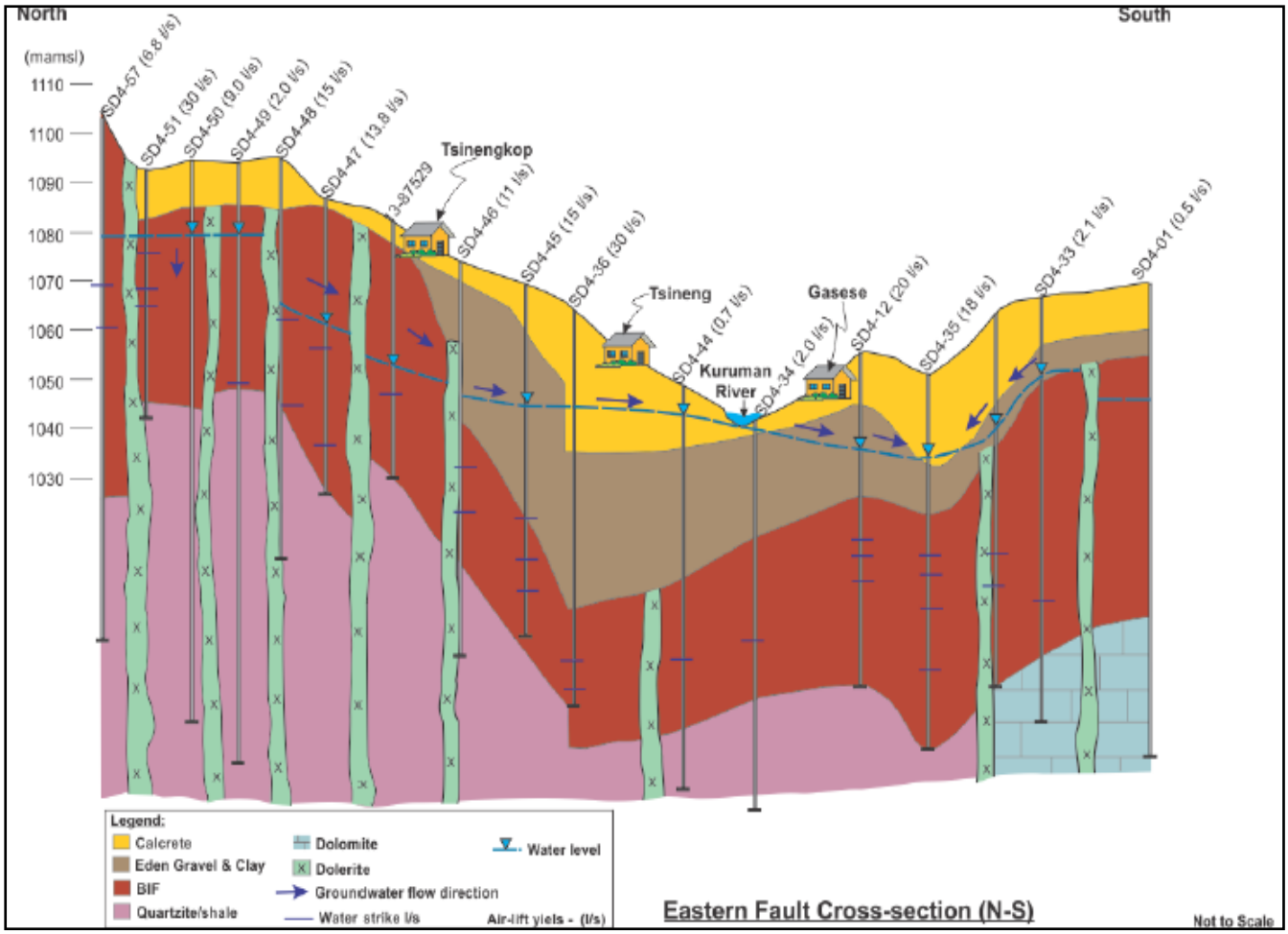

Figure 101: Cross-section of the Eastern Fault in SD4 from north to south (Golder, 2014)

7.3.5.5 Discussion

The transmissivity values of the intersected aquifer systems are variable due to the varying geology of the study area (see Table 10). The boreholes with low transmissitivities are underlain by fresh shale, quartzite, dolomite and lava. The high transmissivity boreholes are underlain by fine weathered and fractured banded iron formation. It was noted that the boreholes with high transmissivities occur near fault zones, indicating that the faults could act as or be associated with flow conduits for groundwater.

Variation in storativity values is evident in the western and eastern part of the study area; the difference is possibly due to the different degree of fracturing and the different geological conditions in the study area. According to Bredenkamp (1995) the *S*-values tend to change with distance because of the pressure relationship between groundwater in the matrix and in the fracture.

The hydraulic conductivities of the study area differ because of the different properties in the respective fault zones. In the Western Fault, permeabilities generally appear to be due to matrix porosity, while in the Eastern Fault permeabilities generally appear to be due to fractured zones and matrix porosity.

7.4 SUSTAINABLE YIELD ASSESSMENT AND ABSTRACTON RECOMMENDATIONS

The sustainable yields of the boreholes was obtained using the end drawdown, meaning that the yields are conservative and regarded as “Safe yield”, however this could also mean that the yield is under-estimated as the main strike position could have not been reached during the constant discharge (van Tonder, 2001).

In this current study the use of end drawdown was opted, to ensure that the water level is not dropped below the main strike position and also to ensure that sinkholes in the dolomite aquifers are not prompted to occur.

The sustainable yields for the selected boreholes were estimated using the FC programme. Figure 102, shows the location and distribution of the production boreholes. Table 11 shows the summarised pumped tested borehole information and abstraction recommendations.

From the table, one can see the recovery rate of the tested boreholes. The recovery rate of the recommended production boreholes are up to 95% within the pumping time. Thirty-one production boreholes with a total water supply of 108.14 l/s for 20 hours per day were recommended. The total recommended abstraction for the 31 production boreholes amounts to 7 786 m^3/day. It was recommended that five of the production boreholes be used as standby boreholes.

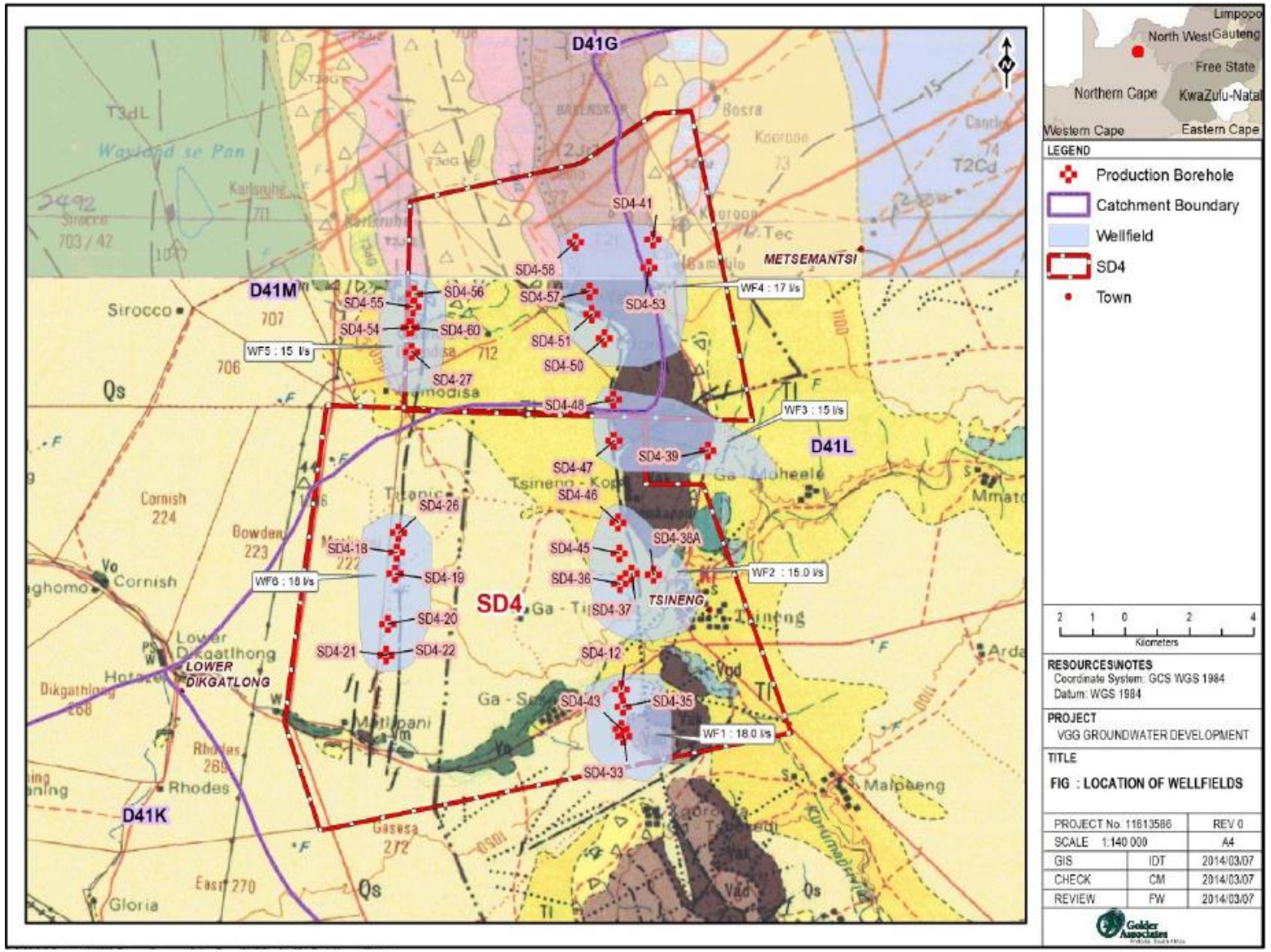

Figure 102: Location and distribution of production boreholes (Golder, 2014)

Table 11: Summarised pumped tested borehole information and the abstraction recommendations.

Borehole	Borehole Depth	Air-lift Yield	Static water level	CDT	CDT Yield	Drawdown	Recovery	Recovery	T	Recommended Abstraction			Borehole status
										Yield	Duration	Volume	
Number	(m)	(*l*/s)	(mbgl)	(hrs)	(*l*/s)	(m)	(m)	(%)	(m^2/day)	(l/s)	(hrs)	(m^3/day)	Prod/Mon/Standby
SD4-05	66.8	2.1	9.81	8	1.5	52.68	0.21	100	4	0.4	12	17.3	Mon
SD4-06	49	8.5	13.38	18	6.1	21.22	0.42	98	45	1.5	12	64.8	Pro/Standby
SD4-11	61.86	2.1	13.6	12	1	8.23	0	100	5	0.4	12	17.3	Mon
SD4-12	70.2	20	20.23	72	10.4	8.35	0.47	94	42	5	20	360	Prod
SD4-13	123.48	0.8	25.58	6	0.5	2.99	0	100	6.4	0.4	12	17.3	Mon
SD4-18	107	6	36.42	48	5.1	19.38	0.46	98	18	2	12	86.4	Prod
SD4-19	110.3	11.2	37.47	72	10.1	14.46	1.07	93	78	7.5	20	540	Prod
SD4-20	132.66	18	36.63	72	10.1	40.46	0.06	100	23	5	20	360	Prod
SD4-21	109.45	4	34.69	24	3	22.95	0.93	96	14	2	12	86.4	Prod/Standby
SD4-21A	61.62	4	35.38	24	2.1	6.76	0.07	99	38	1.5	12	64.8	Mon
SD4-22	94.6	20	34.12	72	10	18.2	0.14	99	59	4	20	288	Prod
SD4-26	107	9.8	15.12	48	6.1	40.16	11.95	70	13.3	2	12	86.4	Prod
SD4-27	91	10	19.42	72	10	7.13	0.63	91	34	3	20	216	Prod
SD4-28	110.65	6	34.37	48	5	26.01	2.14	92	35	2.4	12	103.7	Prod/Standby
SD4-29	99.3	10	31.9	11	2.9	61.42	3.24	95	2.7	1	12	43.2	Mon
SD4-33	109.24	1.5	15.03	No CDT	2	-	-	-	6	0.5	12	21.6	Mon
SD4-34	117.78	2	3.37	No CDT	2.1	-	-	-	4	0.5	12	21.6	Mon
SD4-35	80.33	15	22.06	48	15.1	15.11	0.58	96	100	7	20	504	Prod
SD4-36	81.57	30	21.14	72	15	10.92	2.92	73	27	3	20	216	Prod

Table 11 (Continued): Summarised pumped tested borehole information and the abstraction recommendations.

Borehole	Borehole Depth	Air-lift Yield	Static water level	CDT	CDT Yield	Drawdown	Recovery	Recovery	T	Recommended Abstraction			Borehole status
Number	(m)	(*l*/s)	(mbgl)	(hrs)	(*l*/s)	(m)	(m)	(%)	(m^2/day)	Yield (l/s)	Duration (hrs)	Volume (m^3/day)	Prod/Mon/Standby
SD4-37	73.65	15	21.46	72	10	10.65	0.36	97	48	4	20	288	Prod
SD4-38	92.75	4	23.74	24	3	18.26	0.55	97	48	4	12	86.4	Prod/Standby
SD4-38A	82.02	3	22.07	48	5.1	11.92	0.24	98	49	3	20	216	Prod
SD4-39	106.4	20	17	72	10	23.71	0.63	97	47.4	4	20	288	Prod
SD4-41	117	0.8	74.03	24	2.5	13.46	0.03	100	29	1.8	12	77.8	Prod
SD4-42	120.24	20	13.65	48	8.1	41.5	0.68	98	113	4	20	288	Prod
SD4–43	79.24	15	27.78	48	10.1	13.51	0.38	97	78	6	20	432	Prod
SD4-45	73.6	15	26.46	72	10.3	12.39	2.15	83	61	3	18	194.4	Prod
SD4-46	73.5	11	32.49	72	10.2	12.84	1.46	89	43	5	18	324	Prod
SD4-47	64.2	14	20.71	72	10.1	13.2	1.09	92	59	4	20	288	Prod
SD4-48	82	15	28.82	72	10	12.22	1.83	85	75	3.5	20	252	Prod
SD4-50	120	9.8	15.83	48	8	36.43	0.65	98	32	4	20	288	Prod
SD4-51	56.45	30	15.22	72	20	2.15	0.61	72	133	7	20	504	Prod
SD4-52	82.8	10	8.4	20	4	68.29	1.08	98	7	0.7	12	30.2	Mon
SD4-53	117.51	8	42.92	72	15	8.52	2.01	76	48.2	3	20	216	Prod
SD4-54	53.55	17	21.96	72	15	4.71	0.26	94	87.7	4	20	288	Prod
SD4-55	88	15	24.05	72	10.1	6.91	0	100	72.8	4	20	288	Prod
SD4-56	84.37	15	25.95	72	8	11.81	0.01	100	89.9	4	20	288	Prod
SD4-57	120.4	6.8	27.1	48	8	4.44	0.06	99	84	3	20	216	Prod
SD4-58	59	1.2	40	24	3	6.77	0.54	92	18.6	1.2	12	51.8	Prod/Standby
SD4-60	94.8	2	21.7	24	1.5	13.85	0	100	17.8	0.8	12	34.6	Mon

CHAPTER 8: HYDROCHEMISTRY

8.1 INTRODUCTION

Forty groundwater samples were collected during the drilling exercise and submitted to the UIS laboratory in Pretoria for chemical analyses. The analyses were performed to assess if the groundwater in the study area is of a quality suitable for human consumption and to determine whether pollutants had impacted on the groundwater. Water samples were analysed for the concentrations of the major ion species (macro determinants), as well as for selected trace elements (micro determinants). No bacteriological analyses were conducted.

In this chapter, the results of the inorganic analyses performed on the groundwater samples are discussed. The groundwater chemistries are also plotted in Piper, Expanded Durov and Schoeller Diagrams to allow visual classification of the water types present in the study area.

8.2 RESULTS OF THE WATER CHEMISTRY ANALYSES

To classify the quality of the groundwater from the various boreholes, the results of the inorganic water analyses performed on the water samples were compared against the South African National Standards SANS (241:2011). The results of the analyses are presented in (Table 12). In this table, the measured concentrations of the parameters analysed are displayed and colour-coded according to water quality category. The classification system used to classify the water in different quality categories is as follows:

- Class 0: Very good quality water
- Class1: Good water quality-suitable for use, rare instances of negative effects
- Class 2: Marginal water quality-conditionally acceptable. Negative effects may occur in some sensitive groups; and
- Class 3: Poor water quality - unsuitable for domestic use without treatment. Chronic health effects may occur.
- Class 4: Unacceptable water quality-totally unsuitable for use. Acute effects may occur.

8.2.1 Macro-Determinants

The hydrochemical signature of the groundwater from the study area shows that the groundwater quality is generally good. The pH values (ranging between 6.99 and 8.04) point towards neutral to

slightly alkaline groundwater conditions, and fall within the limits of very good quality water as prescribed by the guidelines of the SANS (241:2011). In the study area, low EC values were observed in the shallow boreholes with borehole SD4-20s and borehole SD-21s having values of 45.6 and 55 mS/m, respectively. The depth of SD-20s was 45 m and of borehole SD-21s was 40 m. The inverse was observed for the deeper boreholes: the EC values of borehole SD4-30 and borehole SD4-31 was (97.1 mS/m and 100 mS/m), respectively. These boreholes were drilled to depths of (120 mbgl and 99.86 mbgl), respectively. At shallow depth the thick Kalahari sediments are present, which could be protecting the shallow aquifers. The TDS concentrations of the borehole water (range between 276 mg/*l* and 1 540 mg/*l*), resulting in the water quality to be classified as very good to marginal according to the SANS (214:2011) guidelines.

The groundwater appears to be characterised by high fluoride and calcium concentrations. This is related to the geological structures and the geological conditions of the study area. According to Gaciri and Davies (1993) certain geological settings that host rocks such as metamorphic, sedimentary and volcanic rocks release fluoride in the groundwater during chemical leaching and weathering process of these rocks. During the drilling of some of the boreholes, lava (volcanic material) was intersected (refer to Chapter 6). The observed high calcium concentrations can possibly be related to the clay, calcrete and dolomite material found in the study area.

The macro determinants analyses were done to include major ions and metals. All the collected samples were analysed for the following major parameters: ammonium (NH_4), calcium (Ca), chloride (Cl), magnesium (Mg), sodium (Na), sulphate (SO_4), potassium (K), nitrate as N, and fluoride (F).

From the results of the chemical analyses performed on the groundwater samples, it is seen that most of the major determinants had concentrations low enough to classify the water as belonging to Class 0 (very good quality) and Class 1 (good quality). However, some of the concentrations at some of the boreholes were high enough to cause a Class 2 (marginal quality) classification. These are discussed below:

- Borehole SD4-21S– Water from this borehole had a higher nitrate concentration (14.2 mg/*l*) than the other boreholes in the study area. The reason for the higher concentration is thought to be due to human activities near the borehole; namely cattle faecal material and the use of septic tanks.
- Borehole SD4-31 – Water from this borehole had elevated chloride (300 mg/*l*) and fluoride (1.3 mg/*l*) concentrations (see Table 12). This borehole is near a dolerite dyke, hence the elevated levels of fluoride and chloride concentration.

The chloride can likely be due to the shale layer in the borehole. According to the geological log of this borehole at 30 m, a dolerite layer was intersected followed by a shale layer.

- Borehole SD4-47–Water from this borehole had an elevated electrical conductivity value (230 mS/m), and high total dissolved solids (1 540 mg/*l*), calcium (250 mg/*l*) and chloride (515 mg/*l*) concentrations. The high calcium concentration is likely to be due to the clay material which is found in the borehole. The chloride can be due to the dolerite layer found in this borehole. The possible reason for high EC and TDS is livestock watering close to this borehole.

8.2.2 Micro Determinants (Trace Elements)

The analysis of the trace elements was conducted using an Induced Couple Plasma-Mass Spectrometer (ICP-MS) and included the following parameters: aluminium (Al), copper (Cu), iron (Fe), and manganese (Mn). The results of the hydrochemical analyses show that only the Mn concentrations at a number of boreholes were high enough to cause a Class 1 (good quality) classification. All the other concentrations were low enough to cause a Class 0 (very good quality) classification.

8.3 WATER TYPE CLASSIFICATION

Water classification based on the hydrochemical results was done to investigate the type of water that is present in the study area. The hydrochemical characteristics are assessed using the Piper Trilinear Diagram (Piper, 1944), Expanded Durov Diagram (Durov, 1948) and Schoeller Diagram (Schoeller, 1964). These diagrams show the chemical distribution of groundwater in the study area. The Windows Interpretation System for Hydro-geologists, developed by the Institute of Groundwater Studies, was used to create these diagrams.

Table 12: Results of hydrochemical analyses

Site Name	pH	EC	TDS	Total Alk	Na	Ca	Mg	K	CL	SO4	F	NO3-as N	Al	Cu	Fe	Mn
		mS/m	Mg/L	Mg/L	Mg/L	Mg/L	Mg/L	Mg/L	Mg/L	Mg/L	Mg/L	Mg/L	Mg/L	Mg/L	Mg/L	Mg/L
SD4-01	7.92	62.4	392	275	54.3	38.8	44.2	4.93	40.8	40.9	0.717	1.22	0.05	0.05	0.05	0.08
SD4-03	7.42	69.2	456	491	22.6	102	38.8	4.61	14.4	24.2	0.816	2.12	0.05	0.05	0.05	0.25
SD4-05	7.57	78	594	442	11.5	140	33.3	2.28	12.9	17.5	0.169	2.81	0.05	0.05	0.05	0.05
SD4-06	7.35	89.1	572	415	28.2	110	66.9	2.78	57.8	49.2	0.212	3.37	0.05	0.05	0.05	0.05
SD4-07	7.51	79.3	504	494	29.3	101	53	2.61	53	35.7	0.366	3.27	0.05	0.05	0.05	0.1
SD4-11	7.45	70.1	440	386	12.2	90.8	50.8	1.04	23.4	9.47	0.337	2.13	0.05	0.05	0.05	0.05
SD4-12	7.54	68.2	454	362	13.6	119	28.4	1.68	19.1	10.9	0.139	4.95	0.05	0.05	0.05	0.05
SD4-13	7.34	117	814	403	51.1	121	71.1	3.13	124	70.8	0.3	8.7	0.05	0.05	0.05	0.11
SD4-15	7.68	72.1	480	433	29.4	34.9	61.8	3.34	17.5	13.5	0.311	2.48	0.05	0.05	0.05	0.18
SD4-16	7.87	69.3	472	396	40	62	58.8	3.75	19.2	17.6	0.413	2	0.05	0.05	0.05	0.1
SD4-18	7.5	81.6	532	414	25.2	95.1	60.7	3.07	43	22.5	0.351	2.43	0.05	0.05	0.05	0.05
SD4-19	7.61	86.8	594	403	32	89.6	67	3.17	61.8	31.6	0.367	3.2	0.05	0.05	0.05	0.05
SD4-20	8.04	91.5	572	472	46.2	74.2	79.9	4.57	47.8	23.8	0.409	1.99	0.05	0.05	0.05	0.05
SD4-20S	7.69	45.6	276	225	18.3	31.3	39.1	2.84	22.9	8.76	0.38	0.3	0.05	0.05	0.05	0.19
SD4-21	7.57	80.1	452	461	18.2	44.6	67.9	2.55	15.6	11.9	0.397	2.28	0.08	0.05	0.05	0.05
SD4-21A	7.54	79.7	468	454	15.1	50.1	68.4	2.13	16.9	10.1	0.434	2.21	0.1	0.05	0.05	0.05
SD4-21S	7.69	55	326	298	23.6	35.8	52.9	2.38	0.856	0.3	0.45	14.2	0.05	0.05	0.05	0.13
SD4-22	7.59	72.2	458	387	17.3	80.3	49.2	2.9	24.4	15.3	0.473	2.27	0.13	0.05	0.05	0.05
SD4-26	7.57	87.6	488	442	24.3	102	52.6	5.85	22.3	23.2	0.364	2.62	0.12	0.05	0.05	0.05
SD4-28	7.25	86.5	526	500	15.4	60.7	76.4	2.2	13.8	8.64	0.42	3.44	0.11	0.05	0.05	0.05
SD4-29	7.97	74.9	428	404	28	60.7	62.8	2.67	29.2	13.6	0.437	1.92	0.11	0.05	0.05	0.05
SD4-30	7.75	97.1	516	462	42.5	65.2	70.1	3.07	65.2	28.9	0.676	3.36	0.05	0.05	0.05	0.06
SD4-31	7.49	100	774	208	60.9	69.4	65.1	5.39	300	0.8	1.3	0.3	0.05	0.05	0.05	0.37
SD4-33	7.39	65.5	384	340	17.8	103	28.4	2.18	0.18	0.8	0.18	4.02	0.05	0.05	0.05	0.11
Class 0	5.0-9.5	<70	<450		<100	<80	<70	<25	<100	<200	<0.7	<6	<0.15	1	<0.5	<0.1
Class 1	4.5-5 & 9.5-10	70-150	450-1000		100-200	80-150	70-100	25-50	100-200	200-400	0.7-1.0	6.0-10	0.15-0.5	1.0-2.0	0.5-1.0	0.1-1.5
Class 2	4.0-4.5 & 10-10.5	150-370	1000-2400		200-400	150-300	100-200	50-100	200-600	400-600	1.0-1.5	10.0-20.0	>0.5	>2.0	1.0-5.0	1.5-4
Class 3	3-4 & 10.5-11	370-520	2400-3400		400-1000	>300	200-400	100-500	600-1200	600-1000	1.5-3.5	20-40			5.0-10	4.0-10
Class 4	<3 & >11	>520	>3400		>1000		>400	>500	>1200	>1000	>3.5	>40			>10	>10

Table 12 (Continued): Results of hydrochemical analyses

Site Name	pH	EC	TDS	Total Alk	Na	Ca	Mg	K	CL	SO4	F	NO3-as N	Al	Cu	Fe	Mn
		mS/m	Mg/L	Mg/L	Mg/L	Mg/L	Mg/L	Mg/L	Mg/L	Mg/L	Mg/L	Mg/L	Mg/L	Mg/L	Mg/L	Mg/L
SD4-34	7.75	78.6	460	398	35.4	89	59.5	3.46	70	36.7	0.231	3.1	0.03	0.02	0.02	0.01
SD4-35	7.79	69.7	486	357	15.4	63.3	29.3	1.81	17.9	14.9	0.16	5.7	0.05	0.05	0.05	0.05
SD4-36	7.56	104	678	423	32.9	133	65.4	3.84	105	36.5	0.203	3.84	0.16	0.05	0.05	0.05
SD4-37	7.59	108	728	430	40.8	112	69.5	3.32	111	38.3	0.268	5.18	0.15	0.05	0.05	0.05
SD4-38	7.69	96.5	618	381	43.9	100	62.7	5.15	84.6	63.2	0.576	1.24	0.05	0.05	0.05	0.28
SD4-38A	7.46	112	742	434	49.7	116	72	4.27	115	46.3	0.429	4.11	0.05	0.05	0.05	0.05
SD4-40	7.86	73.1	452	364	23.7	76.6	56	1.35	38.5	16.6	0.327	2.12	0.05	0.05	0.05	0.05
SD4-41	7.36	93.8	578	325	40.3	102	50.5	5.27	91	86.3	-	0.38	0.05	0.05	0.05	0.39
SD4-42	7.75	75.1	450	382	23.2	84.9	52.5	1.75	37	18.5	0.346	2.35	0.13	0.05	0.05	0.05
SD4-43	7.76	64.5	436	328	14.8	114	26.9	1.58	17.7	9.73	0.163	5.82	0.05	0.05	0.05	0.05
SD4-44	7.5	99.8	544	415	37.4	101	70.6	3.96	103	36.1	0.133	0.74	0.02	0.02	0.05	1.18
SD4-45	7.15	116	800	446	43.5	98.2	68.2	4	118	45	0.252	6.59	0.13	0.05	0.05	0.05
SD4-46	7.79	108	724	268	45	66.6	80	4.55	178	52	0.185	5.24	0.07	0.05	0.05	0.05
SD4-47	7.36	230	1540	423	121	250	127	5.7	515	184	0.116	2.63	0.18	0.05	0.05	0.05
SD4-52	7.65	98.6	658	416	43.1	76.4	75.3	3.25	88.4	47	0.486	1.69	0.12	0.05	0.05	0.05
SD4-58A	6.99	62.1	440	255	19.3	69.6	37.2	5.04	28.3	47.8	-	3.33	0.05	0.05	0.05	0.05
Class 0	5.0-9.5	<70	<450		<100	<80	<70	<25	<100	<200	<0.7	<6	<0.15	1	<0.5	<0.1
Class 1	4.5-5 & 9.5-10	70-150	450-1000		100-200	80-150	70-100	25-50	100-200	200-400	0.7-1.0	6.0-10	0.15-0.5	1.0-2.0	0.5-1.0	0.1-1.5
Class 2	4.0-4.5 & 10-10.5	150-370	1000-2400		200-400	150-300	100-200	50-100	200-600	400-600	1.0-1.5	10.0-20.0	>0.5	>2.0	1.0-5.0	1.5-4
Class 3	3-4 & 10.5-11	370-520	2400-3400		400-1000	>300	200-400	100-500	600-1200	600-1000	1.5-3.5	20-40			5.0-10	4.0-10
Class 4	<3 & >11	>520	>3400		>1000		>400	>500	>1200	>1000	>3.5	>40			>10	>10

The Piper Diagram is a graphical representation of the chemistry of a water sample which plots cations and anions in separate ternary plots. The ternary plots consist of two triangles, one the left and another on the right. Fractional concentration of concentration of major cation (Ca^{2+}, Mg^{2+}, Na^{2+} and K^{2+} are plotted in the left-hand triangle, while fractional concentrations of major anions (SO_4^{2-}, HCO_3^- and CO_3^{2-}, and Cl^-) are plotted on the right-hand triangle. These concentrations are then projected into the central diamond-shaped diagram. Bases on where the ion concentrations plot in the diamond-shaped region, the water type may be classified in terms of the relative abundances of the major cations and anions (refer to Figure 103).

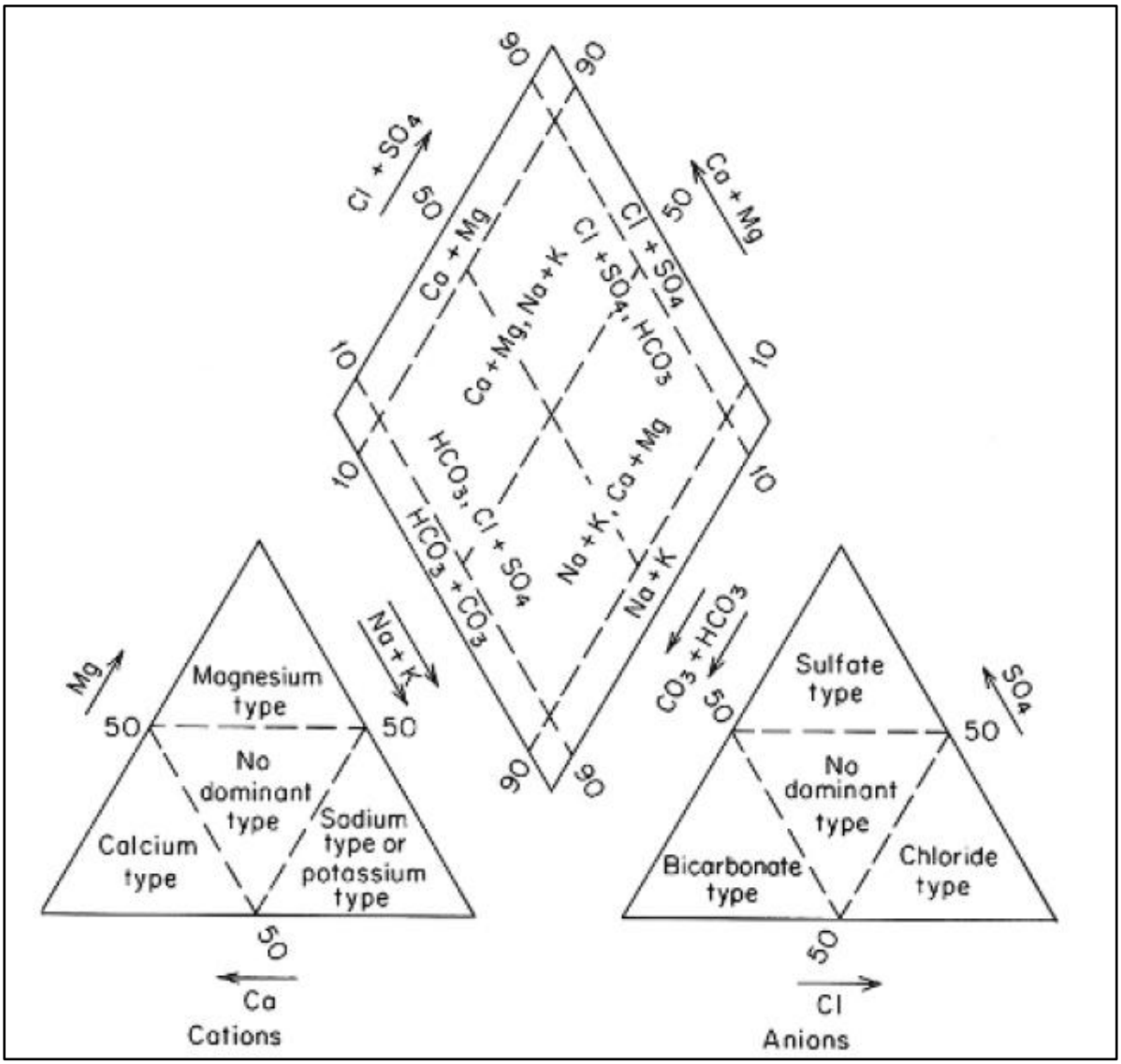

Figure 103: Classification of water type in the Piper Diagram (Freeze and Cherry, 1979)

In (Figure 105), the Piper Diagram classifies the water type as bicarbonate with calcium and magnesium dominating; this dominance can be attributed to the geology and possibly due to the recharged rainfall water in the study area.

It is assumed that groundwater had enough time to be in contact with the rocks in order for the water chemistry to resemble the mineral constituents of the host rocks.

The boreholes in the Western Fault have a groundwater type that indicates magnesium bicarbonate dominance. Mixing of water types is possible in these boreholes because of the thick Kalahari sediments found in this part of the study area.

The boreholes in the Eastern Fault have a groundwater type that indicates calcium bicarbonate, with some boreholes having no cation dominance. The dominance of cations in some of the borehole can be related to the geology. Borehole SD4-31 is an outlier because it indicates a chloride dominance which is possibly due to the shale layer found in the borehole. It is also possible that connate water was released from the shale/clay during fracturing and mixing of fresh water and ion exchanges thus having water of different origin and age.

The Expanded Durov Diagram is a graphic representation similar to the Piper Diagram. The central plotting area is a square rather than a diamond but the principal difference is that in the Expanded Durov Diagram the percentages of the individual ions are calculated as total ions (Cation + Anions). In the Piper Diagram the percentages of cations and anions are plotted separately. The nine blocks in the main square of the diagram represent the hydrochemical facies. These hydrochemical facies are used to distinguish one water type from another (Chadha, 1999) (see Figure 104)

According to the Expanded Durov Diagram shown in (Figure 106), the groundwater from the study area is mostly unpolluted water (plotting in the top right and middle squares). Only four of the forty water samples plot in other squares, with only one sample suggesting some contamination. The chloride could be related to the geological condition while the source of sulphide is unknown.

A Schoeller Diagram is a semi-logarithmic diagram of the concentrations of the main ionic constituents in water (SO_4, HCO_3, Cl, Mg, Ca, Na/K) in equivalents per million per kg of solution (meq/kg). An equivalent is the amount of an anion or cation species needed to add or remove one mole of electrons from a system. Concentrations of each ion in each sample are represented by points on six equally spaced lines and points are connected by a line. The diagram gives absolute concentration, but the line also gives the ratio between two ions in the same sample

If a line joining two points representing ionic concentrations in a single sample is parallel to another line joining a second set of concentrations from another sample, the ratio of those ions in those samples are equal (van Voast and Wayne, 2003). These waters may then be considered to have similar mixing patterns.

According to the Schoeller Diagram shown in (Figure 107), two different water types occur in the study area. Most of the water samples display very similar shapes in the diagram.

However, a few outliers have noticeably lower sulphate concentrations than the majority of the samples. These outliers could be due to the different lithologies in which the boreholes occur.

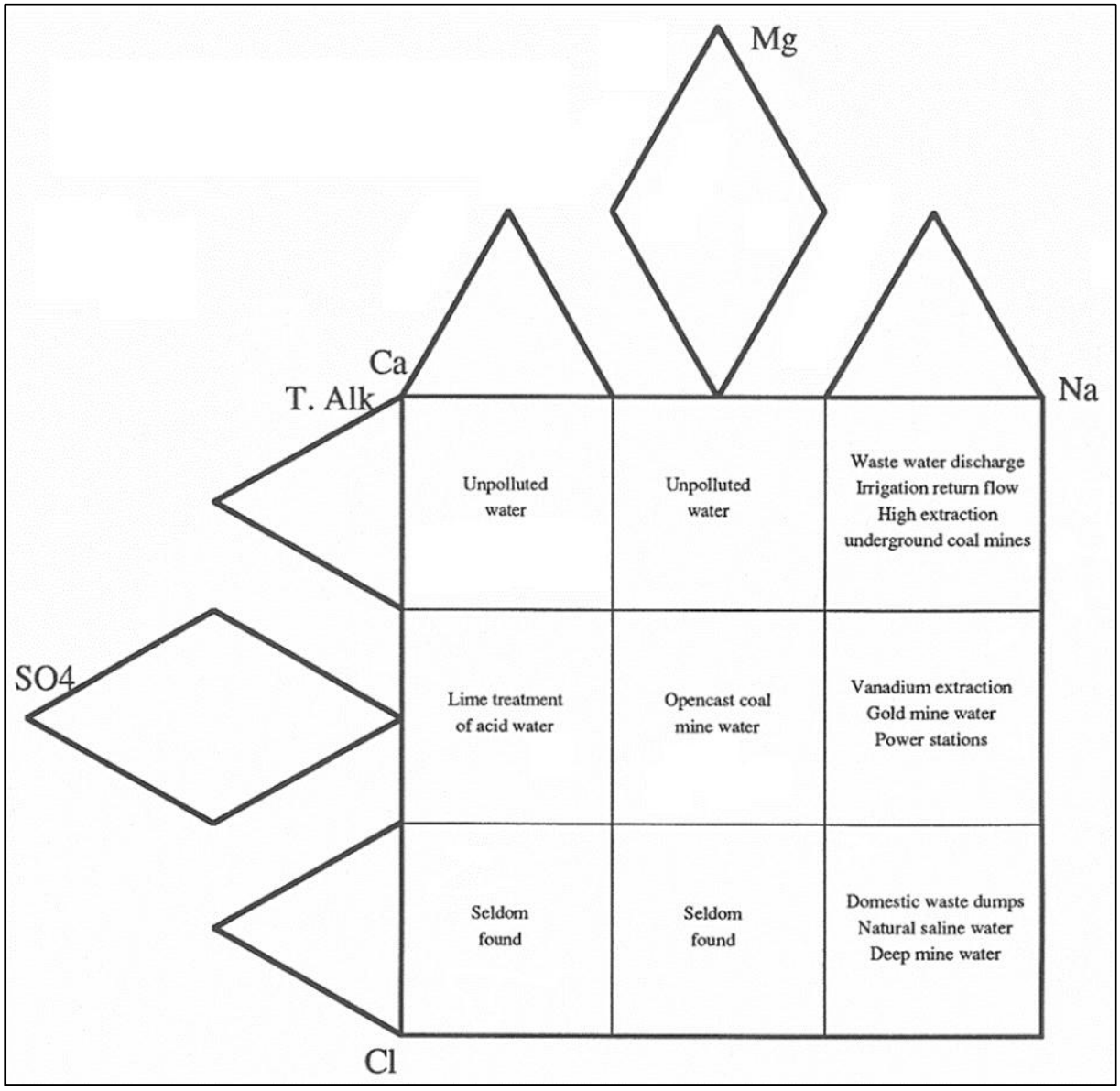

Figure 104: Classification of water type in the Expanded Durov Diagram (Chadha, 1999)

8.4 DISCUSSION

The overall water quality of study area can be classified under Class 1, which means the water is good for human consumption. A few boreholes showed elevated concentrations of chloride and fluoride which could be possibly related to the geological conditions. These few outlier boreholes are classified under Class 2, which is marginal water quality according to SANS (241:2011).

The different groundwater chemistry classification diagrams confirmed that different water types can be found in the study area. The Piper Diagram identified the calcium magnesium bicarbonate cations and anions as being dominant in the study area.

The Expanded Durov Diagram showed that most of the water samples have ion concentrations associated with unpolluted water. The Schoeller Diagram identified two distinct water types in the study area.

Although the quality of the groundwater from the different production boreholes appears to be generally good in terms of the inorganic parameters, no bacteriological analyses were performed on the water samples. It is recommended that further investigations into the water quality focus specifically on possible bacterial contamination of the water. It is further recommended that the water abstracted from the production boreholes be chlorinated as a safety measure prior to distribution and consumption.

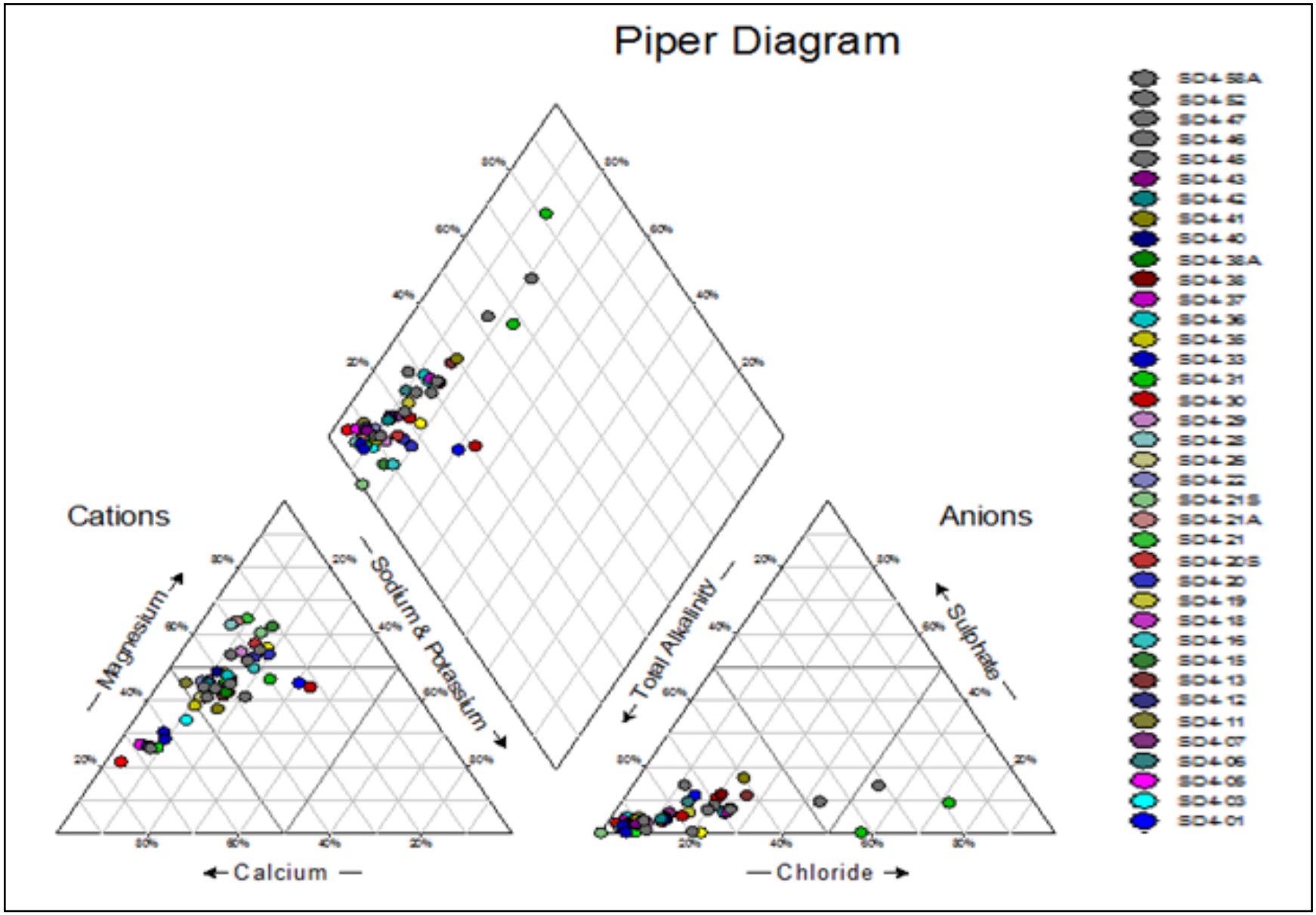

Figure 105: Piper Diagram displaying the hydrochemistry of water samples from the production boreholes

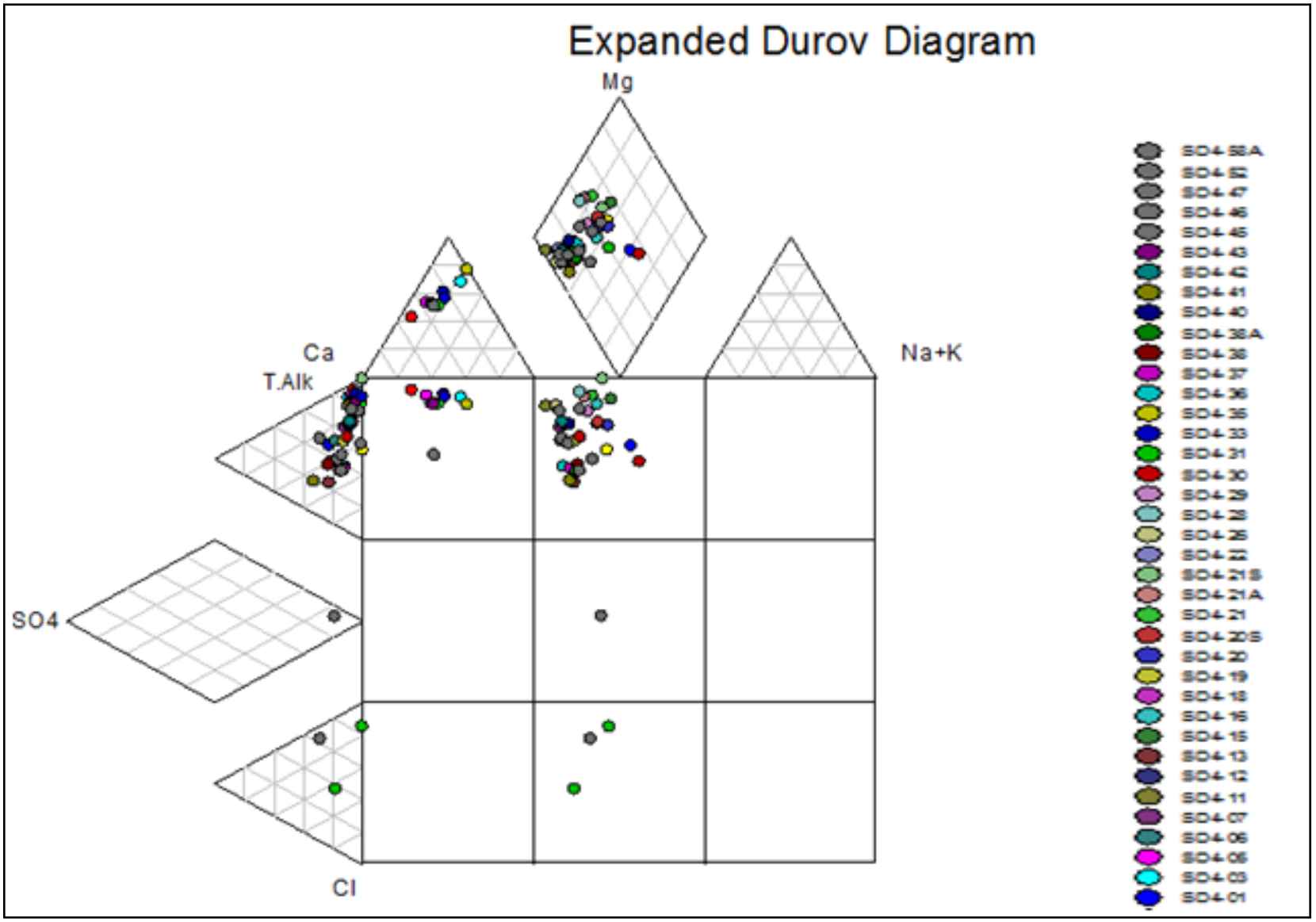

Figure 106: Expanded Durov Diagram displaying the hydrochemistry of water samples from the production boreholes

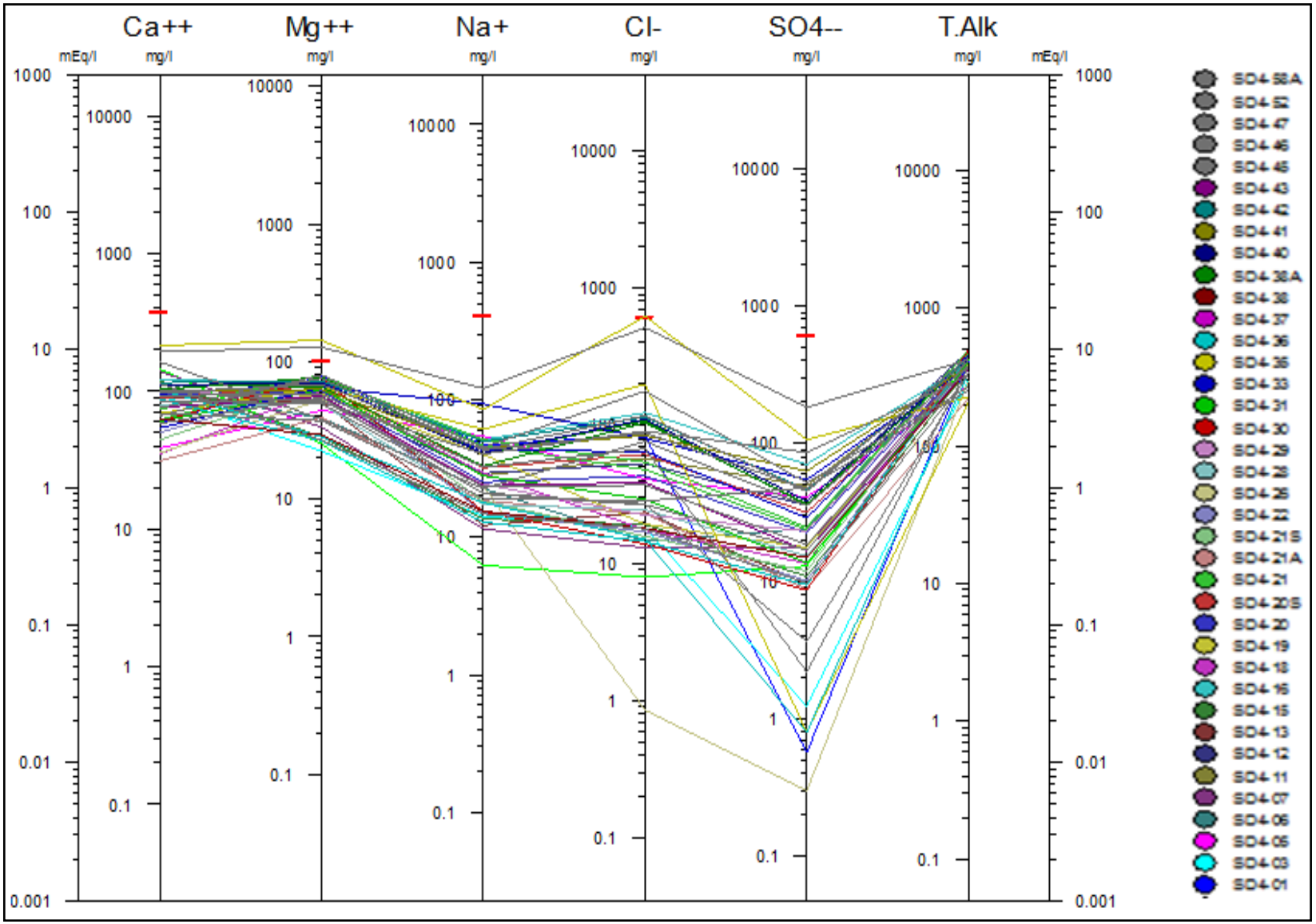

Figure 107: Schoeller Diagram displaying the hydrochemistry of water samples from the production borehole

CHAPTER 9: CONCLUSION AND RECOMMENDATIONS

This study focussed on using airborne and ground geophysical surveys during an investigation aimed at assessing the potential of using groundwater to augment the water supply to the John Taole Gaetsewe District. Due to failing surface water resources and an expected increase in the water demand, the municipality is likely to face water shortages in future if the surface water resources are not augmented from groundwater.

The airborne geophysical investigations consisted of using a helicopter-borne time-domain electromagnetic (TDEM) system (the SkyTEM system) to obtain information on the subsurface resistivity distribution up to depths in excess of 500 mbgl. The results of the TDEM survey were used to identify subsurface contrasts in the resistivity properties related to changes in the geology and the presence of geological structures. Well-defined resistivity anomalies were recorded along two major fault zones known to occur in the study area. In addition, analyses of the TDEM data also indicated that some of the dykes in the study area are associated with detectable resistivity contrasts.

Based on the results of the airborne geophysical survey, as well as knowledge of the local geological conditions, preliminary targets were identified for the ground geophysical investigations. Four methods were employed during the ground surveys, namely: the gravity, magnetic, electromagnetic (EM) and electrical resistivity tomography (ERT) methods. Data were recorded on profiles perpendicularly across the targets identified from the airborne EM data. The ground geophysical investigations confirmed the presence of the structures identified during the TDEM survey. Based on the results of the ground geophysical survey, targets were selected for the installation of production boreholes.

A total of 78 boreholes were drilled at the positions selected from the results of the ground geophysical investigations. Most of these boreholes were drilled along the two major faults mapped during the geophysical surveys. Sixty of the boreholes encountered water strikes and were hence deemed to be successful. These boreholes had a combined total blow-yield of 409 *l*/s. The high-yielding boreholes were located along the two major fault zones in the study area. The banded iron formation underlying the study area proved to be the major aquifer system, and not the dolomites as was suspected prior to the investigations.

Forty of the successful boreholes had blow-yields larger than 2 *l*/s and were selected for aquifer hydraulic testing to determine the hydraulic parameters of the intersected aquifer systems. Analyses of the results of the aquifer hydraulic tests revealed that the transmissivities of the intersected

aquifer systems range from 4 to 133 m^2/day, while storativity values range between 0.0001 and 0.0382. For each of the hydraulically tested boreholes, a sustainable yield was calculated using the values of the aquifer parameters for that particular borehole. The total sustainable yield for all the boreholes was calculated as 7 786 m^3/day.

Groundwater samples were taken from the 40 boreholes selected for aquifer hydraulic testing. These samples were submitted for inorganic hydrochemical analyses at an accredited laboratory, the results of the analyses showed that the groundwater quality in the study area is generally very good, although the concentrations of some macro determinants were high enough at some boreholes to render the water quality only good. The groundwater quality at four of the forty boreholes was classified as marginal.

By considering both the volumes of groundwater available for sustainable abstraction, and the groundwater quality, it is concluded that groundwater may be successfully used to augment the water supply to the John Taole Gaetsewe. However, to protect both the aquifer system from over-exploitation and the human consumers of groundwater from health risks, it is recommended that the following actions be taken:

- Although the total sustainable yield of the production boreholes was calculated at 7 786 m^3/day, the sustainable yield calculations did not compensate for the fact that many of the production boreholes are located on the same geological structures. These boreholes are therefore likely to tap from the same groundwater resource. The true total sustainable yield may therefore be much lower than the simple sum of the individual sustainable yields. If several boreholes on the same geological structure are therefore used to abstract groundwater, careful monitoring of the water levels will have to be done to ensure that the draw downs in the boreholes do not exceed the levels of the major fractures encountered in these boreholes.
- Ongoing monitoring of the groundwater quality will be essential to ensure that the quality remains suitable for human consumption. If it is found that the groundwater quality deteriorates to levels where it becomes unfit for human consumption, the water will have to be treated at one of the existing water treatments facilities currently serving the municipality. It is recommended that water quality testing be done on at least a monthly basis.

This study has shown how the combined use of airborne and ground geophysical surveys can greatly assist in the understanding of the subsurface geological and geohydrological conditions. Such an improved understanding will generally lead to higher success rates of groundwater

exploration programmes, which will in turn reduce the costs associated with the drilling of unsuccessful borehole.

It is therefore recommended that geophysical surveys always form part of groundwater exploration programmes, especially when the programmes focus on regional aquifer systems. For such regional aquifer systems, airborne geophysical surveys may prove invaluable.

REFERENCES

Ahmed, A.M., Ibrahim, A.E., Abbashar, A.R and Mohammed, E.A. (2009). Exploration of groundwater in a basement area using electrical and electromagnetic surveys, Case study : El sunut, North Kordofan State. *University of Africa journal of sciences*. Vol **2**, 1-13

Al-Garni, M.A. (2009). Geophysical investigation for groundwater in complex subsurface terrain, Wadi, KSA : A case study history. *Jordan journal of Civil Engineering*, volume **3**, No.2, 2009

Alla, M.A., Sultan, S.A., Mekhemer, H.M., El-Qady, G. and Santos, F.M. (2007). Integrated geophysical interpretation for groundwater potentiality : case study at the central part of Sinai Peninsula, Egypt. EGM 2007 International workshop innovation in EM, GRAV and MAG methods, Capri, Italy. 15-18 April 2007

Anderson, T. (2011). *Specialist vegetation study on the potential impact of the proposed gravenhage manganese project, Hotazel***.**

Ariyo, S.O & Adeyemi, G.O. (2013). Significant of geology & geophysical investigations in groundwater prospecting . A case study from hard rock terrain of Southwestern Nigeria. *Global journal of Human Social Science Geography, Geo-sciences & Environmental science & Disaster management*, vol**13** version 1, year 2013

Ayta, M., El-Qady, G. and Zaher, A. (2012). CSMT and TEM investigation to evaluate groundwater potentially in Qaret, Abu Rouh, Minya, Egypt. 21stEM induction workshop, Darwin, Australia, July 25-31, 2012

Beukes, N.J. **(1980**). Stratigrafie en lithofasies van die Campbellrand-Subgroep van die Proteroftiese Ghaap-Group, Nord-Kaapland. *Transvaa*l *Geological Society of South Africa.***83**, pp 141-170

Beukes, N.J. (1983). Paleo-environmental setting of Iron-formation in the depositional basin of the Transvaal Supergroup, South Africa. In : Trendall, A.F and Morris, R.*C Iron-formations, facts and problems*. Amsterdam, Elsevier, pp 131-209

Beukes, N.J. (1984). Sedimentology of Kuruman and Griquatown Iron-formation, Transvaal Supergroup, Griqualand West, South Africa. *Precambrian Research*, **24** pp 47-84

Beukes, N.J. (1986). The Transvaal sequence in Griqualand West. In : Anhaeusser, C.R. and Maske, S (Eds). *Mineral deposits of Southern Africa*, Vol 1. *Geological Society of South Africa*, Johannesburg pp 819-828

Beukes, N.J. (1987). Facies relation, depositional environments and diagenesis in a major early - Proterozoic stromatolitic carbonate platform to basinalsequence, Campbellrand subgroup, Transvaal Supergroup, South Africa**.** *Sedimentary Geology***, 54,** pp 1-46

Borehole Water Association of Southern Africa, (Undated) : Groundwater : Guidelines for Boreholes. (Available from either the Directorate Geohydrology of the Dept. of Water Affairs & Forestry or the Borehole Water Assoc. of Southern Africa)

Bradley, C.C., Ali, M.Y., Shawky, I., Levannier, A. and Dawoud, M.A. (2007). Microgravity investigation of an aquifer storage and recovery site in Abu Dhabi. *First Break*, volume **25**, 2007

Bredenkamp, D.B,. **Botha, L.J,.van Tonder, G.J and van Rensberg, H.J., (1995).** *Manual on quatitative estimation of groundwater recharge and aquifer storativity*. Report TT73/95 Water Research Commission. Pretoria

Carrasquilla, A., **Goncalves, C.A and Ulugergerli, E. (2007).** Evaluating the performance of different geophysical methods for groundwater prospecting in Santo basin, Brazil. Researchgate.net/publication/271842756

Chadha, D. K. (1999). A proposed new diagram for geochemical classification of natural waters and interpretation of chemical data: *Hydrogeology Journal***7**:431–439

Christiansen, A.V., Auken, E and Sørensen, I. (2006). The transient electromagnetic method. In: Kirch,R.(Ed), *Groundwatergeophysics a tool for hydrogeology*. Chapter 6, 179-225pp

Cooper, H.H. and C.E. Jacob. (1946). A generalized graphical method for evaluating formation constants and summarizing wellfield history, Am. *Geophys. Union Trans*., vol. **27**, pp. 526-534

Danielsen,V.E., Auken, E., Søndergaard., V, and Sørensen., I. (2003). The application of the transient electromagnetic method in hydrogeophysical survey. *Journal of Applied Geophysics* **53** (2003) pp181-198

Department of Water Affairs. (2013). *Annual national state of water report*, Pretoria

Department of Water Affairs. (2011). *Development of reconciliation strategies for area served/interacting by/with Sedibeng water's vaalgamaga scheme as well as a water master plan* , Pretoria

Department of Water Affairs. (2013). Geohydrological Information directorate, Pretoria

Department of Water Affairs (2013). *National Water Resource Strategy* , Pretoria

Department of Water Affairs. (2005). *Groundwater resource assessment phase 2*. Version **2**, 2005, Pretoria

Department of Water Affairs. (2010). *Groundwater Strategy*, Pretoria

Department of Water Affairs. (1997). *Minimum standards and guidelines for groundwater resource development for the community resource water supply and sanitation programme*. (1st ed), Pretoria

Department of Water Affairs. (2011). *The groundwater dictionary: A comprehensive reference of groundwater related terminology*. (2nd ed), Pretoria

Department of Water and Sanitation. (2014). Water Use Registration System**.** Accessed on 15 September 2014

Dudash, L.W., Morgan, T. and Kennedy, J. (2014). Integrated geophysical investigation of Pauma basin, California**.** Viewed on 24 November 2014 from http://library.serg.org

du Preez, M., van der Merwe., le Roux W., Nel, J., Meyer, R., Murray, K., Paramoer, E., Steyl, G. and Velly, C. (2013). *Investigation of the fate and transport of selected microogarnisms in two simulated aquifer conditions in the laboratory in the field*. Report 1905/1/12. Water research commission, Pretoria

Durov, S.A.(1948). Natural waters and graphic representation of their compositions. Dokl Akad Nauk SSSR **59**:87–90

Fitterman, D.V. and Stewart, M.T.(1986). Transient electromagnetic sounding for groundwater. *Geophysics*. **51**, 995-1005

Fourie, F.D. (2012). Institute of Groundwater Studies lecture notes. Unpublished. University of Free-State, Bloemfontein.

Freeze, R.A. and Cherry, J.A. (1979). *Groundwater*. Prentice Hall. New Jersey

Gaciri, S.J. and Davies, T.C. (1993). The occurrence and geochemistry of fluoride in some waters of Kenya. *Journal of Hydrology*. 143(**3-4**) 395-412

Golder Associates.(2014*).* *Groundwater assessment and development for the Vaal Gamaga pipeline scheme-SD4 area*. Pretoria

Grant, F. S. and West, G. F. (1965), Interpretation theory in applied geophysics:

McGraw-Hill, New York

Institute of Groundwater Studies (2008). Lecture notes. Unpublished. University of Free-State, Bloemfontein.

Institute of Groundwater Studies (2012). Lecture notes. Unpublished. University of Free-State, Bloemfontein.

Harding, C.J (2004).*Origin of the Zeekoebaart and Nauga east high-grade iron ore deposits, Northern Cape Province, South Africa*. Msc thesis. Rand Afrikaans University, Johannesburg.

Hiscock, K. (2005). *Hydrogeology principles and practice*, Blackwell publishing, United kingdom

Healy, R.W. (2010). *Estimating groundwater recharge*. Cambridge

Jones, J.F. (1963). Aquifer testing procedures and other information used evaluating groundwater supplies in Alberta**.** *Research Council of Alberta*. Report 63

Jones and Wagener. (2011). *Gravenhage manganese project, hydrogeological assessment and numerical groundwater model*. Report JW68/11/C525

Keller, R.L., Anscombe, J.R., Bauman, P.D., Hankin, P. and Engelbrecht, L. (2000). Geophysical mapping of groundwater water potential in rural water supply project: Malawi, Africa. Viewed on 24 November 2014 from http://library.serg.org

Kinzelbach W. (2002). A survey of methods for groundwater recharge in arid and semi-arid regions, Zurich, Switzerland.

Kirsch, R. (ed.), (2006*).* *Groundwater geophysics, A tool for hydrogeology*, Springer, Germany

Kirschvink, J.L., Gaidos, E.J., Bertani, L.E., Beukes, N.J., Gutzmer, J., Maepa, L.N. and Steinberger, R.E. (2000). Paleoproterozoic snowball Earth: Extreme climatic and geochemical global change and its biological consequences. *Proceedings of the national academy of sciences of the United States of America*. Vol. **97**15 February, 2000

Kotze, Y and van Tonder ,G. (2012). Groundwater use authorisations as part of groundwater resource management in water scares area within South Africa. Institute of groundwater Studies, University of the Free State, Bloemfontein.

Kruseman, G. P. and de Ridder, N.A. (1992). Analysis and Evaluation of Pumping Test Data. Second Edition. International Institute for Land Reclamation and Improvement. Wageningen. Netherlands.

Lerner, D.N., Issa, A. and Simmers, I. (1990). A guide to understanding and estimating natural recharge. *International contribution to hydrogeology*. Vol **8**. Hannover, Verlag Heinz

Llyod, J.W. (1986). Groundwater in arid and semi arid regions. *Encyclopedia of life support systems***.** Vol **1.** School of Earth Science, University of Birmingham, UK

Loke, M.H. (2000). *Electrical imaging surveys for environmental and engineering studies: a practical guide to 2-D and 3-D surveys*. Penang**,** Malaysia.

Lohman, S.W., (1972). Ground-water hydraulics: *U.S. Geological Survey* Professional Paper 708, 70 p.

McNeil, J.D. (1990). Use of electromagnetic methods for groundwater studies. In: Ward, S.H.(ed). Geotechnical and environmental geophysics, Vol:**02**. *Society of Exploration Geophysicists*, pp 191-218

Milsom, J.(2003). *Field geophysics*, 3rdedn., John Wiley & Sons, England

Mochales, T., Casas, A.M., Pueyo E.L., Pueyo, O., Roman, M.T., Pocovi, A., Soriano, M.A and Anson, D (2007). Detection of underground cavities combining gravity, magnetic and ground penetrating radar surveys. A case study from Zaragora area Spain. Published online Springer.

Monokofala, C. (2010). *Groundwater resource assessment for the Greater Mamusa local municipality North West-Province, South Africa*. Msc thesis, University of Free-State, Bloemfontein.

Monokofala, C. and Wiegmans, F. (2013). Groundwater resource assessment for water supply to the Heuningvlei socio-economic development area. 13thBiennial groundwater division conference. Paper presented at Southern sun Elangeni, Durban. 17-19 September 2013

Morris, B.L., Lawrence, A.R.L., Chilton, P.J.C., Adams, B., Calow, R.C., and Klinck, B.A. (2003). Groundwater and its Susceptibility to Degradation: A Global Assessment of the Problem of Options for Management. Early Warning and Assessment Report series, RS. 03-3. United Nations Environment Programme, Nairobi, Kenya.

Mucina, L and Rutherford, M. (2006). The vegetation of South Africa, Lesotho and Swaziland. Strelitzi**19**. *South African National Biodiversity Institute*, Pretoria

Murray, E.C. (1996). Guidelines for assessing single borehole yields in secondary aquifers. Msc thesis, Rhodes University.

Muturi, E.N, Korowe, M.O., Githiri, J.G., Cezar, I. and Jeffrey, S. (2014). Application of geophysics for groundwater evaluation in hard rock: case Kitui Fault**.** *Scientific Conference Proceeding.*2014

Nabighian, M. N. and Macnae, J. C. (1991). Time domain electromagnetic prospecting methods, In Nabighian, M. N., Ed., Electromagnetic methods in applied geophysics, Vol**2**, Part A: *Soc. Expl. Geophys*., 427-509

Narayan, S., Dusseault, M.B and Nobes, D.C (1994). Inversion techniques applied to resistivity inversion problems. *IOP Science Journal*, Volume **10**,669

Nyabeza, P.K., Shabalala, A. and Gwavava.O. (2013). Using geophysical techniques to delineate groundwater bearing structures at the Sagole hot spring, Limpopo province, South Africa**.**13thBiennial groundwater division conference. Paper presented at Southern sun Elangeni, Durban. 17-19 September 2013

Oladunoye, H.T., Odunaike, R.K., Ogunsola. P and Olaleye. O.A. (2013) Evaluation of groundwater potential using electrical resistivity method in Okenugbo area south west of Nigeria. *Internal journal of Engineering Applied Sciences*. Vol**4.** No.5 November 2013

Parsons R.P and Conrad J.E, (1998). Explanatory notes for the aquifer classification map of South Africa; WRC Report No. 116/98, Water Research Commission, Pretoria.

Parsons, R.P (1999). Water resource protection policy implementation-Groundwater glossary version 1.0

Pinsker, (1972). The effect of variations in local gravity and of aircraft Speed on the effective weight of Aircraft in high performance Cruise. *Ministry of Defence Aeronautical research council*. Report.R. & M. No. 3680

Piper, A.M. (1944). A graphic procedure in geochemical interpretation of water analyses. *Transactions America Geophysical Union*, 25(**6**) 914-928

Porsani, J.L., Almeida, E.R., Bortolozo, C.A. and Sontos, F. (2012). TDEM survey in an area of seismicity induced by water wells in Parana sedimentary basin, northern Sao Paulo state, Brazil. *Journal of applied geophysics*. V**82** no. 1 Part 6, pp 75-83 July 2012

Prabhu, H.M and Ravindran, A. (2012). Groundwater exploration study using wenner-schlumberger-electrode array through W-4 2D resistivity imaging systems at Mahapallipuram,Chennai, India. *Research journal of Recent Sciences*. Vol (**1**) 11 36-40

Reid, J.and Viezzoli, A. (2007). High-resolution near surface airborne electromagnetic-SkyTEM survey for Uranium exploration at Pells Range, WA. *Australian Society of Exploration Geophysics.*

Reynolds, J.M. (1997): *An introduction to applied and environmental geophysics*. John Wiley and Sons, NY, 806 pp.

Roux A.T. (1980). The magnetic method in the South Africa Geophysics Association Manual. Geophysics division of the national physical research laboratory of CSIR, Pretoria

Schoeller,H.(1964). La classification géochimique des eaux. IASH publication, no 64, General assembly of Berkeley 1964. Vol**4**

Shendi, E.H and Abouelmagd, A.A. (2004). New approach for groundwater geophysics in the development of groundwater in the basement terrains (A case study from south Sinai, Egypt). 7th conference geology of Sinai for development , Ismalia. 2004, pp 129-140

SkyTEM. (2012).*SD1, SD2 and SD4 RSA data report.* Denmark

Sørensen, I. and Auken, E. (2000). Large-Scale TEM investigation for groundwater**.**Viewed on 24 November 2014 from http://library.serg.org

Sørensen, I. and Auken, E. (2004). SkyTEM-a new high resolution helicopter transient electromagnetic system.*Exploration Geophysics.*2004**, 35,** 191-199

Struckmeier, W.F (1989). Types and uses of hydrogeological maps. International Symposium Hydrogeological maps. IAH. Hannover. pp 17-30

Standard South Africa, (2011)**.***South African National Standards, Drinking Water*, SANS 241:2005, Edition 6. 2011

Stettler, E.H (1979). *A geological and geophysical investigation of the diamond runs on Ruigtelaagte and vicinity, in the Bakerville area, Lichtenburg district***.** Msc thesis**.** University of Pretoria, Pretoria.

Sultan, A.S and Pek, J., (2014). Delineating groundwater aquifer and subsurface structures using integrated geophysical interpretation at the western part of Aqaba, Sinai Egypt. *International journal of Water Resources and Arid environments.* 3(**1**): 51-62 2014

Telford, W.M., Geldart, L.P and Sheriff, R.E. (1990). *Applied Geophysics* (2nded). Cambridge University Press.

Terblanche, M. and Stroebel, L. (2013). Case study: Groundwater exploration in the basement granite of the Kraaipan Group using aeromagnetic surveys.13thBiennial groundwater division conference. Paper presented at Southern sun Elangeni, Durban. 17-19 September 2013

Thomas, C., Judson,. W., Lehn, F and William, M. (1998*).* *Groundwater and surface water: A single resource.* US Geological Survey circular 1139, Denver

Todd, D.K. (1980). *Groundwater hydrology* (2nd Ed). New York, John Wiley

Ugwu, S.A and Nwsou, J.I. (2009). Detection of fractures for groundwater development in Ona Ukwu using electromagnetic profiling. *Journal of Applied Science and Environmental Management*. Vol**13** (4) 59-63

van Dyk, G.S., Makheta, J., Potgiter, D., Zikali, T., Leeme, V., Moletsane, F. and Vonya, T. (2008). Groundwater resource in the Northern Cape Province, Kimberly

van Niekerk, H.S. (1998).*The paleoproterozoic Olifantshoek-Kheisorogen and it's mineral potential*. Unpublished report, Johannesburg, pp 1-26

van Tonder, G, Bardenhagen I, Rieman K, Van Bosch J, Dzanga P. And Xu, Y. (2001). Manual on Pumping test analysis on fractured rock aquifers prepared by the Institute for Groundwater Studies (IGS) and submitted to Water Research Commission. January 2001

van Tonder, G. and Xu Y.(2001). A guide for the estimation of groundwater recharge in South Africa., Presented at the Workshop on Recharge, at the University of Pretoria (June 2001)

van Voast, W.A and Wayne (2003). A Geochemical signature of formation waters associated with coalbed methane. *American Association of Petroleum Geologists* (AAPG) Bulletin, v**. 87**, no. 4 (April 2003), pp. 667–676.

Vegter, J.R. (1995). An Explanation of a Set of National Groundwater Maps, WRC report TT74/95, *Water Research Commission*, Pretoria.

Vivier, J.J.P. (2013).Determination of sustainable groundwater yield: A system management approach based on the minimum groundwater balance. 13thBiennial groundwater division conference. Paper presented at Southern sun Elangeni, Durban. 17-19 September 2013

Wiegmans, F. (2006).*Groundwater Resources Management Strategy for the Kgalagadi District Municipality: Groundwater Situation Assessment*, Volume **2.** Report No. VSAG/06/08/01. August 2006.

Whightman, W., Hild, J. and Hodges, S. (2001). Geophysical surveys for groundwater in the Gaza strip**.** Viewed on 24 November 2014 from http://library.serg.org

Woodford, A.C **and Chevallier, L. (2002).** *Hydrogeology of the main Karoo basin: Current knowledge and future research needs.* Report TT179/02, *Water Research Commission*, Pretoria.

Internet sources:

Viewed on June 2014

(www.tshipi.co.za).

(http://www.bus-ex.com/article/kudumane-manganese-resources).

Viewed on July 2014

(https://en.wikipedia.org.wiki/groundwater

(texaset.tamu.edu/effrain.php

(www.floodmap.net).

Viewed on August 2014
geoinfo.nmt.edu/geoscience/projects/astronauts/gravitymethod.html)

(http://education.nationalgeographic.org/media/earths-tides/).

(geoinfo.nmt.edu/geoscience/projects/astronauts/gravity_method.html).

www.google.images.com
Viewed on January 2015
(http://www.thefreedictionary.com/
(www.scintrexltd.com).
www.abemlund.com
(https://en.wikipedia.org/wiki/)
www.google.images.com
(http://www.solution4africa.com/
www.encyclopedia.com).
(en.openei.org/wiki/DC/Resistivity/Survey).
(www.geonics.com)

Viewed on September 2016
(www.gamaga.gov.za)
(new.sedibengwater.co.za).

Other sources:
John Taole Gaetsewe memorandum document 2012
Kathu gazette

ABSTRACT

In this study the groundwater resource the in Tsineng area, Northern Cape was assessed in terms of the volumes of water that may be sustainably abstracted from the aquifer system, and the quality of the available groundwater. A strong emphasis was placed on the use of airborne and ground geophysical techniques to gain a better understanding of the geological and geohydrological conditions in the study area.

The airborne geophysical technique employed during the current investigation was the time-domain electromagnetic method (using the SkyTEM system), while ground geophysical surveys employed the gravity, magnetic, frequency-domain electromagnetic and electrical resistivity tomography methods. The geophysical techniques were used to provide information on physical changes in the subsurface conditions that may be related to the presence of geological structures associated with potential groundwater resources. The results of all the geophysical methods used were collated and correlated to the local geology to make an informed decision during the selection of drilling targets for the installation of production boreholes.

From the TDEM data, information on the subsurface distribution of resistivities was obtained. Well-defined resistivity anomalies correlated well with the known presence of two prominent fault zones. Furthermore, resistivity anomalies were also identified at the locations of mapped dolerite dykes known to intersect the study area. The ground geophysical investigations were conducted across preliminary targets defined from the airborne TDEM data. The ground geophysical investigations confirmed the presence of the structures identified from the TDEM data.

Based on the results of the geophysical investigations and the known local geological conditions, drilling targets were selected at positions deemed promising for the installation of successful production boreholes. A total of 78 exploration boreholes were drilled during the current investigations. Sixty of these boreholes had water strikes and were thus considered successful. A combined total blow-yield of 409 *l*/s was measured in the successful boreholes. Forty of the drilled boreholes had blow-yields in excess of 2 *l*/s. These boreholes were selected for aquifer hydraulic tests to assess the hydraulic parameters of the intersected aquifer systems. From the estimated hydraulic parameters, sustainable yields were determined for the tested boreholes. The total estimated sustainable yield from the boreholes was more than 7 500 m^3/day.

Water samples from the 40 high-yielding boreholes were submitted for chemical analyses. The results of the analyses showed that the water in the study area is generally of very good quality,

suitable for human consumption. It is therefore concluded that groundwater may be successfully used to augment the municipal water supply in the Tsineng area.

The results of the current research demonstrate that the use of geophysical techniques could greatly contribute to an understanding of the geological and geohydrological conditions in a study area, which could in turn lead to a higher success rate during groundwater exploration programmes.

OPSOMMING

In hierdiestudie is die grondwaterbronne in die Tsineng-area in die Noord-KaapProvinsiegeëvalueer in terme van die volumes water watvolhoubaaronttrekkan word vanuit die akwifeersisteem, asook die kwalitiet van die beskikbaregrondwater. ‘nSterkklem is geplaas op die gebruik van geofisiesetegniekeom ‘n beterinsig in die geologieseengeohidrologiesetoestande van die studie-area teverkry.

Die lug-geofisiesetegniekwatgebruik is gedurende die huidigeondersoek was die tyd-domeinelektromagnetiesemetode (die SkyTEM-sisteem is gebruik), terwyl die grondgeofisieseopnames die gravitasie-, magnetiese-, frekwensie-domeinelektromagnetiese-enelektrieseweerstandtomografie-metodesgebruik het. Die geofisiesetegnieke is gebruikominligtingtebekomoor die fisieseveranderingeondergrondswatverband mag hou met die teenwoordigheid van geologiesestrukturegeassosieer met potensiëlegrondwaterbronne. Die resultate van al die geofisiesemetodes is gesamentlikbeskouengekorreleer met die plaaslikegeologieomingeligtebesluiteteneemtydens die seleksie van boorteikensvir die installering van produksieboorgate.

Vanaf die TDEM data is inligtingoor die ondergrondseverspreiding van soortlikeweerstandeverkry. Goed-gedefinieerdeweerstands-anomalië het goedooreengestem met die bekendeteenwoordigheid van twee prominenteverskuiwingsones. Verder is weerstands-anomaliëookgeïdentifiseer by die posisiesvanbekendedolerietgangewat die studie-area deurkruis.Diegrondgeofisieseondersoeke is gedoenoorvoorlopigeteikens, soosgedefinieervanaf die TDEM-data.Diegrondgeofisieseondersoekehet die teenwoordigheidbevestig van die strukturewatvanaf die TDEM-data geïdentifiseer is.

Vanaf die resultate van die geofisieseondersoeke,asook die bekendeplaaslikegeologiesetoestande, is boorteikensgekies op plekkewat as belowendbeskou is vir die installering van suksesvolleproduksieboorgate.‘nTotaal van 78 eksplorasieboorgate is geboortydens die huidigeondersoeke.Sestig van hierdieboorgate het water getrefen is gevolglik as suksesvolbeskou.‘nGekombineerdetotaleblaaslewering van 409 *l*/sis gemeet in die suksesvolleboorgate.Veertig van die boorgate het blaaslewerings van meer as 2 *l*/sgehad. Hierdieboorgate is gekiesvirhidrouliesetoetsing van die akwifeerom die hidrouliese parameters van die akwifeer-sisteemtebepaal.Vanaf die geskattehidrouliese parameters, is volhoubareleweringsvir die getoetsteboorgatebepaal.Dietotalegeskattevolhoubarelewering van die boorgate was meer as 7 500 m^3/day.

Watermonsters van die 40 hoë-leweringboorgate is ingedienvirchemieseanalises. Die resultate van die chemieseanalises het getoondat die water in die studie-area oor de algemeen van baiegoeiekwaliteit is, geskikvirmenslikegebruik. Die water kandussuksesvolgebruik word om die munisipalewatertoevoer in die Tsineng-area aantevul.

Die resultate van die huidigeondersoektoondat die gebruik van geofisiesetegniekegrootlikskanbydra tot die begrip van die geologieseengeohidrologiesetoestande in ‘n studie-area, watweerkan lei tot ‘n hoërsukseskoersgedurendegrondwatereksplorasieprograme

APPENDIX A

A1 WESTERN FAULT

Borehole No.	Latitude	Longitude	Traverse No	Drill Depth (m)	Casing Depth (m)	Water Strike (m)	Air-Lift yield (l/s)
SD4-15	-27.09951	23.00059	E11A/600	115	96	33;84	0.5
SD4-16	-27.09956	22.99757	E11A/300	161	96	93	2.1
SD4-17	-27.0509	23.00087	E4A/165	126	4	69	0.1
SD4-18	-27.07232	22.99858	E9A/145	126	72	86; 90	**6.1**
SD4-19	-27.07789	22.99812	E9B/150	122	74	76	**12.5**
SD4-20	-27.09127	22.99613	E10B/100	120	120	94, 115	**18**
SD4-20A	-27.09137	22.99617	E10/100	100	-	76	0
SD4-20S	-27.09102	22.99617	E10B/100	45	45	31	**0.01**
SD4-21	-27.09954	22.99557	E11A/100	110	110	81, 98	**4**
SD4-21A	-27.09959	22.99526	E11A/70	115	55	74, 93	4
SD4-21S	-27.09925	22.99563	E11A/100	40	40	33	0.01
SD4-22	-27.06709	22.99902	E8B/175	95	95	20, 70, 86	**20**
SD4-23	-27.06168	22.99969	E7B/150	120	52	23	0.5
SD4-24	-27.05629	22.99886	E5B/40	112	53	84	0.4
SD4-25	-27.04271	23.00055	E1A/50	115	54	29	0.6
SD4-26	-27.0252	23.00355	Geological	109	109	39, 65	**9.8**
SD4-27	-27.0193	23.00273	Geological	91	79	49, 57	**10**
SD4-28	-27.10489	22.99496	Geological	110	110	66, 82	**4**
SD4-28A	-27.10484	22.99465	Geological	90	61	-	0.01
SD4-29	-27.1101	22.99439	Geological	100	100	82	**10**
SD4-30	-27.11596	22.99389	Geological	120	50	52	0.6

A2 EASTERN FAULT

Borehole No.	Latitude	Longitude	Traverse No	Drill Depth (m)	Casing Depth (m)	Water Strike (m)	Air-Lift yield (l/s)
SD4-35	-27.11305	23.06177	E12/2400	79	79	38, 41, 50	**18**
SD4-43	-27.11894	23.06123	N03/8400	79	79	49, 52, 59	**15**
SD4-36	-27.08059	23.06086	E9D/300	82	63	76, 80	**30**
SD4-44	-27.09466	23.06115	N03/5700	95	64	79	**0.7**
SD4-37	-27.07791	23.06402	E9C/600	80	80	63, 67	**25**
SD4-38	-27.07788	23.07008	E9C/1200	91	91	60, 67	**4**
SD4-38A	-27.07813	23.0702	E9C/1200	80	40	44	**6**
SD4-39	-27.04535	23.08534	E02/300	110	100	48,106	**20**
SD4-40	-27.08112	23.10039	N12/4350	120	100	33, 76, 82	**5**
SD4-40A	-27.08105	23.10037	N12/4350	100	-	93	**3**
SD4-42	-27.04805	23.10045	N12/600	120	120	54, 105, 118	**20**
SD4-45	-27.0725	23.06067	Geological	73	73	55, 58, 66	**15**
SD4-46	-27.06437	23.06037	Geological	82	66	42, 46, 58	**11**
SD4-47	-27.04271	23.05916	E01/420	64	60	36, 53	**13.8**
SD4-48	-27.03187	23.05905	Geological	82	60	36, 49	**15**
SD4-50	-27.01561	23.05646	Geological	124	124	69, 93	**9**
SD4-51	-27.00917	23.05303	Geological	57	36	19, 26, 31	**30**
SD4-52	-27.01793	23.08425	Geological	99	99	54	**2.2**
SD4-53	-26.997	23.0689	Geological	117.5	110	28.85.99	**8**
SD4-54	-27.01277	23.00202	Geological	53.5	40	39,45,50	**17**
SD4-55	-27.00736	23.0031	Geological	88	62	36,48,56	**15**
SD4-57	-27.00328	23.05237	Geological	120	80	34,47,50	**6.8**
SD60-60	-27.01271	23.00261	Geological	94.8	90	54	**2.2**

A3 SOUTH BOUNDARY

Borehole No.	Latitude	Longitude	Traverse No	Drill Depth (m)	Water Strike (m)	Air-Lift yield (l/s)
SD4-01	-27.1359	23.06121	N03/10280	170	84	0.5
SD4-03	-27.12235	23.09449	N11/8850	82	17	0.2
SD4-04	-27.12253	23.09449	N11/8900	100	58	0.1
SD4-05	-27.12302	23.09439	N11/8925	67	19	2.1
SD4-06	-27.11881	23.09449	N11/8450	49	19; 25	**8.5**
SD4-07	-27.11845	23.09453	N11/8410	82	19;58	0.5
SD4-08	-27.12125	23.08839	N10/8710	80	33	0.1
SD4-10	-27.12139	23.08844	N10/8730	40	-	0
SD4-09	-27.12054	23.0881	N10/8745	26	0	0
SD4-11	-27.11303	23.09425	E12/5630	61	25;26	2.1
SD4-13	-27.10162	23.07026	N05/1680	124	50	0.8
SD4-14	-27.11307	23.07027	E12/3250	45	-	0
SD4-31A	-27.11306	23.06976	E12/3200	37	-	0
SD4-31	-27.11305	23.06929	E12/3150	100	45	0.2
SD4-33	-27.1209	23.06127	N03/8620	112	42, 61	2.1
SD4-34	-27.09955	23.06067	E11/2300	120	35, 46	2

ABSTRACT

In this study the groundwater resource the in Tsineng area, Northern Cape was assessed in terms of the volumes of water that may be sustainably abstracted from the aquifer system, and the quality of the available groundwater. A strong emphasis was placed on the use of airborne and ground geophysical techniques to gain a better understanding of the geological and geohydrological conditions in the study area.

The airborne geophysical technique employed during the current investigation was the time-domain electromagnetic method (using the SkyTEM system), while ground geophysical surveys employed the gravity, magnetic, frequency-domain electromagnetic and electrical resistivity tomography methods. The geophysical techniques were used to provide information on physical changes in the subsurface conditions that may be related to the presence of geological structures associated with potential groundwater resources. The results of all the geophysical methods used were collated and correlated to the local geology to make an informed decision during the selection of drilling targets for the installation of production boreholes.

From the TDEM data, information on the subsurface distribution of resistivities was obtained. Well-defined resistivity anomalies correlated well with the known presence of two prominent fault zones. Furthermore, resistivity anomalies were also identified at the locations of mapped dolerite dykes known to intersect the study area. The ground geophysical investigations were conducted across preliminary targets defined from the airborne TDEM data. The ground geophysical investigations confirmed the presence of the structures identified from the TDEM data.

Based on the results of the geophysical investigations and the known local geological conditions, drilling targets were selected at positions deemed promising for the installation of successful production boreholes. A total of 78 exploration boreholes were drilled during the current investigations. Sixty of these boreholes had water strikes and were thus considered successful. A combined total blow-yield of 409 *l*/s was measured in the successful boreholes. Forty of the drilled boreholes had blow-yields in excess of 2 *l*/s. These boreholes were selected for aquifer hydraulic tests to assess the hydraulic parameters of the intersected aquifer systems.

From the estimated hydraulic parameters, sustainable yields were determined for the tested boreholes. The total estimated sustainable yield from the boreholes was more than 7 500 m^3/day.

Water samples from the 40 high-yielding boreholes were submitted for chemical analyses. The results of the analyses showed that the water in the study area is generally of very good quality, suitable for human consumption. It is therefore concluded that groundwater may be successfully used to augment the municipal water supply in the Tsineng area.

The results of the current research demonstrate that the use of geophysical techniques could greatly contribute to an understanding of the geological and geohydrological conditions in a study area, which could in turn lead to a higher success rate during groundwater exploration programmes.

Keywords: Geophysical techniques, Groundwater exploration, Groundwater resource assessment, SkyTEM, Aquifer parameters, Borehole sustainable yield, Water quality.

OPSOMMING

In hierdiestudie is die grondwaterbronne in die Tsineng-area in die Noord-Kaap Provinsiegeëvalueer in terme van die volumes water wat volhoubaaronttrekkan word vanuit die akwifeersisteem, asook die kwalitiet van die beskikbaregrondwater. ‘nSterkklem is geplaas op die gebruik van geofisiesetegnieke om ‘n beterinsig in die geologieseengeohidrologiesetoestande van die studie-area teverkry.

Die lug-geofisiesetegniek wat gebruik is gedurende die huidigeondersoek was die tyd-domeinelektromagnetiesemetode (die SkyTEM-sisteem is gebruik), terwyl die grondgeofisieseopnames die gravitasie-, magnetiese-, frekwensie-domeinelektromagnetiese-enelektrieseweerstandtomografie-metodesgebruik het. Die geofisiesetegnieke is gebruik om inligtingtebekomoor die fisieseveranderingeondergronds wat verband mag hou met die teenwoordigheid van geologiesestrukturegeassosieer met potensiëlegrondwaterbronne. Die resultate van al die geofisiesemetodes is gesamentlikbeskouengekorreleer met die plaaslikegeologieomingeligtebesluitete neem tydens die seleksie van boorteikensvir die installering van produksieboorgate.

Vanaf die TDEM data is inligtingoor die ondergrondseverspreiding van soortlikeweerstandeverkry. Goed-gedefinieerdeweerstands-anomalië het goedooreengestem met die bekendeteenwoordigheid van twee prominenteverskuiwingsones. Verder is weerstands-anomaliëookgeïdentifiseer by die posisiesvan bekendedolerietgange wat die studie-area deurkruis.Die grondgeofisieseondersoeke is gedoenoorvoorlopigeteikens, soosgedefinieervanaf die TDEM-data.Die grondgeofisieseondersoekehet die teenwoordigheidbevestig van die strukture wat vanaf die TDEM-data geïdentifiseer is.

Vanaf die resultate van die geofisieseondersoeke, asook die bekendeplaaslike geologiesetoestande, is boorteikensgekies op plekke wat as belowendbeskou is vir die installering van suksesvolle produksie boorgate. ‘n Totaal van 78 eksplorasie boorgate is geboortydens die huidigeondersoeke.Sestig van hierdieboorgate het water getrefen is gevolglik as suksesvolbeskou.‘n Gekombineerde total eblaaslewering van 409 *l*/sis gemeet in die suksesvolleboorgate.Veertig van die boorgate het blaaslewerings van meer as 2 *l*/s gehad. Hierdieboorgate is gekiesvirhidrouliesetoetsing van die akwifeerom die hidrouliese parameters van die akwifeer-sisteemtebepaal.

Vanaf die geskattehidrouliese parameters, is volhoubareleweringsvir die getoetsteboorgatebepaal. Die total egeskattevolhoubarelewering van die boorgate was meer as 7 500 m^3/day.

Watermonsters van die 40 hoë-leweringboorgate is ingedienvirchemieseanalises. Die resultate van die chemieseanalises het getoondat die water in die studie-area oor de algemeen van baiegoeiekwaliteit is, geskikvirmenslikegebruik. Die water kandussuksesvolgebruik word om die munisipalewatertoevoer in die Tsineng-area aantevul.

Die resultate van die huidigeondersoek toon dat die gebruik van geofisiesetegniekegrootlikskanbydra tot die begrip van die geologieseengeohidrologiesetoestande in ‘n studie-area, wat weerkan lei tot ‘n hoërsukseskoersgedurendegrondwatereksplorasieprogramme